Multisubstituted Corannulene Derivatives: from Photophysics to Metal Complexes

Dissertation

zur

Erlangung der naturwissenschaftlichen Doktorwürde

(Dr. sc. nat.)

vorgelegt der

Mathematisch-naturwissenschaftlichen Fakultät

der

Universität Zürich

von

Davide Bandera

aus Italien

Promotionskomitee:

Prof. Dr. Jay S. Siegel (Vorsitz und Leitung)

Prof. Dr. Kim K. Baldridge

Prof. Dr. Franco Cozzi

Prof. Dr. Karl-Heinz Ernst

Zürich, 2009

Die vorliegende arbeit wurde von

der Mathematisch-naturwissenschaftlichen Fakultät

der Universität Zürich im Mai 2009

als Dissertation angenommen

Promotionskomitee:

Prof. Dr. Jay S. Siegel

Vorsitz

Prof. Dr. Kim K. Baldridge

Prof. Dr. Franco Cozzi

Prof. Dr. Karl-Heinz Ernst

Universität Zürich

2009

Table of contents

LIST OF FIGURES

LIST OF SCHEMES

LIST OF TABLES

ACKNOWLEDGEMENTS

Prof. Dr. J. S. Siegel

Prof. Dr. K. K. Baldridge
Prof. Dr. R. Dorta
PD. Dr. N. S. Finney
Prof. Dr. Y.-T. Wu
PD. Dr. A. Linden and X-ray team
PD. Dr. L. Bigler

Simon Jurt and the NMR team

Jui-Cheng Tseng, Arif Karim, Fitore Kasumaj,
Paola Romanato, Fabienne Furrer, Derik Frantz, Karla Arias, Ashley Sullivan,
Anna Butterfield, Tomoharu Hayama, Silvia Rocha
and
all Siegel, Finney and Baldridge group members past and present

My family

CURRICULUM VITAE

EDUCATION

1/2004 - 5/2009 **University of Zürich**, Zürich, Switzerland
Ph. D. in Organic Chemistry
-Thesis on "Multisubstistuted corannulene derivatives: from photophysics to metal complexes" . Research advisor Prof. J. S. Siegel.
-Took courses in X-ray crystallography, NMR spectroscopy, gaschromatography and HPLC.

12/2003 - 1/2004 **Università degli Sudi di Milano**, Milano, Italy
Italian State Certificate for the Practice of the Chemist Profession

9/1998 - 10/2003 **Università degli Studi di Milano**, Milano, Italy
Laurea in Industrial Chemistry
-Thesis: " In search of new chiral ligands for asymmetric catalysis: synthesis of macrocyclic and enantiomerically pure bipyridine and phenanthroline structures". Thesis advisor Prof. F. Cozzi.

9/1993 - 7/1998 **Istituto Tecnico Industriale Statale per Chimici "S. Cannizzaro"**
Qualified Chemist Diploma (high school)

WORK EXPERIENCE

1/2004 - 5/2009 **Research Associate**, *University of Zürich, Organic Chemistry Institute*, Zürich, Switzerland
-Research on corannulene derivatives and their application in photophysic and organometallic complexes. Research advisor Prof. J. S. Siegel.

11/2002 - 10/2003 **Undergraduate Researcher**, *Università degli Studi di Milano*, Milano, Italy
-Research of new chiral ligand for asymmetric catalysis. Research advisor Prof. F. Cozzi.

6/1997 - 7/1997 **Summer Student**
Research Institute for Pharmacology "Mario Negri", Milano,
-Molecular biology methodologies for cytokines gene expression research in a neurochemistry laboratory. Supervisor Dr. Liana Terreni.

6/1996 - 7/1996 **Summer Student**
Department for Public Health and Environmental Protection, Parabiago, Milano, Italy
-Analysis of pollutants in water for public consumption.

ACHIEVEMENTS AND HONORS

Awards **ISU Università degli Studi di Milano**, *Laurea Prize year 2003*

Scholarships 1999-2003 **ISU Università degli Studi di Milano**, *Scholarship* for the period

SNF Post-doctoral Fellowship (June 2009-May 2010), Post-doc at Eindhoven University of Technology (Prof. Dr. E. W. Meijer), Eindhoven, Netherlands.

POSTERS, PRESENTATIONS AND PAPERS

Poster s **Swiss Chemical Society National Meeting**, Lausanne, September 2007, Switzerland
"Synthesis and Properties of Ir(I) and Rh(I) Metal Complexes of Pentaalkyl Substituted Corannulene Derivatives", D. Bandera, R. Dorta, A. Linden, K. K. Baldridge, J. S. Siegel.

12th International Symposium on Novel Aromatic Compounds, Awaji Island, July 2007, Japan
"Synthesis and Properties of Ir(I) and Rh(I) Metal Complexes of Pentaalkyl Substituted Corannulene Derivatives", D. Bandera, R. Dorta, A. Linden, K. K. Baldridge, J. S. Siegel.

236th ACS National Meeting, Philadelphia, August 2008, USA
"Synthesis and Properties of Ir(I) and Rh(I) Complexes of Alkylsubstituted Corannulene Derivatives", D. Bandera, R. Dorta, A. Linden, K. K. Baldridge, J. S. Siegel.

Presentations

Swiss Chemical Society National Meeting, Zürich, October 2005, Switzerland
"Synthesis and Photophysical Properties of Multiethynyl Substituted Corannulene Derivatives", D. Bandera, Y.-T. Wu, R. Maag, A. Linden, K. K. Baldridge, J. S. Siegel

Multisubstiututed Corannulene Derivatives: Synthesis, Properties and their Ir(I) and Rh(I) Metal Complexes, Prof. E. W. Meijer group meeting, TU Eindhoven, NL, May 2008.

Papers **Syntheis of [Ru(II)bis(2,2'-bipyridine)(5-{ethynyl-corannulene}-2,2'-bipyridine)](PF6)2**, C. S. Jones, A. Linden, D. Bandera, J. S. Siegel, *manuscript in preparation*.

Synthesis and Properties of Multiethynyl Substituted Corannulene Derivatives, Y.-T. Wu, D. Bandera, R. Maag, A. Linden, K. K. Baldridge, J. S. Siegel, *J. Am. Chem. Soc.,* **2008**, *130*, 10729.

Synthesis and Properties of (4-Substituted-phenyl)corannulene Derivatives, C. S. Jones, D. Bandera, K. K. Baldridge, J. S. Siegel. *manuscript in preparation*.

Chiral Rh(I) Complexes of Corannulene Derivatives, D. Bandera, R. Dorta, A. Linden, K. K. Balbridge, J. S. Siegel., *manuscript in preparation*.

Building 2D Crystals from 5-Fold-Symmetric Molecules, T. Bauert, L. Merz, D. Bandera, M. Parschau, J. S. Siegel, K.-H. Ernst, *J. Am. Chem. Soc.* **2009**, *131*, 3460.

Synthesis, Structure and Dynamic Properties of Rh(I) and Ir(I) Complexes of Penta-alkyl Corannulene Derivatives, D. Bandera, R. Dorta, K. K. Baldridge, A. Linden, J. S. Siegel, *manuscript in preparation*.

ABSTRACT OF THE DISSERTATION

Multisubstituted Corannulene Derivatives: from Photophysics to Metal Complexes

By

Davide Bandera

Doctor of Philosophy

University of Zurich, 2009

Prof. Dr. Jay S. Siegel, Chair and Advisor

Corannulene, $C_{20}H_{10}$ is a fragment of buckminsterfullerene, C_{60}. Among the interesting properties of corannuelene are: its bowl structure, photophysics and symmetry. The improved synthetic route for the synthesis of corannulene provides abundant starting material for the preparation of a wide variety of derivatives of which the physical properties can be studied. This dissertation is divided in three areas: 1) study of the properties of multi-alkynyl substituted corannulene derivatives, 2) synthesis and dynamic properties of Rh(I) and Ir(I) metal complexes of C_5-symmetric alkyl derivatives of corannulene, and 3) preparation and study of the properties of Rh(I) complexes of corannulene and derivatives, which bear a chiral, enantiomerically pure ligand.

The synthesis of multisubstituted corannulene derivatives having varied symmetry (C_1, C_s-1,2,5,6-tetrasubstituted or C_5-1,3,5,7,9-pentasubstituted) is accomplished from the corresponding halogenated compounds by means of palladium or nickel catalyzed coupling reactions. Recently improved reaction conditions provide quantities of compounds sufficient for detailed study of properties.

The photophysical behavior of multi-arylalkynyl substituted derivatives has been investigated in dichloromethane solution. The results show that it is possible to tune the luminescence of these derivatives by changing the aryl substituents. The derivatization of corannulene leads to greatly enhanced photophysical properties thus opens the possibility for application as photoactive materials. The X-ray crystallographic analyses of some of these multi-arylalkynyl derivatives unveil the possibility of preparing materials in which the corannulene motifs are stacked in a columnar fashion in contrast with the parent compound corannulene. Quantum chemical calculations provide geometric parameters in agreement with the experimental data and help explain the photophysical properties of this class of compounds.

Rh(I) and Ir(I) complexes of C_5-symmetric alkyl derivatives of corannulene are prepared by reaction of the corannuelene derivatives with the $[L_2M(\mu^2\text{-}Cl)]_2$ dimer in the presence of a silver salt (M = Rh or Ir, L = mono- or bidentate- olefin). X-ray crystallographic analyses show the metal η^6 bound to the polyaromatic surface. Quantum chemical calculations provide estimate of the geometric parameters in good agreement with the experimental data. The 1D and 2D ^{1}H NMR study of these compounds show interesting dynamic properties: some of the Rh(I) compounds display metal migration on the corannulene surface whereas Ir(I) derivatives show rotation along the metal-corannulene bond. The dynamics can be tuned by changing the olefinic ligand (L) and/or the metal.

The Rh(I) compound bearing a chiral, enantiomerically pure ligand provides, for the first time, an example in which, during the complex formation, a dynamic kinetic resolution (DKR) of the C_5-symmetric alkylderivatives is performed. Such DKR is more efficient when the substituents on the corannulene core are bulky.

ZUSAMMENFASSUNG

Mehrfach substituierte Corannulen Derivate: von Photophysik zu Metallkomplexen

By

Davide Bandera

Dr. sc. Nat.

Universität Zürich, 2009

Prof. Dr. Jay S. Siegel, Vorsitz und Leitung

Corannulen, $C_{20}H_{10}$, ist ein Fragment des Buckminsterfulleren C_{60}. Interessante Eigenschaften von Corannulen sind unter Anderem seine Schalenform, die Photophysik und die Symmetrie. Ein verbesserter Syntheseweg von Corannulen verschafft Zugriff zu genügend Startmaterial für die Synthese von einer Vielzahl von Derivaten, deren physikalische Eigenschaften untersucht werden können. Diese Doktorarbeit ist in drei Abschnitte unterteilt: 1) Untersuchung der Eigenschaften von multi-alkynyl substituierten Corannulen Derivaten, 2) Synthese und dynamische Eigenschaften von Rh(I) und Ir(I) Metallkomplexen C_5-symmetrischer Alkylderivate von Corannulen, und 3) Herstellung und Untersuchung der Eigenschaften von Rh(I) Komplexen des Corannulen und Derivaten, welche einen chiralen, enantiomerenreinen Liganden enthalten.

Die Synthese von mehrfach substituierten Corannulen Derivaten unterschiedlicher Symmetrie (C_1, C_s-1,2,5,6-tetrasubstituiert oder C_5-1,3,5,7,9-pentasubstituiert) erfolgt von den entsprechenden halogenierten Verbindungen durch Palladium- oder

Nickelkatalysierte Kupplungsreaktionen. Die kürzlich optimierten Reaktionsbedingungen liefern genügend Material für eine detaillierte Untersuchung der jeweiligen Eigenschaften.

Das Photophysikalische Verhalten multi-arylalkynyl substituierter Derivate in Dichlormethan wurde untersucht. Die Resulate zeigen, dass es möglich ist, die Lumineszenz dieser Derivate durch Austausch der Arylderivate zu steuern. Die Derivatisierung von Corannulen führt zu stark verbesserten photophysikalischen Eigenschaften und eröffnet somit die Möglichkeit einer Anwendung als photoaktive Materialien. Die Röntgenkristallanalyse einiger der multi-arylakynyl Derivate enthüllt die Möglichkeit, Materialien, in denen Corannulen Motive – im Gegensatz zum unsubstituierten Corannulen - säulenartig gestapelt vorkommen, herzustellen. Quantenchemische Berechnungen liefern geometrische Parameter in Übereinstimmung mit den experimetellen Daten und helfen bei der Erklärung der photophysikalischen Eigenschaften dieser Klasse von Verbindungen.

Rh(I)- und Ir(I)-Komplexe der C_5-symmetrischen Alkylderivate von Corannulen werden durch Reaktion der Corannulenderivate mit dem $[L_2M(\mu^2\text{-}Cl)]_2$ Dimer in Anwesenheit eines Silbersalzes (M= Rh oder Ir, L= mono-oder bidentat-Olefin) hergestellt. Röntgenstrukturanalyse zeigt, dass das Metall auf der polyaromatischen Oberfläche η^6-gebunden ist. Quantenchemische Berechnungen ergeben Abschätzungen der geometrischen Parameter, die gut mit den experimentellen Daten übereinstimmen. Die 1D- und 2D-^{1}H NMR Untersuchung dieser Verbindungen zeigen interessante dynamische Eigenschaften: einige der Rh(I)-Verbindungen stellen Migration auf der Corannulenoberfläche dar, wohingegen Ir(I)-Derivate Rotation

längs der Metall-Corannulen-Bindung zeigen. Diese Dynamik kann durch Austausch des Olefinliganden (L) und/oder des Metalls verändert werden.

Die Rh(I)-Verbindung mit einem chiralen, enantiomerenreinen Liganden stellt, zum ersten Mal, ein Beispiel dar, bei welchem während der Komplexbildung eine dynamische kinetische Auflösung (DKA) der C_5-symmetrischen Alkylderivative ausgeführt wird. Eine soche DKA ist je effizienter je grösser die Substituenten am Corannulenkern sind.

Chapter 1.

Discovery of corannulene, syntheses and properties.

1.1 Introduction

In the modern chemical era, a class of compounds that is driving great research efforts in the chemical community comprises the polycyclic aromatic hydrocarbons (PAHs).[1] These molecules are especially abundant in oil and coal as well as in the atmosphere, due to the extensive combustion still necessary for energy production and locomotion.[2] The use of this class of compounds spans from the preparation of pharmaceuticals, organometallic catalysts, dyes, polymers and applications in nanotechnology.[3] In this chapter a historical background concerning a class of PAHs having bowl-shaped structure (Figure 1.1), in particular: corannulene (**1**, $C_{20}H_{10}$) and buckminsterfullerene (**2**, C_{60}) will be presented.

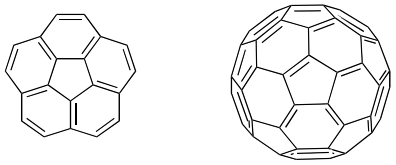

1 2

Figure 1.1. Corannulene (1) and buckminsterfullerene (2).

1.1.1. The discovery of Corannulene and Fullerene

Corannulene was synthesized by Lawon et. al. in 1966[4] in what was a continuing challenge in the design and construction of molecules which must compromise between the factors of strain and aromaticity.[5] The structure, a central five-membered ring fused with five six-membered rings, provides an unusual strain resulting from geometrical requirements that force the molecule to be curved.[6] Buckminsterfullerene was observed for the first time by Kroto et. al. during laser vaporization experiments of graphite.[7] These experiments aimed at understanding the mechanism by which long-chain carbon molecules are formed in interstellar space. The results evidenced that a particularly stable C_{60} carbon cluster was formed. After this observation, concern arose regarding which kind of structure this compound could have. A truncated icosahedron was proposed and named as buckminsterfullerene. The confirmation arrived when Krätschmer et. al.[8] and later Kroto et al.[9] were able to get X-ray analyses. Following the discovery of **2**, scientists have found that several other carbon-rich based compounds[10] (e.g. higher fullerenes

and single–walled carbon nanotubes), and new forms of carbon allotropes were proposed.[11]

1.1.2. The first synthesis of corannulene

The first synthesis started from acenaphtalene (**3**) and was designed in such a way that strain distortion and aromatization were introduced over the last few steps.[4] This synthetic path included 17 steps and the overall yield was below 1% (Scheme 1.1). The small amount of material prepared by this first synthesis made it possible to characterize **1** and confirm the bowl-shaped structure.[12]

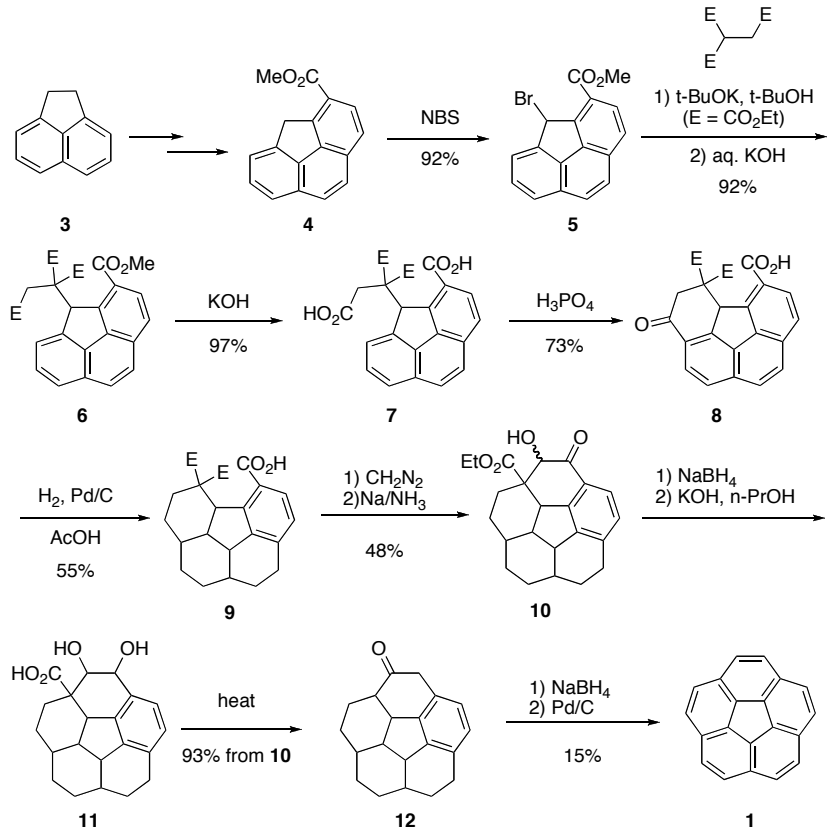

Scheme 1.1. First synthesis of 1.

Other research groups unsuccessfully attempted to find a new synthetic procedure to afford **1**. In particular, Robins[13] tried to prepare **1** starting from the construction of the corannulene core, namely, substituted 7,10-fluoranthenes (**15**) which would subsequently undergo cyclization (Scheme 1.2) to the final product corannulene.

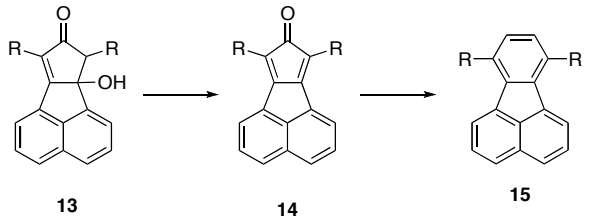

Scheme 1.2. Robins synthetic path to 15.

An alternative approach by Reiss included the preparation of cyclophane dienes (**16**), followed by an oxidative photochemical ring-closure (Scheme 1.3) to afford **1**.[14] After these attempts by Robins and Reiss failed, research on **1** was very limited for almost 20 years.[15] In 1985, the discovery of **2** brought new interest to **1**; new solution-phase synthetic procedures and flash vacuum pyrolysis (FVP) were used to prepare **1** and its derivatives.

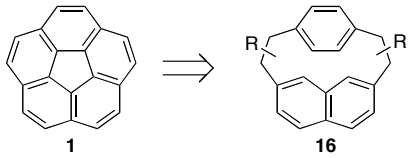

Scheme 1.3. Reiss' synthetic path to 1.

1.1.3. Synthesys of 1 by means of FVP[16]

The inspiration of using flash vacuum pyrolysis in the synthesis of **1** came after Brown observed the formation of acenaphtalene from ethynylnaphtalene.[17] Scott and Siegel were the first two groups to accomplish the synthesis of **1** by FVP (Scheme 1.4). Scott's method[18] starts from **17,** with the formation of terminal alkynes that then rearrange to vinylidene carbenes, which insert to the CH bonds of the naphthalene, affording **1** after double cyclization.[17] Later, it was found that **18**, precursor to **17**, could afford **1** directly, thereby shortening the synthesis by another step and avoiding thermal polymerization of the starting material.

At the same time, Siegel envisioned a possible synthetic route starting from **19**.[19] This synthesis, performed in static–condition FVP, involves the elimination of SO_2 followed by rearomatization with Pd/C. The same group, based on work by Boekhelheide,[20] also prepared **1** from **20**. The transformation involves a series of HBr

eliminations combined with an electrocyclic reaction of the intermediates affording the target compound **1**.

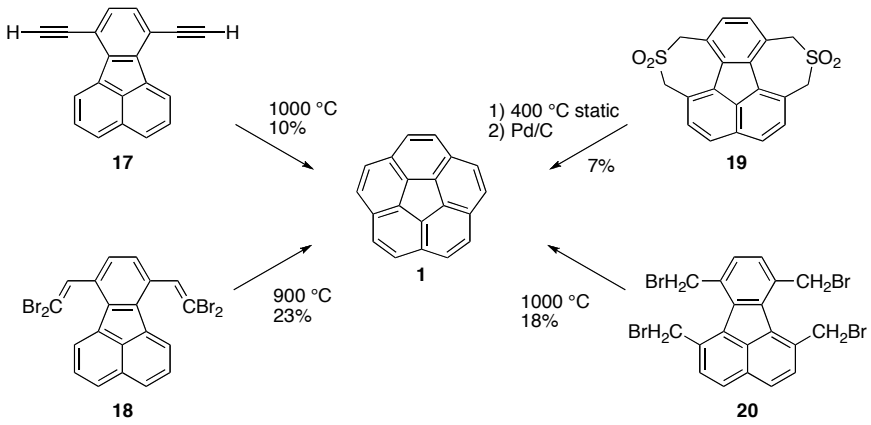

Scheme 1.4. First synthesis of 1 by FVP by Scott and Siegel .

Driven by the challenge of finding more efficient ways to yield **1,** these first synthetic successes inspired other groups to join the field, and stimulated new efforts from the researchers already in the field (Scheme 1.5). Rabideau[21] started from the vinyl silylether **21**, precursor to a vinyl carbene that rearranges to form **1**; alternatively, **22** is reported to afford the target molecule in low yield by the loss of methane.[22] Other synthetic approaches did not start from a pre–formed fluoranthene intermediate. Zimmermann's[23] approach begins from the diyne **23**, which loses TMS groups during FPV due to the free Si–OH groups on the hot quartz surface. Metha and Panda[24] used substituted [4]helicene **24** that, by means of a cyclodehydrogenation, forms a benzo[ghi]floranthene. Subsequent ring closure and rearomatization leads to **1**. Knölker was capable of improving the reaction starting from **17**, which affords **1** in 36% yield.[25] Of all these attempts the path that afforded **1** with the highest yield was the one reported by Scott, in which **25** loses two molecules of HCl and then cyclizes twice to give the target compound **1**.

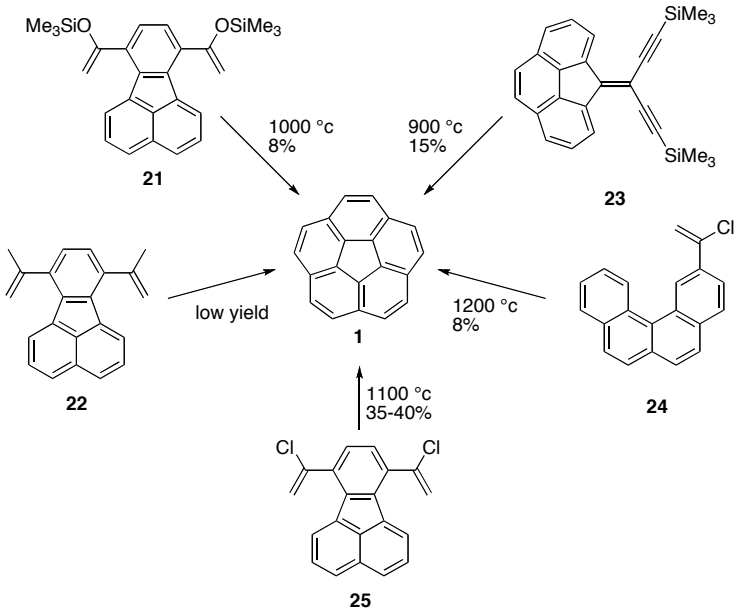

Scheme 1.5. Alternative FVP synthesis of 1.

Although FVP allowed the preparation of corannulene in much higher yield than Lawton and Barth's methodology, it had some limitations: first, the difficulty of preparing large amounts of **1** in high yield and the possibility of forming side products, due to the drastic reaction condition (e.g thermal rearrangements);[26] second, the low tolerance to the introduction of substituents and functional groups on the corannulene nucleus. These limitations led to the development of new solution-phase synthesis of **1**.

1.1.4. Solution-phase synthesis of 1[27]

The first attempt towards a solution-phase synthesis of **1** was a continuation of the synthesis of **20**[19] (Scheme 1.6) by the Siegel group. In particular, starting from **26**, compound **29** was prepared from **28**.[13] Subsequent by bromination of **29** yielded **30**. The latter was then reduced and dehydrogenated to give **31**.[28]

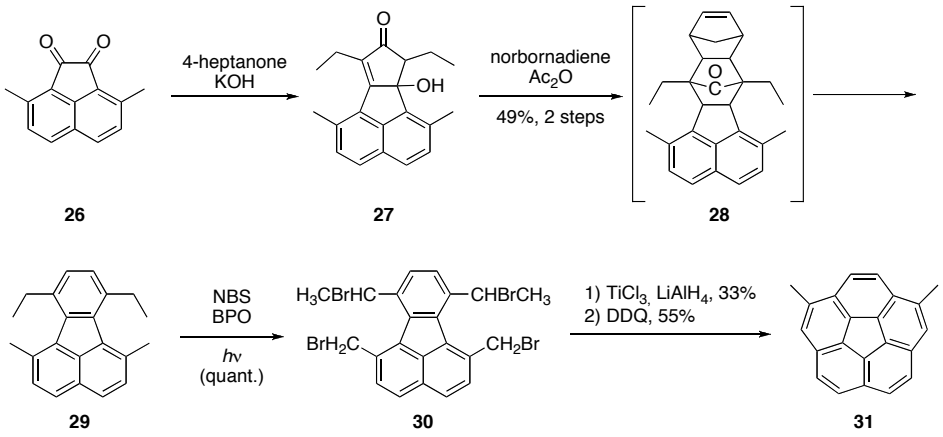

Scheme 1.6. The first synthesis of corannulene derivatives.

In 1999, Siegel[29] and Rabideau,[30] (Scheme 1.7) independently introduced two low-valent metal-based reductive couplings to afford **1** from octabromide **33**, which was obtained by the forced NBS bromination of **32**. Both these methods afforded **1** in good yields.

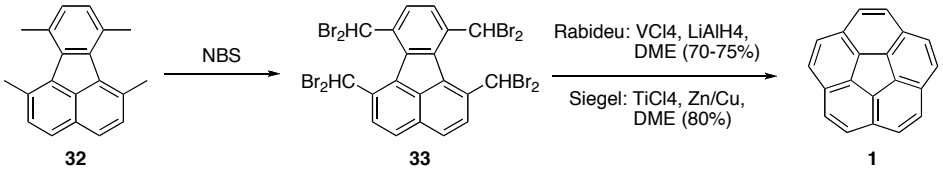

Scheme 1.7. Siegel and Rabideau's method from synthesis of 1 with low valent metal.

Another method to afford **1** was introduced by Sygula and Rabideau.[31] This method involves the ring-closure of of **33** by sodium hydroxide; the deprotonation of the benzylic proton initiates the C–C bond formation (Scheme 1.8). This ring-closing step results in different bromides, **34** or **35**, depending on the solvent. Compound **34** affords **1** upon treatment with *n*-BuLi, followed by quenching with water, whereas **35** is reduced with Zn and KI.[31b]

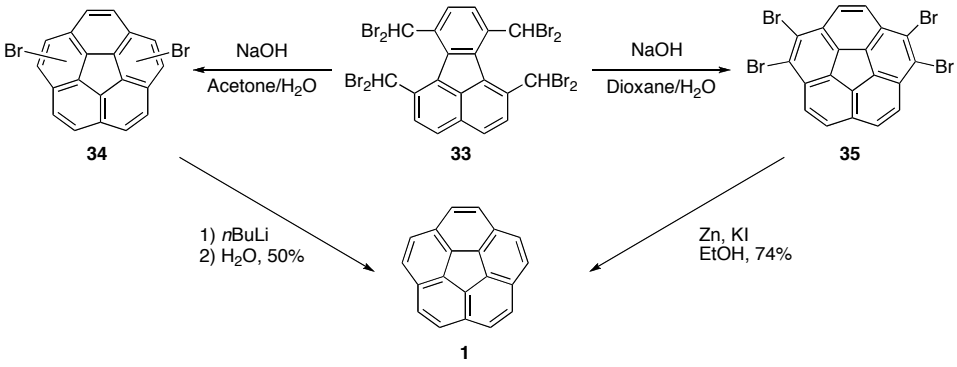

Scheme 1.8. Rabideau's method for the preparation of 1

The methods to synthesize **1** and derivatives that have been discussed so far do not allow the introduction of reactive functional groups on the corannulene nucleus. To overcome this issue, Sygula and Rabideau introduced a mild Ni–based method in 2002.[32] Treatment of **36** with nickel forms **38**, via **37**, according to the postulated mechanism for Ni–mediated reductive couplings of benzyl/benzylidene bromides (Scheme 1.9).[33] These synthetic methodologies allow for the preparation of a variety of substituted corannulene derivatives *via* solution-phase synthesis (Table 1.1).

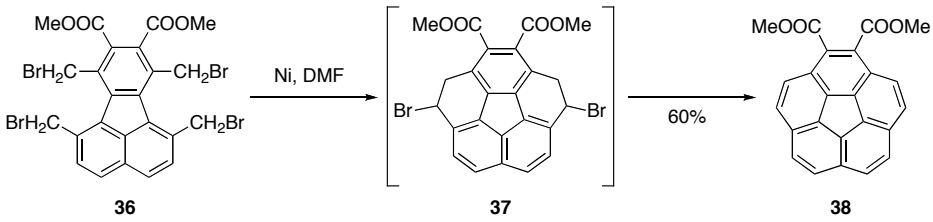

Scheme 1.9. Ni based method for the santhesis of 38.

Table 1.1. Summary of the solution-phase methods for 1 and derivatives.

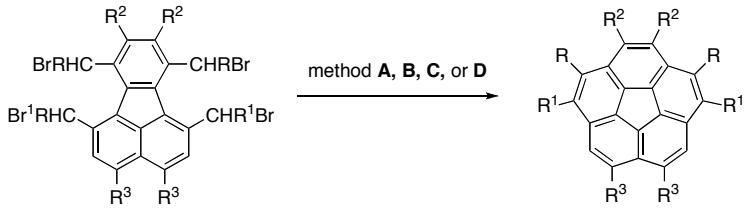

A: $TiCl_4$, Zn/Cu, DME or VCl_4, $LiAlH_4$, DME
B: 1)NaOH, dioxane/H_2O; 2) Zn, KI, EtOH or DMF
C: 1)$TiCl_3$, $LiAlH_4$ or $TiCl_4$, Zn/Cu, DME; 2) DDQ
D: Ni, DMF

Entry	R	R^1	R^2	R^3	Method	Yield (%)	ref
1	Br	Br	H	H	A	80	29
2	Br	Br	H	H	A	70-75	30
3	Br	Br	H	H	B	74	31
4	Br	Br	H	Cl	A	85	29
5	Me	Br	H	H	B	66	34
6	2-BrPh	Br	H	H	B	96	35
7	Me	H	H	H	C	24	29
8	H	Me	H	H	C	48	29
9	H	Me	H	Cl	C	45	29
10	Me	Me	H	H	C	6	29
11	H	H	COOMe	H	D	60	32
12	H	H	COOMe	Cl	D	49	36
13	H	H	COOMe/Ph	Cl	D	51	36

So far, only the synthetic procedures for **1** and its derivatives have been introduced. Although tedious, such synthetic procedures allow for the preparation of different corannulene derivatives and, as a consequence, the study of their properties.

The synthesis of **2** has been performed by vaporization of graphite [8,37] or by combustion of hydrocarbons [38] and these methods allow production of **2** on industrial scale providing enough material for the study of not only its properties but also of its

applications. The Scott group reported in 2002 a procedure to prepare **2** *via* solution-phase synthesis and FVP but with low yield.[39]

1.1.5. A look at the structure and properties of 1

Structurally, corannulene **1** is a fragment ($C_{20}H_{10}$) of **2**. From X-ray crystallographic analyses,[40] it was noted that **1** due to lack of symmetry in the crystal has four different C–C bonds lengths: 1.38 Å (rim), 1.44 Å (flank), 1.42 Å (hub), and 1.38 Å (spoke). Instead, **2** was showed to have only two different C–C bond lengths: 1.45 and 1.38 Å for pentagon/hexagon and hexagon/hexagon fusions, respectively (Figure 1.2).[41]

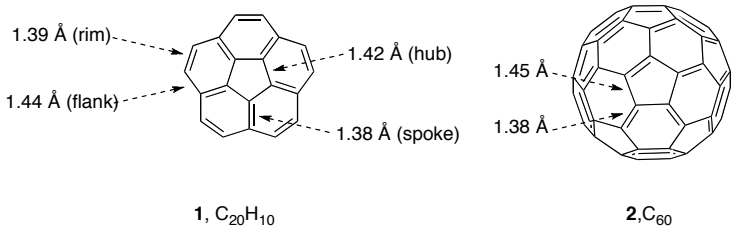

Figure 1.2. Structural comparison of 1 and 2.

The distance between the plane of the hub rings and the rim atoms is defined as the bowl depth of this curved structure. For compound **1**, this distance is 0.875 Å[40] (Figure 1.3) whereas for **2** is 1.5 Å[41]

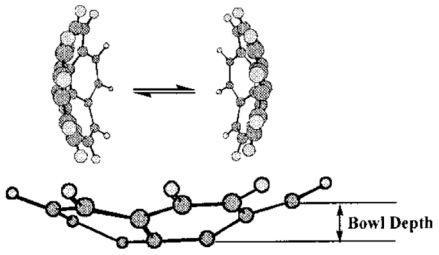

Figure 1.3. Definition of bowl depth.

The curved polyaromatic arene **1** has, like **2**, a bowl-shaped structure. The consequence of this curvature is that the alignment of the p-orbitals leads to a poorer overlap and so to a weaker π bond. The deviation of the p-orbital from the planar geometry is called pyramidalization (Figure 1.4).

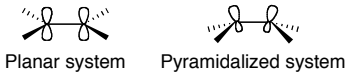

Figure 1.4. Planar vs pyramidalized system.

Haddon[42] introduced the concept of π-orbital axis vector (POAV) as a measure of the curvature of individual carbon atoms. Specifically, an imaginary vector is defined such that its location is equidistant between the three σ-bonds of an sp^2 hybridized carbon atom so that the maximum angle is achieved. If the angle between the vector and the C-C axis is q_{sp}, then POAV angle is defined as $\phi_{POAV} = \theta_{\sigma\pi} - 90$ (Figure 1.5). In general, an sp^2-hybridized carbon atom prefers to form a planar σ-framework with its neighbors, leaving its p-orbital perpendicular to the σ-bonds. For planar aromatics, the $\phi_{POAV} = 0$, in **2** it is 11.6°[42] and in **1** three different ϕ_{POAV} are present: 8.7° (hub), 5.5° (spoke), and 1.1° (rim).[40]

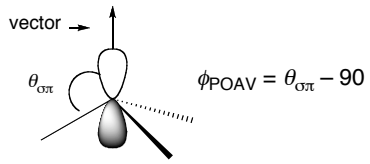

Figure 1.5. Definition of POAV.

In 1971, Barth and Lawton observed that **1** had a bowl-shaped structure and proposed that interconvertion takes place through a planar transition state (Figure 1.6).[5] They were however, not able to directly measure the inversion barrier associated with this process due to the C_{5v} symmetry of **1**. To circumvent this problem, derivatives of **1** were prepared and the inversion barrier was estimated to be 11.5 kcal mol^{-1}.[18a,43]

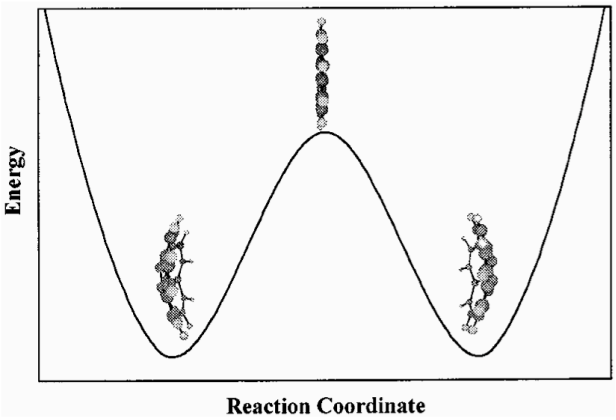

Figure 1.6. Energetic diagram for the bowl to bowl inversion.

The oxidation and reduction potentials for **1** have been measured by means of cyclovoltammetry,[44,12] which reveals a non-reversible oxidation at + 1.6 V and two reversible recuctions at -1.9 V and -2.3 V. Scott et al. have reported the reduction of **1** with Li and K.[45] During these experiments in THF-d_8, four different color changes were evidenced and each of them belongs to the reduction states going from monoanion to the tetraanion, that was characterized as a sandwich dimer (Figure 1.7).[46] The dianion is produced when K is used

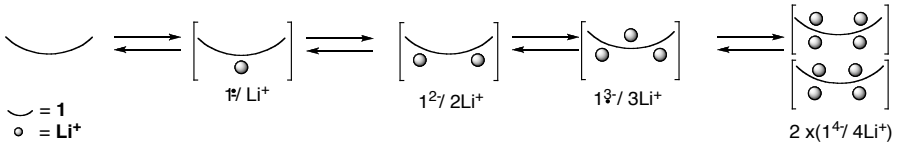

Figure 1.7. Step by step reduction of 1.

Extended PAHs usually display luminescence but the reduced orbital overlap in **1** reduces this phenomenon. Nevertheless, **1** displays fluorescence and phosphorescence.[47] In particular, **1** shows λ_{em} = 420 nm, 440 nm in the fluorescence spectrum and λ_{em} = 475 nm, 485 nm, 512 nm in the phosphorescence spectrum. The measured fluorescence quantum yield for **1** is 0.07.[47] The fluorescence lifetime, 10.3 ns, implies that **1** should not have time to complete a full inversion during the fluorophore's lifetime, whereas the phosphorescence lifetime, 2.6 s, should permit many inversions. Fluorescence quenching experiments revealed that **1** is quenched by nitromethane.[48]

Corannulene offers the possibility of functionalization, which could afford a variety of compounds whose properties could be studied. In this thesis work, the properties of multi-alkyne derivatives will be investigated to unveil the effects of such kinds of substituents on the corannulene nucleus. A detailed study on the photophysical properties of these compounds and the solid-state structures will be presented. Corannulene and its derivatives can also be used as ligands in organometallic complexes. The effect of alkyl sustituents is the subject of a study aimed at the elucidating the dynamic processes in metal complexes with Rh(I) and Ir(I) and olefinic ligands. The study of these dynamics served as the basis for the preparation and investigation of the properties of complexes of corannulene and its derivatives with a Rh(I) metal fragment bearing an enantiomerically pure ligand.

1.2 References

[1] Harvey, R. G. *Polycyclic Aromatic Hydrocarbons*, Wiley-VCH: NY, 1997.

[2] Calvert, J.G.; Atkinson, R.; Becker, K. H.; Kamens, R. M.; Seinfeld, J. H.; Wallington, T. J.; Yarwood, G. *The Mechanism of Atmospheric Oxidation of Aromatic Haydrocarbons*, Oxford University Press: NY, 2002.

[3] (a) Zollinger, H. *Color Chemistry: Syntheses, Properties, and Applications pf Organic Dyes and Pigments*, Wiley-VCH: Weinheim, Germany, 2003. (b) Tsuji, J. *Transition Metal Reagents and Catalyst: Innovation in Organic Synthesis*, Wiley, NY, 2002. (c) Steed, J. W.; Turner, D. R.; Wallace, K. J. *Core Concepts in Supramolecular Chemistry and Nanochemistry*, Wiley, The Atrium, Southern Gate, Chichester, West Sussex, UK, 2007.

[4] Barth, W. E.; Lawton, E. G. *J. Am. Chem. Soc.* **1966**, *88*, 380.

[5] Barth, W. E.; Lawton, E. G. *J. Am. Chem. Soc.* **1971**, 93, 1730.

[6] Hanson, J. C.; Nordnam, C. E. *Abstract of Am. Crystallographic Ass. Summer Meeting* **1967**, 69 (N8).

[7] Kroto, H. W.; Heath, J. R.; O'Brein, S. C.; Curl, R. F.; Smalley, R. E. *Nature* **1985**, *318*, 162.

[8] Krätschmer, W.; Lamb, L. D.; Fostiropoulos, K.; Huffman, D. R. *Nature* **1990**, *347*, 354.

[9] David, I. F.; Ibberson, R. M.; Matthewman, J. C.; Pressides, K.; Dennis, T. J. S.; Hare, J. P.; Kroto, H. W.; Taylor, R.; Walton, D. R. M. *Nature* **1991**, *353*, 147.

[10] (a) Kroto, H. W. *Nature* **1987**, *329*, 529. (b) Ettl, R.; Chao, I.; Diederich, F.; Whetten R. L. *Nature* **1991**, *353*, 149. (c) Iijima, S.; Ichihashi, T.; Ando, Y. *Nature* **1992**, *356*, 776.

[11] (a) Iijima, S. *Nature* **1991**, *354*, 56. (b) Smith, B. W.; Monthioux, M.; Luzzi, D. E. *Nature* **1998**, *396*, 323.

[12] Janata, J.; Gendell, J.; Ling, C.; Barth, W. E.; Backes, L.; Mark, H. B.; Lawton, R. G. *J. Am. Chem. Soc.* **1967**, *89*, 3056.

[13] Craig, J. T.; Robins, M. D. W. *Aust. J. Chem.* **1968**, *21*, 2237.

[14] Davy, J. R.; Iskander, M. N.; Reiss, J. A. *Aus. J. Chem.* **1979**, *32*, 1067.

[15] (a) Wynberg, H. *Tetrahedron Lett*. **1973**, *46*, 4623; (b) Agramat, I.; Hess, B. A.; Shaad, L. J. *Pure Appl*. *Chem*. **1980**, *52*, 1399; (c) Trinajstic, N.; Randic, M. *J*. *Am*. *Chem*. *Soc*. **1984**, *106*, 4428.

[16] Tsefrikas, M. V.; Scott, L. T. *Chem*. *Rev*. **2006**, *106*, 4868.

[17] (a) Brown, R. F. C.; Eastwood, F. W.; Jackman, G. P. *Aust*. *J*. *Chem*. **1977**, *30*, 1757. (b) Brown, R. F. C.; Harrington, K. J.; McMullen, G. L. *J*. *Chem*. *Soc*., *Chem*. *Comm*. **1974**, *123*. (c) Brown. R. F. C. *Recl*. *Trav*. *Chim*. *Pays-Bas* ***1988****, 107*, 655.

[18] (a) Scott, L. T.; Hashemi, M. M.; Bratcher, M. S. *J*. *Am*. *Chem*. *Soc*, **1992***, 114*, 1920. (b) Scott, L. T.; Cheng, P.-C.; Hashemi, M. M.; Bratcher, M. S.; Meyer, D. T.; Warren, H. B. *J*. *Am*. *Chem*. *Soc*. **1997**, *119*, 10963.

[19] Borchardt, A.; Fuchicello, A.; Kilway, K. V.; Baldridge, K. K.; Siegel, J. S. *J*. *Am*. *Chem*. *Soc*. **1992**, *114*, 1921.

[20] Harruff, L. G.;, Krymowski, J.; Peterson, J.; Boekhelheide, V. *J*. *Am*. *Chem*. *Soc*. **1978**, *100*, 2892.

[21] Liu, C. Z.; Rabideu, P. W. *Tetrahedron Lett*. **1996**, *37*, 3437.

[22] Preda, D. V. Ph. D. Dissertation, Boston College, Chesnut Hill, MA, 2001.

[23] Zimmermann, G.; Nuechter, T.; Hagen, S.; Nuechter, M. *Tetrahedron Lett*. **1994**, *35*, 4747.

[24] Mehta, G.; Panda, G. *Tetrahedron Lett*. **1997**, *38*, 2145.

[25] Knölker, H.-J.; Braier, A.; Bröcher, D. J.; Jones, P. G.; Piotrowski, H. *Tetrahedron Lett*. **1997**, *38*, 2145.

[26] Reisch, H. A.; Bratcher, M. S.; Scott, L. T. *Org*. *Lett*. **2000**, *2*, 1427.

[27] Wu, Y.-T.; Siegel, J. S. *Chem*. *Rev*. **2006**, *106*, 4843.

[28] Seiders, T. J.; Baldridge, K. K.; Siegel, J. S. *J*. *Am*. *Chem*. *Soc*. **1996**, *118*, 2754.

[29] Seiders, T. J.; Elliot, E. L.; Grube, G. H.; Siegel, J. S. *J*. *Am*. *Chem*. *Soc*. **1999**, *121*, 7804.

[30] Sygula, A.; Rabideau, P. W. *J*. *Am*. *Chem*. *Soc*. **1999**, *121*, 7800.

[31] (a) Sygula, A.; Rabideau, P. W. *J*. *Am*. *Chem*. *Soc*. **2000**, *122*, 6323. (b) Xu, G.; Sygula, A.; Marcinow, Z.; Rabideau, P. W. *Tetrahedron Lett*. **2000**, *41*, 9931. (c) Sygula, A.; Xu, G.; Marcinow, Z.; Rabideau, P. W. *Tetrahedron* **2001**, *57*, 3637.

[32] Sygula, A.; Karlen, S. D.; Sygula, R.; Rabideau, P. W. *Org*. *Lett*. **2002**, *4*, 3135.

[33] (a) Yamamoto, T; Wakabyashi, S.; Osakada, K. J. *J*. *Organomet*. *Chem*. **1992**, *428*, 223. (b) Stanger, A.; Schachter, A; Boese, R. *Tetrahedron* **1998**, *54*, 1207.

[34] Maag, R. Diplomarbeit, University of Zürich, 2006.

[35] Marcinow, Z.; Grove, D. I.; Rabideu, P. W. *J. Org. Chem.* **2002**, *67*, 3537.

[36] Wu, Y.-T.; Hayama, T.; Linden, T.; Baldridge, K. K.; Siegel, J. S. *J. Am. Chem. Soc.* **2006**, *128*, 6870.

[37] Alekseyev, N. I.; Dyuzhev, G. A. *Carbon* **2003**, *41*, 1343.

[38] (a) Howard, J. B.; McKinnon, J. T.; Makarovsky, Y.; Lafleur, A. L.; Johnson, M. E. *Nature* **1991**, *352*, 139. (b) Goel, A.; Howard, J. B. *Carbon* **2003**, *41*, 1949.

[39] (a) Boorum, M. M.; Vasil'ev, Y. V.; Drewello, T.; Scott, L. T. *Science* **2001**, *294*, 828. (b) Scott, L. T.; Boorum, M. M.; McMahon, B. J.; Hagen, S.; Mack, J.; Blank, J.; Wegner, H.; de Meijer, A. *Science* **2002**, *295*, 1500.

[40] (a) Hanson, J. C.; Nordman, C. E. *Acta. Crystallogr., Sect. B* **1976**, *B32*, 1147. (b) Sevryugina, Y.; Rogachev, A. Y.; Jackson, E. A.; Scott, L. T.; Petrukhina, M. A. *J. Org. Chem.* **2006**, *71*, 6615.

[41] Fedurco, M.; Olmstead, M. M.; Fawcett, W. R. *Inorg. Chem.* **1995**, *34*, 390.

[42] (a) Haddon, R. C.; Scott, L. T. *Pure Appl. Chem.* **1986**, *58*, 137. (b) Haddon, R. C. *Acc. Chem. Res.* **1988**, *21*, 243. (c) Haddon, R. C. *J. Am. Chem. Soc.* **1990**, *112*, 3385. (d) Haddon, R. C. *Science* **1993**, *261*, 1545.

[43] Seiders, T. J.; Baldridge, K. K.; Siegel, J. S. *J. Am Che, Soc.* **2001**, *123*, 1920.

[44] (a) Seiders, T. J.; Baldridge, K. K.; Siegel, J. S.; Gleiter, R. *Tetrahedron Lett.* **2000**, *41*, 4519.

[45] Ayalon, A.; Rabinovitz, M.; Cheng, P.; Scott, L. T. *Angew. Chem. Int. Ed. Engl.* **1992**, *31*, 1636.

[46] (a) Ayalon, A.; Sygula, A.; Cheng, P.; Rabinovitz, M.; Rabideau, P. W.; Scott, L. T. *Science* **1994**, *265*, 1065. (b) Becker, H.; Javahery, G.; Petrie, S.; Cheng, P.; Schwarz, H.; Scott, L. T.; Bohme, D. K. *J. Am. Chem. Soc.* **1993**, *115*, 11636.

[47] (a) Verdieck, J. F.; Jankowski, W. A. *Mol. Lumin. Int. Conf.* **1969**, 829. (b) Dey, J.; Will, A. Y.; Agbaria, R. A.; Rabideu, P. W., Abdourazak, A. H.; Sygula, R., Warner, I. M. J. *J. Fluoresc.* **1997**, *7*, 231.

[48] (a) Pandey, S., Acree, W.E. Jr., Fetzer,, J. C. *Phy. Chem. Liq.* **1999**, *37*, 565. (b) Tucker, S. A.; Bates, H. C., Acree, W. E., Jr.; Fetzer, J. C. *Appl. Spectrosc.* **1993**, *47*, 715.

Chapter 2.

Properties of Multiethynyl Substituted Corannulene Derivatives

2.1. Introduction

The effect of substituents on a polyaromatic hydrocarbon nucleus has been extensively studied. In particular, investigation of such effects on the photophysical and solid-state properties has led to some applications.[1]

Corannulene is only a modest fluorophore,[2] despite its similar dimension to pyrene, which is an extremely good fluorophore that has been used in several applications.[3] The effect of substitution on the properties of corannulene has only been investigated in a few cases, some of which are monoarylethynyl-substituted. These substituents cause a remarkable red shift in the UV spectrum and an increased fluorescence quantum yield. These results have generated interest not only in the academic environment, but also in industry, and a few patents on corannulene-based materials have been recently filed.[4]

Corannulene packs in a non-columnar mode in the solid state and so do some of its derivatives.[5] Multi-substituted corannulene derivatives are mostly prepared from the corresponding halogenated compounds by means of metal-catalyzed coupling reactions. The focus of this chapter is the study of the effect that arylethynyl substituents have on corannulene. In particular: 1) effects on the crystal packing; and 2) the photophysical behavior in solution.

2.1.1. Halogenated corannulene derivatives.

In the previous chapter we have seen that substituted corannulene derivatives can be prepared by building up the corannulene core using the appropriately substituted reagents. In this chapter, the use of halogenated corannulene derivatives (Figure 2.1) will be the basis for the preparation of different compounds.

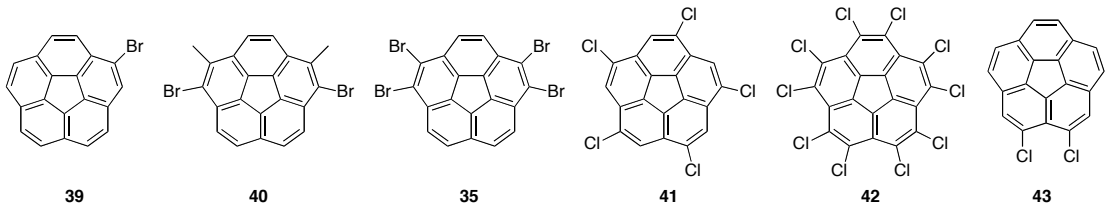

Figure 2.1. Common halogenated corannulene derivatives.

Compound **39** can be synthesized by a monohalogenation (Scheme 2.1) of the parent compound corannulene **1** with bromine.[6] In contrast to **39**, compound **40** is

prepared from a synthetic route that begins with **29**. Derivative **29** is halogenated with NBS to give intermediate **30**, which is then subjected to conditions developed by Maag, analogous to Rabideau's[7] ring closing, to yield **40** (Scheme 2.2).

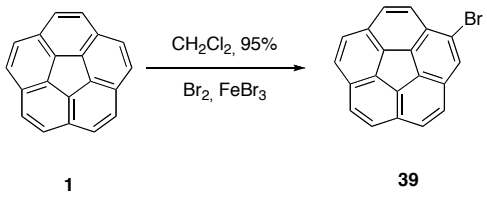

Scheme 2.1. Synthesis of 39.

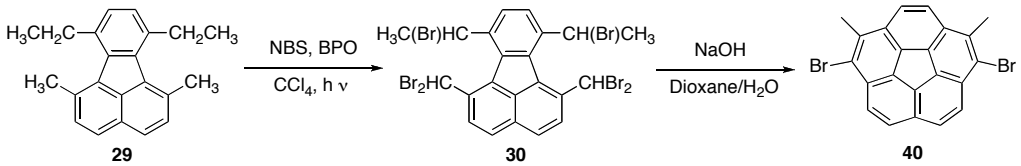

Scheme 2.2. Synthesis of 40.

Compound **43** (Figure 1.2) was prepared by starting from acenaphtalene and building the corannulene core.[8] Compound **35** is an intermediate in the synthesis of corannulene, and the synthetic procedure is reported in Chapter 1 (Scheme 1.8). *Sym*-pentachlorocorannulene **41**, is prepared by halogenation of **1** with ICl by a procedure reported by Scott.[9,6a] In this reaction, one of the hub carbons of **1** likely reacts with the iodine in the ICl molecule. This step is followed by addition of the Cl^- on the *rim* carbon and subsequent rearomatization to give the target compound (Scheme 2.3).

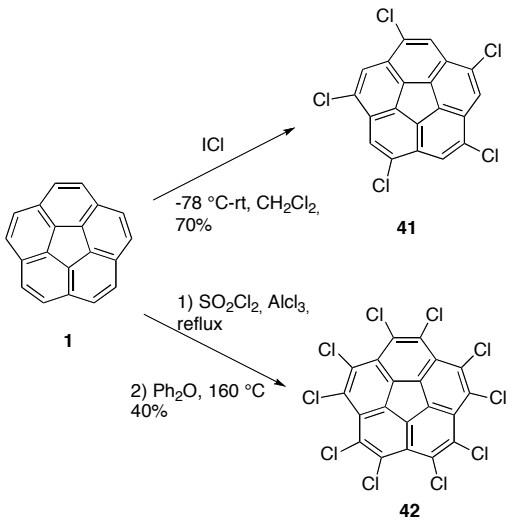

Scheme 2.3. Synthesis of 41 and 42.

Decachlorocorannulene is prepared from corannulene by the procedure reported by Scott.[10] In particular harsh conditions, **1** is first converted to tetradecachlorannulene and then, by heating in Ph_2O, it rearomatizes, losing Cl^- to afford **42**.[11]

2.1.2. Synthesis of alkyl- and aryl- monosubstituted corannulene derivatives.

Monosubstituted corannulene derivatives are readily available by means of coupling reactions between **39** and several reagents. In particular, methylcorannulene has been prepared from **39** by reaction with trimethylaluminium[8] or methylmagnesium bromide[12] in the presence of catalytic amounts of Ni(0). Reactions of **39** with alkyllithium reagents such as *i*-PrLi, *t*-BuLi and BnLi, gives the corresponding alkyl-1,2-dehydrocorannulene; after treatment with Pd/C, monosubstituted compounds of the type **46** are obtained.[13]

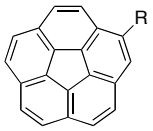

45-49

Table 2.1. Synthesis of monosubstituted corannulene derivatives.

Entry	Product	R	Method	Yield (%)	ref
1	**45**	CH_3	$AlMe_3$, cat. $NiCl_2$(dppp), DME	90	13
2	**45**	CH_3	MeMgBr, cat. $NiCl_2$(dppp), THF	63	14
3	**46**	Alkyl	1) RLi, 2) Pd/C	low	15
4	**47**	$C(CH_3)_2OH$	1) *n*-BuLi, 2) Acetone	40	16
5	**48**	Ar	ArZnCl, cat. $NiCl_2$(dppp), THF	-	17
6	**49**	R—≡—§	R^1—≡—H , cat $PdCl_2(PPh_3)_2$, CuI, Et_3N	67-97	30

Treatment of **39** with *n*-BuLi, followed by quenching with acetone, provides **47**.[14] Arylcorannulne derivatives are synthesized from **39** by a reaction with an arylzinc reagent in the presence of a Ni(0) catalyst to give compounds of type **48**.[15] Compounds of the **49** series (with substituent R = H, TMS, Ph, C_6F_5, **1**) are prepared

by means of a Sonogashira-type[16] coupling reaction, between **39** and the corresponding trimethylsilylacetylene or arylacetylene in the presence of catalytic Pd(0).[30]

2.1.3. Synthesis of tetrasubstituted corannulene derivatives.

The synthesis of tetrasubstituted derivatives of **1** (Scheme 2.4) is performed starting from **35** by means of various coupling reactions. Compound **50** was prepared by the reaction of **35** with trimethylsilylacetylene under Sonogashira-type conditions,[17] while **51** was instead obtained by a coupling with trimethylaluminium in the presence of a Ni(0) catalyst.[17]

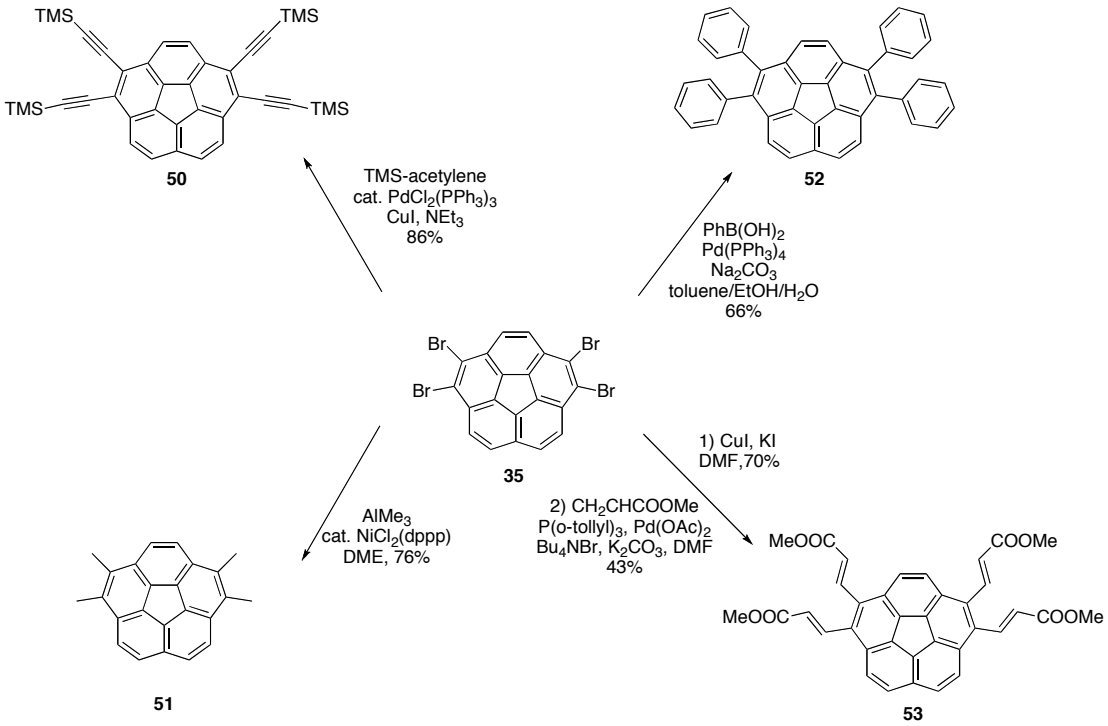

Scheme 2.4. Synthesis of some tetrasubstituted corannulene derivatives.

Compound **52** results from the conversion of **35** with the corresponding boronic acid by means of a Suzuki-type coupling reaction[18].[17] The bromide **35** was first converted to the tetraiodide and then to the tetrakis[(methylcarboxy)ethenyl]corannulene **53**[19] by Heck-type coupling conditions.[20]

2.1.4. Synthesis of *sym*-penta- and decasubstituted corannulene derivatives.

Sym-pentachlorocorannulene (**41**) can be converted to several under various reaction conditions (Table 2.2).[21,8] Reaction with trialkylamuminium derivatives in the presence of a Ni(0) catalyst gives compounds **54**–**56**.[8] Negishi-type coupling in the presence of a Ni(0) catalyst with the corresponding arylzinc chloride give compounds of the series **57**–**61**.[21] Recently, Hayama[22] improved the conditions for these type of coupling with sterically-hindered arylzinc chlorides by using a Nolan-type catalyst.[23]

Table 2.2. Synthesis of *sym*-pentasubstituted corannulene derivatives.

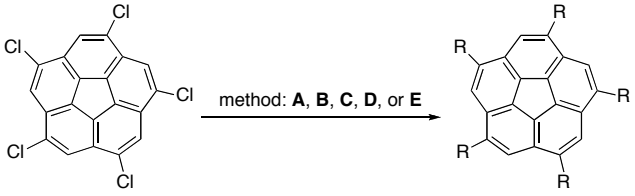

41 **54-66**

A: AlR_3, $Ni(Cl)_2(dppp)$, DME
B: ArZnCl, $Ni(Cl)_2(dppp)$, THF
C: TMSA, Cs_2CO_3, $ZnCl_2$, 160-170 °C, 4d
D: RSH, NaH, DMEU, 120 °C, 1d
E: ROH, NaH, 180 °C, 2d

Entry	Compound	R	Method	Yield (%)	Ref.
1	**54**	CH_3	A	33	21
2	**55**	C_2H_5	A	51	21
3	**56**	C_8H_{17}	A	31	21
4	**57**	Ph	B	49	21
5	**58**	(*n*-octyl)Ph	B	31	21
6	**59**	(2-methyl)Ph	B	28	21
7	**60**	1-Naph	B	38	21
8	**61**	Manisyl[a]	B	7	21
9	**62**	TMS—≡—§	C	53	21
10	**63**	SPh	D	38	21
11	**64**	Ph-S-Ph	D	13	21
12	**65**	SC_2H_5	D	14	21
13	**66**	$(CH_2)_2O(CH_2)_2OCH_3$	E	41	21

[a] Manisyl = (2,6-dimetoxy-4-methyl)phenyl

Sym-pentakis(trimethylsilylethynyl)corannulene **62** is synthesized from **41** by Eberhard's procedure, which involves the use of a pincer Pd(II) catalyst.[24] Thioaryl- and thioalkyl derivatives can be prepared by nucleophilic aromatic substitution. This method was first introduced by Scott for the preparation of *sym*-pentakis(4-methoxyphenylthio)-corannulene and *sym*-pentakis(2-naphtylthio)corannulene.[25] Siegel applied the same method, but with longer reaction times to prepare compounds **63**–**65**.[21] Nucleophilic substitution with alkoxides requires harsher conditions, and compound **66** was prepared by running the reaction at 180 °C for 2 days.[21]

The synthesis of decasubstituted derivatives (Scheme 2.5) starts from **42**. Coupling with trimethylaluminium in the presence of a Ni(0) catalyst yields **67**.[8] Nucleophilic aromatic substitution was used by Scott[25] for the preparation of decaalkylthiocorannulenes of the type **68** (with R = $-SC_3H_7$, $-SC_6H_{13}$ and $-SC_{12}H_{13}$). Reaction with benzene1,2-dithiol gave **69**, which was prepared as a model for possible host-guest complexes with C_{60}.

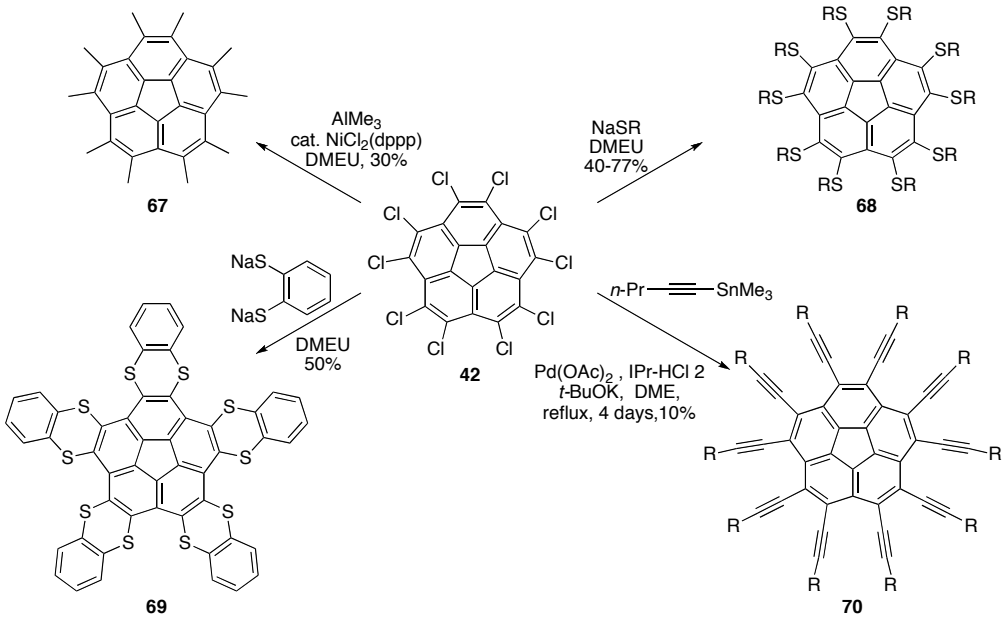

Scheme 2.5. Synthesis of decasubstituted corannulene derivatives.

Hayama reported the preparation of **70** by a coupling between **42** and a tin-acetylide,[26] which applied the procedure reported by Wu[27] for the synthesis of 2,3-diethynylcorannulene derivatives. Derivative **70** a potential precursor for the preparation of a carbon nanotube end-cap *via* solution-phase synthesis.[26]

2.1.5. Photophysical properties of known substituted corannulene derivatives.

Grube et al. reported the synthesis of compounds **54–66**.[21] The properties of these compounds in solution were investigated. The alkyl derivatives **54–56** display a small red shift (9-10 nm) of the π-π* absorption band in the UV-vis spectra, similar to that observed in alkyl-substituted benzene derivatives (Table 2.3).[28]

Table 2.3. Photophysical properties of *sym*-pentaalkyl-and pentaarylcorannulene derivatives[a]

Entry	Compound	λ_{abs} (nm)	λ_{em} (nm)	λ_{exc} (nm)
1	**1**	251	421	247, 286
2	**54**	295	431	261, 297
3	**55**	297	431	262, 298
4	**56**	298	433	263, 299
5	**57**	319	447	286, 321
6	**58**	324	452	291, 326
7	**59**	308	440	273, 308
8	**60**	311	445	321
9	**61**	305	439	262, 310
10	**62**	337, 366*sh*	474	337
11	**63**	349	-	-
12	**64**	356	508	254, 296, 357
13	**65**	337	-	-
14	**66**	308	433	274

[a] Measurement in acenonitrile

This red shift suggests a slight increase in electron density on the aromatic system. Compound **19** has a substantial red shift (31 nm) compared to corannulene, suggesting conjugation between the corannulene core and the phenyl substituents. As the steric size of the *ortho* aryl groups increases, a decreasing red shift is observed for the series (**61 < 59 < 60**), likely due to the aryl substituents twisting out of plane and a consequent partial loss of conjugation. A large red shift in the π-π* absorption for **66** is correlated with the stronger π-donating power of the alkoxy, over the alkyl

substituents. Compounds **63–65** display a substantial red shift in the π-π* absorption compared to **1**, a clear effect of the sulfur substitution.[29] Emission spectra show a red shift of 10 nm in the alkyl series with respect to corannulene. More pronounced is the red shift observed for the aromatic substituted derivatives (18-30 nm), similar in range to the shift caused by the alkoxy sustituent in **66**. The derivative **62** shows an emission maximum at 474 nm due to the extension of the core π conjugation with the alkynyl units. Perhaps surprising is the emission maximum for **13**, occuring at 508 nm probably due also to an even more extended π core. In general, the Stokes' shifts are in the order of 130-150 nm. Overall, we can say that alkyl and aromatic substitutions affect the properties of corannulene by a red shift both in absorption and emission spectra (Table 2.3).

The study of monoarylethynyl-substituted corannulene derivatives (Table 2.4) was reported in 2004.[30] These compounds proved to be considerably more fluorescent than **1**. This relates to the extended π-conjugation. A more careful investigation of the photophysical properties of these compounds allows for some considerations: the π-π* transitions are red-shifted with respect to parent compound **1** (285 nm), around 10 nm for **49**-(TMS, H, Ph) and 15 nm for **49**-C_6F_5 and **49**-(**1**). Even in this case, this effect is believed to arise from the extended conjugation of the corannulene π-framework. Changing the R substituent results in an increased red-shift going from H < TMS < Ph < C_6F_5 < **1**.

In the emission spectra of compounds of the **49** series, the emission maxima are essentially the same as for parent compound **1** (417, 432 nm) for compounds **49**(TMS)-**49**(C_6F_5) and slightly red-shifted for **49**-(**1**) (418 and 443 nm). This suggests a change in geometry upon electronic excitation, similar to what has been observed for **1**.[2b] In **49**-(**1**). The increased red shift is also considered a consequence of an enhanced conjugated network. Stokes' shifts are on the order of 140 nm and comparable with those reported for *sym*-pentasubstituted derivatives (Table 2.4).

Table 2.4. Photophysical properties of a series of arylethynyl- substituted corannulene derivatives [a]

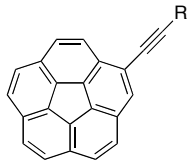

49

R = H, TMS, Ph, C_6F_5, **1**

Entry	R	λ_{abs}[logε] (nm)	λ_{em} (nm)	ϕ_F
1	TMS	256[4.8], 295[4.7]	407^{Sh}, 425	0.14
2	H	261[4.9], 295[4.6]	409^{Sh}, 426	0.08
3	Ph	254[4.6], 297[4.7]	409, 429	0.31
4	C_6F_5	255[4.5], 300[4.7]	411^{Sh}, 431	0.26
5	Corannulene	249[4.3], 302[4.2]	418, 443	0.57

[a] (measurement in cyclohexane, ϕ_F relative to 9,10- DPA)

Recently Mack[31] reported the synthesis and properties of 1,2- and 1,4-di(ethynylcorannulenyl)benzene derivatives. The synthesis was performed starting from bromocorannulene **39**, which, after conversion to ethynylcorannulene, was coupled by standard Sonogashira conditions to 1,2- and 1,4-dibromobenzene to give **71** and **72** (Figure 3.3).

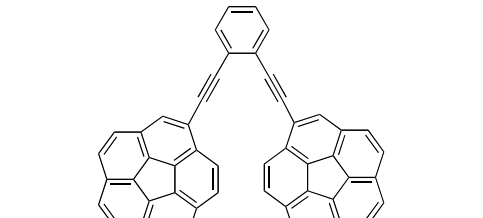

71

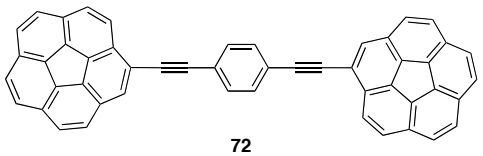

72

Figure 2.2. Structure of benzene-substituted corannulene derivatives.

These compounds were designed with the aim that extended conjugation between corannulene moieties would provide new materials with enhanced luminescent

properties (Table 2.5). Compound **71** displays two maxima at 254 and 299 nm and a long tail that trails into the visible region. Derivative **72** has maxima at 250, 302, and 371 nm and a tail into the visible region. DFT and TD-DFT calculations were performed on the geometric and absorption properties of this molecule to understand the spectra. The calculations provide a comparison between theory and experimental values. In **71**, the outer *rim* of each corannulene moiety is placed over the interior of the other one and each corannulene is twisted with respect to benzene ring. In **72**, the structure is calculated to be planar, and the corannulene moieties are only slightly twisted with respect to the benzene ring. For **1** and **71**, the agreement is high (within 10 nm); for **71**, a transition is predicted at 293 nm but observed at 299 nm. In the same compound, the HOMO-LUMO transition is predicted at 425 nm, but observed at 360 nm. This is believed to be due to the fact that the intramolecular interactions are not accounted at the level of theory used. For **72**, the calculated values at 244, 303, and 401 nm correlate with the experimental ones. The emission spectrum of this molecule has essentially the same maxima observed for corannulene, but different intensities. When excited at 300 nm, the ϕ_F are 0.08 for **71** and 0.60 for **72**. Excitation at 400 nm gives high fluorescence intensity for **72** but not for **71**. The viability of these molecules as blue emitters was tested by irradiation of a solution with a 405 nm laser beam: **71** displays soft blue fluorescence while **72** shows bright fluorescence as reported in this work.

Table 2.5. Photophysycal properties of 1,2- and 1,4-di(ethynylcorannulenyl)benzene derivatives[a]

Entry	Compound	λ_{abs}[logε] (nm)	λ_{abs}[calc] (nm)	λ_{em} (nm)	ϕ_F
1	**1**	254(4.8), 289(4.5)	254, 283	420, 440	-
2	**71**	254(4.5), 299(4.3)	293	420, 440	0.08
3	**72**	250(4.6), 302(4.5), 371(4.4)	303, 401	420, 440	0.60

[a] Measurement in dichloromethane; [b] calculation at the level of theory B3LYP-6-31G*.

2.2. Present Work[32]

In this section, the synthesis and properties of multi-ethynyl corannulene derivatives will be discussed. Particular emphasis will be given to the effect that aryl-ethynylsubstitution on the corannulene core exerts on its photophysics in solution and in the solid state. Computational DFT calculations will also be presented and help explaining the properties of this class of compounds.

2.2.1. Synthesis of multi-ethynyl substituted corannulene derivatives.

In 2006, Wu introduced the use of tin acetilyde compound for the preparation of 2,3-diethynyl-substituted corannulene derivatives for the first time (this methodology is derived from a modified Nolan protocol[27]). These reaction conditions were applied by Yao-Ting Wu for the preparation of the compounds herein studied (Figure 2.3).

The diethynylcorannulenes **73**-R_2 and the tetraethynylcorannulenes **74**-R_4 were synthesized by Sonogashira coupling reactions.[16] Reaction of 1,6-dibromo-2,5-dimethylcorannulene (**40**) or 1,2,5,6-tetrabromocorannulene (**45**) with the desired terminal alkyne afforded products in good yields (Scheme 2.6, Table 2.6).

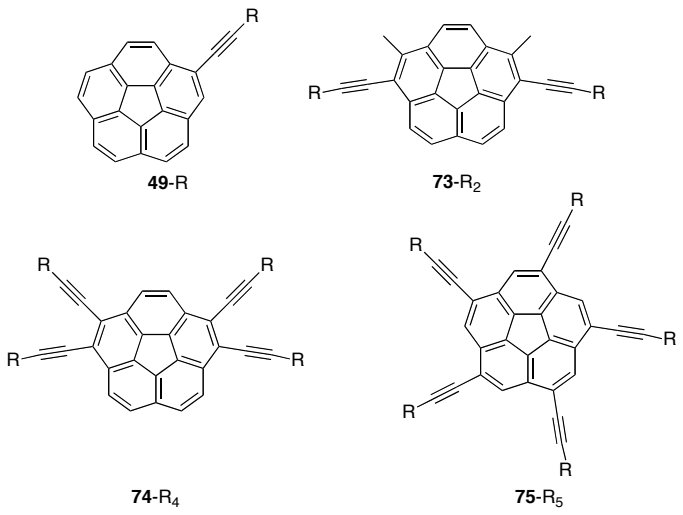

Figure 2.3. General structures of the derivatives studied in this work.

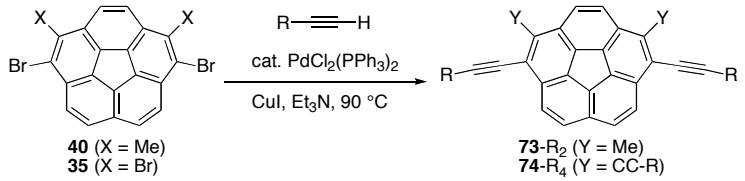

Scheme 2.6. Synthesis of di- and tetraalkynylcorannulenes.

A modification of the Nolan's protocol[27] was applied to the synthesis of compounds in the **75**-R_5 series. Reaction of 1,3,5,7,9-pentachlorocorannulene (**41**) with various trimethyltin alkynes afforded the desired product in reasonable to good yields (Scheme 2.7, Table 2.6). The starting material (**41**) is sparingly soluble in the reaction solvent but, after the first coupling partners associate, the solubility of the intermediates increase, enhancing the efficiency of the subsequent coupling reaction.

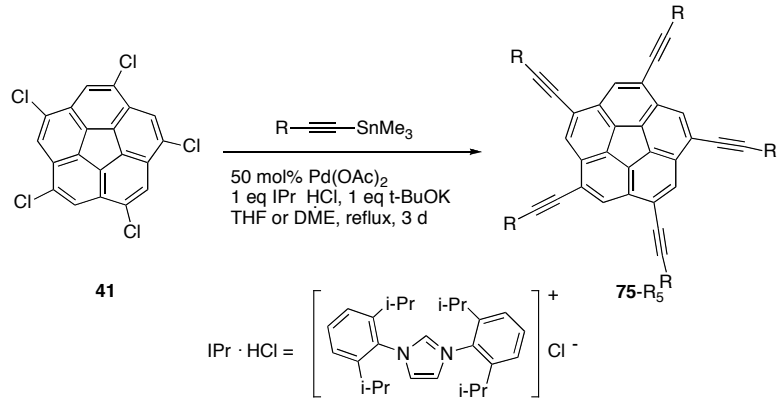

Scheme 2.7. Synthesis of pentaethynyl corannulene derivatives.

Table 2.6. Synthesis of compounds of the classes 73, 74 and 75.

Entry	Halide	R	Product	Yield (%)
1	**40**	$SiMe_3$	**73**-TMS_2	79
2	**40**	Ph	**73**-Ph_2	92
3	**35**	$SiMe_3$	**74**-TMS_4 (**50**)	85
4	**35**	Ph	**74**-Ph_4	86
5	**35**	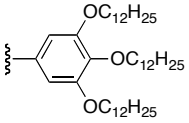	**74**-$Ar(a)_4$	83
6	**35**	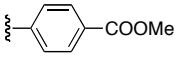	**74**-$Ar(b)_4$	55
7	**35**	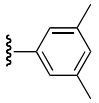	**74**-$Ar(c)_4$	82
8	**35**	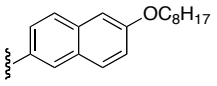	**74**-$Ar(d)_4$	91

9	**35**	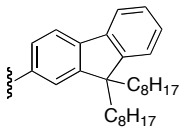	**74**-Ar(e)$_4$	85
10	**41**	$SiMe_3$	**75**-TMS_5 (**62**)	47
11	**41**	Ph	**75**-Ph_5	45
12	**41**	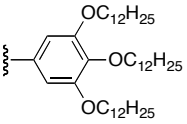	**75**-Ar(a)$_5$	71
13	**41**	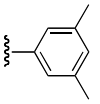	**75**-Ar(c)$_5$	57
14	**41**	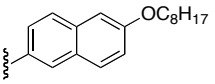	**75**-Ar(d)$_5$	93
15	**41**	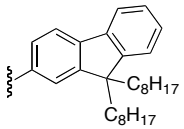	**75**-Ar(e)$_5$	76
16	**41**	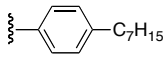	**75**-Ar(f)$_5$	91
17	**41**	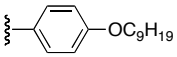	**75**-Ar(g)$_5$	87

2.2.2. X-Ray structures of 73-Ph_2, 74-Ar(c)$_4$ and 75-Ar(c)$_5$.

X-ray quality crystals of **73**-Ph_2, **74**-Ar(c)$_4$ and **75**-Ar(c)$_5$ were obtained and their structures were determined as representative of their corresponding classes. All of these compounds show the characteristic bowl structure of corannulene and an internal geometry consistent with their constituent structure (Table 2.7). An interesting part of these structures is their stacking order. All three compound classes adopt an essentially columnar packing motif along a stacking axis. This property is unobserved in simple corannulene derivatives, except for 1,2,5,6-tetrabromocorannulene (**35**), which crystallizes in a polar orthorhombic space group *Pna*2$_1$. Compound **35** forms columns of perfectly stacked bowls (the normal to the plane of the hub ring is collinear with the stacking axis).[33] In general, this type of unidirectional columnar packing is observed in large, non-planar polycyclic compounds, such as circumtrindene ($C_{36}H_{12}$),[34] hemibuckminsterfullerene ($C_{30}H_{12}$),[35] diindeno[1,2,3,4-defg,1',2',3',4'-mnop]chrysene ($C_{26}H_{12}$),[36] semibuckinsterfullerene ($C_{30}H_{12}$),[37] and sumanene.[38]

A crystal of **73**-Ph_2 was obtained by slow evaporation of a CH_2Cl_2/MeOH solvent mixture at room temperature (Figure 2.5, Table 2.7). The structure was solved in a polar orthorhombic space group *Pca*2$_1$, but here the translational element along the *c* axis moves two steps along the column. Hub rings of each molecular pair are oriented

in opposite direction with respect to their centroids. The bowls have the same directions along the stack but are slightly tilted with respect to the stacking axis of 12.2° (i.e. the normal to the hub plane respect the *c* axis). Neighboring columnar stacks have the same bowl orientation.

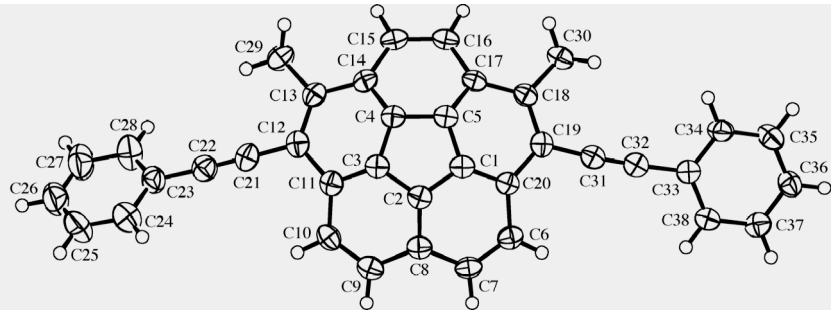

Figure 2.4. Crystal structure of 73-Ph_2.

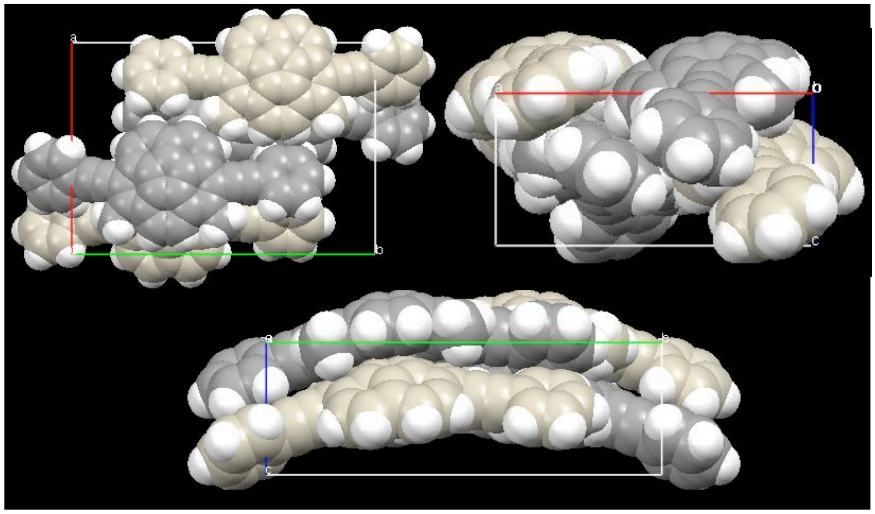

Figure 2.5. Crystal packing of 73-Ph_2 along the (bottom) *c*, (top right) *b* and (bottom) *a* axes.

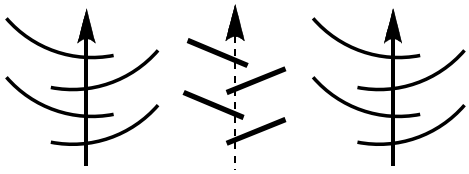

Figure 2.6. Orientation of the corannulenyl units and adjacent arylethynyl arms in the stacking of 73-Ph_2. Arrows define the stacking axes (bold for foreground, dashed for background). Curves represent corannulene, and bars represent arylalkynyl arms.

The molecular order in the *ab* plane places the body of one molecule next to the arm of the adjacent one and the arylalkynyl units adopt a conformation that optimizes arene–arene T interactions (Figure 2.5, Figure 2.6).

74-Ph_4 and **75**-Ph_5 are only sparingly soluble in most organic solvents and this hampered the growth of suitable crystals. Therefore, more soluble compounds were prepared, in particular **74**-Ar(c)$_4$ and **75**-Ar(c)$_5$, which both have short side chains on the phenyl rings. Crystals were grown by slow evaporation of a CH_2Cl_2/$CHCl_3$/MeOH mixture at room temperature. The diffraction data for these compound were recorded at 273 and 260 K respectively, because at lower temperatures the crystals cracked.

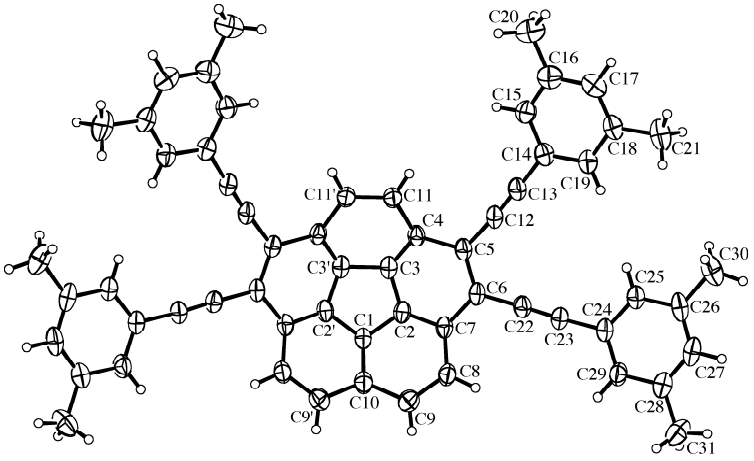

Figure 2.7. Crystal structure of 74-Ar(c)$_4$.

The structure of **74**-Ar(c)$_4$ (Figure 2.7) was solved in the space group *Pnma* with one molecule sitting on a special position of crystallographic C_s symmetry. During the structure solution modeling, it was found that the unit cell contained two voids, each having a volume of 173 Å^3. Different Fourier maps revealed four unconnected peaks distributed on and about a mirror plane within each void. It was assumed that the voids represented water molecules. The formula was $C_{60}H_{42}\cdot 1.5H_2O$. Attempts were made to include the water molecules in the model, but without success. The contribution of the solvent molecules to the intensity data was removed using the SQUEEZE[39] routine of the PLATON[40] program.

The modeled structure for **74**-Ar(c)$_4$ (Figure 2.8, Table 2.7) shows that translation along the *a* axis coincides with moving two steps along the column of stacked bowls. The hub rings in each molecular pair are oriented in opposite

directions about their centroids. Along the stack, the bowl direction is the same and the hub planes are slightly tilted (4.8° with the *a* axis) with respect to the stacking axis. Neighboring columnar stacks along the *c* axis have the same direction; adjacent columns define (along the *c* axis) a columnar channel hosting the solvent molecule. A layer is defined along the *ac* plane by these columnar stacks and the bowl direction in neighboring planes is antiparallel (Figure 2.8).

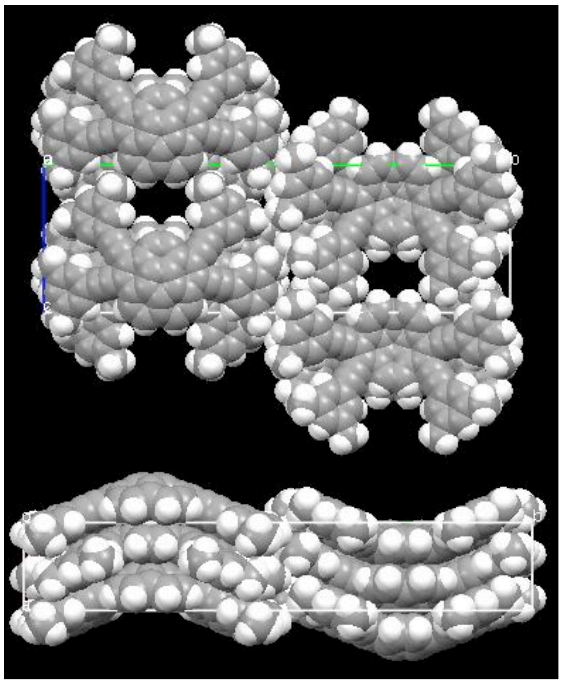

Figure 2.8. Crystal structure of 74-Ar(c)$_4$ along the (top) *a* and (bottom) *c* axes.

The structure of **75**-Ar(c)$_5$ was solved in the monoclinic space group $P2_1/n$ (Figure 2.9, Table 2.7). Two molecules of **75**-Ar(c)$_5$ are present in the asymmetric unit, and each of them sit on a general position, because the C_5 molecular symmetry is incompatible with any space group. The achiral space group indicates that a racemic mixture of left- and right-handed bowls are present. Translation along the *b* axis coincides with moving two steps along the column of stacked bowls. The hub rings of each molecular pair are oriented about their centroids.

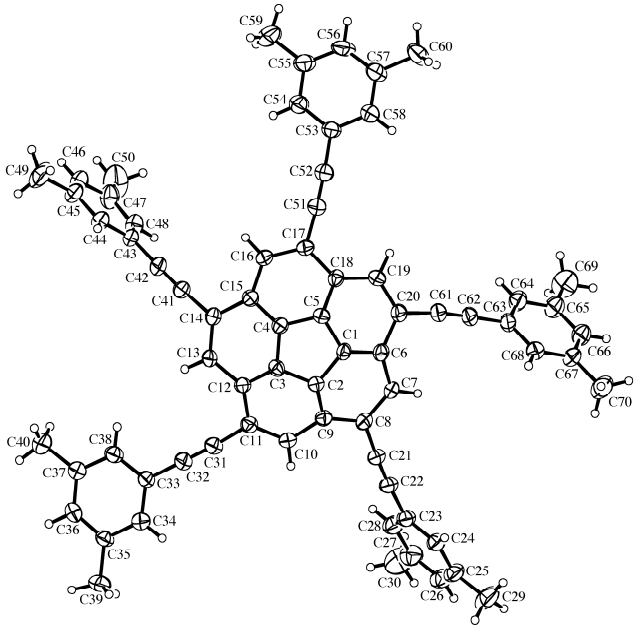

Figure 2.9. Crystal structure of 75-Ar(c)$_5$.

The pairs have the same handedness, and this combines with the opposite orientations of the hub rings to place their arms in a staggered relationship to one another. The bowl direction is the same along the column and the hub planes are slightly tilted with respect to the stacking axis (6.6° with respect to the *b* axis). Neighboring columnar stacks along the *a* axis have the same orientation, whereas they have antiparallel bowl directions along the *c* axis (Figure 2.10). These three structures show that it is possible to obtain columnar stacking in substituted corannulenes (Figure 2.11).

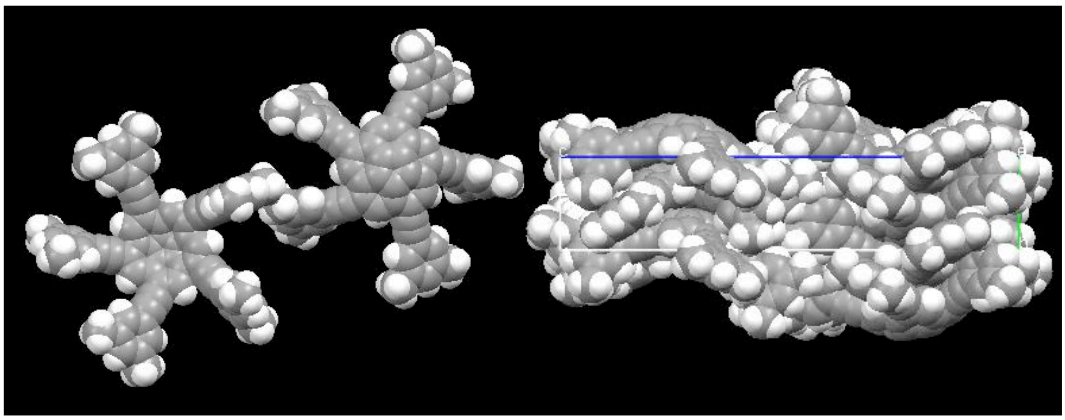

Figure 2.10. Crystal packing of 75-Ar(c)$_5$ (left) the two-molecule asymmetric unit, (right) view along the *c* axis.

Table 2.7. Crystal structure data for corannulene derivatives 73-Ph_2, 74-Ar(c)$_4$ and 75-Ar(c)$_5$[a]

	73-Ph_2	**74**-Ar(c)$_4$	**75**-Ar(c)$_5$
Formula	$C_{38}H_{22}$	$C_{60}H_{45}O_{1.5}$	$C_{70}H_{50}$
Molecular weight	478.59		
Solvent	CH_2Cl_2/MeOH	CH_2Cl_2/$CHCl_3$/MeOH	CH_2Cl_2/$CHCl_3$/MeOH
T (K)	160(1)	273(1)	260(1)
Crystal system	Orthorhombic	Orthorhombic	Monoclin
Space group	*Pca*2$_1$	*Pnma*	*P*2$_1$/*n*
Z	4	4	8
a (Å)	15.4564(6)	7.4846(5)	33.414.4(19
b (Å)	22.1901(1)	43.341(3)	7.8392(3)
c (Å)	7.4161(2)	13.684(1)	41.096(2)
b (deg)	90	90	109.8771(8)
V (Å^3)	2543.68(2)	4438.9(5)	10123.5(7)
Bowl depth (Å)	0.8467(7), **0.861[0.879]**	0.884(2), **0.848[0.888]**	0.936(5), **0.853[0.892]**
POAV$_{hub}$ angle	8.00(14), **8.1[8.3]**	8.2(3), **8.0[8.4]**	8.7(2), **8.0[8.4]**

[a]bold numbers for bowl depth and POAV$_{hub}$ angle are BL3LYP/cc-pVDZ and [MO6-2X/cc-pVDZ] calculated value respectively

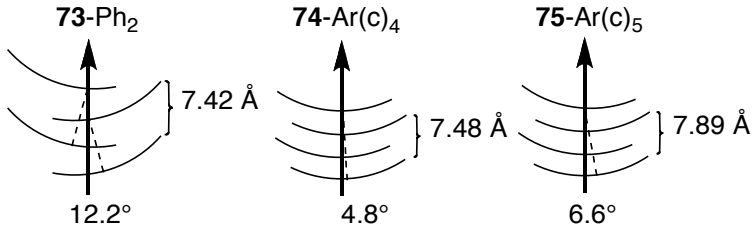

Figure 2.11. Comparison of the stacking order parameters for 73-Ph_2, 74-Ar(c)$_4$ and 75-Ar(c)$_5$. Arrows define the stacking axes, and curves represent corannulene fragments.

All three arylethynylcorannulenes **73**-Ph_2, **74**-Ar(c)$_4$ and **75**-Ar(c)$_5$ follow the standard geometry in their core fragments. Correlative trends involve the bowl depth and POAV$_{hub}$[41] angle. The bowl depth is positively correlated with the POAV$_{hub}$ angle, because the hub atoms are the principal sites of out-of-plane distortion. A comparison highlights bowl depth of 0.846(7), 0.884(8) and 0.936(5) Å, respectively for **73**-Ph_2, **74**-Ar(c)$_4$ and **75**-Ar(c)$_5$. The corresponding POAV$_{hub}$ angles are 8.00(14), 8.2(3), and 8.7(2)°, respectively. This trend suggests that *rim* substitution with an increasing number of arylalkynyl substituents correlates with an increase in the bowl depth. This

result is in constrast with the previously reported data, where it had been observed that alkyl *rim* substitution flattens the bowl and decreases the inversion barrier.[42] This consideration leads to the supposition that, in **75**-Ar(c)$_5$, the inversion barrier might be higher than in corannulene (11.5 kcal mol^{-1}).

This set of compounds have also been the object of quantum chemical calculations and these results are compared to the experimental data. The DFT calculations were performed on the set of compounds with the BL3LYP/cc-pVDZ and M06-2X/cc-pVDZ levels of theory. The results (Table 2.7) show a good agreement between experimental values and calculated ones and that only M06-2X could account for the increase in the bowl depth with respect to the increase in the number of alkynyl substituents although the calculated effect was less dramatic than that observed experimentally.

2.2.3. Photophysical properties.

Previously, the photophysical properties of compound **1**, **49**-TMS and **49**-Ph were investigated and these compounds were found to be modest fluorophores in cyclohexane solution.[30] The study of this new class of multiaryalkynyl derivatives (**73**, **74**, and **75**, Table 2.8) of corannulene will provide an in-depth analysis of the properties of these molecules.

For discussion purposes, this class of compounds is seen as having a central corannulene fragment and a perturbing substituent field. The principal subsymmetries of C_{5v} are a C_5 axis and five mirror planes (σ), each of which represents C_s symmetry. The symmetry perturbations due to arylalkyne substituents for **49**, **73**, **74**, and **75** are C_1, C_s, C_s, and C_5.

Compopund **1** is C_{5v} symmetric and has a quadruply degenerate HOMO (2 x E_1, 2 x E_2); the highest occupied orbital of A-Type is HOMO-4 (Figure 2.12). The principal transition involved is π-π^* with several cryptic transition because of the small extinction coefficients.

For molecules of the **75** class, where the C_5 symmetry allows for effective interaction between the substituent field and the A symmetry orbital of the corannulene core, the resulting A symmetry orbital (HOMO-4) represents an antibonding interaction.

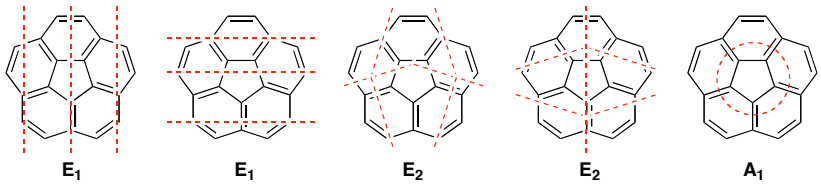

Figure 2.12. Nodal planes for the degenerate orbitals HOMO to HOMO-3, and for HOMO-4 orbital (A_2 symmetry) in 1.

The two sets of E-type orbitals remain degenerate, forming a complex HOMO-to-HOMO-3. Computations predict manifold π-to-π* transitions among degenerate HOMO and LUMO levels that have essentially no transition moment because of their symmetry. The first transition falls at 360 nm [358 nm, (log ε 5.0) exptl.]. As for benzene, frontier orbitals with mutually exclusive nodal structures lead to poor Frank-Condon factors for HOMO-LUMO transitions.

In the case of series **73** and **74** the resulting intersection between the C_s symmetry of the field and the C_{5v} of the core gives a C_s molecular symmetry. For **73**, the substituents at the 1 and 6 positions lie along the nodal planes of two of the E-type orbitals (Figure 2.13). A consequence of this substituent position is no core-to-field perturbation, and these orbitals remain essentially at their "non-interacting" energies. On the other hand, the other two E-type orbitals are well-suited spatially and symmetrically to interact with the field orbitals: HOMO and HOMO-1 are the resulting antibonding combinations of this core-to-field interaction. According to symmetry arguments, these four orbitals are energetically separated, but HOMO-2 and HOMO-3 are degenerate. The longest absorption wavelength (377 nm explt.) is predicted to be a strong HOMO-LUMO transition with calculated wavelengths at 368 and 396 nm (Table 2.8, depending on the method).

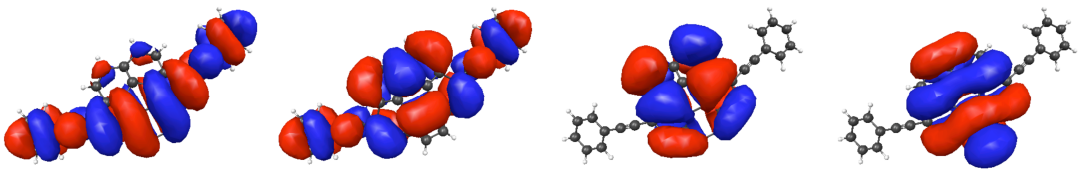

Figure 2.13. HOMO to HOMO-3 (left to right) for 73-Ph_2, HOMO and HOMO-1 represent core-to-field interactions, while HOMO-2 and HOMO-3 are effectively degenerate core orbitals.

In class **74**, the four substituents have a symmetry field similar to that of class **73**, although they present a different spatial distribution of orbital densities and phases. An interaction of the core with four E-type orbitals is possible, and results in HOMO to HOMO-3 antibonding core-to-field interactions (Figure 2.14). In contrast with compound **73**-Ph_2, these orbitals are energetically separated, practically and by symmetry arguments. The longest absorption wavelength (400 nm exptl.) is predicted as a HOMO-LUMO transition with calculated values at 363 and 393 nm (Table 2.8).

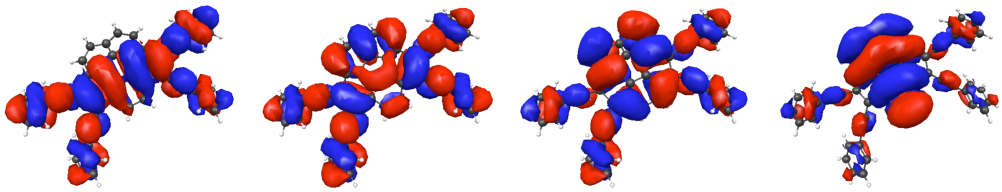

Figure 2.14. HOMO to HOMO-3 (left to right) for 74-Ph_4. All are core-to-field interactions.

The absorption at longer wavelengths for class **74**, respect to **71**, comes from a stronger interaction between filled-field and core orbitals (HOMO) and between unfilled-field and core orbitals (LUMO). Better antibonding and bonding interactions, between core and field lead to energetically higher HOMOs and energetically lower LUMOs respectively. In class **75**, the longer absorption wavelengths are seen computationally, but with nominal transition probabilities, which mirrors the cryptic nature observed experimentally. The first absorption wavelength (358 nm explt.) is a HOMO-LUMO manifold transition that lies computationally at 365 and 360 nm (Table 2.8).

This simplified model makes it possible to foresee a similarity between compounds of the class **73** and **74** with compounds like mono- and disubstituted fluorenes or biphenyls, compounds that are important in OLED materials.[43] In this view, the orbital structure and photophysical behavior of **76** relative to **77** serves as a good analogy to the relative behavior of **73**-Ph_2 *versus* **74**-Ph_4.[44] **73**-Ph_2, **74**-Ph_4, and **45** show a common orbital density and phase pattern (Figure 2.15). Do these compounds also have the same fluorescence behavior?

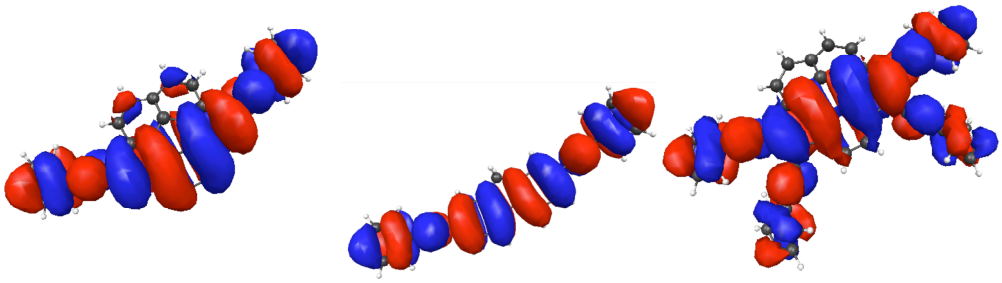

Figure 2.15. HOMOs of 73-Ph_2, 77 and 74-Ph_4 (left to right). All have common nodal number and structure.

Computations on the fluorescence of corannulene are ongoing, but some empirical observation can be made from the collected data (Table 2.8). In general, for the tetra- and pentasubstituted series, the compounds with more substituents display longer emission wavelengths (λ_F) for a given aryl type. The Stokes' shifts increase with the number of substituents on the corannulene core; this is possibly due to the fact that the emission for **75**-Ph_5 comes from the reverse HOMO-LUMO state, which is blocked to absorption by a poor transition moment. A geometric molecular change in the excited state could result in a better overlap between states.

Fluorescence lifetimes (τ_F) for the series **49**-Ph, **73**-Ph_2, **74**-Ph_4, and **75**-Ph_5, are of the order of 5–10 ns (in particular 6.6, 4.8, 10.3, and 10.5 ns) and are 10 times longer respect to **76** and **77**. The fluorescence quantum yields (ϕ_F) for the series **49**-Ph, **73**-Ph_2, **74**-Ph_4, and **75**-Ph_5 are 20, 75, 83 and 12%, respectively. The high quantum yields for **73**-Ph_2 and **74**-Ph_4 mirror the almost quantitative yield observed for **76** and **77**. **49**-Ph has instead a behavior that parallels more closely the behavior of 3-phenylethynylphenathroline, which presumably suffers quenching due to an activated and/or intersystem crossing. This observation is supported by preliminary low-temperature measurements on **49**-Ph, which display a low phosphorescence similar to that which has been observed for 3-phenylethynylphenanthroline.

Compound **75**-Ph_5 displays a surprisingly low quantum yield. There are conflicting reports in the literature regarding symmetry effects on quantum yield. Nizhegorodov[45] described an increase in quantum yield due to an increase in radiative states. The Ham[46] effect also accounts for the fact that higher symmetry leads to forbidden transitions between ground and excited states, as observed for benzene. Nakajima[47] and Dong[48] reported that vibrational, environmental, or substitutional

perturbation of the molecular symmetry allows for previously forbidden states, resulting in increased absorption and emission properties.

Table 2.8. Photophysical properties of multiethynyl-substituted corannulene derivatives.[a]

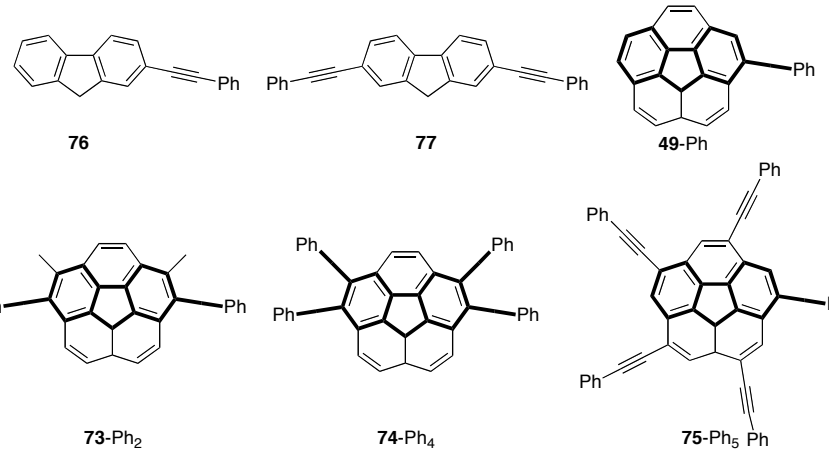

76 **77** **49**-Ph

73-Ph_2 **74**-Ph_4 **75**-Ph_5

entry	compound	λ_{abs}[nm] (log ε)	λ_{calc}[nm][b]	λ_F[nm]	ϕ_F[c]	τ_F (ns)
1	**1**	320^{sh}(4.0), 288(4.7), 254(5.0)		423	0.03	7.3
2	**49**-TMS	297(4.6)		435	0.07	8.0
3	**49**-Ph	400^{sh}, **363-345**(**4.1**), 298^{br}(4.7)	**340**, 313, 272 [**375**, 315,292]	434, 415	0.2	6.6
4	**40**	292(4.8), 259^{br}(5.0)		446, 426	0.03	7.8
5	**73**-TMS_2	416^{sh}(3.3), 371^{sh}(4.0), 320^{sh}(4.1), 307(4.6)		455, 442^{sh}	0.25	5.5
6	**73**-Ph_2	425^{sh}, **378**-**359**(**4.4**), 320^{sh}, 298(4.6)	**368**, 315, 275 [**396**, 347, 313]	469, 446	0.75	4.8
7	**74**-TMS_4	331(4.8)		475, 449,	0.17	11.1
8	**74**-Ph_4	450^{weak}, **400**^{sh}, **356**(**4.9**), 305(4.9), 288	**399**, **363**, 328,314,28 [429, **399**,**352**/**344**, 321, 285]	500, 473	0.83	10.3
9	**74**-Ar(a)$_4$	370(4.8)		529	0.67	7.9
10	**74**-Ar(b)$_4$	458^{sh}(3.8), 361(4.9), 332(4.9), 312^{sh}(4.9)		504, 476	0.58	9.1
11	**74**-Ar(d)$_4$	381(4.9), 361^{sh}(4.9), 319^{sh}(4.9)		506	0.71	6.5
12	**74**-Ar(e)$_4$	382(4.9), 331(4.9)		527, 501	0.73	6.0

13	**75**-TMS_5	339(4.7), 303(4.9)		468, 452	0.05	9.5
14	**75**-Ph_5	**358**(**5.0**), **324**(**5.0**), 284(4.9)	**365**, **332**, 286, [**360**, **348**/**325**, 290]	485, 465	0.12	10.5
15	**75**-$Ar(a)_5$	376(5.0), 332^{sh}(4.9)		542	0.37	8.4
16	**75**-$Ar(d)_5$	383(5.0), 354^{sh}(4.9), 306(5.0), 287(5.0)		503	0.24	5.8
17	**75**-$Ar(e)_5$	385(5.0), 345^{sh}(5.0), 321(5.0)		449, 485	0.44	8.9
18	**75**-$Ar(f)_5$	364(4.9), 328(4.9)		491, 465	0.16	11.0
19	**75**-$Ar(g)_5$	374(5.0), 334(4.9), 322^{sh}(4.8)		498, 479	0.26	10.2
20	**76**	335(4.6), 319(4.6)		357, 340	0.89	0.75
21	**77**	363^{sh}(4.7), 346(4.9), 317^{sh}(4.6)		391, 370	0.94	0.65
22	**77**[d]	362^{sh}, 347(4.9)		387, 368	1	0.67

[a]all measurements performed by exciting at 306 nm in degassed DCM solution at rt; bold values correspond to those used for comparison between experiment and computation; [b]M06-2X/6-311+G(d,p)//M06-2X(cc-pVDZ [ZINDO//M06-2x/cc-pVDZ]. [c] Quantum yields[49] relative to 9,10-DPA (ϕ_F = 0.95)[50] in ethanol. [d] Values from ref 45.

Studies that reflect the situation in **75**-Ph_5 are those reporting that, upon desymmetrization of carbon-based nanotubes, an increase in quantum yield is observed.[51] This would correctly correlate with the cases of **73**-Ph_2 and **74**-Ph_4 *vs* **75**-Ph_5, where the molecules of lower symmetry show higher quantum yields. The lifetimes for **74**-Ph_4 and **75**-Ph_5 are essentially the same and, therefore, this is not a differentiating factor. A hypothetical explanation is that the symmetry of the ground state in **75**-Ph_5 allows various non-radiative relaxation modes and thus results in lower quantum efficiency (increased rate of nonradiative decay).

Warner and co-workers[2b] have observed that cyclopentacorannulene display a lower quantum yield respect to **1** (1 and 7%, respectively). This does not agree with the symmetry argument cited above. One supposition is that the bowl depth and its relation to strain plays a role. Warner noted that the radiative decay of cyclopentacorannulene is slower than that of **1** and hypothesized that this is a possible result of its greater out-of-plane distortion, which leads to greater strain and loss of oscillator strength.

A comparison of the experimental absorption and emission spectra (Figure 2.16, 2.17, and 2.18) shows their complex nature. In the phenyl-substituted series, the tetrasubstituted compound shows longer emission wavelength and higher quantum yields (Figure 2.16). Among the **74**-R_4 series, **75**-$Ar(a)_4$, whose arene is tris(dodecyloxy)phenyl group, displays the longest emission wavelength; this behavior is characteristic of some electron transfer from the arylalkynyl unit to the corannulene core. Following the derivatives as a function of the electron-reach character, the **74** series (Figure 2.17) organizes in the following manner: **74**-$Ar(b)_4$ < **74**-Ph_4 < **74**-$Ar(e)_4$ < **74**-$Ar(d)_4$ < **74**-$Ar(a)_4$. This same trend is observed also in the **75** series (Figure 2.18). In all cases, compounds in the **74** series have higher quantum yields with respect to their analogs in the **75** series.

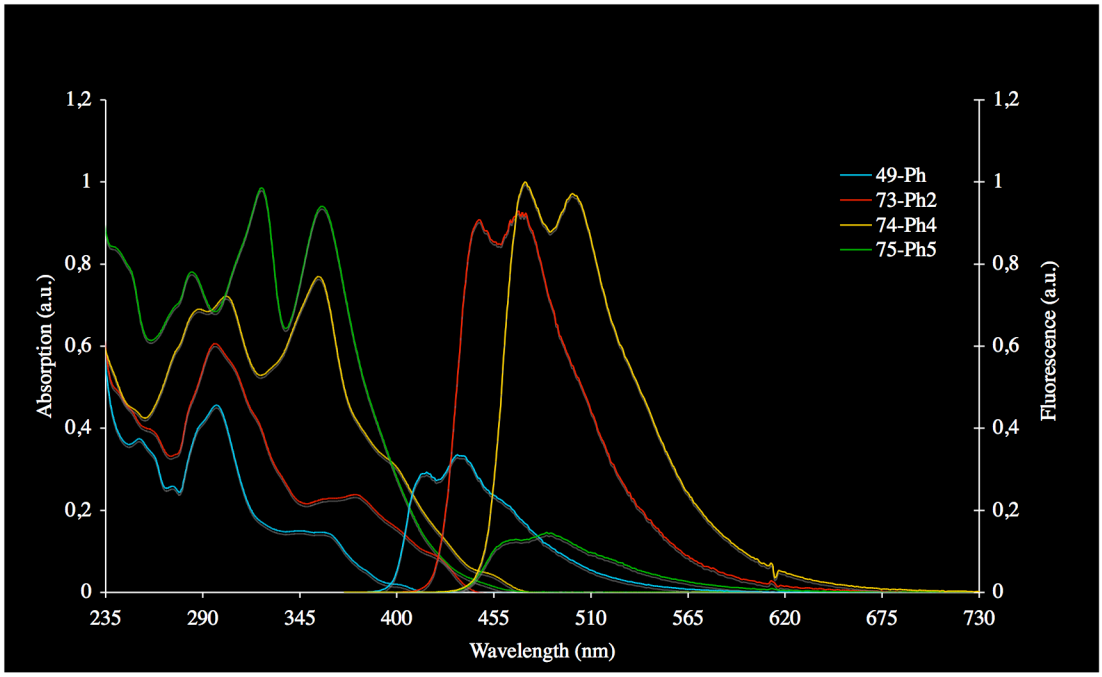

Figure 2.16. Absorption and emission spectra for the Ph substituted series.

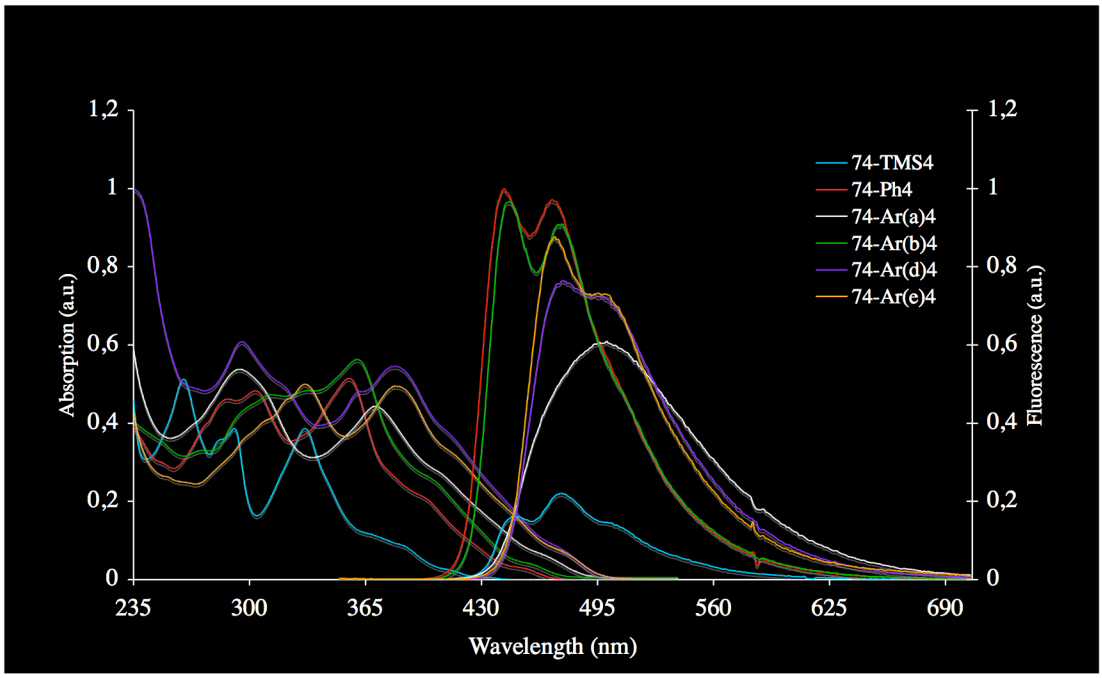

Figure 2.17. Absorption and emission spectra for the tetrasubstituted series 74-R_4.

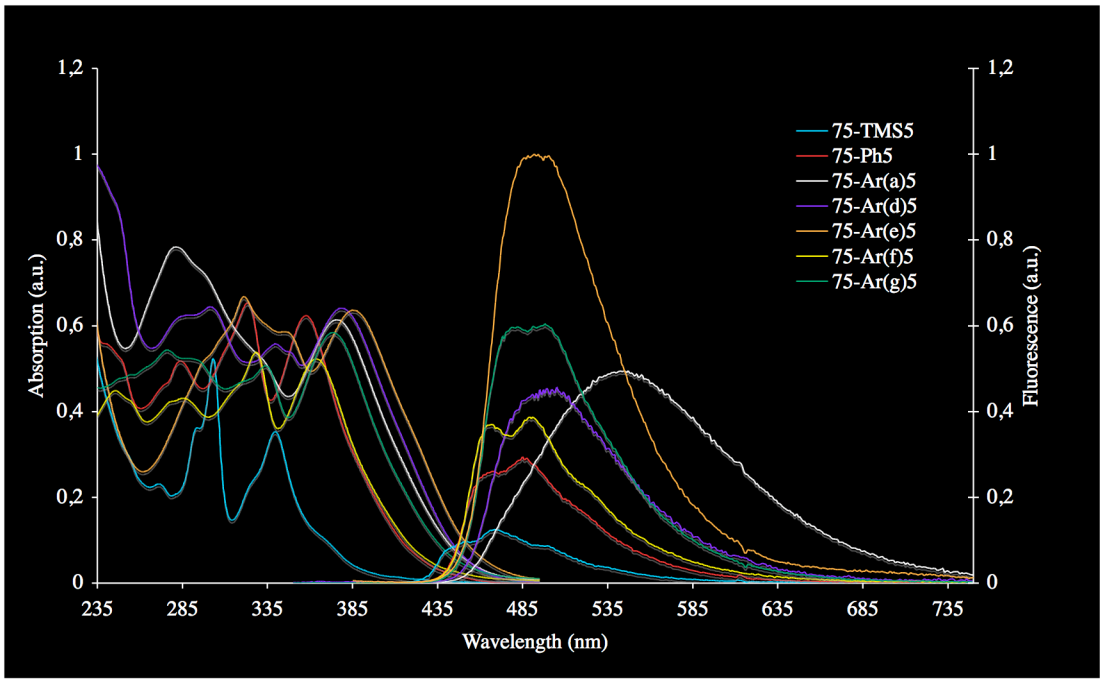

Figure 2.18. Absorption and emission spectra for the pentasubstituted series 75-R_5.

2.2.4. Conclusion and outlook

Two of the fundamental questions at the basis of this study have been addressed: 1) it is possible to prepare compounds displaying columnar stacking in the solid state by means of the arylalkynyl-substitution on the corannuelene core (**73**-Ph_2,

74-Ar(c)$_4$, and **75**-Ar(c)$_4$; and 2) it is possible to tune and enhance the photophysical properties of corannulene by means of the opportune arylalkynyl-substituent, presenting the possibilities for application in photoactive devices.

2.3. Experimental part

2.3.1. Methods

UV-vis: Perkin Elmer spectrometer Lambda 19 – Fluorescence emission: Edinburgh Instrument F900 fluorimeter equipped with S900 single photon photomultiplier detection system and Xe 900 xenon arc lamp (450 W) – Lifetime: Edinburgh Instrument F900 equipped with a nF900 nanosecond flash lamp filled with hydrogen (operating at 0.4 bar and frequency 40 KHz).

X-Ray crystal structures were obtained from measurements made on a *Nonius KappaCCD* area-detector diffractometer using graphite-monochromated Mo *K*α radiation (λ = 0.71073 Å) and an *Oxford Cryosystems Cryostream 700* cooler.

For the syntheses of the compounds object of this study see ref. 32 (supporting informations).

2.3.2. X-ray data

Table 2.9. Crystallographic Data for 73-Ph_2

Crystallised from		CH_2Cl_2 / MeOH
Empirical formula		$C_{38}H_{22}$
Formula weight [g mol^{-1}]		478.59
Crystal colour, habit		yellow, plate
Crystal dimensions [mm]		0.02 × 0.22 × 0.35
Temperature [K]		160(1)
Crystal system		orthorhombic
Space group		$Pca2_1$ (#29)
Z		4
Reflections for cell determination		2602
2θ range for cell determination [°]		4 – 50
Unit cell parameters	a [Å]	15.4564(6)
	b [Å]	22.190(1)
	c [Å]	7.4161(2)
	α [°]	90
	β [°]	90
	γ [°]	90
	V [Å^3]	2543.6(2)
F(000)		1000

D_x [g cm^{-3}]	1.250
μ(Mo $K\alpha$) [mm^{-1}]	0.0708
Scan type	ϕ and ω
$2\theta_{(max)}$ [°]	50
Total reflections measured	31639
Symmetry independent reflections	2448
R_{int}	0.088
Reflections with $I > 2\sigma(I)$	1931
Reflections used in refinement	2446
Parameters refined; restraints	346; 1
Final *R(F)* [$I > 2\sigma(I)$ reflections]	0.0433
wR(F^2) (all data)	0.1059
Weights:	$w = [\sigma^2(F_o^2) + (0.0616P)^2 + 0.0189P]^{-1}$ where $P = (F_o^2 + 2F_c^2)/3$
Goodness of fit	1.044
Secondary extinction coefficient	0.009(1)
Final Δ_{max}/σ	0.001
$\Delta\rho$ (max; min) [e Å^{-3}]	0.16; -0.14
$\sigma(d_{(C-C)})$ [Å]	0.004 – 0.006

Table 2.10. Crystallographic Data for 74-Ar(c)$_4$

Crystallised from	CH_2Cl_2 / MeOH
Empirical formula	$C_{60}H_{45}O_{1.5}$
Formula weight [g mol^{-1}]	790.01
Crystal colour, habit	colourless, plate
Crystal dimensions [mm]	0.10 × 0.23 × 0.38
Temperature [K]	273(1)
Crystal system	orthorhombic
Space group	*Pnma* (#62)
Z	4
Reflections for cell determination	3412
2θ range for cell determination [°]	4 – 46
Unit cell parameters *a* [Å]	7.4846(5)
b [Å]	43.341(3)
c [Å]	13.684(1)
α [°]	90

β [°]	90
γ [°]	90
V [Å^3]	4438.9(5)
F(000)	1668
D_x [g cm^{-3}]	1.182
μ(Mo $K\alpha$) [mm^{-1}]	0.0690
Scan type	ϕ and ω
$2\theta_{(max)}$ [°]	46
Total reflections measured	24969
Symmetry independent reflections	3080
R_{int}	0.074
Reflections with $I > 2\sigma(I)$	1939
Reflections used in refinement	3074
Parameters refined	278
Final $R(F)$ [$I > 2\sigma(I)$ reflections]	0.0819
$wR(F^2)$ (all data)	0.2663
Weights:	$w = [\sigma^2(F_o^2) + (0.1670P)^2]^{-1}$ where $P = (F_o^2 + 2F_c^2)/3$
Goodness of fit	1.099
Final Δ_{max}/σ	0.001
$\Delta\rho$ (max; min) [e Å^{-3}]	0.39; -0.30
$\sigma(d_{(C-C)})$ [Å]	0.004 – 0.007

Table 2.11. Crystallographic Data for 75-Ar(c)$_5$

Crystallised from	CH_2Cl_2 / $CHCl_3$ / MeOH
Empirical formula	$C_{70}H_{50}$
Formula weight [g mol^{-1}]	891.16
Crystal colour, habit	yellow, plate
Crystal dimensions [mm]	0.05 × 0.15 × 0.25
Temperature [K]	260(1)
Crystal system	monoclinic
Space group	$P2_1/n$ (#14)
Z	8
Reflections for cell determination	14858
2θ range for cell determination [°]	4 – 46
Unit cell parameters a [Å]	33.414(1)

b [Å]	7.8392(3)
c [Å]	41.096(2)
α [°]	90
β [°]	109.8771(8)
γ [°]	90
V [Å^3]	10123.5(7)
F(000)	3760
D_x [g cm^{-3}]	1.169
μ(Mo $K\alpha$) [mm^{-1}]	0.0660
Scan type	ϕ and ω
$2\theta_{(max)}$ [°]	46
Total reflections measured	73976
Symmetry independent reflections	13975
R_{int}	0.094
Reflections with $I > 2\sigma(I)$	7007
Reflections used in refinement	13957
Parameters refined	1282
Final $R(F)$ [$I > 2\sigma(I)$ reflections]	0.0635
$wR(F^2)$ (all data)	0.1798
Weights:	$w = [\sigma^2(F_o^2) + (0.0635P)^2 + 0.268P]^{-1}$ where $P = (F_o^2 + 2F_c^2)/3$
Goodness of fit	1.026
Secondary extinction coefficient	0.0007(2)
Final Δ_{max}/σ	0.001
$\Delta\rho$ (max; min) [e Å^{-3}]	0.20; -0.16
$\sigma(d_{(C-C)})$ [Å]	0.004 – 0.006

2.4. References

[1] (a) Müllen, K.; Scherf, U. *Organic Light-Emitting Devices*, Wiley-VCH, Weinheim, 2006. (b) Gogotsi, Y. *Carbon Nanomaterials*, Taylor & Francis Gr., Boca Raton, Fl, 2006.

[2] (a) Verdieck, J. F.; Jankowski, W. A. *Mol. Lumin. Int. Conf.* **1969**, 829. (b) Dey, J.; Will, A. Y.; agbaria, R. A.; Rabideu, P.W., Abdourazak, A. H.; Sygula, R., Warner, I. M. J. *J. Fluoresc.* **1997**, *7*, 231.

3 (a) Malashikin, S.; Finney, N. S. *J. Am. Chem. Soc.* **2008**, *130*, 12846. (b) Fages, F.; Leroy, S.; Tirapattur, S.; Sohna Sohna, J.-E. *Pure & Appl. Chem.* **2001**, *73*, 411. (c) Figueira-Duarte, T. M.; Simon, S. C.; Wagner, M.; Druzhinin, S. I., Zachariasse, K. A.; Müllen, K. *Angew. Chem. Int. Ed.* **2008**, *47*, 10175. (d) Kumar, C. V.; Buranaprapuk, A. *Angew. Chem. Int. ed.* **1997**, *36*, 2085.

[4] (a) Yamada, N.; Ueno, k.; Nishimura, J. ; Okada, Y. *U.S. Pat. Appl. Publ.* **2007**, 19. (b) Jarkov, V. V. *U.S. Pat. Appl. Publ.* **2004**, 108.

[5] a) Hanson, J. C.; Nordman, C. E. *Acta. Crystallogr., Sect. B* **1976**, *B32*, 1147. (b) Sevryugina, Y.; Rogachev, A. Y.; Jackson, E. A.; Scott, L. T.; Petrukhina, M. A. *J. Org. Chem.* **2006**, *71*, 6615.

[6] (a) Cheng, P.-C. Ph.D. Dissertation, Boston College: Boston, MA, 1996; p212. (b) Jones, C. S. *unpublished results*, synthesis uses Br_2 with catalytic I_2.

[7] (a) Maag, R. Master Thesis, Universität Zürich, 2006; (b) Sygula, A.; Xu, G.; Marcinow, Z.; Rabideau, P. W. *Tetrahedron* **2001**, *57*, 3637.

[8] Seiders, T. J.; Baldridge, K.K.; Elliott, E. L.; Grube, G. H.; Siegel, J. S. *J. Am. Chem. Soc.* **1999**, *121*, 7439

[9] Scott, L. T. *Pure Appl. Chem.* **1996**, *68*, 291.

[10] Samdal, S.; Hedberg, L.; Hedberg, K.; Richardson, A. D.; Bancu, M.; Scott, L. T. *J. Phys. Chem.* **2003**, *107*, 411.

[11] Butterfield, A. M. Master Thesis, Universität Zürich, 2008.

[12] Aprahamian, I.; Eisenberg, D.; Hoffman, R. E.; Sternfeld, T.; Matsuo, Y.; Jackson, E. A.; Nakamura, E.; Scott, L. T.; Sheradsky, T.; Rabinovitz, M. *J. Am. Chem. Soc.* **2005**, *127*, 9581.

[13] Sygula, A.; Sygula, R.; Fronczek, F. R.; Rabideau, P. W. *J. Org. Chem.* **2002**, *67*, 6487.

[14] Scott, L. T.; Hashemi, M. M.; Bratcher, M. S. *J. Am. Chem. Soc.* **1992**, *114*, 1920.

[15] Jones, C. S.; Bandera, D.; Baldridge, K. K.; Siegel, J. S. *manuscript in preparation*.

[16] (a) Sonogashira, K; Tdha, Y.; Hagihara, N. *Tetrahedron Lett*. **1975**, *6*, 4467. (b) Sonogashira, K. in *Metal-Catalyzed Cross Coupling Reactions*; Diederich, F.; Stang, P. J., eds., Wiley-VHC, Weinheim, Germany, 1998.

[17] (a) Sygula, A.; Rabideau, P. W. *J. Am. Chem. Soc*. **2000**, *122*, 6323. (b) Xu, G.; Sygula, A.; Marcinow, Z.; Rabideau, P. W. *Tetrahedron Lett*. **2000**, *41*, 9931.

[18] Fürstner, A., Leitner, A. *Synlett* **2001**, 290.

[19] Sygula, A.; Xu, G.; Marcinow, Z.; Rabideau, P. W. *Tetrahedron* **2001**, *57*, 3637.

[20] (a) Dounay, A. B.; Overman, L. E. *Chem. Rev*. **2006**, *106*, 116. (b)

[21] Grube, G. H.; Elliott, E. L.; Steffens, R. J.; Jones, C. S.; Baldridge, K. K.; Siegel, J. S. *Org. Lett*. **2003**, *5*, 713.

[22] (a) Hayama, T. Ph.D. Dissertation, Universität Zurich, Zürich, 2008, p30-34; (b) Hayama, T; Baldridge, K. K.; Wu, Y.-T.; Linden, A.; Siegel, J. S. *J. Am. Chem. Soc*. **2008**, *130*, 1583.

[23] For review on NHC, see: (a) Regitz, M. *Angew. Chem. Int. Ed. Engl*. **1996**, *35*, 725. (b) Bourissou, D.; Guerret, O.; Gabbai, F. P.; Bertrand, G. *Chem. Rev*. **2000**, *100*, 39. (c) Jafarpour, L.; Stevens, E. D.; Nolan, S. P. *J. Organomet. Chem*. **2000**, *606*, 49. (d) Scott, N. M.; Nolan, S. P. *Eur. J. Inorg. Chem*. **2005**, 1815.

[24] Eberhard, M. R.; Wang, Z; Jensen, C. M. *Chem. Commun*. **2002**, 818.

[25] Mizyed, S.; Georghiou, P. E.; Bancu, M.; Cuadra, B.; Rai, A. K.; Cheng, P.; Scott, L. T. *J. Am. Chem. Soc*. **2001**, *123*, 12770.

[26] Hayama, T.; Wu. Y.-T.; Linden, A.; Baldridge, K. K.; Siegel, J. S. *J. Am. Chem. Soc*. **2007**, *129*, 12612.

[27] Wu, Y.-T.; Hayama, T.; Baldridge, K. K.; Linden, A.; Siegel, J. S. *J. Am. Chem. Soc*. **2006**, *128*, 6870.

[28] (a) Leclerq, J.; Leclerq, J. M. *Chem. Phys, Lett*. **1973**, *18*, 411. (b) Etzkorn, T.; Klotz, b.; Sørensen, s.; Patroescu, I.V.; Barnes, I.; Becker, K. H.; Platt, U. *Atm. Env*. **1999**, *33*, 525.

[29] Woodward-Fieser rules: Lambert, J. B.; Shurvell, H. F.; Lghtner, D. A.; Cooks, R. G., *Organic Sructural Spectroscopy*; Prentice Hall: Upper Saddle River, NJ, 1998: chapter 11.

[30] Jones, C. J.; Elliott, E. L.; Siegel, J. S. *Synlett* **2004**, 187

[31] Mack, J.; Vogel, P., Jones, D.; Kaval, N.; Sutton, A. *Org. Biomol. Chem.* **2007**, *5*, 2448.

[32] Wu, Y.-T.; Bandera, D.; Maag, R. ; Linden, A.; Baldridge, K.K.; Siegel, J. S. *J. am. Chem. Soc.* **2008**, *130*, 10729.

[33] Work on modeling of the relative packing of **3** is ongoing: Wu, Y.-T.; Maag, R.; Potier, Y.; Ciurash, J. G.; Baldridge, K. K.; Hardcastle, K. I.; Linden, A.; Gavezzotti, A.; Siegel, J. S. Unpubished results, 2008

[34] Forkey, D. M.; Attar, S.; Noll, B. C.; Koerner, R.; Olmstead, M.M.; Balch, A. L. *J. Am. Chem. Soc.* **1997**, *119*, 5766.

[35] Petrukhina, M. A. ; Andreini, K. W.; Peng, L.; Scott, L. T. *Angew. Chem. Int. Ed.* **2004**, *43*, 5477.

[36] Bronstein, H. C. ; Choi, N., Scott, L. T. *J. Am Chem. Soc.* **2002**, *124*, 8870.

[37] Sygula, A.; Marcinow, Z.; Fronczek, F. R.; Guzei, I.; Rabideu, P. W. *Chem. Comm.* **2000**, 2439.

[38] Sakurai, H.; Daiko, T.; Sakane, H.; Amaya, T.; Hirao, T. *J. Am. Chem. Soc.* **2005**, *127*, 11580.

[39] van der Sluis, P; Spek, A. L. *Acta Crystallogr.* **1990**, *A46*, 194.

[40] Spek, A. L. PLATON, Program for the Analysis of Molecular Geometry; University of Utrecht: Utrecht, the Netherlands, 2005.

[41] a) Haddon, R. C.; Scott, L. T. *Pure. Appl. Chem.* **1986**, *58*, 137. (b) Haddon, R. C. *Acc. Chem. Res.* **1988**, *21*, 243. (c) Haddon, R. C. *J. Am. Chem. Soc.* **1990**, *112*, 3385. (d) Haddon, R. C. *Science* **1993**, *261*, 1545.

[42] Seiders, T. J.; Baldridge, K. K.; Grube, G. H.; Siegel, J. S. *J. Am. Chm. Soc.* **2001**, *123*, 517.

[43] Li, Z.; Meng. H., *Organic Light-Emitting Materials and Devices*; Taylor & Francis: Boca Raton, FL, 2007.

[44] Birckner, E.; Grummt, U.-W.; Göllr, A. H.; Pautzsch, T.; Egbe, D. A. M.; Al-Higari, M.; Klemm, E. *J. Phys. Chem. A* **2001**, *105*, 10307.

[45] Nizhegorodov, N. I. *Zh. Prikl. Spektrosk.* **1992**, *57*, 477.

[46] Ham, J. S.; *J. Phys. Chem.* **1953**, *21*, 756.

[47] Nakajima, A. *Bull. Chem. Soc. Jpn.* **1971**, *44*, 3272.

[48] Dong, D. C. ; Winnik, M. A. *Photochem. Photobiol.* **1982**, *35*, 17.

[49] (a) Demas, J. N.; Crosby, G. A. *J. Phys. Chem.* **1971**, *75*, 991. (b) Fery-forgues, S.; Lavrabe, D. *J. Chem. Ed.* **1999**, *76*, 1260.

[50] Morris, J. V.; Mahaney, M. A.; Huber, J. R. *J. Phys. Chem.* **1976**, *80*, 969.

[51] (a) Shavar, J.; Kono, J. ; Portugall, O.; Krstic', V; Rikken, G. L. J. A.; Miyaushi, Y.; Maruyama, S.; Perebeinos, V. *Nano Lett.* **2007**, *7*, 1851. (b) Sun, Y.-P. *supramol. Photochem.* **1997**, *1*, 325.

Chapter 3.

Synthesis and Properties of Ir(I) and Rh(I) Metal Complexes of Multi–alkyl Corannulene Derivatives.

3.1 Introduction.

The discovery of fullerene has shed light on a new area of organometallic chemistry in which the properties of metals bound to non-planar aromatic compounds can be investigated. As a result, a great number of exohedral transition metal complexes of fullerene have been synthesized over the past two decades.[1] However chemical synthesis of endohedral fullerene complexes is still challenging.[2]

The progress and advances in fullerene chemistry have also driven attention toward complexes of non-planar aromatic compounds. From a coordination viewpoint, buckybowls are unique ligands that have multiple coordination sites, as well as edge and rim carbon atoms capped with hydrogen atoms. Like fullerenes, they comprise a convex, three-dimensional surface of unsaturated carbon atoms and have convex and concave surfaces that are both potentially available for coordination. The coordination of metals on the concave surface is expected to provide fundamental building blocks for the synthesis of inclusion complexes of fullerene and nanotubes. The coordination of a metal ion on the convex surface could provide insights onto the activation and functionalization of the surface of fullerenes and nanotubes.

Metal complexes of buckybowls have been studied over the past 11 years.[3] In particular, complexes of corannuelene (**1**) and some of its alkyl derivatives, dibenzo[a,g]corannulene (**78**), hemibuckminsterfullerene (**79**) and, lately, sumanene (**80**) have been reported (Figure 3.1) with metals such as Ru(II), Ir(I), Ir(II), Rh(I) and Rh(II). These compounds where prepared by solution-phase synthesis or gas-phase co-deposition. Complexes with Cr, Mo, W, U, Fe and Ti have been observed in laser plasma experiments[4] or their synthesis has been attempted by direct metallation.[5]

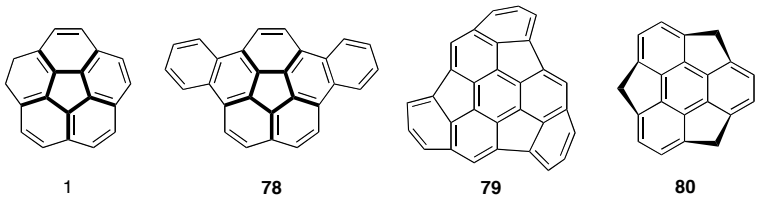

Figure 3.1. Buckybowls for which metal complexes have been reported.

The subjects of this chapter are the synthesis and the study of the properties of Rh(I) and Ir(I) metal complexes of *sym* multi-alkyl derivatives of corannulene. The effects of introducing alkyl substituents to the corannulene core will be investigated by ^{1}H 1D and 2D NMR techniques and will likely provide insight into the dynamic

processes of these compounds. X-ray crystallographic analyses will provide data on the solid state structure of these compounds and, in particular, the binding mode.

3.1.1. Complexes of Buckybowls

3.1.1.1. η^6 complexes

In 1997, the first example of a metal complex in which one of the ligands was a fullerene fragment, namely corannulene (**1**) was reported. By reacting $[(C_5Me_5)Ru(NCCH_3)_3](O_3SCF_3)$[6] with **1** in dichloromethane–d_2 (DCM-d_2) it was found that the ratio **1**/$[(C_5Me_5)Ru(\eta^6\text{-}C_{20}H_{10})](O_3SCF_3)$ (**81**) stabilizes to 1:1 after 20 h. After solvent evaporation and addition of fresh DCM-d_2, the conversion was complete (Figure 3.2).[7]

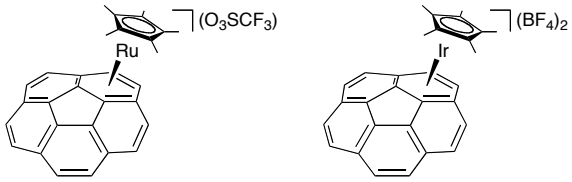

81 82

Figure 3.2. $[(C_5Me_5)Ru(\eta^6\text{-}C_{20}H_{10})](O_3SCF_3)$ (81) and $[(C_5Me_5)Ru(\eta^6\text{-}C_{20}H_{10})](BF_4)_2$ (82).

Complex **81** was particularly air sensitive and, therefore, it was characterized only by HRMS and NMR techniques. Addition of acetonitrile to a DCM-d_2 solution of **5** led to arene-corannulene exchange with regeneration of the starting materials. An exchange process was observed also with the addition of benzene, which generated free **1** and $[(C_5Me_5)Ru(\eta^6\text{-}C_6H_6)](O_3SCF_3)$. Quantum chemical calculations predicted *exo*-**81** to be 6 kcal mol^{-1} more stable than the *endo* isomer. Variable temperature NMR experiment on **81** excluded intramolecular arene exchange (high temperature experiment) but could not provide insights into the presence or absence of a rapid *exo*/*endo* interconversion due to the inversion of **1**.[8] In this study, it was also observed that addition of more than one equivalent of metal fragment led to a product that was presumably dimetallated but never isolated.

Six year passed before another successful synthesis of complexes of corannulene would be reported although an attempt to synthesize Fe complexes in the gas-phase by Bohme was published earlier.[9] Angelici and co-workers performed a reaction in which **1** was subjected to treatment with $[(C_5Me_5)Ir((OCMe_2)_3](BF_4)_2$ in

nitromethane-d_3. The reaction appeared to give quantitative conversion to $[(C_5Me_5)Ir((\eta^6\text{-}C_{20}H_{10})](BF_4)_2$ (**82**) at room temperature within 5 minutes (Figure 3.2).[10]

More interesting are the results of the same reaction using 1,2,5,6-tetramethylcorannuelene. After 3 minutes, ^{1}H NMR showed the presence of three isomers (Figure 2.3) in a 23:16:61 ratio (**83A**: **83B**: **83C**). After 15 minutes the ratio changed to 36:21:43 and, after 6 h, only isomers **83A** and **83B** were present (88:12). This ratio did not change in the following 24 h. When the reaction was carried out at 101 °C for 3 h, **83C** was not observed and the ratio **83A**: **83B** was the same (88:12). The stabilities of $[(C_5Me_5)Ir((\eta^6\text{-arene})](BF_4)_2$ were observed to be greater when the arene is alkyl-substituted[11] thus the observation for compounds **83A**-**C**. Initially, isomer **83C** in which the $[(C_5Me_5)Ir]^+$ unit is coordinated to a non-methylated ring, was observed. However, it is followed by isomerization of **83C** to the more stable **83A**, where $[(C_5Me_5)Ir]^+$ unit is bonded to an alkylated ring. These observations do not suggest the nature of this isomerization; in fact it could occur via migration of the $[(C_5Me_5)Ir]^+$ on the corannulene derivative surface or by a dissociation/association process.[10] Reaction of the final mixture of **83A**-**B** with benzene or acetone produced complete exchange of the corannulene with benzene.The derivative **83B** was found to disappear faster than **83A**, indicating the more labile nature of **83B**, where the metal is coordinated to a non-methylated ring.

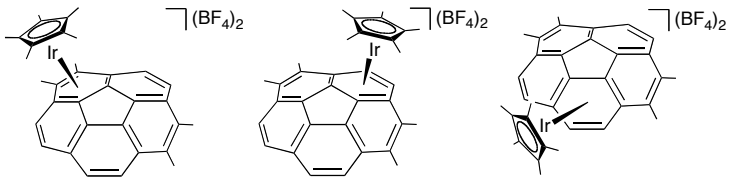

Figure 3.3. Isomers formed from the reaction of 1,2,5,6-tetramethylcorannuelene and $[(C_5Me_5)Ir((OCMe_2)_3](BF_4)_2$.

Another example in which a partial selectivity is observed upon reaction of a metal fragment with a corannulene derivative was shown by Siegel.[12] The reaction of acecorannulene[13] with $[(C_5Me_5)Ru(NCCH_3)_3](O_3SCF_3)$ in DCM-d_2 produced a mixture of isomers **84B**-**C** in a 2:1 ratio, together with free acecorannulene (Figure 3.4). Evaporation of the solvent and addition of fresh DCM-d_2 converted all the acecorannulene to **84B**-**C** maintaining the same isomeric ratio. When the reaction is

carried out at -80 °C, only **84B**, together with free acerocorannuelene, is observed. Upon warming to 25 °C, a 2:1 ratio of **84B-C** is observed in 1 h. It was found, deducing from the symmetry needed to account for the present signals, that the first isomer that forms is **84B**. The metal arene migration barrier was estimated to be ca. 25 kcal mol^{-1}.

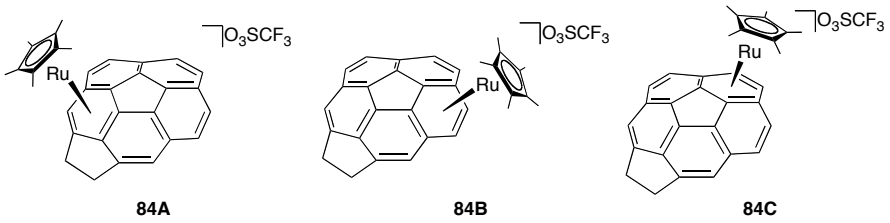

84A **84B** **84C**

Figure 3.4. Isomers formed from the reaction of acecorannulene and $[(C_5Me_5)Ru((NCCH_3)_3](O_3SCF_3)$.

In this example the diastereotopic protons on the acecorannulene provided a probe for *endo vs exo* facial complexation to the ruthenium fragment. Indipendent irradiation of the methylene protons of either **84B** or **84C** and the methyl groups on Cp*, showed no signal enhancements, which suggested an *exo* facial binding. Although the ring involved in this complex shows the larger POAV[14] and thus the orbital alignment is poor for the formation of a η^6 complex, this ring might play a role in the migration process. A possible explanation was given and was based on the fact that, in fullerene, the most stable η^2 complexes are the one in which the metal is coordinated to the most pyramidalized pair of carbons.[15] Assuming that η^6 metal complexation is likely to occur *via* a stepwise mechanism passing through η^2 and η^4 complexes with sequencial loss of ancillary ligands, $[(C_5Me_5)Ru(NCCH_3)_2]^+$ reacts first with acecorannulene to form an η^2 complex with the most pyramidalized pair of carbons. Thereafter, a η^2 slippage towards the ring that gives **84B** occurs and, by loss of acetonitrile, the η^6 complex is formed (the process might be catalyzed by the presence of free acetonitrile).

In an similar study, the reaction of 1,2,5,6-tetramethylcorannulene with $[(C_5Me_5)Ru(\mu_3\text{-}Cl)]_4$ in the presence of different silver salts was performed to test if any coordinative ring selectivity was present.[16] The results showed that a mixture of products **85B**-**C** was found in a 1:2 ratio while none of **85A** was ever observed

(Figure 3.5). This observation led to the conclusion that, in this case, ring migration of $[(C_5Me_5)Ru]^+$ was very slow.

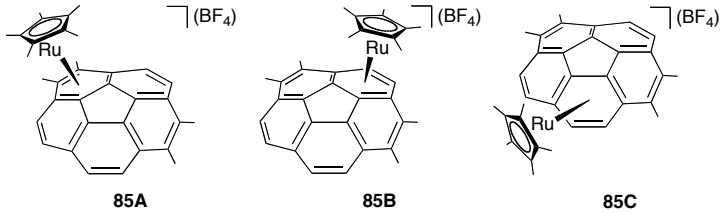

Figure 3.5. Isomers formed from the reaction of 1,2,5,6-tetramethylcorannuelene and $[(C_5Me_5)Ru(\mu_3\text{-}Cl)]_4$

A competitive test to check whether $[(C_5Me_5)Ru]^+$ binds stronger to **1** or 1,2,5,6-tetramethylcorannulene was performed.[16] Corannulene (**1**), the tetramethylated derivative (**51**), $[(C_5Me_5)Ru(\mu_3\text{-}Cl)]_4$ and, $AgPF_6$ were dissolved in nitomethane-d_3 in a 1:1:0.25:1 ratio and the mixture stirred for 2 h at room temperature (Figure 3.6). A stable average 1:2.9 ratio (**86**:**85B**+**85C**) was observed, suggesting that the coordination is kinetically more rapid with the tetramethylated compounds.

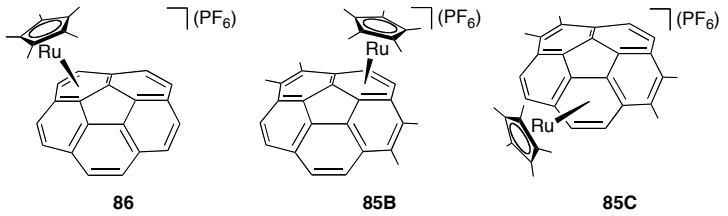

Figure 3.6. Competitive test products.

In 2004 the first dimetallated complex of corannuelene (**1**) as well as the first X-ray-characterized structure in which a metal is η^6 bound to **1** was reported.[17] The reaction of **1** with $[(C_5Me_5)Ru(\mu_3\text{-}Cl)]_4$ in the presence of $AgPF_6$ in nitomethane-d_3 afforded **87** in good yield (Figure 3.7).

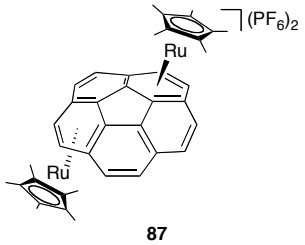

Figure 3.7. $[(C_5Me_5)Ru(\mu_2\text{-}\eta^6, \eta^6\text{-}C_{20}H_{10})](PF_6)_2$.

Dissolution of **87** in acetone causes the displacement of the $[(C_5Me_5)Ru]^+$ units. Decomposition was observed for a solution of **87** in nitomethane-d_3 after a week. The X-ray crystal structure of **87** (Figure 3.8) showed that the two $[(C_5Me_5)Ru]^+$ units are bonded to both the *exo* and *endo* faces of corannulene.

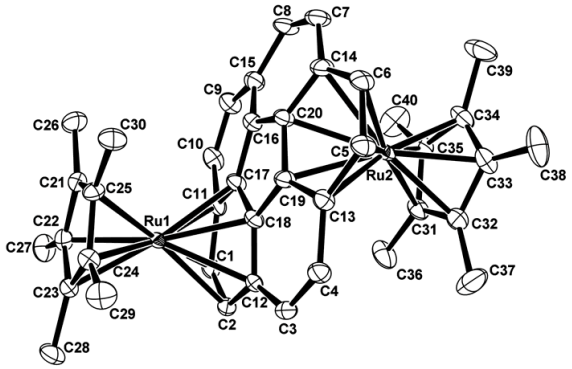

Figure 3.8. X-ray crystal structure of 87.

The analysis of the of the crystal data suggests that the coordinated ruthenium fragments have great influence on the corannulene structure. The *rim* C–C bond length was lengthened from 1.402(5) in **1** to 1.454(11) in **87**. The POAV angles[14] of the five central carbon atoms and those attached to them are on average 8.4° and 3.8°, respectively, in **1**, while they are 4.2° and 1.3° respectively in **11**. In free **1**, the bowl depth is 0.87 Å,[18] while, in **87** and in the mono coordinated analogous **88**[16] are 0.42 Å and 0.78 Å, respectively (Figure 3.9). These observations allowed to the conclusion that in **9** the curvature of **1** was greatly reduced.

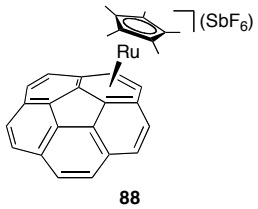

88

Figure 3.9. $[(C_5Me_5)Ru(\eta^6\text{-}C_{20}H_{10})](SbF_6)$.

In 2007, the first examples in which corannulene is bound to $[M(\eta^6\text{-arene})]^{2+}$ metal fragments were reported.[19] The reaction of **1** with $[M(\eta^6\text{-arene})Cl_2]_2$ in the presence of a silver salt afforded compounds **89–91** (Figure 3.10), in which M = Ru or Os, and arene = C_6Me_6, C_6EtMe_5 or cymene, respectively (each of them with SbF_6^- as

counteranion). In the crystal structure, a partial flattening of corannulene together with a boat-like structure for the coordinated ring was noted.

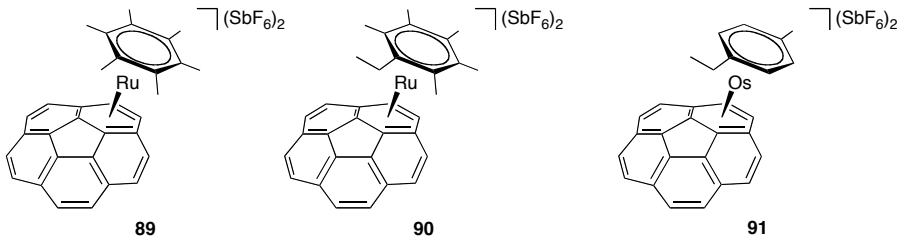

89 90 91

Figure 3.10. Structure of compounds 89-91.

The reactivity of [Ru(η^6-C_6Me_6)(η^6-corannulene)]$(SbF_6)_2$ with nucleophiles was tested because such reactivity was reported in complexes of the type [Ru(η^6-C_6Me_6)(η^6-C_6Me_4)]$^{2+}$.[20] Treatment of **89** with *t*-BuOK, CH_3ONa and Et_3N all resulted in decomposition of the complex.[19] Complexes of the type [(Fe, Ru or Os)(η^6-$C_6H_6)_2$]$^{2+}$ react with tertiary phopshines to give ring adducts.[21] The reaction of **89** with a 5-fold excess of different phosphine leads to a new compound but, to date its isolation failed.[19]

The organometallic chemistry of **1** has been dominated by [(Ru(II) or Ir(II))(C_5Me_5)] metal fragments. The effects due to complexation on the bowl structure of **1** and, in same cases, on the migration properties of a metal fragment have been discussed and chemical reactivity was not observed at the metal center while **1** is bound.

In 2006, Ir(I) and Rh(I) complexes of **1**, in which the ligands on the metal fragment are cyclic alkenes were reported.[22] These complexes where prepared by treating **1** with [M$(COE)_2(OCMe_2)$]PF_6,[23] where M = Rh(I) or Ir(I) in a suspension in diethyl ether for 12 h, to yield compound **92–93** in quantitative yields (Scheme 3.1). The X-ray analyses of these compounds disclosed that the nature of the binding mode is η^6 (with M–C bond slightly shorter in Ir(I) than in Rh(I)), with a boat-like conformation of the metal-coordinated ring.

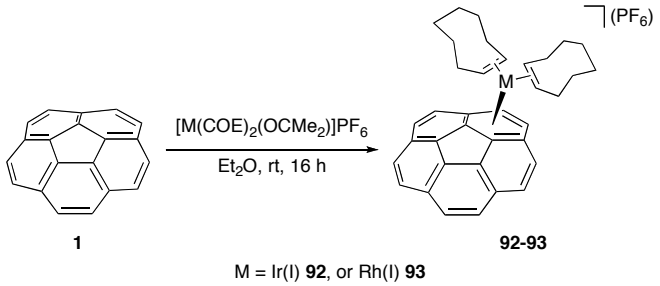

Scheme 3.1. Synthesis of compounds 92–93.

Compound **93** showed a broad signal (aromatic region) in the ^{1}H NMR spectrum at 300 K. Upon cooling, this broad signal decoalesced to a set of five signals. This observation led to the hypothesis that the metal migrated on the corannuelene surface. This process could occur by one of two distinct mechanisms (Figure 3.11). Either the metal fragment $[Rh(COE)_2]^+$, migrates through the central, five-membered ring in an $\eta^6 \rightarrow \eta^5 \rightarrow \eta^6$ process (**A**, *hub*-migration), or follows the outer edge of **1** and migrates from one arene ring to the next *via* an $\eta^6 \rightarrow \eta^4(\eta^2) \rightarrow \eta^6$ mechanism (**B**, *rim*-migration). In 2D EXSY experiments at 278 K, **93** displayed cross-peaks between the singlet of the η^6-coordinated ring and all of the other four aromatic ring signals at long mixing times (500ms). Changing the mixing times between 3 10^{-3} s and 500 ms showed rapid onset of cross-peaks among all signals between 1 and 5 ms without distinction between vicinal and distal fragments. This observation supports the idea that the favored migration path is the *hub* (**A**, Figure 3.11).

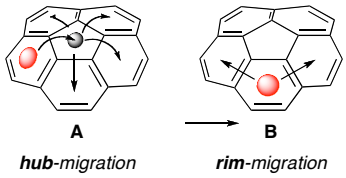

Figure 3.11. Possible migration paths of the metal fragment in 93.

Compound **92** upon heating underwent a transformation that gave rise to a new set of aromatic signals which were explained with the presence of **94** that has one COD-bound ligand (Scheme 3.2). Independent synthesis of **94** by application of a procedure introduced by Shrock for the synthesis of benzene complexes[24] involved the reaction of $[Ir(COD)(\mu_2\text{-}Cl)]_2$ with **1** in the presence of $AgPF_6$ to form the desired compound **94**. The transformation of **92** to give **94** highlights the fact that these

$[Rh(COE)_2]^+$ fragment can undergo chemical reactions while bound to **1**. In a related example, **93** was treated with $(i\text{-Pr})_3P$ at -40 °C, resulting in the substitution of one COE with the phosphine to give **95** (Scheme 3.2). ^1H NMR data suggested that the migration of the metal fragment in **97** was faster since decoalescence of the signals in the aromatic region occurs at 253 K and at 273 K in **17**.

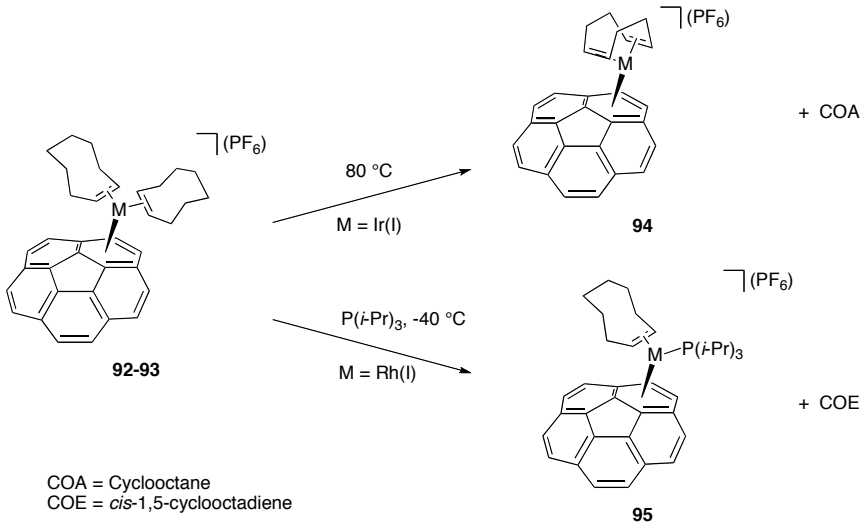

Scheme 3.2. Reactivity of 94 and 95.

In 2007, Hirao and co-workers[25] prepared the first complex of sumanene (**80**) by a ligand exchange reaction with ferrocene in the presence of aluminum powder and aluminum chloride at 120 °C in a solvent free environment, which afforded **96** in 91% yield (Scheme 3.3). ^1H NMR indicated that the metal was bound to one of the outer benzene rings, rather than the central one. Further NMR studies, including NOE experiments, indicated that the metal was bound on the *endo* face. X-ray crystallographic analyses confirmed the structure in which the $[CpFe]^{2+}$ fragment is η^6-coordinated on the *endo* face, providing the first example of an *endo* η^6-coordinated buckybowl.

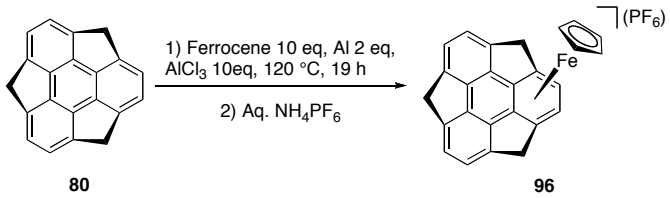

Scheme 3.3. Synthesis of 96.

3.1.1.2 η^2 and η^1 complexes

Solution-phase synthesis is not the only way to prepare complexes of **1**. In 2003, Petrukhina and co-workers introduced the use of vapor-phase co-deposition[26] to the synthesis of new corannulene-metal complexes. Compound **1** was combined with $[Rh_2(O_2CCF_3)_4]$ in a sublimation-deposition apparatus at 160 °C in different ratios ($[Rh_2(O_2CCF_3)_4]$:**1**, 1:1 or 3:2).[27] After three days, crystals of new complexes were found. The X-ray crystallographic analyses of these substances led to their structural identification as $\{([Rh_2(O_2CCF_3)_4]_m[C_{20}H_{10}]_n\}$ where *m*:*n* are 1:1 (**97**) and 3:2 (**98**). Furthermore, these analyses revealed two unique structural motifs built on weak η^2 coordination. Compound **97** is a 1D network polymer consisting of alternating dirhodium units and **1** (zigzag chains, Figure 3.12). Each molecule of **1** is bound to two dirhodium units by an η^2 bond to *rim* carbons; one on the *exo* face and the other one on the *endo* face. The Rh-C length was found to be slightly longer for the Rh bound to the *exo* face with respect to the *endo* one (2.643(4) Å and 2.580(4) Å).

Compound **98** is an infinite 2D layered network consisting of giant hexagonal cells consisting of six dirhodium units and six molecule **1**. Each molecule of **1** is coordinated to three dimetal units, two on the *exo* side and one on the *endo* side. In **98** only *rim* carbons of **1** are involved in coordination to the rhodium atoms in an η^2 fashion with Rh-C bond lengths of 2.636(3) Å and 2.548(3) Å for *exo* bonding and 2.570(3) Å for *endo* bonding. In both cases, coordination to rhodium, does not significantly perturb the structure of **1**.[27]

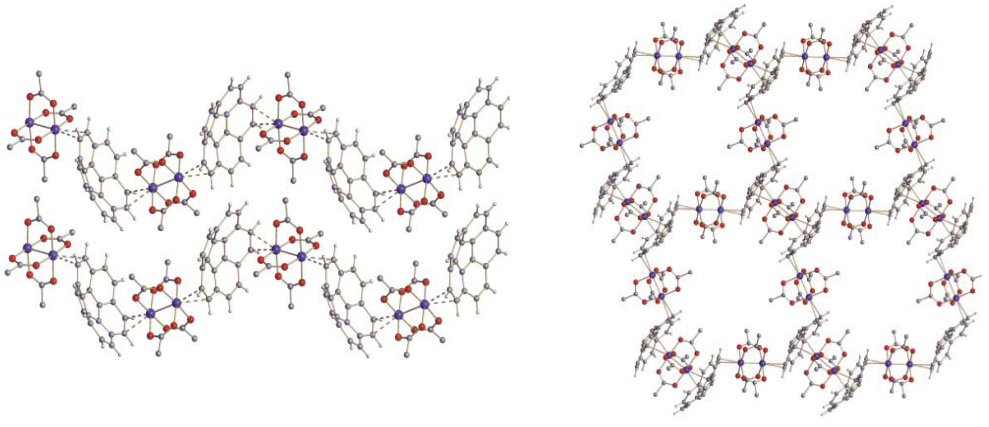

97 **98**

Figure 3.12. Crystal packing for $\{([Rh_2(O_2CCF_3)_4]\ [C_{20}H_{10}]\}$ (97) and $\{([Rh_2(O_2CCF_3)_4]_3[C_{20}H_{10}]_2\}$ (98), Rh blue, O red, C gray, H light gray.

The vapor-phase co-deposition of hemibuckminsterfullerene (**79**) with $[Rh_2(O_2CCF_3)_4]$ at 164 °C for three days afforded dark red crystals that allowed for the identification of the structure as $\{([Rh_2(O_2CCF_3)_4]_3(C_{30}H_{12})\}$ (**99**).[28] X-ray crystallographic analyses showed that **99** has an infinite 2D layered structure built on weak Rh–C interactions with an η^2 binding mode with only *rim* carbon atoms (Figure 3.13). Four metal centers from three independent dirhodium units are bound to each molecule of **79**, resulting in a tetradentate coordination mode that was previously observed only in the planar chrysene.[26b] Three of the rhodium centers are bound from the *exo* face and, one from the *endo* face. More in depth analyses revealed that the *endo* bound units is more appropriately described as η^1.

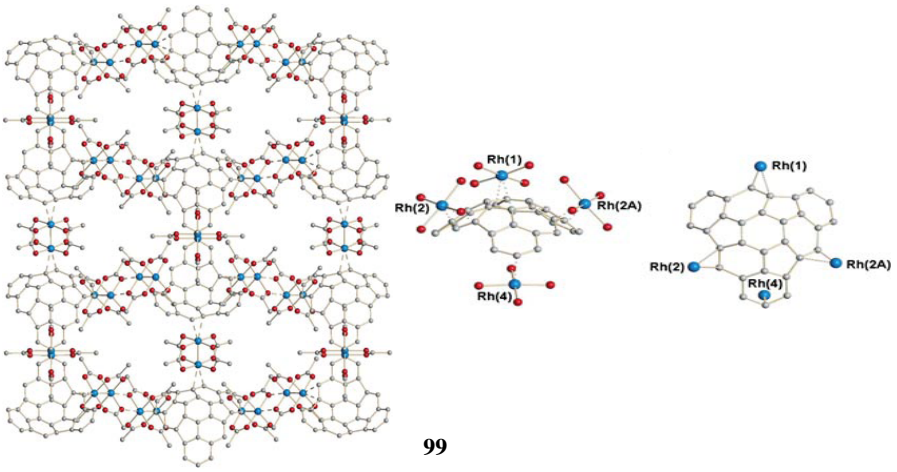

Figure 3.13. Crystal packing (left) and binding mode for 99 (side and top view, center and left respectively), Rh(1), Rh(2), and Rh(2A) η^2 bounded; Rh(4) η^1 bound (Rh blue, O red, C gray, H light gray) .

In an analogous study, **78** was combined with $[Rh_2(O_2CCF_3)_4]$ in a vapor-phase co-deposition apparatus for 7-10 days at 160 °C. The resulting red plates were analyzed and the structure was assigned as $\{([Rh_2(O_2CCF_3)_4]_3$(dibenzo[a,g]corannulene)} (**100**).

The 2D network found for **100** is similar to that of **97**. Each molecule of **78** is bound to three dirhodium units (Figure 3.14). Two of them are bound to *rim* carbons of the corannulene core in an η^2 mode (*endo* face, Rh1 and Rh2) and one (Rh3) is bound on the *exo* face in an η^2 mode. In this case, in contrast to the observations on **91**, the coordination of three metal centers induces a flattening of the bowl, with bowl depth reduce4 from 0.83 Å to 0.77 Å.

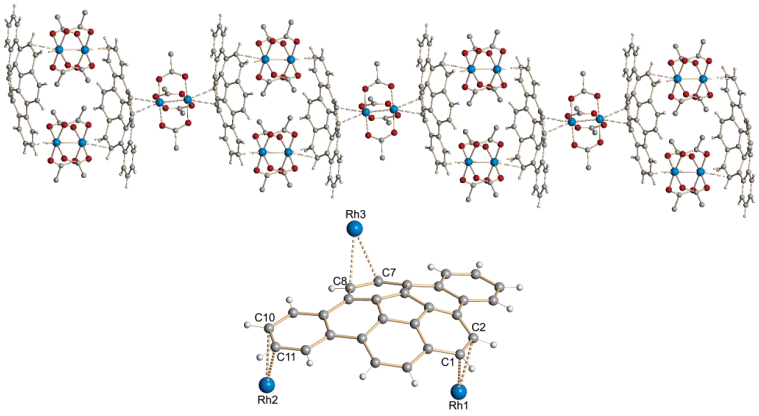

100

Figure 3.14. Crystal packing for 100 (top) and binding mode: Rh1, Rh *endo* and, Rh3 *exo* (Rh blue, O red, C gray, H light gray).

Petrukhina and co-workers,[29] studying the influence of the metal center acidity on the coordination mode, combined **1** with the Ru(II) complex {(Ru_2[(3,5-CF_3)$_2$$C_6H_3$]$_2$$(CO)_5$} in a vapor-phase co-deposition apparatus at 165 °C. X-ray analyses of the product disclosed the identity of the compounds as {(Ru_2[(3,5-CF_3)$_2$$C_6H_3$]$_2$$(CO)_5$($C_{20}H_{10}$)}(1/4 $C_{20}H_{10}$). In particular, one corannulene functions as a guest, occupying a cavity in the crystal lattice,[29] whereas the others function as ligands coordinated to the diruthenium units. Two crystallographically independent diruthenium(I,I) units were present with bound corannulene in the same crystal (Figure 3.15). One has a η^2-*rim* bound **1** (with average Ru-$C_{1\text{-}2}$ bond length of 2.545(3) Å) (**101**) and, a second one (**102**) where the dimetallic unit is η^1 bound to a single *hub* carbon atom (with length Ru-C_{12B} of 2.611(3) Å).

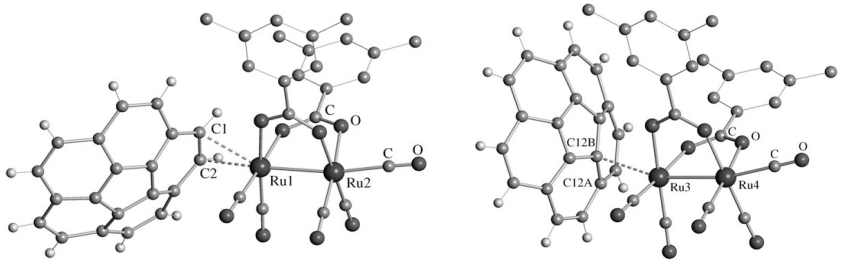

101 **102**

Figure 3.15. Crystal structures of 101 and 102.

The POAV[14] angles for the four uncomplexed carbon atoms of the ligand in the *hub* η^1 complex are 8.3°±0.2°. On the other hand, the *hub* η^1 bound carbon has a POAV of 10.6°, which is significantly different and a clear indication of bonding to Ru. This observation, together with a longer Ru-C_{12A} bond length between (2.965(4) Å, Figure 3.15) confirms the η^1 binding mode. The Ru-C bond length of 2.545(3) Å (*rim*) and 2.611(3) Å (*hub*) are appreciably longer than the average bond length observed in the bis-corannulene adduct $[(Ru_2(O_2CCF_3)_2(CO)_4(C_{20}H_{10})_2]$ (2.508(3) Å) (**103**, Figure 3.16).[30]

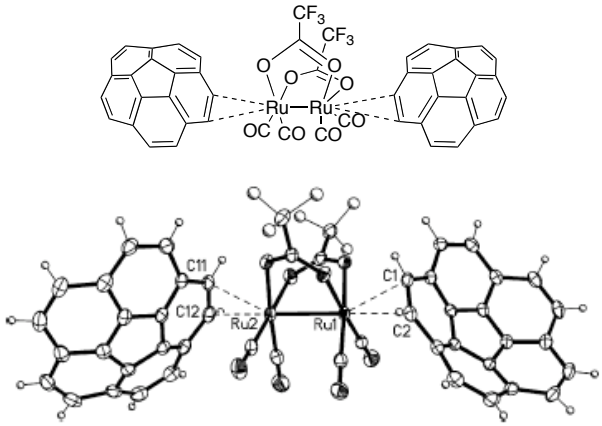

103

Figure 3.16. Crystal structure of 103.

Siegel and co-workers studied the effect of different counteranions in Ag(I) metal complexes of **1**.[31] The result showed an η^2 or η^1 binding mode always on the *exo* face and different 2D networks induced by the presence of different anions (Figure 3.17). In this study were not found significant differences on the structure of **1** due to the metal binding.

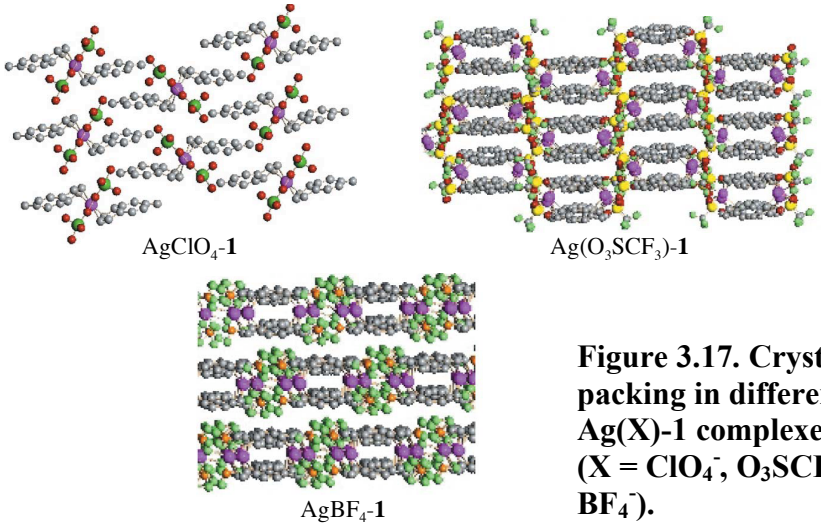

$AgClO_4$-**1** $Ag(O_3SCF_3)$-**1**

$AgBF_4$-**1**

Figure 3.17. Crystal packing in different Ag(X)-1 complexes ($X = ClO_4^-$, $O_3SCF_3^-$, BF_4^-).

3.2 Present work

In this section, *sym*-pentaalkyl corannulene derivatives will be used for the preparation of Rh(I) and Ir(I) metal fragments containing olefinic ligands such as diethylene, *cis*-cyclooctene (COE) *cis*-1,5-cyclooctadiene (COD) and bicyclo[2.2.1]hepta-2,5-diene (NBD). The use of these corannulene derivatives will provide new molecular species, the physical properties of which will be studied in the solution-phase and solid state. Specifically, the solution-phase study by 1D and 2D NMR techniques will allow for the qualitative and, in same cases quantitative determination of the dynamic processes that take place in these complexes, such as rotation and migration. A haptotropic ring migration[32] process was reported in a study in which the parent compound, corannulene, was complexed with the metal fragment $[Rh(COE)_2]^+$.[22] The solid state study by X-ray crystallographic analyses will unveil the molecular geometry and the binding modes. The possibility of modifying the corannulene ligands by changing the alkyl substituents on the periphery of the corannulene core furnishes a unique way to study the effects of such substitution on the properties of these new compounds. Analogously, changing of the metal fragment within a series of complexes with the same corannulene derivative will provide insights into the effects of the olefinic ligand on dynamic and structural properties. Quantum chemical computations on some of the complexes will aid in understanding the results provided by NMR and crystallographic analyses.

3.2.1. The π-metal complexes bond and d^8-arene-ML_2 complex

The interaction of a metal with an olefin or a triene to form η^6, η^4 or η^2 are controlled by two factors. The first, is the interaction of the filled and unfilled orbitals of the olefin with the unfilled and filled orbitals of the metal. Donation occurs between the filled π orbitals of the olefin and the unfilled orbital of the metal having the suitable orientation (p_z, d_{z^2} , $d_{x^2-y^2}$) and, from the metal (p_x or d_{xz}) to the unfilled π* orbitals of the olefin (back bonding).[33] In general the description of this type of bond is referred to as the Dewar-Chatt model (Figure 3.18).[34]

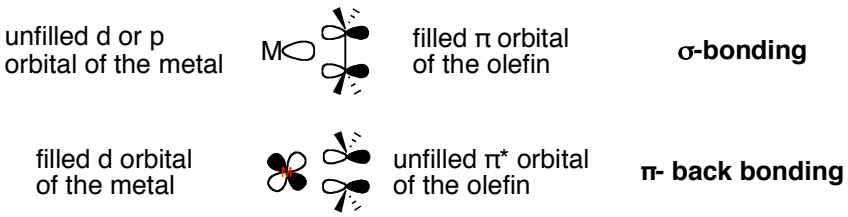

Figure 3.18. Dewar-Chatt model.

The second factor is the spatial requirement for the orbitals of the metal to overlap with the orbital of the complete π system. In a η^2 olefin complex, the degree of back bonding is controlled by the energy of the filled metal orbitals and the unfilled π* of the olefin. Electron deficient metals or electron rich olefins decrease the amount of back bonding, because of large differences in the orbital energies of the filled orbitals of the metal and the unfilled orbitals of the olefin. When in a complex the back bonding is small than the effect on the C–C bond length of the olefin will be small and the coordinated olefin substantially planar (e.g. Zeise's salt $K[PtCl_3(C_2H_4)]$[35,1]). Electron rich metals and electron deficient olefins, increase the amount of back bonding and, as a consequence, substantial geometric distortion are observed in the olefin. In particular it can lead to an extreme where the olefin carbons approach an sp^3 hybridization and the metal olefin bonds seen as part of a metallocyclopropane.

It is also important to consider the effect associated with the pyramidalization of the olefin carbons.[36] A first effect is a decreased overlap between the two p orbitals that causes an increase in the energy of the HOMO and a decrease of the LUMO by the same amount. The second effect is an acquisition of s character by the two p orbitals. The acquisition of s character, lowers the energy of both HOMO and LUMO because of the relative s-p energy differences. As an overall effect there is a slight increase in the HOMO energy and a large decrease in the LUMO (Figure 3.19).

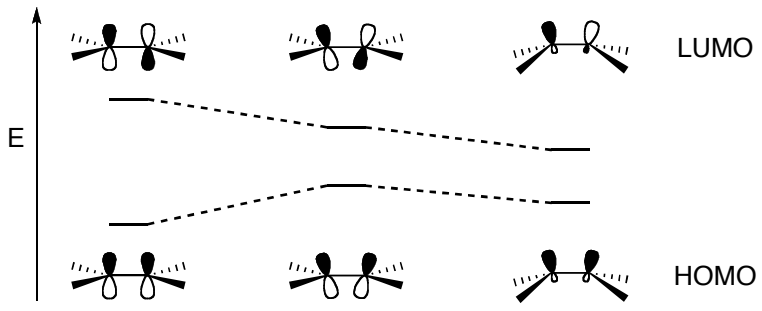

Figure 3.19. Effect of pyramidalizatin on the HOMO-LUMO gap.

In η^6 and η^4 π-metal complexes is required that the orbitals of the metal interact with the HOMO or LUMO of a diene or triene, respectively.[36a] Because of their dimensions, the orbital overlap is diminished and a distortion towards metallocyclopropanes decreases it as well.

In d^8-arene ML_2 systems (like the complexes object of this study), there are two limiting conformations.[36a] Both of them have a non-planar folded arene ligand, but each are directly bonded to different sides of the folded arene ligand. In the conformation **A**, the ML_2 group eclipses two C–C bonds. The two *para* carbons, which form a vector normal to the plane of ML_2, are bent out of plane of the other four carbons, away from the metal. In the alternative orientation, **B**, the ML_2 fragment group eclipses two carbon atoms and, the four non-eclipsed carbon move out of plane, away from the metal. A structurally equivalent view of generating this conformation from a planar d^8-arene-ML_2 of C_{2v} symmetry is that the two eclipsed carbon atoms, move out of plane and the other four, toward the metal.

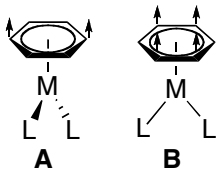

This displacements seen in arene-ML_2 complexes have electronic origin. Figure 3.20 shows an orbital interaction diagram for a d^8-benzene-ML_2 complex where the benzene ligand has been kept planar. The lowest π orbital of a_1 symmetry in benzene forms a three orbital interaction with $1a_1$ and $3a_1$ of the ML_2. The lowest two molecular orbitals are filled. The $2a_1$ and a_2 fragment orbitals are of δ symmetry so they will be stabilize by the π* orbitals (upper left, Figure 3.20). They are also stabilized by two relatively high-lying benzene ring orbitals which are also of δ symmetry. That leaves b_2 and b_1 of the ML_2 and two π orbital. The b_2 of ML_2 forms a very strong interaction with the b_2 of the π orbital. The bonding combination is filled. ML_2b_1 and benzene b_1 form a bonding and antibonding combination both of which are filled. The antibonding b_1, to the two *para* carbons can be relieved by puckering of the benzene. The occupation of this b_1 also causes a lengthening of the metal-benzene

carbon lengths and is probably responsible of the rapid arene exchange reactions that these complexes undergo.

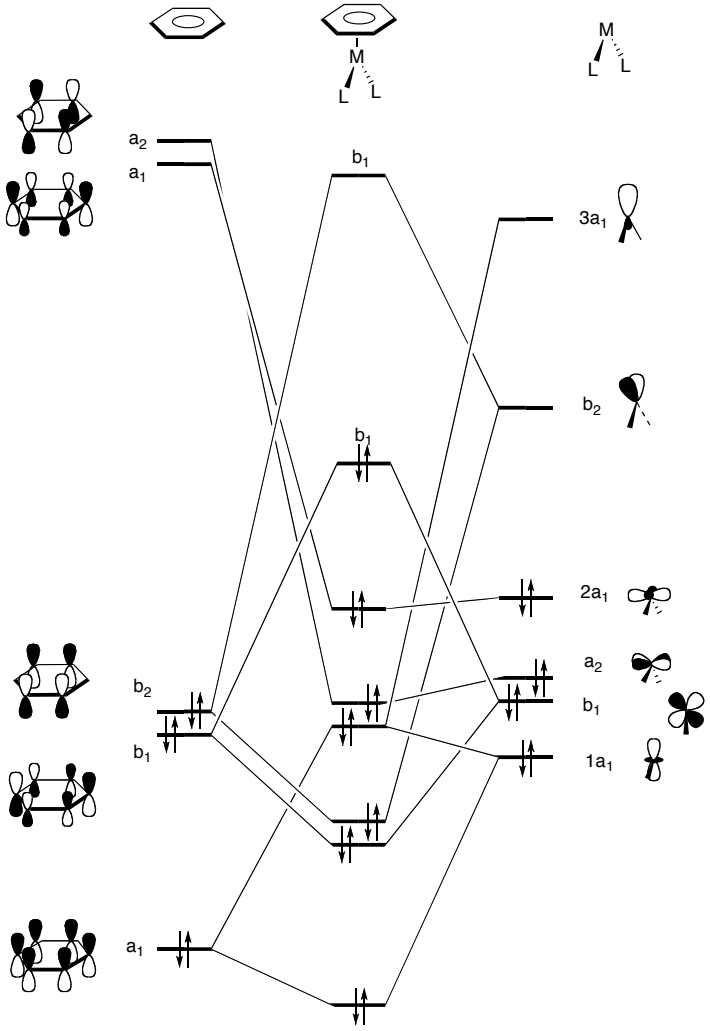

Figure 3.20. Construction of the valence orbitals for a benzene-d^8-benzene-ML$_2$ fragment.

3.2.2. Synthesis of Rh(I) and Ir(I) metal complexes of *sym*-pentaalkylcorannulene

The *in situ* procedure introduced in a previous report[22] for the synthesis of the complex [Ir(COD)(η^6-$C_{20}H_{10}$)]PF_6 is here extensively applied to the synthesis of new organometallic derivatives of **1**, 1,3,5,7,9-pentamethylcorannulene (**54**) and 1,3,5,7,9-penta(*t*-Butyl)corannulene (**104**).

The treatment of **1** with the [Rh(NBD)(μ_2-Cl)]$_2$ or [Rh(C_2H_4)$_2$(μ_2-Cl)]$_2$ in the presence of $AgPF_6$ in dichloromethane solution affords compound **105** and **106**, respectively, in good yield (Scheme 3.4). Compound **106** is sparingly soluble in dichloromethane, chloroform and 1,1,2,2-tetrachloroethane.

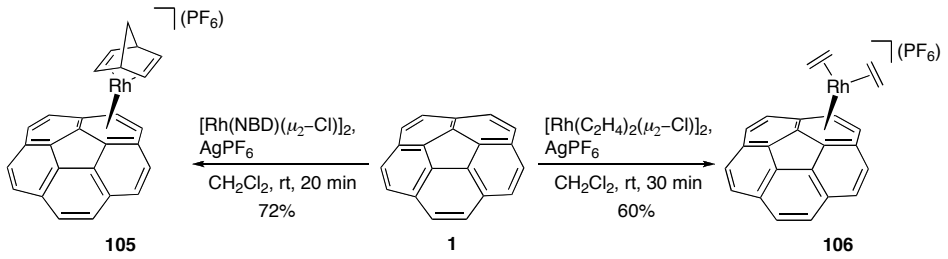

Scheme 3.4. Synthesis of complexes 105 and 106.

When **54** reacts with the dimers $[Rh(NBD)(\mu_2\text{-}Cl)]_2$ or $[Rh(COD)(\mu_2\text{-}Cl)]_2$ in dichloromethane solution in the presence $AgPF_6$, compounds **107** and **108** are formed, respectively, in high yields (Scheme 3.5). In analogous syntheses, in which **54** is treated with the monodentate ligand containing dimers $[Rh(C_2H_4)_2(\mu_2\text{-}Cl)]_2$ or $[Rh(COE)_2(\mu_2\text{-}Cl)]_2$ the adducts **109** and **110** are formed (Scheme 3.5).

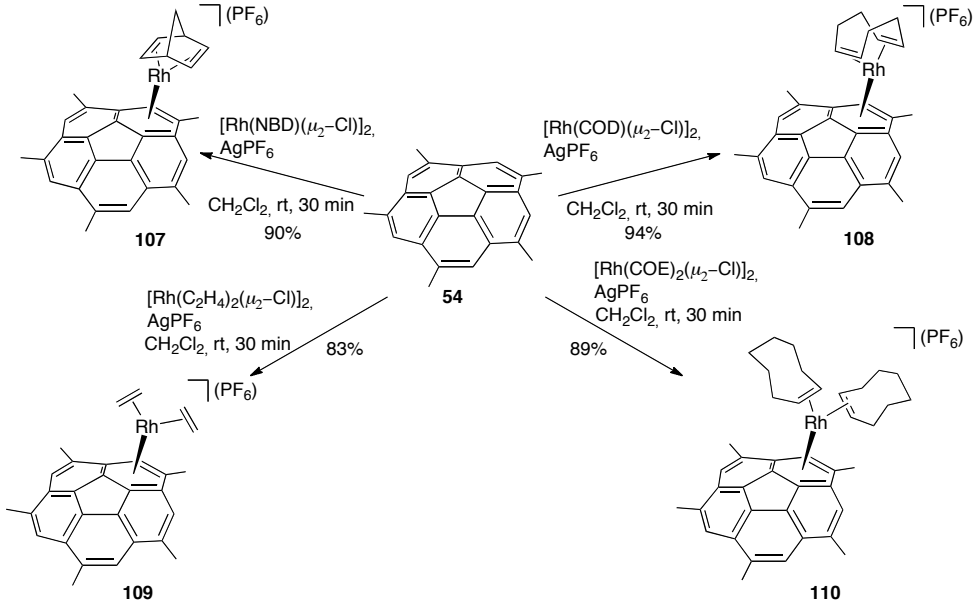

Scheme 3.5. Synthesis of the complexes 107-110.

The same methodology was applied to the syntheses of compounds **111-113**, derivatives of the more sterically hindered corannulene derivative **104** in high yields (Scheme 3.6).

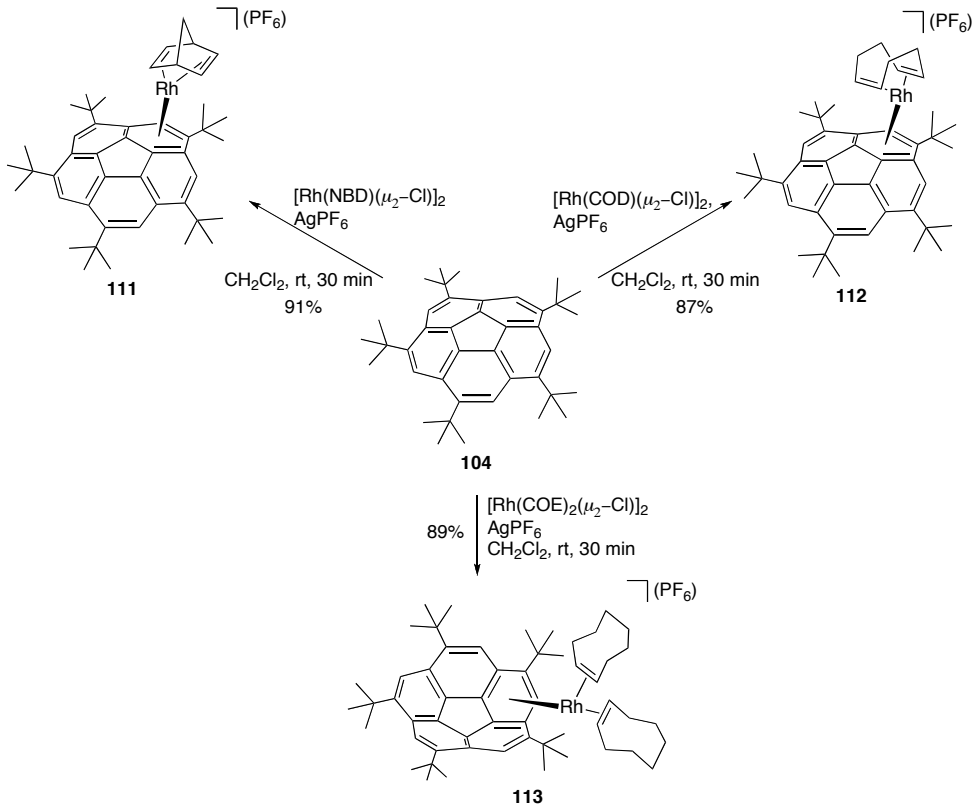

Scheme 3.6. Synthesis of the complexes 111-113.

The reaction of **54** and **104** with $[Ir(COD)(\mu_2\text{-}Cl)]_2$, in the presence of $AgPF_6$, affords compounds **114** and **115**, respectively (Scheme 3.7). The treatment of **54** and **104** with $[Ir(COE)_2(\mu_2\text{-}Cl)]_2$, on the other hand, did not efficiently afford the desired adducts **116**-**117** but only forms traces of the desired compounds. 1D NMR experiments showed that the conversion of the corannulenes **54** and **104** into the desired compounds are low and even prolonged reaction times (1h, 2h, 6h) do not result in an efficient preparation of the desired compounds. In other attempts, the $AgPF_6$ was added to a cold solution of **54** or **104** with $[Ir(COE)_2(\mu_2\text{-}Cl)]_2$ but only traces of the desired **116**-**117** were detected. However the same procedure was applied successfully for the preparation of $[Ir(COE)_2(\eta^6\text{-}C_{20}H_{10})]PF_6$ (94% yield). Thus, the negative result with **54** and **104** is likely due to the different electronic properties of the substituted corannulene ligands.

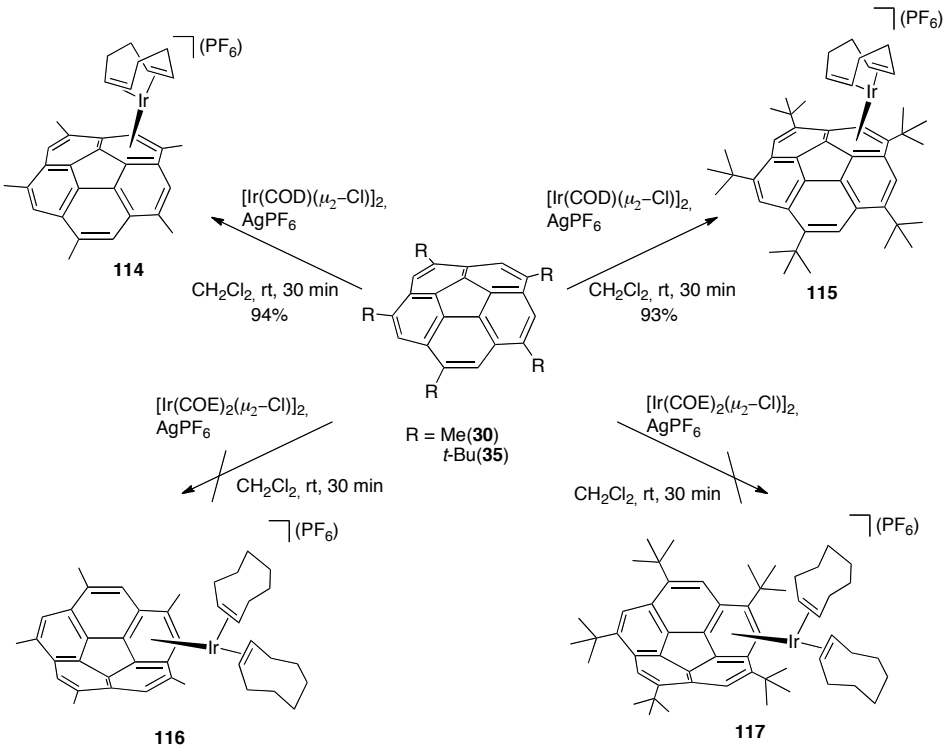

Scheme 3.7. Synthesis of the complexes 114 and 115.

Derivatives of compound **32** were expected to be model compounds for structural comparison (as previously reported with other aromatic compounds[22]) to the newly synthesized complexes presented above. Treatment of **32** with $[Ir(COD)(\mu_2\text{-}Cl)]_2$ or $[Rh(COD)(\mu_2\text{-}Cl)]_2$ in DCM solution with $AgPF_6$ afforded compounds **118A-B** and **119**, respectively (Scheme 3.8). The reaction of $[Ir(COD)(\mu_2\text{-}Cl)]_2$, $AgPF_6$ and **32** results in the formation of two products in a 1:1 ratio, as determined by ^1H NMR. In **118A**, the $[Ir(COD)]^+$ fragment is coordinated to a benzene ring whereas in **118B** it is coordinated to the naphthalene moiety. Upon heating to 360 K, a solution of the mixture in 1,1,2,2-tetrachloroethane-d_2, the proton signals (aromatic region) belonging to compound **118B** (**δ** (ppm) = 7.85, 7.76, 7.36, 7.30, 6.99, 6.60) disappear and only the proton signals accounting for **118A** are observed ((**δ** (ppm) = 8.06, 7.53, 6.44). This transformation is irreversible and, upon cooling, only **118A** is present in solution. These NMR observations led to the conclusion that **118B** is the kinetic product while **118A** is the thermodynamically more stable product. Furthermore, this isomerisation process likely occurs through an $\eta^6 \rightarrow \eta^4 (\eta^4) \rightarrow \eta^6$ migration process from the naphthalene ring to the benzene ring *via* the central five membered ring. A previous report by Muetterties[37] also showed a non selective binding of the metal fragment $[Ir(COD)]^+$ to anthracene. The reaction of anthracene with $[Ir(COD)(\mu_2\text{-}Cl)]_2$

in the presence of $AgBF_4$ afforded two complexes that were assigned to products in which the $[Ir(COD)]^+$ is coordinated, in one case, to one of the side benzene rings and, in the other, to the central benzene ring, in a 3:1 ratio.

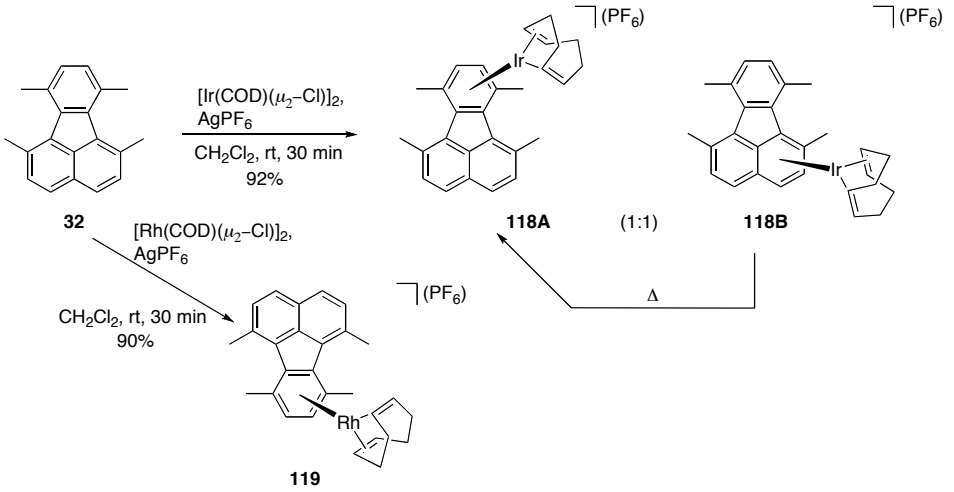

Scheme 3.8. Synthesis of compounds 118A-B and 119.

3.2.3. Crystal structure and results the DFT quantum chemical calculations

New structures of corannulene metal complexes were obtained. In particular, we report compound $[Rh(NBD)(\eta^6\text{-}C_{20}H_{10})]PF_6$ (**105**) and $[Rh(COD)(\eta^6\text{-}C_{20}H_{10})]PF_6$ (**120**) which were previously synthesized[22] but the X-ray crystal structure not solved.

Compound $[Rh(NBD)(\eta^6\text{-}C_{20}H_{10})]PF_6$, **105**, crystallizes from DCM/ether (Figure 3.21). The asymmetric unit contains one cation and one anion. The Rh(I) ion is bound in an η^6 mode to the *exo* face of corannulene. This binding mode was observed in corannulene complexes with $[Ir(COE)_2]^+$, $[Rh(COE)_2]^+$ and, $[Rh(COE)(i\text{-}Pr)_3P]^+$ metal fragments, and is also common in compounds with benzene and phenanthrene.[22] The average Rh–C bond lengths are 2.289(4) Å (for C1, C2, C7 and C8) for the *rim* and *hub* carbon atoms, whereas, for the metal-*flank*/*spoke* carbon, they are slightly longer 2.249(2) Å (Rh–C6) and 2.507(2) Å (Rh–C9) (Table 3.1). These bond lengths differences were also displayed in the previously reported derivatives from Dorta[22] in which a bending of the benzene ring towards the metal center, resulting in a boat-like conformation of the ring. Calculated values for the Rh-C bond length are in agreement with the experimental data within an average of 0.06 Å.

Table 3.1. Summary of the Rh–C bond length (Å) for complexes 105, 106, 107, 109, 110, 120, 121, 122.

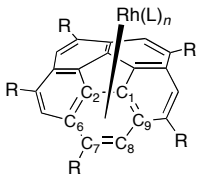

R = H, Me, *t*-Bu

Cor.	L	Com.	Rh-C_1	Rh-C_2	Rh-C_6	Rh-C_7	Rh-C_8	Rh-C_9
$C_{20}H_{10}$	NBD	**105**	2.283(2)	2.364(3)	2.429(2)	2.272(2)	2.255(2)	2.507(2)
			2.401	**2.439**	**2.574**	**2.299**	**2.298**	**2.531**
	COD	**120**	2.268(7)	2.274(7)	2.46(1)	2.26(1)	2.31(2)	2.431(8)
	$(COE)_2$	**121**[a]	2.385(4)	2.453(4)	2.472(3)	2.239(3)	2.262(3)	2.567(3)
	$(C_2H_4)_2$	**106**[b]	**2.377**	**2.289**	**2.465**	**2.279**	**2.270**	**2.548**
$C_{25}H_{20}$	$(C_2H_4)_2$	**109**	2.349(13)	2.281(12)	2.540(13)	2.291(12)	2.253(12)	2.420(13)
			2.342	**2.345**	**2.507**	**2.332**	**2.296**	**2.587**
	$(COE)_2$	**110**	2.384(4)	2.380(4)	2.532(4)	2.376(4)	2.291(4)	2.521(4)
			2.507	**2.455**	**2.617**	**2.465**	**2.393**	**2.644**
	NBD	**107**[b]	**2.410**	**2.378**	**2.528**	**2.316**	**2.277**	**2.544**
$C_{40}H_{50}$	NBD	**122**	2.279(4)	2.356(4)	2.444(4)	2.302(5)	2.241(5)	2.503(4)
			2.352(4)	2.352(4)	2.490(4)	2.312(4)	2.213(4)	2.438(4)

In bold the result from DFT quantum chemical calculation at the level TZVP + LANL2TZ+f. [a]data from ref. 22 for $[Rh(COE)_2(\eta^6\text{-}C_{20}H_{10})]PF_6$ (**121**) for comparison. [b]only calculated values for $[Rh(C_2H_4)_2(\eta^6\text{-}C_{25}H_{20})]PF_6$ (**106**) and $[Rh(NBD)(\eta^6\text{-}C_{25}H_{20})]PF_6$ (**107**).

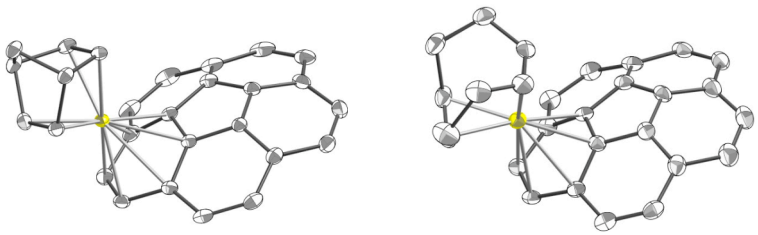

105 **120**

Figure 3.21. Crystal structures for compounds 105 and 120 (H omitted, 50% probability).

The structure of $[Rh(COD)(\eta^6\text{-}C_{20}H_{10})]PF_6$ (**120**) has been solved from a crystal obtained from a DCM/ether solvent system. The asymmetric unit contains one cation and one anion. The Rh-atom sits above one of the six-membered rings of the

corannulene moiety on the *exo* face in an η^6 mode (Figure 3.21). The entire corannulene moiety of the cation is disordered over a range of orientations that result from an in-plane twist of the bowl about a point approximately in the middle of the C1–C6 bond (Figure 3.22), which is one of the radial C–C bonds of the corannulene system. This disorder was modeled by defining two complete sets of atoms for the corannulene moiety. Refinement of the site occupation factor led to a value of 0.586(7) for the major orientation. Similarity restraints were applied to all sets of chemically equivalent bond lengths and angles within both orientations of the molecule. Neighbouring atoms within and between each orientation were restrained to have similar atomic displacement parameters. The restraints applied to the geometric and atomic displacement parameters tend to make the two orientations of the corannulene moiety look discrete. The unrestrained model suggests that the "wagging" motion of the corannulene moiety is dynamic and may adopt a continuum of orientations encompassed by the orientations employed in the restrained disordered model. The average Rh–C bond lengths are 2.268(4) Å, 2.274(7) Å, 2.26(1) Å, 2.31(1) Å (for C1, C2, C7 and C8) for the *rim* and *hub* carbon atoms, while, for the metal-*flank*/*spoke* carbon atoms, they are slightly longer 2.46(1) Å (Rh–C6) and 2.431(8) Å (Rh–C9) (Table 3.1).

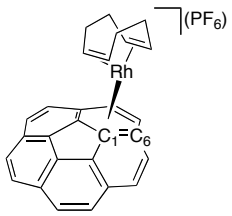

120

Figure 3.22. Structure of 120.

The structure of **109** was solved as $[Rh(C_2H_4)_2(\eta^6\text{-}C_{25}H_{20})]PF_6 \cdot 2(CH_2Cl_2)$ from a crystal obtained from DCM/pentane/ether. The metal is bound on the *exo* face in an η^6 fashion (Figure 3.23). Although the data appear to be reasonable and the diagrams look good, the R-factors remain high (9.4%). As a result, the geometric parameters have high standard uncertainties. The space group is centrosymmetric ($P2_1/n$), the cations, which possess a symmetry axis, are racemic. The asymmetric unit contains two cations and two anions, one of which is disordered, plus four molecules of CH_2Cl_2. The average Rh–C bond lengths are 2.349(13) Å, 2.281(12) Å, 2.291(12) Å,

2.253(12) Å (for C1, C2, C7 and C8) for the *rim* and *hub* carbon atoms, while for the metal-*flank*/*spoke* carbon atoms, they are slightly longer at 2.540(13) Å (Rh–C6) and 2.420(13) (Rh–C9) (Table 3.1). The blue value are data from quantum chemical calculation on the geometry of **109** and these results are in good agreement with the experimental values within an average 0.05 Å. Calculated values are also reported for the analogous compound $[Rh(C_2H_4)_2(\eta^6\text{-}C_{20}H_{10})]PF_6$ (**106**) and they display the same trend observed for the pentamethylcorannulene derivative and they have a mean difference of 0.04 Å.

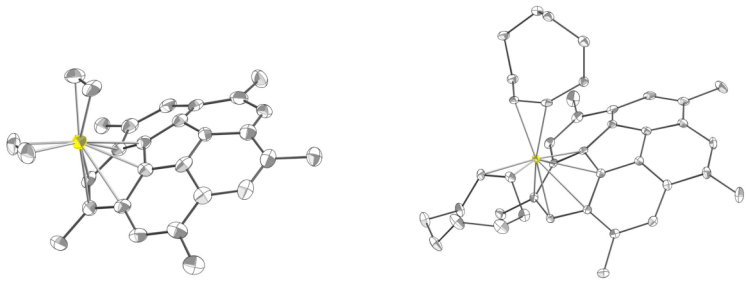

109 **110**

Figure 3.23. Crystal structure for compounds 109 and 110 (H omitted, 50% probability).

The structure of **110** was solved, from crystal grown from DCM/pentane/ether, as $[Rh(COE)_2(\eta^6\text{-}C_{25}H_{20})]PF_6{\cdot}2(CH_2Cl_2)$. The metal is bound on the *exo* face in an η^6 binding mode (Figure 3.23). Since the space group is centrosymmetric (P^{-},1), the compound in the crystal is racemic. The asymmetric unit contains one cation, one anion and two molecules of CH_2Cl_2. The PF_6^- anion and two CH_2 groups in one of the cyclooctene rings are disordered. The average Rh–C bond lengths are 2.348(4) Å, 2.380(4) Å, 2.376(4) Å, 2.291(4) Å (for C1, C2, C7 and C8) for the *rim* and *hub* carbon atoms, while, for the metal-*flank*/*spoke* carbon atoms, they are slightly longer 2.532(4) Å (Rh–C6) and 2.521(4) (Rh–C9) (Table 3.1). Compared to the previously reported analog compound $[Rh(COE)_2(\eta^6\text{-}C_{20}H_{10})]PF_6$ (**121**),[22] the Rh–C bond lengths are shorter in **110** for C1 and C2 but slightly longer in C7, C8, C6 and, C9. The calculated values for this compound are in agreement with the experimental data within an average of 0.1 Å.

Interesting is the different alignment of the metal fragment on the coordinated benzene ring in **109** and **110**. In **109** it is aligned with the methyl ring, while in **110** with the proton. Preliminary results on the difference in energy between the methyl-

aligned fragment with respect to the proton-aligned one **109** (Figure 3.24), in **33,** show a small difference of ca. 1.2 kcal mol^{-1}. Calculations on **110** are ongoing and will possibly help explaining this difference.

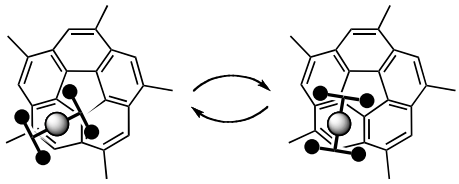

Figure 3.24. Different possible alignments for the metal fragment on pentamethyl derivatives.

A crystal of compound **111** was submitted for X-ray analyses and the result was surprising. Regression of the diffraction data revealed the structure to be $\{[Rh(NBD)]_2(\eta^6, \eta^6\text{-}C_{40}H_{50})\}(PF_6)_2 \cdot 1.5(Et_2O)$ (**122**, Figure 3.25). Two metal fragments are bound on the penta-(*t*-butyl)corannulene moiety and, they are both bound on the *exo* face. This double binding contrasts all of the η^6-dimetallated derivatives of corannulene reported so far where one metal is bound to the *exo*, and the other to the *endo* face.[16,17] This result also contrasts with our initial hypothesis that an increased bulckiness of the substituents in *sym*-pentasubstituted derivatives might lead to coordination at the central five-membered ring. The reported structure for **104**,[38] shows a bowl depth of 0.72 Å, which is a remarkable decrease with respect to that of the parent compound **1** (0.875 Å). This difference could favor coordination to more than one metal center. Although the quality of the crystal was low and the refinement only partially successful (R = 8.9%) some considerations can be made. The average bond lengths in the two fragments are similar for the Rh–C distances in C1, C2, C7 and C8 (Table 3.1) and slightly longer for the Rh-C in C6 and C9.

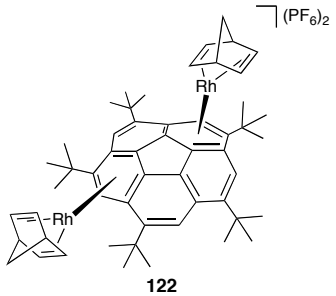

122

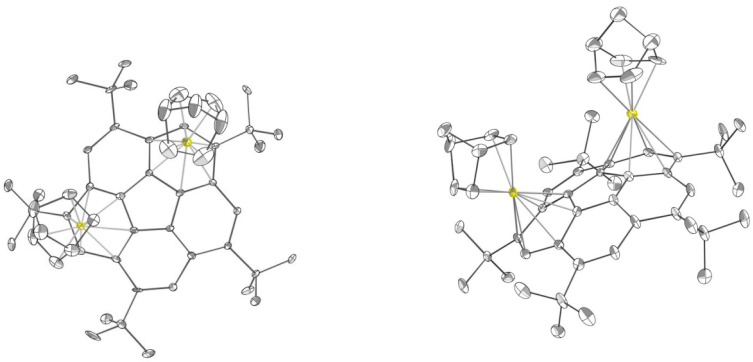

Figure 3.25. Crystal structure of 122, side view (left) and top view (right).

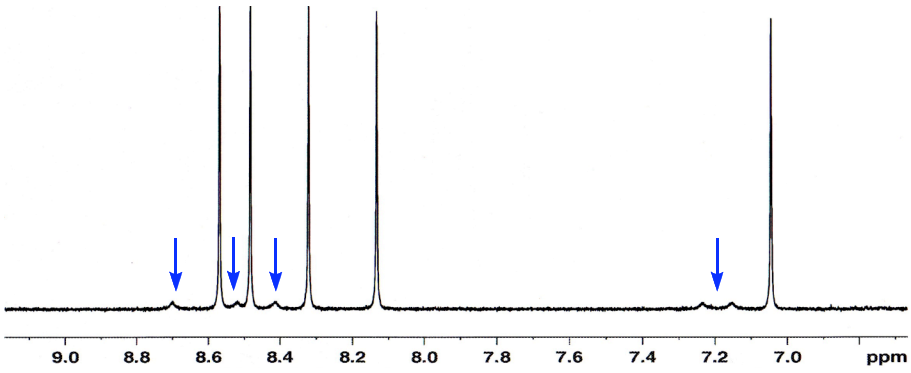

Figure 3.26. ^{1}H NMR of the aromatic region of mixture of compounds 11 (major) and 122 (minor).

A retrospective analyses of the ^{1}H NMR data of **111** showed the presence of five resonances in the coordinated **104** (aromatic region only), plus a second set in which two protons, in the same region, were shifted up-field instead of one (Figure 3.26). This observation is consistent with the presence of the complex $\{[Rh(NBD)]_2(\eta^6, \eta^6\text{-}C_{40}H_{50})\}(PF_6)_2$ (**122**).

The structure and novelty of compound **122** led us to put some efforts into understanding how it could have formed. One proposal is that during the first reactions, when the isolation methodology was not robust, the compound was crystallized several times from DCM/pentane/ether and always resulted in a viscous oil. It is likely that, under these conditions, some of the formed **111** might have decomposed, resulting in $[Rh(NBD)]^+$ fragments in solution. These fragments could have reacted with **111**, possibly forming **122**. All attempts that were made to selectively prepare **122** did not lead to the desired compound (Scheme 3.9). One

possibility for its formation was the reaction of **104** in the presence of one equivalent of the desired $[Rh(NBD)(\mu_2\text{-}Cl)]_2$ with $AgPF_6$ to afford **122** but none of the desired compound was observed (direct synthesis); instead **111** was obtained. Treatment with more equivalents of metal led to the same negative result. An alternative route could have been a stepwise synthesis, starting with formation of **111** and then a reaction with a second equivalent of the metal fragment to afford **122**. However, this reaction also resulted in isolation of **111**. A possible reason for this unsuccessful result could be that the excess $[RhNBD]^+$ can react to form dimers and trimers of norbornadiene as observed by Katz [39] and this path removes the metal from the solution avoiding the formation of the desired **122**.

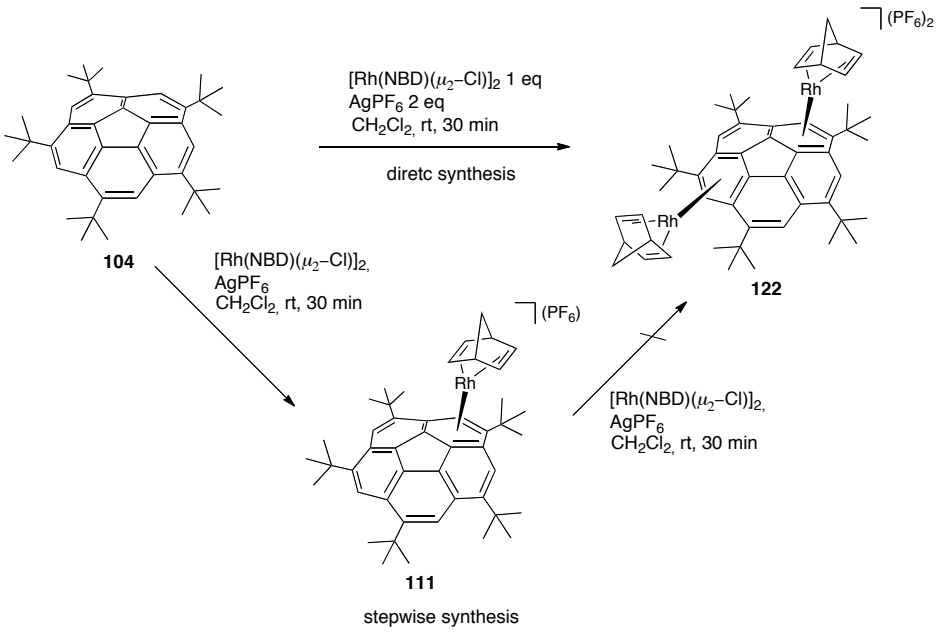

Scheme 3.9. Attempted synthesis of 122.

The structures of the model compounds **118A** and **119** were solved from crystals grown, in both cases, from DCM/pentane/ether. The solved structures were the expected complexes $[Ir(COD)(\eta^6\text{-}C_{20}H_{18})]PF_6$ and $[Rh(COD)(\eta^6\text{-}C_{20}H_{18})]PF_6$, respectively (Figure 3.27). The unit cell, in both cases, contains four cations and four anions. The metals are bound to the benzene ring in an η^6 fashion. The average M–C bond lengths are comparable with those observed for the corannulene derivatives (Table 3.2). The longer bond length is observed in both cases between the metals and C6.

Table 3.2. Summary of Rh–C bond length (Å) for 118A and 119.

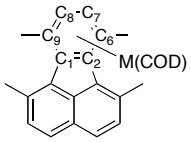

Compound	M-C_1	M-C_2	M-C_6	M-C_7	M-C_8	M-C_9
118A	2.347(2)	2.262(2)	2.415(2)	2.327(2)	2.220(2)	2.343(2)
119	2.253(2)	2.340(2)	2.401(3)	2.319(3)	2.216(3)	2.334(3)

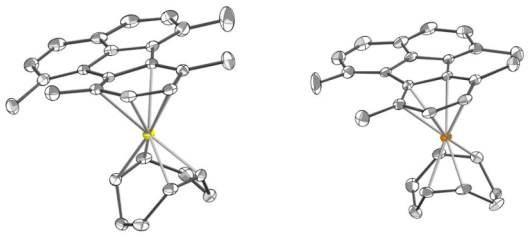

118A **119**

Figure 3.27. Crystal structure of 118A and 119 (H omitted, 50% probability).

The DFT calculations also provided molecular parameters, HOMO/LUMO energies and electrostatic potential map, in addition to the Rh-C(corannulene) bond lengths for compounds **105**, **106**, **107**, **109**, **110**. The distances between the metal centers and the carbons on the olefinic ligands are denominated Rh-$C_{A\text{-}D}$ (Table 3.3). For the corannulene series, the average bond length are slighter shorter for the NBD derivative (**105**, 2.154(4) Å exp.) with respect to the diethylene (**106**, 2.164 Å calc.). In the pentamethyl series, the COE complex shows the longest bond lengths (**110**, 2.164(4) Å) with respect to diethylene (**109**) and NBD (**107**) where they are similar (average 2.144 Å but for the 109 the R = 9.4% and thus the uncertainties high, 0.018Å). The calculated values are in agreement with the experimental.

Table 3.3. Distances Rh-C(olefin) in Å.[a]

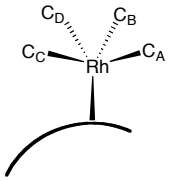

Cor.	L	Com.	Rh-C_A	Rh-C_B	Rh-C_C	Rh-C_D
$C_{20}H_{10}$	NBD	**105**	2.214(2) **2.120**	2.116(2) 2.**117**	2.140(2) **2.169**	2.148(2) **2.176**
	$(C_2H_4)_2$	**106**	**2.140**	**2.150**	**2.185**	**2.181**
$C_{25}H_{20}$	$(C_2H_4)_2$	**109**	2.126(9) **2.137**	2.140(9) **2.137**	2.150(9) **2.193**	2.16(1) **2.187**
	$(COE)_2$	**110**	2.183(3) **2.185**	2.138(3) **2.145**	2.172(4) **2.206**	2.164(4) **2.208**
	NBD	**107**	**2.114**	**2.115**	**2.171**	**2.177**

[a] In bold result of DFT quantum chemical calculations at the level TZVP + LANL2TZ+f.

Table 3.4. Bond angles as explained from the scheme.

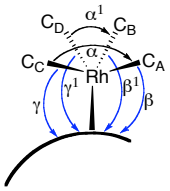

1	L	Com.	α	α^1	β	β^1	γ	γ^1
$C_{20}H_{10}$	NBD	**105**	66.51(9) **66.56**	66.7(1) **66.3**	106.72(8) **103.2**	104.42(9) **103.7**	108.67(8) **105.9**	107.29(8) **106.0**
	$(C_2H_4)_2$	**106**	**88.0**	**89.0**	**94.5**	**95.1**	**94.7**	**94.7**
$C_{25}H_{20}$	$(C_2H_4)_2$	**109**	88.7(4) **88.2**	89.4(4) **88.98**	95.4(3) **94.6**	99.8(4) **95.3**	98.6(4) **94.3**	97.6(3) **95.2**
	$(COE)_2$	**110**	87.5(2) **87.3**	84.3(2) **86.6**	100.0(1) **88.2**	99.6(2) **100.9**	102.7(1) **99.5**	97.8(3) **99.1**
	NBD	**107**	**66.55**	**66.32**	**103.2**	**102.2**	**106.3**	**105.6**

[a] In bold result of DFT quantum chemical calculations at the level TZVP + LANL2TZ+f.

The bond angles are shown in Table 3.4, according to the reported scheme. The angles α and α^1 are significantly smaller in the NBD derivatives **105** (66.6(1)°, exp.) and **107** (66.4°, calc.). For the diethylene compounds **106** and **109**, the average angles α and α^1 are in the range 88.0-89.4°(exp. and calc.) and for the COE derivative, **110**, 84.3-87.5° (exp.). The calculated values are in good agreement with the experimental values. The angles β, β^1, γ and γ^1 are defined in the plane between the corannulene surface and various Rh-C_{A-D} bonds. Compound **105** and **107** show angles in the range 104.42(9)-108.67(8)° and 102.2-106.3°(calc.), respectively. The derivatives **106** and **109** have angles in the range 94.5-95.1° (calc.) and 95.4(3) 99.8(4)° (exp.), respectively. Compound **110** has angles in the range 97.8(3)-100.0(1)°. These data for the angles show similar results for the COE and diethylene series.

A closer look at the calculated orbital energies (Figure 3.28) for LUMO and HOMO to HOMO-8, show that the LUMO and HOMO energies are higher for the COE derivative and the lower energies are found for the diethylene derivatives. Furthermore, the LUMO and HOMO energies of the complexes, for a given olefinic ligand, are always lower for the corannulene derivative with respect to the pentamethyl derivatives and, within the corannulene and pentamethyl series, the energies decrease in the order COE<NBD<diethylene. These data are supported by the values of the calculated (TZVP + LANL2TZ+f) dissociation energies for the pentamethyl series. Compounds **110**, **107** and **109** have dissociation energies equal to 40.90, 62.53, 63.80 kcal mol^{-1}, respectively, confirming the trend observed for the HOMO and LUMO energy levels.

The molecular orbital pictures are shown in Tables 3.5-3.7. Specifically, Table 3.5 shows that compound **106** and **109** display a similar nodal and phase pattern for the LUMO and from HOMO to HOMO-2. In Table 3.6 and 3.7, a comparison of the pentamethyl series show that, for LUMO and HOMO to HOMO-1, similar nodal and phase patterns are also present, although the energies are different as shown in Figure 3.28. Corannulene and pentamethylcorannulene also show similar nodal and phase pattern (see experimental section).

The electrostatic potential map for **105**, **106**, and **110** provided in Table 3.8 shows that the charge densities are localized either on the *rim* carbon atoms opposite to the side where the metal is bound or on the methyl groups. The LUMO and HOMO densities

reveal that the electron density is strongly localized on the olefinic ligand and that at least one of the benzene rings of corannulene, opposite to the coordinated one, displays a low electron density.

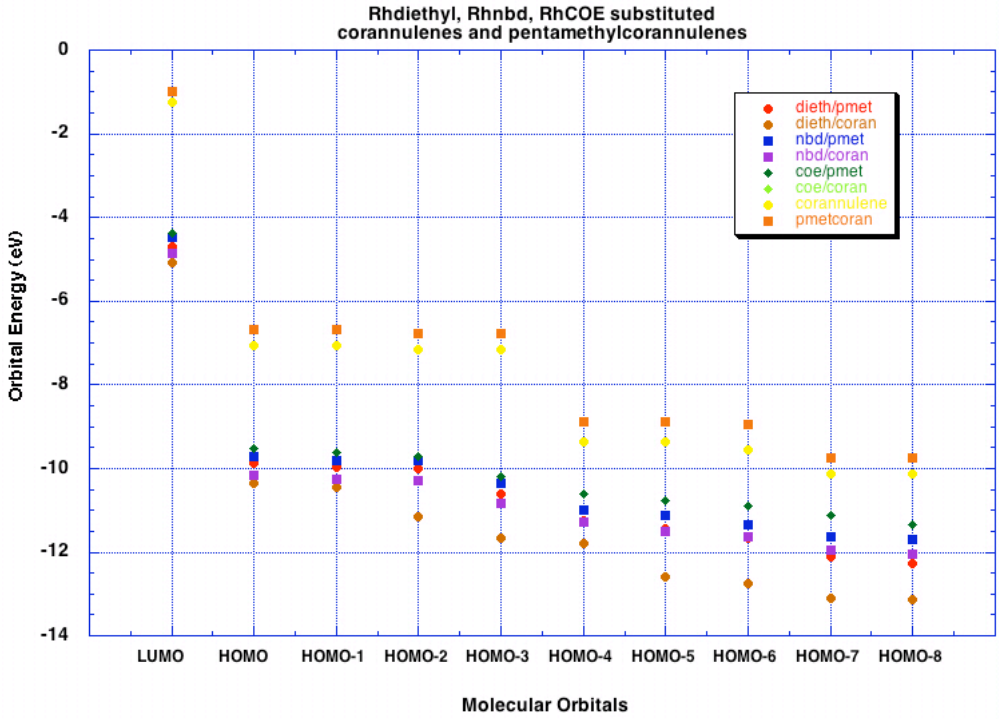

Figure 3.28. Plot of HOMO and LUMO Energy levels for selected compounds calculated at the level TZVP + LANL2TZ+f.

Table 3.5. $[Rh(C_2H_4)_2]$ complexes with different ligands: $C_{25}H_{20}$ and $C_{20}H_{10}$[a]

Orbital	$[Rh(C_2H_4)_2(C_{25}H_{20})]$	$[Rh(C_2H_4)_2(C_{20}H_{10})]$
LUMO		
HOMO		
HOMO-1	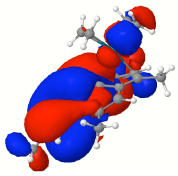	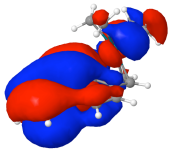
HOMO-2	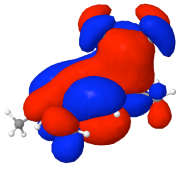	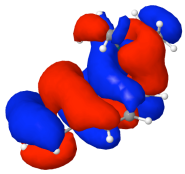
HOMO-3	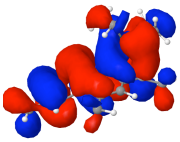	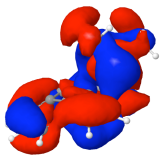
HOMO-4	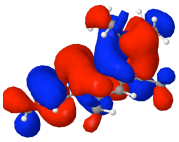	

[a] side views for LUMO and from HOMO to HOMO-4, calculated at the level TZVP + LANL2TZ+f.

Table 3.6. [Rh($C_{25}H_{20}$)] complexes with different ligands: COE, NBD, diethylene[a]

Orbital	[Rh(COE)$_2$($C_{25}H_{20}$)]	[Rh(NBD)($C_{25}H_{20}$)]	[Rh(C_2H_4)$_2$($C_{25}H_{20}$)]
LUMO	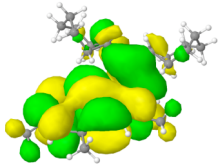	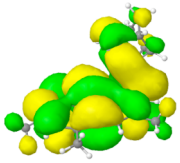	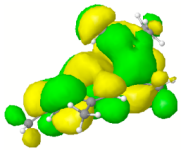
HOMO	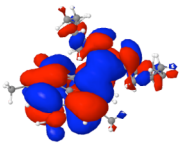		
HOMO-1		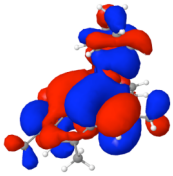	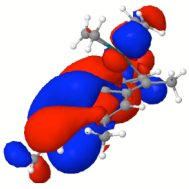
HOMO-2	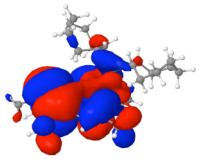		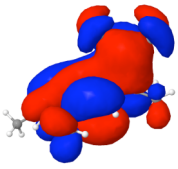
HOMO-3	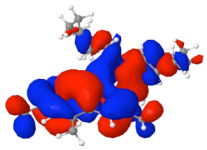	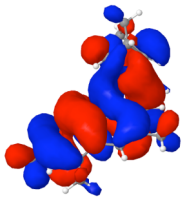	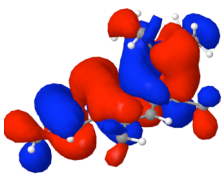
HOMO-4		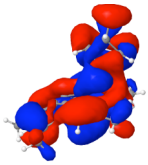	

[a] side views for LUMO and from HOMO to HOMO-4, calculated at the level TZVP + LANL2TZ+f.

Table 3.7. [Rh($C_{25}H_{20}$)] complexes with different olefinic ligands: COE, NBD, diethylene[a]

Orbital	[Rh(COE)$_2$($C_{25}H_{20}$)]	[Rh(NBD)($C_{25}H_{20}$)]	[Rh(C_2H_4)$_2$($C_{25}H_{20}$)]
LUMO	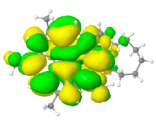	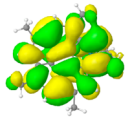	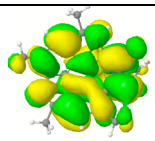
HOMO	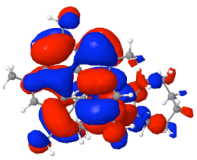	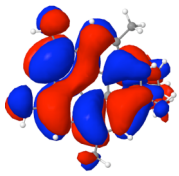	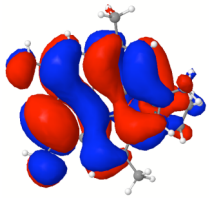
HOMO-1	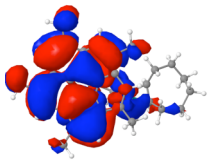	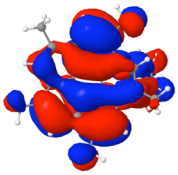	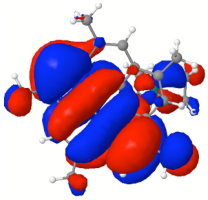
HOMO-2	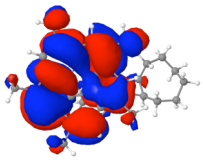	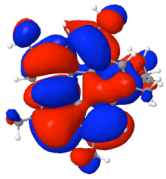	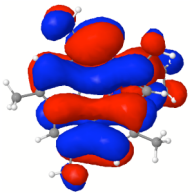
HOMO-3	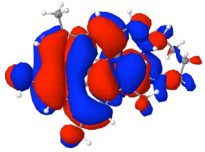	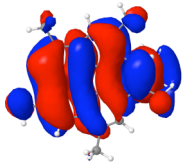	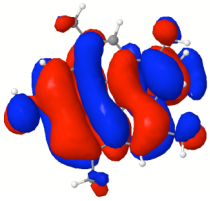
HOMO-4	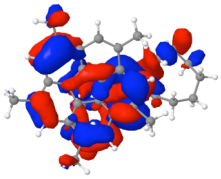	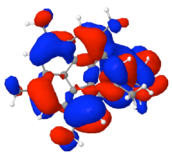	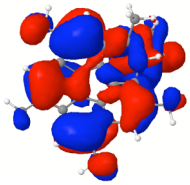

[a] bottom views for LUMO and from HOMO to HOMO-4, calculated at the level TZVP + LANL2TZ+f.

Table 3.8. Electrostatic potential map (EPM), HOMO and LUMO electron densities for 105, 106 and, 110.[a]

Compound	EPM	HOMO	LUMO
$[Rh(C_2H_4)_2(C_{20}H_{10})]$	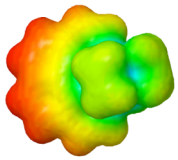	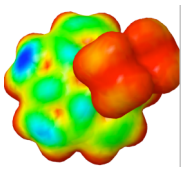	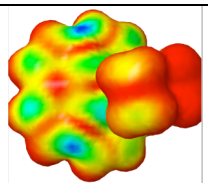
$[Rh(NBD)(C_{20}H_{10})]$	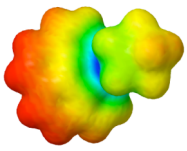	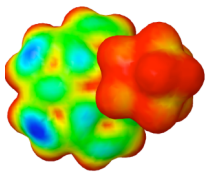	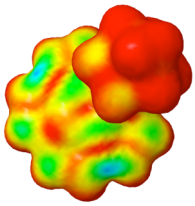
$[Rh(COE)_2(C_{25}H_{20})]$	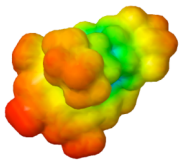	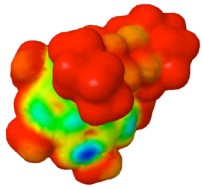	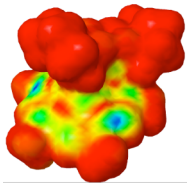

[a] calculated at the level TZVP + LANL2TZ+f. displayed only top views

3.2.4. NMR study

In this section, considerations about the dynamic properties of the compounds previously discudssed will be presented. It is important to take into account some symmetry considerations that will help to explain the structure of the ^{1}H NMR spectra 2D experiments that will be shown.

The lower symmetry of the 1,3,5,7,9-pentaallkylsubstituted derivatives will provide spectra that show five proton signals in the aromatic region if the exchange process is slow on the NMR timescale at a certain temperature. In a reported example,[22] this behavior was observed for $[Rh(COE)_2(\eta^6\text{-}C_{20}H_{10})]PF_6$ when cooled to 273 K. Slowing the migration process allows for the detection of five signals for the ten aromatic protons of corannulene. In the olefinic region, two proton signals A and B will be present when the rotation along the metal-corannulene bond is fast and the exchange between A and B is quick (balls represent olefin protons, fast rotation, **a**, and slowed, **b**. Figure 3.29). When the rotation is slowed the AB signals will result split in couples AA' and BB' and four proton signals observed (**b**, figure 3.29).

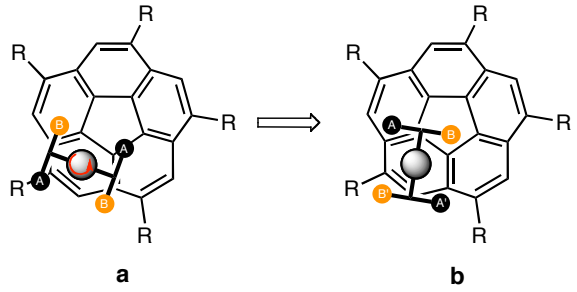

Figure 3.29. Schematic consideration of the effect of symmetry in the NMR spectra in complexes of C_5-symmetric substituted corannulene derivatives.

3.2.4.1. Observation and discussion on NMR data

3.2.4.1.1. Diethylene and COD compounds

In compounds **106** and **109**, corannulene (**1**) and pentamethylcorannulene (**54**) are bound to the metal fragment $[Rh(C_2H_4)_2]^+$. The ^{1}H NMR spectra of the two compounds show five proton signals in the aromatic region at 300 K. EXSY[40] experiments show that haptotropic ring migration does not occur. On the other hand, there is evidence that the ethylene ligands do rotate along the metal-ligand bond, as described in $[Rh(Cp)(C_2H_4)_2]$[41] and in other Rh and Ir complexes with indene and substituted derivatives.[42] Compound **106** shows a broad olefinic proton signal at

300 K while **109** shows split signals, although one of the two signals is overlapped with the methyl groups of pentamethylcorannulene (Figure 3.30, right).

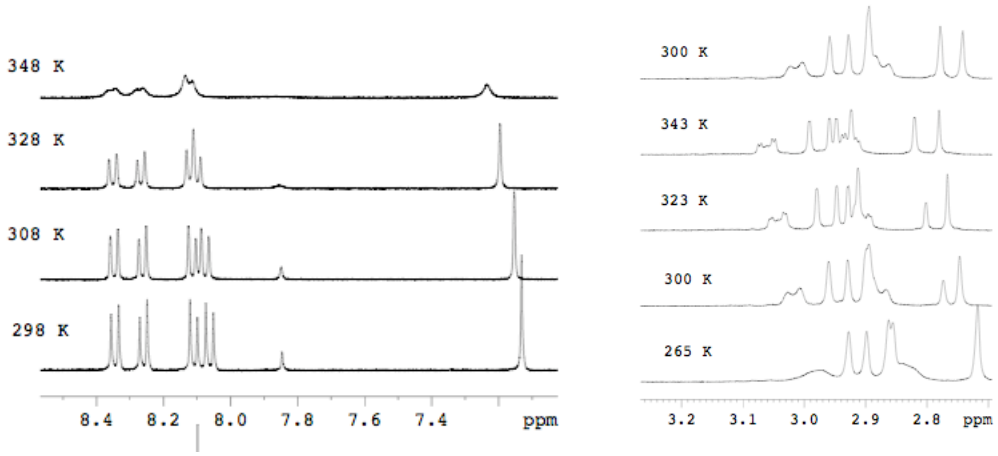

Figure 3.30. VT NMR for 106 (left) and 109 (right) in $C_2D_2Cl_4$.

Upon heating compound **109** decomposes as shown from the appearance of the free **54** (2.7 ppm). When **106** is warmed we can see (Figure 3.30, left) that the signals broadens in the aromatic region, but further increase of the temperature also leads to decomposition as described for **109**.

In the compounds **108** and **112** the corannulene derivatives **54** and **104** are bound to the metal fragment $[Rh(COD)]^+$. In compound **114** and **115** the same corannulene derivatives are bound to the metal fragment $[Ir(COD)]^+$. These four compounds show five proton signals in the aromatic region and do not show haptotropic ring migration as investigated by ESXY experiments. Upon heating, **108**, **112**, **114** and **115** show decomposition by release of the corannulene moiety. In the olefinic region, they show two proton signals due to fast rotation along the (M–L)–arene bond (Figure 3.29). This rotational behavior was also observed in other metal–arene systems.[43] All the complexes display decoalescence of the two olefinic protons into four signals upon cooling (Figure 3.31, **108**; Figure 3.33, **115**). The rotational barriers along the olefin-Rh-corannulene were calculated from the measured coalescence temperatures (T_c) according to the Gutowski-Holm approximation for equally populated signals.[44]

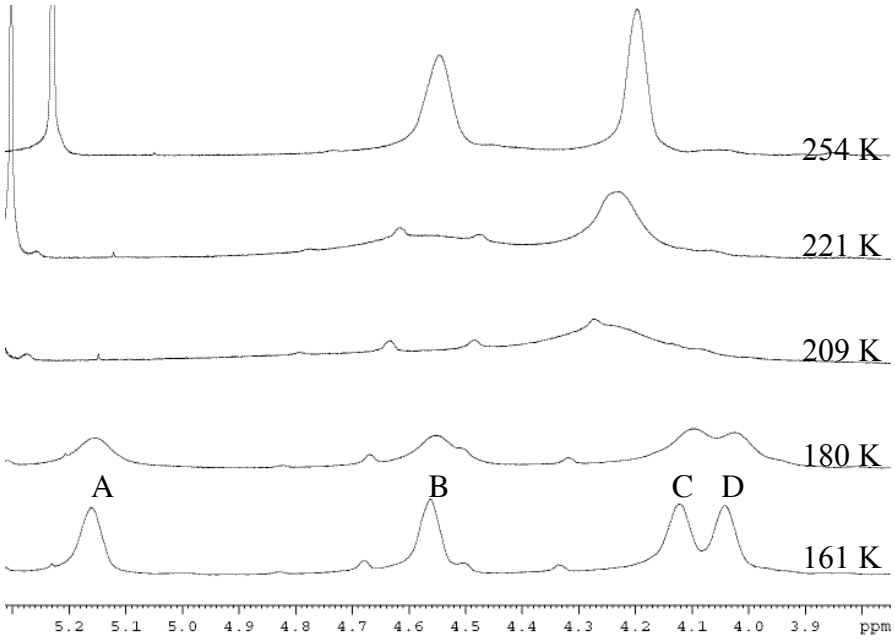

Figure 3.31. VT NMR for 108 in $CDFCl_2$.

The fact that the AB system splits into an ABCD pattern requires the determination of which protons are exchanging. For this purpose, a 2D EXSY experiment was performed on **108** at 170 K with mixing time (τ_m) of 0.5 ms. The result is shown in Figure 3.32 as example. The proton A-C and B-D are exchanging while A-B and C-D belong to the same double bond as established by COSY NMR. The same splitting pattern was observed for **112** in an analogous EXSY measurement. For compounds **114** and **115**, a splitting of the olefin protons of the type A-D/ C-B was observed whereas for **108** and **112** an A-B/ C-D type.

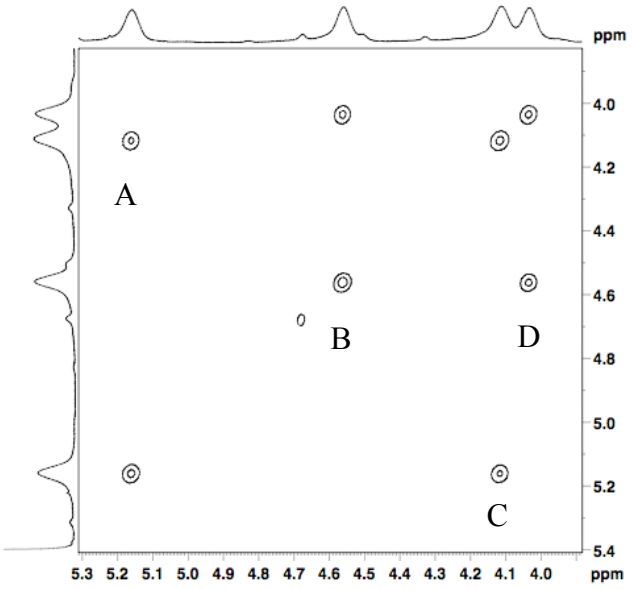

Figure 3.32. EXSY for 108 in $CDCl_2F$ at 170 K, τ_m = 0.5 ms.

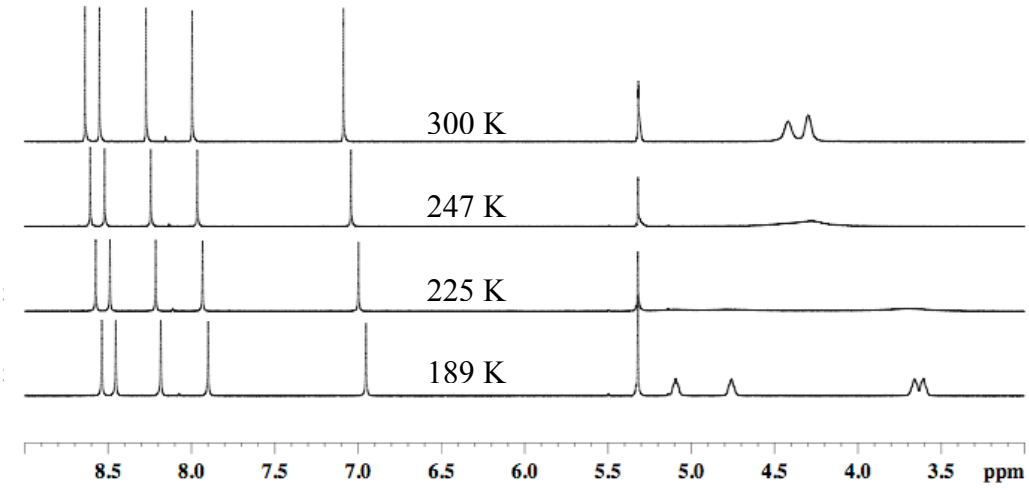

Figure 3.33. VT NMR for 115 in CD_2Cl_2.

The measurements resulted in the following calculated rotational barriers along the olefin-Rh-corannulenes bonds (Table 3.9): **108** (T_c = 209 K) $\Delta G^{\neq}$ = 38.8 ± 0.9 kJ mol^{-1}, **112** (T_c = 237 K) $\Delta G^{\neq}$ = 43.2 ± 0.3 kJ mol^{-1}, **114** (T_c = 237 K) $\Delta G^{\neq}$ = 42.7 ± 0.9 kJ mol^{-1}and, **115** (T_c = 247 K) $\Delta G^{\neq}$ = 45.0 ± 0.9 kJ mol^{-1} (**108** measured in $CDCl_2F$, **112**, **114**, **115** in CD_2Cl_2). The rotational barrier for **112**, **114** and **115** are of

the same magnitude and in agreement with the very small deviations reported for RhCpCOD and IrCpCOD.[43a] For compound **108** the barrier of rotation is significantly lower, possibly due to a weaker bond with the corannulene core together with the reduced steric interactions with the smaller methyl substituents. Fast rotation is restored upon warming to room temperature for all the compounds.

Table 3.9. Summary of rotational barrier along the olefin-Rh-(substituted corannulene) measured for selected compounds.

Compound	Formula	T_C (K)	Δν (Hz)	$\Delta G^{\neq}$ (kJ mol^{-1})
107	[Rh(NBD)($C_{25}H_{20}$)]PF_6	169	71.92 / 59.87[c]	[a]33.5 ± 0.2
108	[Rh(COD)($C_{25}H_{20}$)]PF_6	209	519.6 / 260.7[d]	[a]38.8 ± 0.9
114	[Ir(COD)($C_{25}H_{20}$)]PF_6	229	521.9 / 256.7[e]	[b]42.7 ± 0.9
112	[Rh(COD)($C_{40}H_{50}$)]PF_6	237	738.4 / 581.9[d]	[b]43.2 ± 0.3
115	[Ir(COD)($C_{40}H_{50}$)]PF_6	247	719.6 / 576[e]	[b]45.0 ± 0.3

[a]measured in $CDFCl_2$. [b]measured in CD_2Cl_2. [c] AB splitting of the bridge head and bridge protons signals of NBD. [d] AC/BD splitting of the olefinic protons of COD. [e] AB/CD splitting of the olefinic protons of COD.

3.2.4.1.2 NBD complexes

In compounds with the metal fragment $[Rh(NBD)]^+$, **105**, **107** and **111** multiple dynamic processes are observed. For **105**, two proton signals are observed in the aromatic region, one of which is very broad at 300 K. The broad signal and this signal splits into four upon cooling to 260 K to make a total of five. This result suggests a haptotropic migration on the corannulene core. Upon heating, a single signal is observed at 323 K.

Compound **107** displays five signals in the aromatic region and evidence from an EXSY NMR experiment suggests that ring migration is occurring on some time scale (this will be discussed in next session). Upon heating (in $C_2D_2Cl_4$), the five proton signals in the aromatic region coalesce to a broad singlet at 361 K. After cooling, **107** does not show significant decomposition displaying the typical splitting pattern described (Figure 3.34).

Low temperature NMR measurements (in $CDFCl_2$) showed that the two olefinic signals observed at 300 K splits in four as observed for the COD complexes. The same is observed for the proton on the bridge and on the bridgehead position, which split into two signals A-B and C-D respectively (Figure 3.35). The latter were used to evaluate the rotational barrier according to the coalescence approximation[44] resulting in a value for **107** of (T_c = 169 K) $\Delta G^{\neq}$ = 33.5 ± 0.2 kJ mol^{-1}. This value is significantly lower than the values observed for compounds **108**, **114**, **112** and **115**. This might be explained by the different orbital overlap due to the higher pyramidalization degree of the olefin double bond in NBD and, with the reduced steric interactions between the NBD and the methyl groups on the corannulene core.

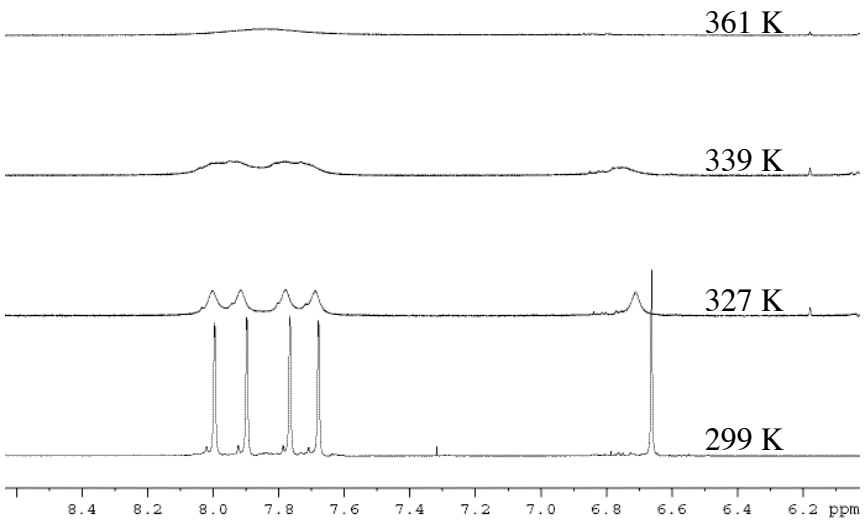

Figure 3.34. VT ^{1}H NMR for 107 in $C_2D_2Cl_4$.

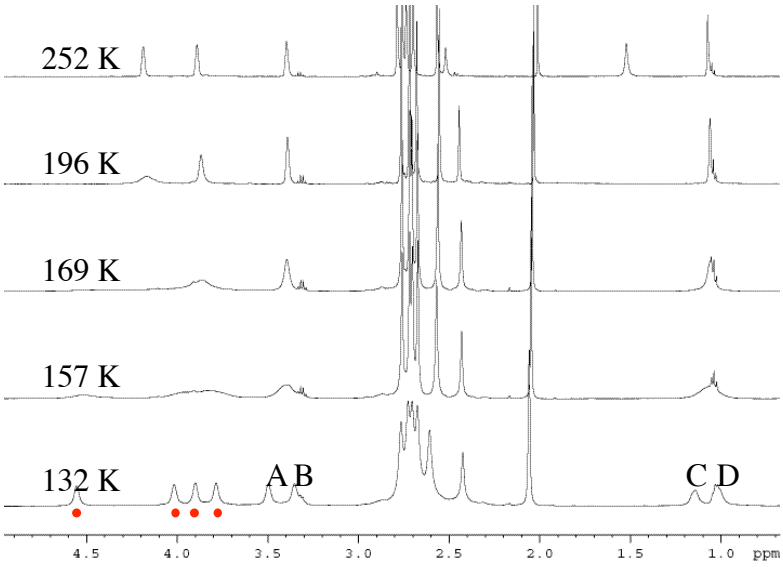

Figure 3.35. VT ^{1}H NMR for 107 in $CDFCl_2$ (red dots indicate the olefinic protons).

Compound **111** displays a set of five proton signals in the aromatic region and EXSY shows an exchange in magnetization among the set of signals suggesting that migration is occurring (this will be discussed in the next session). Upon heating the sample to 394 K, the five proton aromatic signals coalesce to a broad signal, which, upon cooling to room temperature, converts back to the set of five signals with partial decomposition displayed by the signal of free **104**.

To first approximation, we can observe that the ring migration process is faster in the complex with corannulene than in the alkyl substituted derivatives. A higher temperature is required for coalescencence to one signal in the aromatic region (**105** 323 K, **107** 363 K, **111** 394 K). In these systems, both rotation and migration are reversible.

3.2.4.1.3 $(COE)_2$ complexes

For complex **113**, a single signal is displayed in the aromatic region at 300 K, meaning that the migration on the corannulene core in fast. Upon cooling to 263 K, five proton signals for the aromatic region are observed (Figure 3.36).

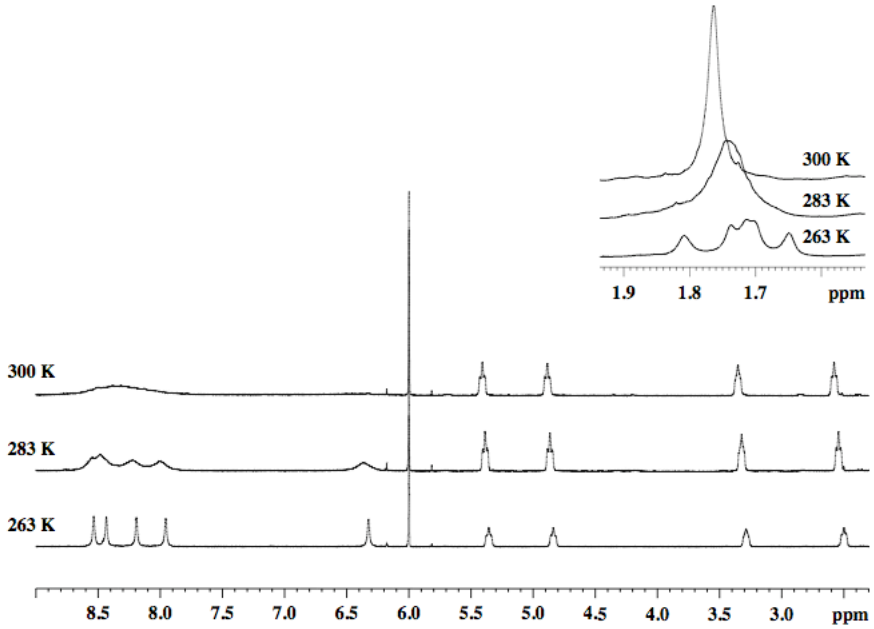

Figure 3.36. VT ^{1}H NMR for 113 in $C_2D_2Cl_4$.

An important observation is the existence of four proton signals in the olefinic region, meaning that rotation is slow on the NMR timescale. An EXSY experiment indicate that the olefinic protons exchange at 300 K but, the process is likely associated with the migration on the corannulene core. The EXSY experiment at 263 K confirms the migration process, by showing exchange of magnetization among the five aromatic signals. For the olefinic protons, the exchange is slow and exchange in magnetization among the signals is not seen, linking the olefinic exchange to a fast migration process. The observation of four olefinic proton signals is due to the asymmetric environment provided from the C_5-symmetric **104**. Thus, if the exchange process would be dissociative, the four signals in the olefinic region would not be observed while the migration occurs quickly.

The derivative **110** displays broad proton signals in the aromatic region at room temperature and, upon heating to 314 K, displays a broad signal in the aromatic region. When cooled at 263 K, a set of five aromatic protons is observed, typical of this series of compounds. At this low temperature, is clear that more than one species are present (Figure 3.37). These species could be a dimetallated compound as suggested by the traces signals in the aromatic region.

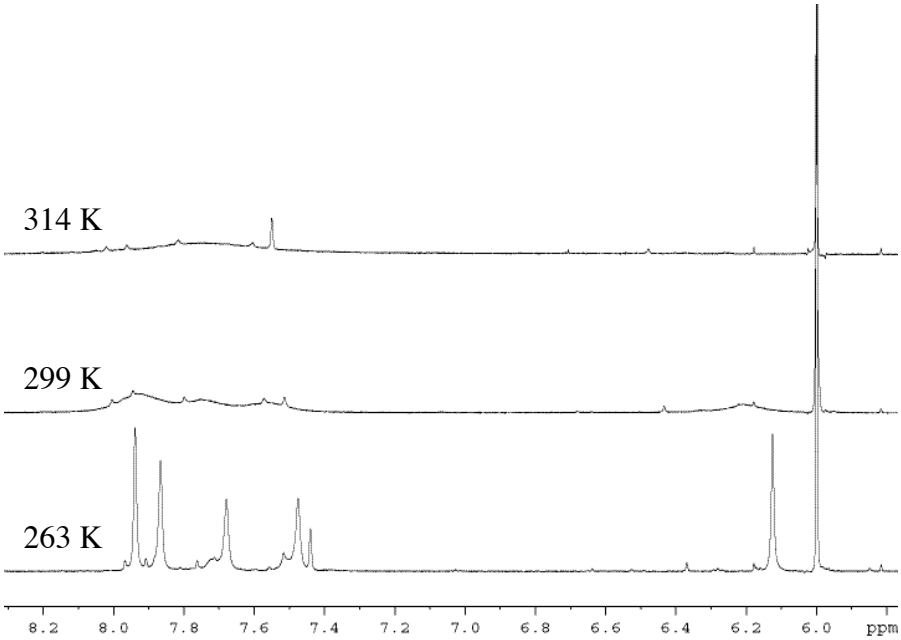

Figure 3.37. VT ^{1}H NMR for 110 in $C_2D_2Cl_4$.

Further cooling to 250 K (not shown) gives a spectrum in which a major and a minor compounds are observed as two sets of five-aromatic protons. The minor product displays also two small signal at 4.2 and 4.7 ppm. The nature of this minor product is, to date, unknown. Discussion of the olefinic region is impossible because of overlap with the methyl groups on **54**. Nevertheless, it is plausible to expect rotation of the $[Rh(COE)_2]^+$ moiety along the metal-corannuelne bond. Rotation of the COE ligands along the M-COE bond is possible as observed for ethylene in Rh and Ir compounds.[42] EXSY experiment showed exchange of magnetization between major and minor products but further investigations are necessary to elucidate the phenomenon.

In summary, diethylene and COD complexes show rotational dynamics only of the ML_2 fragments, whereas the NBD and COE complexes show more complex behavior in which rotation and migration are observed. There are empirical observations that 3rd row metals have slower ligand dynamics than 2nd row metals. The 2nd row is thought to be anomalously fast. In each pair **108**/**114** and **112**/**115**, this empirical rule is held (Table 3.9). Because methyl groups are smaller than *t*-butyl groups, the differences in rotational barriers (**32**<**37** and **39**<**40**) are likely due to the reduced steric interactions between the rotating ML_2 fragment and the alkyl substituents on the corannulene core (Table 3.9).

3.2.4.2. The migration path

It is clear that, in the complexes with the metal fragments [Rh(NBD)] and [Rh(COE)$_2$], haptotropic ring migration[32,45] occurs. In the case of corannulene, some hypotheses were given for compounds similar to the one discussed here.[22] The migration in corannulene could occur *via* a *hub* or a *rim* migration (Figure 3.38). Data suggested that in the reported case the migration was occurring *via* the *hub* path.

To study the migration path, the NMR technique of choice is 2D EXSY[40]. This experiment allows for the determination of the magnetization exchange rates for protons and is displayed as a cross-peak.[46] The intensities (volumes) of the cross-peak are related to the exchange magnetization rate. In our case, the system is composed of a proton (the one on the ring where the metal is coordinated) that exchanges with the other four aromatic signals of a typical complex of the series described herein.

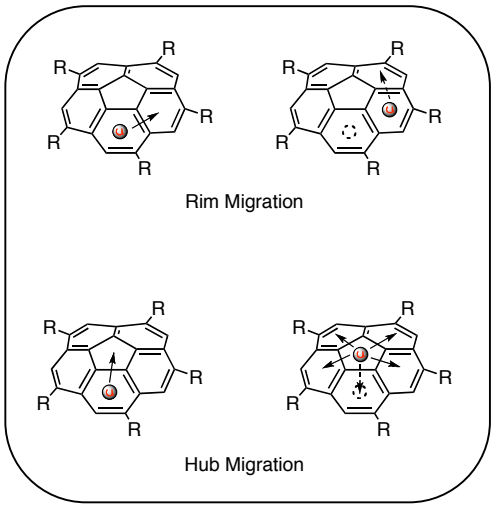

Figure 3.38. Possible migration path, associated with rotation, in substituted corannulene derivatives.

This substantially complicate system, was at first, believed to require a full matrix analyses (FMA)[47] for the determination of the exchange rate. A more careful look at the preliminary data for compounds **107**, **111** and **113**, together with the help of Prof. S. Macura,[48] unveiled the possibility to study this system by simply constructing the build up curves.[49] In fact, plotting the mixing time *vs* the intensity of the cross-peak, corrected for the diagonal peak volume, gave a curve in which slope is equal to the magnetization exchange rate.

The analyses requires the acquisition of the EXSY spectra at several different mixing times (τ_m = 1 μs, 0.02 s , 0.08s, 0.15 s, 0.30 s , 0.60 s, 1.00 s, 1.60 s , 2.20 s, 2.80 s for **107** and **111**). For each selected column (Figure 39 and Figure 3.40), the cross peaks were divided by the diagonal peak and a plots of $I = \left(\frac{I_{ij}}{I_{ii}}\right)$ *vs* τ_m were constructed. A total of twenty build up curves were plotted (see exp. Section) and they were fit to the parabolas with the zero order term = 0. The first terms of these parabolas are the magnetization exchange rates (k, s^{-1}). From the data, we can construct a scheme for which the twenty-five exchange rates are represented as a 5 x 5 matrix in which terms are k.

$$\begin{bmatrix} k_{11} & k_{12} & k_{13} & k_{14} & k_{15} \\ k_{21} & k_{22} & k_{23} & k_{24} & k_{25} \\ k_{31} & k_{32} & k_{33} & k_{34} & k_{35} \\ k_{41} & k_{42} & k_{43} & k_{44} & k_{45} \\ k_{51} & k_{52} & k_{53} & k_{54} & k_{55} \end{bmatrix} \quad (1)$$

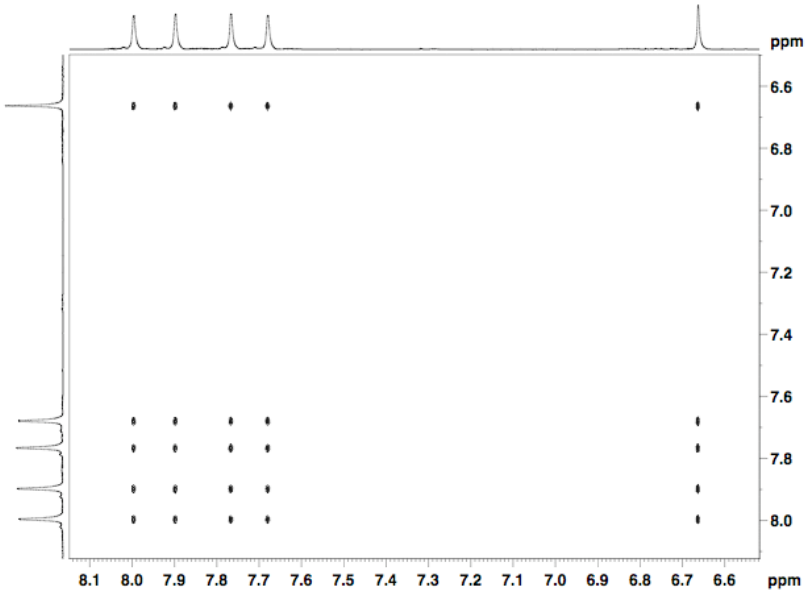

Figure 3.39. EXSY for 107 (τ_m = 2.2 s, T = 278 K, CD_2Cl_2).

For the compounds **107** and **111**, the analyses resulted in k values for the matrix (1) that were similar, suggesting that the *hub* path is favored for these two compounds. Thus, an $\eta^6 \rightarrow \eta^5 \rightarrow \eta^6$ migration process occurs. The values of the exchange rates (k, s^{-1}) and $\Delta G^{\neq}$ (kJ mol^{-1}) are listed in Table 3.10. In particular **107**, (Figure 3.39) shows a

$\Delta G^{\neq}$ in the range 68.3-68.8 kJ mol^{-1} (T = 277 and 282 K, CD_2Cl_2). The value for **111** (Figure 3.40) were calculated from a single measurement at 314 K and displays a $\Delta G^{\neq}$ of 76.8 kJ mol^{-1} (a second set of data was collected at 309 K but the result showed an anomalous reduction of some of the peak volumes, leading to the impossibility of extrapolating the k values correctly). At lower temperature **111** does not show appreciable exchange.

These observations suggest that the ligand-corannulene interactions is more likely stronger in **111** and it is probably due at the better overlap between the orbitals of the metal and the corannuelene. This observation is supported by calculations on the orbital energies for which, within a series having the same NBD ligand, the orbital energies are higher for the substituted derivative (Figure 3.28). By analogy the energy of the *t*-butyl derivative is likely higher with respect to the methylated one.

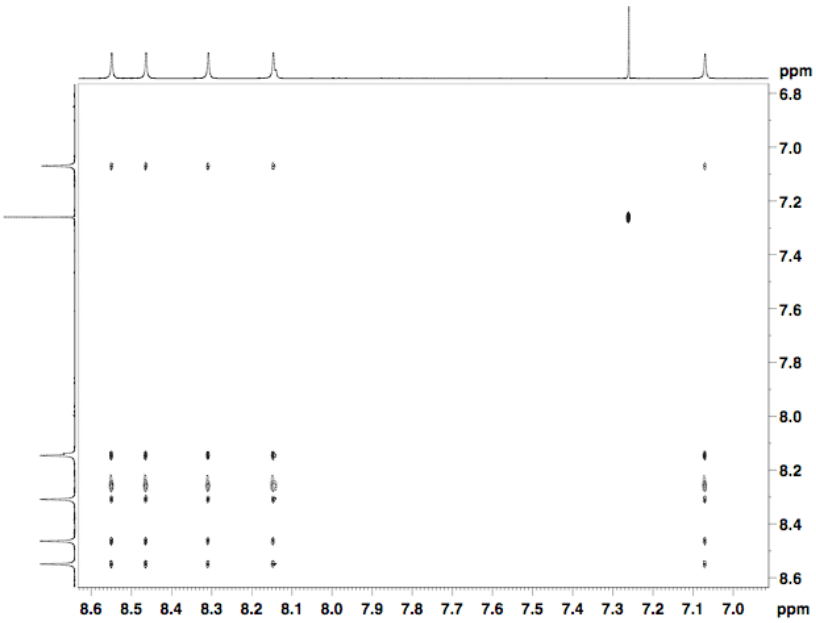

Figure 3.40 EXSY for 111 (τ_m = 2.2 s, T = 314 K, $CDCl_3$).

The reduced bowl depth in **104**[38] might facilitate the strength of the Rh-corannulene bond. A recent computational report on the effect of the curvature on the migration of $Cr(CO)_3$ suggests that an increased curvature makes the migration slower.[50] This contrasts our observation where **104** has a lower bowl depth with respect of **54**. Calculations are ongoing and will help to clarify this behavior.

For **113**, the data on the exchange of magnetization in the aromatic region showed a partial reduction of the volume of some exchange peaks, which does not

allow the use of the build up curve method for the determination of the *k*. On the other hand, it was possible to estimate the exchange rate of the olefinic protons (Figure 3.41). The procedure followed for this evaluation was similar to that used in **107** and **111** but was easier here because the system consists of a two-site exchange. The build-up curves were constructed and the values obtained for the exchange rates in (Table 3.10) calculated (see exp. Section) from measurement at τ_m = 1 μs, 0.20 s, 0.80 s, 0.15 s, 0.3 s, 0.5 s, 0.6 s, 1.00 s, 1.60 s at two different temperatures (302 and 297 K). The resulting $\Delta G^{\neq}$ are in the range 72.5-73.5 kJ mol^{-1} (T = 277 and 282 K, CD_2Cl_2).

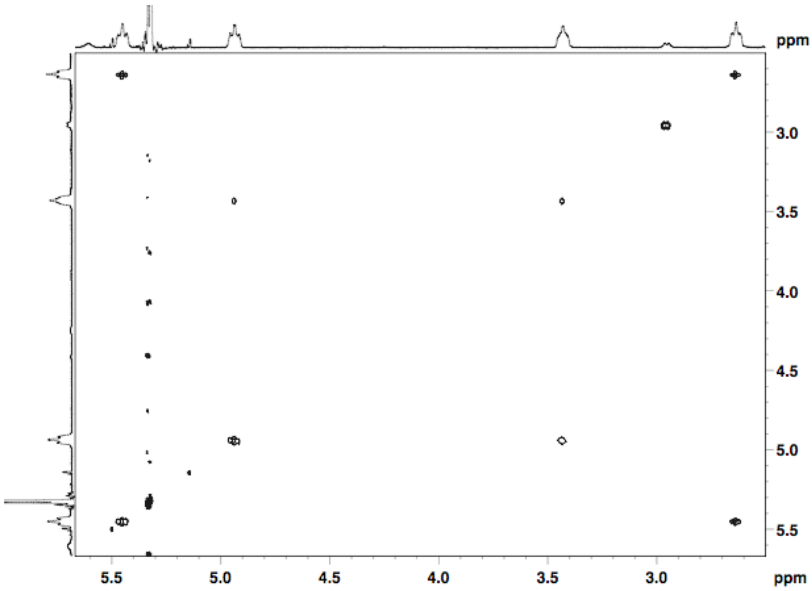

Figure 3.41. EXSY for 113 (τ_m = 1.6 s, T = 297 K, CD_2Cl_2).

Table 3.10. Summary of the calculated exchange rates and energy barriers of haptotropic migration for 107, 111 and, 113.

Compound	Formula	T (K)	k (s^{-1})	$^{c}\Delta G^{\neq}$ (kJ mol^{-1})
107	$[Rh(NBD)(C_{25}H_{20})]PF_6$ [a]	277	0.755 ± 0.030	68.3
		282	1.05 ± 0.02	68.8
111	$[Rh(NBD)(C_{40}H_{50})]PF_6$ [b]	314	1.11 ± 0.2	76.8
113	$[Rh(NBD)(C_{40}H_{50})]PF_6$ [a]	298	1.10 ± 0.05	72.5
		302	1.19 ± 0.04	73.5

[a]measured in CD_2Cl_2, [b]measured in $CDCl_3$ [c]calculated with the Eyring equation[51]

The data collected in this study for the dynamic properties of the selected compounds can be summarized with the overall motion shown in Scheme 3.10. The migration *via* the *hub* path is associated with a rotation along the Rh–corannulene bond in a mode described in the scheme.

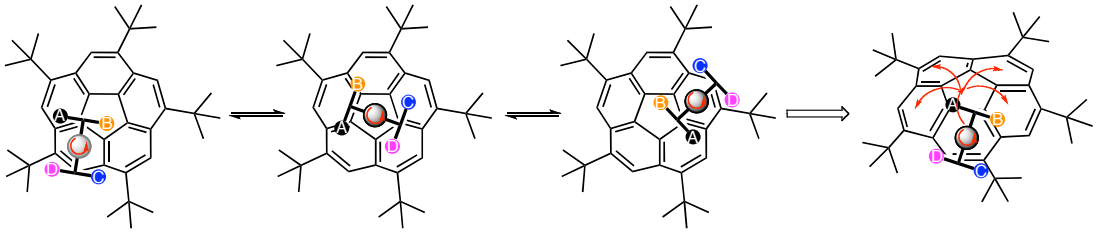

Scheme 3.10. The overall motion: (*hub*-migration)–rotation.

3.2.5. Conclusion

The VT-NMR study, together with EXSY experiments, has allowed for the establishment that the migration path in substituted corannulene occurs *via* the *hub* path. This migration is observed for the complexes with metal fragment RhNBD and $Rh(COE)_2$. In the RhNBD series, the energies of migration, as well as the exchange rates, result higher for **111**, and likely due to the stronger interaction between the corannulene and the metal fragment. The observations done for the olefinic protons in **113** suggest that the migration likely occurs intramolecularly, due to the consistent observation of split olefinic signals while the migration occurs. The other compounds with metal fragments Rh(COD), Ir(COD) and, $Rh(C_2H_4)_4$ show only rotational dynamics.

3.3. Experimental section

3.3.1. Material and methods

General: ^{1}H and ^{13}C NMR were recorded using Bruker AV2-400 (400 and 101 MHz) or AV2-500 using as internal reference the solvent. – 2D EXSY spectra were recorded on Bruker AV2-500 equipped with BBI probe (2048 x 256 data points and SW 3-3.3 Hz) at the mixing time indicated in the build-up curves section. The integration of the peak volume carried out with the Topspin 1.3 software from Bruker – ESI-MS: Bruker EsquireLC MS. – The operational NMR temperature were calibrated respect to DMSO for T > 300K and with respect to methanol for 160 < T < 273 K - Chromatography: Merck silica gel 60 (230–400 mesh) or Fluka neutral alumina (Brockmann I, Activity II). – Fluka acid washed celite was use for the organometallic complexes. – All experiments were carried out under nitrogen in anhydrous solvents (by passage on through alumina colums in a MC Brown solvent system and degassed with N_2 for organometallic complexes) unless otherwise noted. – Solvent for NMR spectroscopy were degassed with nitrogen and dried over molecular sieves. – Solvents for chromatography were technical grade and freshly distilled before use – Corannulene,[52] *sym*-pentachlororcorannulene,[53] *sym*-pentamethylcorannulene,[53] 1,3,5,7,9-penta(*t*-Butyl)corannuelene,[54] tetramethylfluoranthene,[52] Rh and Ir complexes were prepared according to the literature procedures and the spectral data in agreement with them.[55] All the other chemical were purchased – The synthesis of the organometallics complexes **35**-**36** were performed in a MCBrown glove box with a nitrogen atmosphere. – Reaction involving the use of silver salts were carried out in the dark.

3.3.2. Experimental procedures

[Rh(bicyclohepta[2.2.1]-2,5-diene)(corannulene)]PF_6 (105)

To a vial containing corannulene (25 mg, 0.100 mmol) and $[Rh(NBD)Cl]_2$ (23.0 mg, 0.050 mmol) in CH_2Cl_2 (0.5 ml) was added dropwise a solution of $AgPF_6$ (25.3 mg, 0.109 mmol) in CH_2Cl_2 (0.3 ml) and the mixture (yellow) stirred in the dark for 30 min. The resulting suspension was filtered through a pad of cotton/celite to eliminate the AgCl and the filtrate evaporated until ca. 0.1 ml. Ether (1.2 ml) and pentane (1 ml) were carefully layered and put in a freezer at -20 °C overnight. The resulting yellow

precipitate was decanted and washed with ether (2 x 2 ml) and pentane (2 x 1 ml) and dried in vacuo, yielding 42.5 mg (72%) of the desired compound.

^{1}H NMR (500 MHz, CD_2Cl_2, 233 K) δ (ppm) = 8.24 (d, *J* = 9.00, Hz 2H), 8.13 (d, *J* = 8.50, Hz 2H), 8.02 (s, 2H), 8.00 (s, 2H), 6.98 (s, 2H), 4.40-4.35 (br, 4H), 3.54-3.49 (br, 2H), 1.18-1.15 (br, 2H).

^{13}C NMR (125 MHz, CD_2Cl_2, 233 K) δ (ppm) = 140.0, 136.5, 133.6, 133.4, 133.0, 130.5, 128.8, 123.9, 119.0, 108.9, 97.7, 60.7 (d, $J_{Rh\text{-}C}$ = 6.88 Hz), 53.3 (d, $J_{Rh\text{-}C}$ = 9.00 Hz), 48.8

MS-ESI: m/z 445.2 $[RhC_{27}H_{18}]^+$ in chloroform. HRMS-ESI: calcd for $RhC_{27}H_{18}$: 445.0464; found: 445.0468

[Rh(ethylene)$_2$(corannulene)]PF$_6$ (106)

To a vial containing corannulene (20 mg, 0.080 mmol) and $[Rh(C_2H_4)_2Cl]_2$ (15.6 mg, 0.04 mmol) in CH_2Cl_2 (0.5 ml) was added dropwise a solution of $AgPF_6$ (20.2 mg, 0.08 mmol) in CH_2Cl_2 (0.2 ml) and the mixture (orange) stirred in the dark for 20 min. The resulting suspension was filtered through a pad of cotton/celite to eliminate the AgCl and the filtrate evaporated until ca. 0.1 ml. Ether (1 ml) and pentane (1 ml) were carefully layered and put in a freezer at -20 °C overnight. The resulting orange-red precipitate was decanted and washed with ether (2 x 2 ml) and pentane (2 x 1 ml) and dried in vacuo, yielding 26.6 mg (60%) of the desired compound (the product is not very soluble).

^{1}H NMR (400 MHz, $C_2D_2Cl_4$, 300 K) δ (ppm) = 8.34 (d, *J* = 9.20, Hz 2H), 8.26 (d, *J* = 8.80, Hz 2H), 8.11 (d, *J* = 8.80, Hz 2H), 8.06 (d, *J* = 9.20, Hz 2H), 7.13 (2, 2H), 3.14-3.10 (br, 8H).

^{13}C NMR (125 MHz, $C_2D_2Cl_2$, 300 K) δ (ppm) = 141.1, 135.6, 134.6 (2C), 133.5, 131.4, 129.4, 123.6, 119.5, 108.9 (d, $J_{Rh\text{-}C}$ = 2.25 Hz), 97.0 (d, $J_{Rh\text{-}C}$ = 4.00 Hz), 60.6

MS-ESI: m/z 403.2 $[RhC_{24}H_{18}]^+$ in chloroform. HRMS-ESI: calcd for $RhC_{24}H_{18}$: 403.0464; found: 403.0438

[Rh(bicyclohepta[2.2.1]-2,5-diene)(1,3,5,7,9-pentamethylcorannulene)]PF$_6$ (107)

To a vial containing 1,3,5,7,9-pentamethylcorannuelene (35 mg, 0.109 mmol) and $[Rh(NBD)Cl]_2$ (25.4 mg, 0.055 mmol) in CH_2Cl_2 (1.0 ml) was added dropwise a solution of $AgPF_6$ (27.6 mg, 0.109 mmol) in CH_2Cl_2 (0.5 ml) and the mixture (yellow)

stirred in the dark for 30 min. The resulting suspension was filtered through a pad of cotton/celite to eliminate the AgCl and the filtrate evaporated until ca. 0.1 ml. Ether (1.2 ml) and pentane (1 ml) were carefully layered and put in a freezer at -20 °C overnight. The resulting yellow precipitate was decanted and washed with ether (2 x 2 ml) and pentane (2 x 1 ml) and dried in vacuo, yielding 64.9 mg (90%) of the desired compound.

^{1}H NMR (500 MHz, CD_2Cl_2, 283 K) δ (ppm) = 7.98 (d, *J* = 1.1 Hz, 1H), 7.88 (d, *J* = 1.0 Hz, 1H), 7.75 (d, *J* = 1.0 Hz, 1H), 7.67 (d, *J* = 1.0 Hz, 1H), 6.63 (s, 1H), 4.35-4.27 (br, 2H), 4.07 -3,98 (br, 2H), 3.57-3.49 (br, 2H), 2.92 (d, *J* = 0.90, 3H), 2.88 (d, *J* = 0.96, 3H), 2.87 (d, *J* = 0.78, 3H), 2.83 (d, *J* = 0.78, 3H), 2.69 (s, 3H), 1.21-1.18 (br, 2H).

^{13}C NMR (125 MHz, CD_2Cl_2, 270 K) δ (ppm) = 144.6, 141.1, 138.9, 138.7, 135.2, 135.0, 134.4, 134.0, 133.6, 132.9, 129.0, 126.6, 124.9, 120.4, 119.3, 118.7, 110.9 (d, $J_{Rh\text{-}C}$ = 5.00 Hz), 108.1 (d, $J_{Rh\text{-}C}$ = 2.50 Hz), 106.9, 92.5 (d, $J_{Rh\text{-}C}$ = 5.00 Hz), 60.6 (d, $J_{Rh\text{-}C}$ = 7.50 Hz), 53.4 (d, $J_{Rh\text{-}C}$ = 10.0 Hz), 52.8 (d, $J_{Rh\text{-}C}$ = 10.0 Hz), 48.9 (d, $J_{Rh\text{-}C}$ = 2.50 Hz), 19.9, 19.5, 19.23, 19.17, 18.1.

MS-ESI: m/z 515.2 $[RhC_{32}H_{28}]^+$ in chloroform. HRMS-ESI: calcd for $RhC_{32}H_{28}$: 515.1246; found: 515.1241

[Rh(1,5-cyclooctadiene)(1,3,5,7,9-pentamethylcorannulene)]PF_6 (108)

To a vial containing 1,3,5,7,9-pentamethylcorannuelene (35 mg, 0.109 mmol) and $[Rh(COD)Cl]_2$ (27.1mg, 0.055 mmol) in CH_2Cl_2 (1.2 ml) was added dropwise a solution of $AgPF_6$ (27.6 mg, 0.109 mmol) in CH_2Cl_2 (0.5 ml) and the mixture (orange) stirred in the dark for 30 min. The resulting suspension was filtered through a pad of cotton/celite to eliminate the AgCl and the filtrate evaporated until ca. 0.1 ml. Ether (1.2 ml) and pentane (1 ml) were carefully layered and put in a freezer at -20 °C overnight. The resulting orange precipitate was decanted and washed with ether (2 x 2 ml) and pentane (2 x 1 ml) and dried in vacuo, yielding 69.5 mg (94%) of the desired compound.

^{1}H NMR (400 MHz, CD_2Cl_2, 273 K) δ (ppm) = 8.00 (d, *J* = 1.2 Hz, 1H), 7.93 d, *J* = 1.2 Hz, 1H), 7.79 (d, *J* = 1.2 Hz, 1H), 7.66 (d, *J* = 1.2 Hz, 1H), 6.64 (s, 1H), 4.55-4.62 (m, 2H), 4.21-4.29 (m, 2H), 2.93 (d, *J* = 1.2 Hz, 3H), 2.89 (d, *J* = 1.2 Hz, 3H), 2.87

(d, J = 1.2 Hz, 3H) 2.85 (d, J = 1.2 Hz, 3H), 2.74 (s, 3H), 2.13-2.24 (m, 4H), 1.93-2.24 (m, 4H).

^{13}C NMR (100 MHz, CD_2Cl_2, 273 K) δ (ppm) = 145.1, 141.7, 139.3, 139.0, 134.7 (d, J_{Rh-C} = 2.90 Hz), 134.4, 134.2, 134.0, 133.1, 129.1, 127.0, 125.3, 121.0, 119.2, 119.0, 112.5 (d, J_{Rh-C} = 3.70 Hz), 109.2 (d, J_{Rh-C} = 2.50 Hz), 106.8 (d, J_{Rh-C} = 2.90 Hz), 92.8 (d, J_{Rh-C} = 4.10 Hz), 83.5 (d, J_{Rh-C} = 12.4 Hz), 82.7 (d, J_{Rh-C} = 11.8 Hz), 31.4, 31.3, 20.0, 19.5, 19.3, 19.2, 18.0

MS-ESI: m/z 531.2 $[RhC_{33}H_{32}]^+$ in chloroform. HRMS-ESI: calcd for $RhC_{33}H_{32}$: 531.1559; found: 531.1564

[Rh(ethylene)$_2$(1,3,5,7,9-pentamethylcorannulene)]PF_6 (109)

To a vial containing 1,3,5,7,9-pentamethylcorannuelene (20 mg, 0.06 mmol) and $[Rh(C_2H_4)_2Cl]_2$ (12.1 mg, 0.03 mmol) in CH_2Cl_2 (0.5 ml) was added dropwise a solution of $AgPF_6$ (15.2 mg, 0.05 mmol) in CH_2Cl_2 (0.2 ml) and the mixture (orange) stirred in the dark for 20 min. The resulting suspension was filtered through a pad of cotton/celite to eliminate the AgCl and the filtrate evaporated until ca. 0.1 ml. Ether (1 ml) and pentane (1 ml) were carefully layered and put in a freezer at -20 °C overnight. The resulting orange-red precipitate was decanted and washed with ether (2 x 2 ml) and pentane (2 x 1 ml) and dried in vacuo, yielding 27.7 mg (83%) of the desired compound.

^{1}H NMR (500 MHz, CD_2Cl_2, 300 K) δ (ppm) = 8.06 (d, J = 1.0 Hz, 1H), 7.99 (d, J = 1.5 Hz, 1H), 7.84 (d, J = 1.0 Hz, 1H), 7.68 (s, 1H), 6.73 (s, 1H), 3.06-3.00 (m, 4H), 2.95 (d, J = 1.0 Hz, 3H), 2.93 (s, 3H), 2.91-2.87 (m, 10H), 2.75 (s, 3H).

^{13}C NMR (125 MHz, $CDCl_3$, 293 K) δ (ppm) = 145.3, 141.9, 139.38, 139.37 135.2, 135.0, 134.4, 133.9, 133.7, 133.0, 129.3, 127.2, 125.4, 120.8, 119.20, 119.17, 114.4 (d, J_{Rh-C} = 3.63 Hz), 108.1 (d, J_{Rh-C} = 2.63 Hz), 106.2 (d, J_{Rh-C} = 3.00 Hz), 95.1 (d, J_{Rh-C} = 4.00 Hz), 60.5 (d, J_{Rh-C} = 12.00 Hz), 19.9, 19.5, 19.3, 19.2, 17.3.

MS-ESI: m/z 479.3 $[RhC_{29}H_{28}]^+$ in chloroform. HRMS-ESI: calcd for $RhC_{29}H_{28}$: 479.1246; found: 479.1250.

[Rh(*cis*-cyclooctene)$_2$(1,3,5,7,9-pentamethylcorannulene)]PF_6 (110)

To a vial containing 1,3,5,7,9-pentamethylcorannuelene (40 mg, 0.125 mmol) and $[Rh(COE)_2Cl]_2$ (44.8 mg, 0.063 mmol) in CH_2Cl_2 (1.5 ml) was added dropwise a

solution of $AgPF_6$ (31.6 mg, 0.125 mmol) in CH_2Cl_2 (0.5 ml) and the mixture (orange) stirred in the dark for 30 min. The resulting suspension was filtered through a pad of cotton/celite to eliminate the AgCl and the filtrate evaporated until ca. 0.1 ml. Ether (2 ml) and pentane (1 ml) were carefully layered and put in a freezer at -20 °C overnight. The resulting orange-red precipitate was decanted and washed with ether (2 x 2 ml) and pentane (2 x 1 ml) and dried in vacuo, yielding 87.8 mg (89%) of mixture of compounds.

^{1}H NMR (500 MHz, CD_2Cl_2, 248 K, H = H major, **H** = H minor, H = H non assigned) δ (ppm) = 7.95 (s, 1H + 1**H**), 7.97 (s, 1**H**), 7.89 (s, 1H), 7.75 (s, 1**H**), 7.71 (s, 1H), 7.57 (s, 1**H**), 7.53 (s, 1H), 6.25 (s, 1**H**), 6.22 (s, 1H), 4.72-4.63 (br, 1**H**), 4.30-4.21 (br, 1**H**), 3.25-3.04 (m, 3H), 2.88 (br, 6H), 2.84—2.79 (m, 9H), 2.78-2.72 (br, 5H), 2.63-2.59 (m, 1H), 2.21-2.12 (m, 2H), 2.04-1.93 (m, 2H), 1.89-1.81 (m, 2**H**), 1.80-1.38 (m, 10H), 1.40-1.16 (m, 15H), 1.15-1.05 (br, 3H).

^{13}C NMR (125 MHz, CD_2Cl_2, 250 K) δ (ppm) = 145.7, 144.7, 141.2, 141.0, 139.7, 139.3, 139.0, 138.7, 136.4, 134.9, 134.25, 134.22, 133.9, 133.7, 133.6, 133.2, 132.4, 129.3, 128.8, 126.5, 126.1, 125.2, 125.1, 123.0, 121.5, 119.2 (d, J_{Rh-C} = 2.38 Hz), 118.9, 118.8, 116.7, 107.2 (d, J_{Rh-C} = 2.38 Hz), 94.5 (d, J_{Rh-C} = 2.75 Hz), 86.6, 78.6 (d, J_{Rh-C} = 12.25 Hz), 31.7, 31.5, 31.3, 31.2, 31.0, 30.2, 30.0, 29.3, 27.5, 27.1, 25.9, 25.7, 25.6, 25.5, 20.0, 19.9, 19.43, 19.37, 19.25, 19.19, 19.15, 19.0 16.9

MS-ESI: m/z 533.2 $[RhC_{33}H_{34}]^+$ in chloroform. HRMS-ESI: calcd for $RhC_{33}H_{34}$: 533.1716; found: 533.1714

[Rh(bicyclohepta[2.2.1]-2,5-diene)(1,3,5,7,9-penta(*t*-butyl)corannulene)]PF_6 (111)

To a vial containing 1,3,5,7,9-penta(*t*-Butyl)corannulene (43.2 mg, 0.080 mmol) and $[Rh(COD)Cl]_2$ (18.4 mg, 0.040 mmol) in CH_2Cl_2 (1.2 ml) was added dropwise a solution of $AgPF_6$ (20.2 mg, 0.080 mmol) in CH_2Cl_2 (0.3 ml) and the mixture (yellow) stirred in the dark for 30 min. The resulting suspension was filtered through a pad of cotton/celite to eliminate the AgCl and the filtrate evaporated. The yellow solid was washed with pentane (3 x 2 ml) and dried in vacuo, yielding 63.2 mg (91%) of the desired compound.

^{1}H NMR (400 MHz, CD_2Cl_2, 260 K) δ (ppm) = 8.53 (s, 1H), 8.44 (s, 1H), 8.28 (s, 1H), 8.10 (s, 1H), 6.96 (s, 1H), 4.02-4.05 (bs, 2H), 4.10-4.05 (m, 2H), 4.00-3.95 (m, 2H), 1.75 (s, 9H), 1.74-1.71 (m, 27H), 1.70(s, 9H), 1.17 (m, 2H).

^{13}C NMR (100 MHz, CD_2Cl_2, 260 K) δ (ppm) = 157.2, 153.5, 150.9, 146.1, 137.4, 135.3, 134.2, 131.5, 130.2, 129.9, 128.62, 128.56 (d, J_{Rh-C} = 3.60 Hz), 125.8, 124.6, 118.5, 117.1, 114.7, 109.5 (d, J_{Rh-C} = 2.70 Hz), 104.4 (d, J_{Rh-C} = 3.60 Hz), 90.9 (d, J_{Rh-C} = 3.90 Hz), 60.9 (d, J_{Rh-C} = 7.00 Hz), 54.1 (d, J_{Rh-C} = 9.30 Hz, DEPT 135), 50.2(d, J_{Rh-C} = 9.40 Hz), 48.7 (d, J_{Rh-C} = 2.00 Hz), 38.4, 37.82, 37.67, 37.64, 37.5 32.4 (2C), 32.2, 32.0, 31.9

MS-ESI: m/z 725.5 $[RhC_{47}H_{58}]^+$ in chloroform. HRMS-ESI: calcd for $RhC_{47}H_{58}$: 725.3594; found: 725.3560

[Rh(1,5-cyclooctadiene)(1,3,5,7,9-penta(*t*-butyl)corannulene)]PF_6 (112)

To a vial containing 1,3,5,7,9-penta(*t*-Butyl)corannulene (45.1 mg, 0.085 mmol) and $[Rh(COD)Cl]_2$ (21.0 mg, 0.043 mmol) in CH_2Cl_2 (1.5 ml) was added dropwise a solution of $AgPF_6$ (21.5 mg, 0.085 mmol) in CH_2Cl_2 (0.5 ml) and the mixture (orange) stirred in the dark for 30 min. The resulting suspension was filtered through a pad of cotton/celite to eliminate the AgCl and the filtrate evaporated The resulting orange solid was washed with pentane (2 x 1 ml) and dried in vacuo, yielding 65.7 mg (87%) of the desired compound.

^{1}H NMR (500 MHz, CD_2Cl_2, 300 K) δ (ppm) = 8.60 (s, 1H), 8.53 (s, 1H), 8.35 (s, 1H), 8.17 (s, 1H), 6.96 (s, 1H), 4.48-4.38 (br, 2H), 4.30-4.21 (br, 2H), 2.30-2.18 (m, 4H), 2.13-1.96 (m, 4H), 1.81 (s, 9H), 1.78 (s, 9H), 1.77 (s, 9H), 1.75-1.73 (br, 18H).

^{13}C NMR (125 MHz, CD_2Cl_2, 260 K) δ (ppm) = 157.9, 153.7, 151.2, 145.6, 137.8, 134.9, 133.3, 132.3, 131.4 (d, J_{Rh-C} = 3.13 Hz), 130.3, 130.0, 128.5, 125.8, 124.9, 118.2, 117.7, 116.5, 112.8 (d, J_{Rh-C} = 1.50 Hz), 101.1 (d, J_{Rh-C} = 3.50 Hz), 89.1 (d, J_{Rh-C} = 3.38 Hz), 80.9, 80.7, 77.3, 77.2, 38.5, 37.9, 37.8, 37.7, 37.5, 32.6, 32.4 (2C), 32.15, 32.12, 31.9, 31.2 (d, J_{Rh-C} = 4.13 Hz), 30.9, 29.8

MS-ESI: m/z 741.2 $[RhC_{48}H_{62}]^+$ in chloroform. HRMS-ESI: calcd for $RhC_{48}H_{62}$: 741.3907; found:_

[Rh(*cis*-cyclooctene)$_2$(1,3,5,7,9-penta(*t*-butyl)corannulene)]PF_6 (113)

To a vial containing 1,3,5,7,9-penta(*t*-Butyl)corannulene (30 mg, 0.057 mmol) and $[Rh(COE)_2Cl]_2$ (20.4 mg, 0.0285 mmol) in CH_2Cl_2 (1.2 ml) was added dropwise a solution of $AgPF_6$ (14.4 mg, 0.057 mmol) in CH_2Cl_2 (0.5 ml) and the mixture (orange) stirred in the dark for 30 min. The resulting suspension was filtered through a pad of

cotton/celite to eliminate the AgCl and the filtrate evaporated.The resulting orange-red solid was washed with (3 x 2 ml) and dried in vacuo, yielding 50.7 mg (89%) of the desired compound.

^{1}H NMR (500 MHz, $C_2D_2Cl_4$, 263 K) δ (ppm) = 8.53 (s, 1H), 8.43 (s, 1H), 8.19 (s, 1H), 7.95 (s, 1H), 6.32 (s, 1H), 5.36 (br, 1H), 4.84 (br, 1H), 3.28 (br, 1H), 2.50 (br, 1H), 1.81 (br, 9H), 1.77-1.67 (br, 27H), 1.65 (br, 9H), 1.59-1.43 (m, 4H), 1.38-1.16 (m, 10H), 1.16-0.98 (brm, 6H), 0.93 (br, 2H), 0.66 (br, 2H)

^{13}C NMR (125 MHz, CD_2Cl_2, 248 K) δ (ppm) = 157.9, 152.7, 150.4, 145.3, 138.4, 136.4, 133.8, 131.9, 130.9, 130.4, 129.1, 128.9, 125.3, 124.4, 122.1, 118.6, 118.2, 117.6, 104.0 (d, J_{Rh-C} = 2.88 Hz), 91.4, 85.9 (d, J_{Rh-C} = 12.75 Hz), 75.8 (d, J_{Rh-C} = 11.88 Hz), 73.3 (d, J_{Rh-C} = 12.88 Hz), 64.6 (d, J_{Rh-C} = 13.13 Hz), 38.2, 37.9, 37.7, 37.4, 37.3, 32.4, 32.3, 32.1, 31.95, 31.91, 31.6, 30.3, 30.1, 29.9, 27.7, 27.3, 26.9, 26.3, 26.0, 25.9, 25.7, 25.2

MS-ESI: m/z 743.6 $[RhC_{48}H_{64}]^+$ in chloroform. HRMS-ESI: calcd for $RhC_{48}H_{64}$: 743.4063; found: 743.4052

[Ir(1,5-cyclooctadiene)(1,3,5,7,9-pentamethylcorannulene)]PF_6 (114)

To a vial containing 1,3,5,7,9-penta(*t*-Butyl)corannulene (35 mg, 0.109 mmol) and $[Ir(COD)Cl]_2$ (36.9 mg, 0.055 mmol) in CH_2Cl_2 (1.5 ml) was added dropwise a solution of $AgPF_6$ (27.6 mg, 0.109 mmol) in CH_2Cl_2 (0.5 ml) and the mixture (orange) stirred in the dark for 30 min. The resulting suspension was filtered through a pad of cotton/celite to eliminate the AgCl and the filtrate evaporated until ca. 0.1 ml. Ether (1.0 ml) and pentane (1 ml) were carefully layered and put in a freezer at -20 °C overnight. The resulting orange precipitate was decanted and washed with ether (2 x 2 ml) and pentane (2 x 1 ml) and dried in vacuo, yielding 78.2 mg (94%) of the desired compound.

^{1}H NMR (400 MHz, CD_2Cl_2, 300 K) δ (ppm) = 8.06 (d, *J* = 1.2 Hz, 1H), 7.99 (d, *J* = 1.2 Hz, 1H), 7.75 (d, *J* = 1.2 Hz, 1H), 7.55 (d, *J* = 1.2 Hz, 1H), 6.73 (s, 1H), 4.62-4.53 (m, 2H), 4.39-4.31 (m, 2H), 2.96 (d, *J* = 1.6 Hz, 3H), 2.94 (d, *J* = 1.2 Hz, 3H), 2.85-2.83 (4, 6H), 2.78 (d, *J* = 1.2 Hz, 3H), 2.11-1.98 (m, 6H), 1.79-1.89 (m, 2H).

^{13}C NMR (100 MHz, CD_2Cl_2, 283 K) δ (ppm) = 148.2, 141.3, 140.4, 140.2, 135.0, 134.44, 134.37, 134.2, 133.2, 133.0, 131.2, 126.8, 126.3, 119.6, 117.9, 117.2, 105.4, 104.6, 98.9, 84.8, 68.3, 66.6, 33.3, 31.8, 20.2, 19.6, 19.24, 19.22, 17.4.

MS-ESI: m/z 621.2 $[IrC_{33}H_{32}]^+$ in chloroform. HRMS-ESI: calcd for $IrC_{33}H_{32}$: 621.2133; found: 621.2132

[Ir(1,5-cyclooctadiene)(1,3,5,7,9-penta(*t*-butyl)corannulene)]PF_6 (115)

To a vial containing 1,3,5,7,9-penta(*t*-Butyl)corannulene (40.0 mg, 0.075 mmol) and $[Ir(COD)Cl]_2$ (25.2 mg, 0.0375 mmol) in CH_2Cl_2 (1.5 ml) was added dropwise a solution of $AgPF_6$ (19.0 mg, 0.075 mmol) in CH_2Cl_2 (0.5 ml) and the mixture (orange) stirred in the dark for 30 min. The resulting suspension was filtered through a pad of cotton/celite to eliminate the AgCl and the filtrate evaporated. The resulting orange solid was washed with pentane (3 x 1 ml) and dried in vacuo, yielding 68.0 mg (93%) of the desired compound.

^1H NMR (500 MHz, CD_2Cl_2, 283 K) δ (ppm) = 8.63 (s, 1H), 8.54 (s, 1H), 8.27 (s, 1H), 8.00 (s, 1H), 7.08 (s, 1H), 4.61-4.15 (br, 4H), 2.12-1.99 (m, 4H), 1.99-1.88 (m, 2H), 1.79 (s, 9H), 1.75-1.73 (m, 27H), 1.67 (s, 9H).

^{13}C NMR (125 MHz, CD_2Cl_2, 283 K) δ (ppm) = 161.5, 153.5, 152.3, 145.3, 139.0, 135.2, 134.0, 131.6 (d, J_{Rh-C} = 4.88 Hz), 130.7, 129.9, 126.0, 125.8, 124.6, 117.4, 115.7, 115.1, 107.8, 94.9, 81.3, 76.7, 64.8, 38.8, 18.1, 37.8, 37.7, 37.6, 33.9, 32.6, 32.5, 32.4, 32.3, 31.8, 31.4

MS-ESI: m/z 831.7 $[IrC_{48}H_{62}]^+$ in chloroform. HRMS-ESI: calcd for $IrC_{48}H_{62}$: 831.4481; found: 831.4490

[Ir(COD)($C_{20}H_{18}$)]PF_6 (118)

To a vial containing tetramethylfluoranthene (40 mg, 0.155 mmol) and $[Ir(COD)Cl]_2$ (38.5mg, 0.078 mmol) in CH_2Cl_2 (1.2 ml) was added dropwise a solution of $AgPF_6$ (39.2 mg, 0.155 mmol) in CH_2Cl_2 (0.5 ml) and the mixture (orange) stirred in the dark for 30 min. The resulting suspension was filtered through a pad of cotton/celite to eliminate the AgCl and the filtrate evaporated until ca. 0.1 ml. Ether (1.2 ml) and pentane (1 ml) were carefully layered and put in a freezer at -20 °C overnight. The resulting orange precipitate was decanted and washed with ether (2 x 2 ml) and pentane (2 x 2 ml) and dried in vacuo, yielding 85.7 mg (90%) of the desired compound.

^1H NMR (500 MHz, $C_2D_2Cl_4$, 298 K) δ (ppm) = 8.06 (d, J = 8.2, 2H), 7.85 (d, J = 8.75, 1H[1]), 7.76 (d, J = 8.75, 1H[1]), 7.53 (d, J = 8.2, 2H), 7.36 (d, J = 7.75, 1H[1]), 7.30

(d, J = 7.75, 1H[1]), 6.99 (d, J = 6.25, 1H[1]), 6.60 (d, J = 6.25, 1H[1]), 6.44 (s, 2H), 4.08-4.15 (m, 2H[1]), 3.74-3.79 (m, 4H), 3.56-3.62 (m, 2H[1]), 3.16 (s, 3H[1]), 3.06 (s, 6H), 2.88 (s, 6H), 2.85 (s, 3H[1]), 2.76 (s, 3H[1]), 2,73 (s, 3H[1]), 2.01-2.10 (m, 4H+H[1]), 2,00-1.79 (m, 12 H+H[1]), 1.72-1.64 (m, 4H+H[1]).

^{13}C NMR (125 MHz, $C_2D_2Cl_4$, 298 K) δ (ppm) = 140.2, 140.1, 137.5, 137.4, 135.9, 135.2, 135.0, 134.9, 134.5, 133.13, 133.06, 129.6, 128.8, 128.3, 123.3, 121.4, 115.2, 114.2, 111.8, 109.8, 107.0, 105.9, 98.9, 97.4, 89.7, 69.6, 68.7, 68.1, 33.2, 33.08, 32.1, 26.6, 26.1, 25.2, 24.4, 23.7, 23.6.

MS-ESI: m/z 559.2 $[IrC_{28}H_{30}]^+$ in chloroform. HRMS-ESI: calcd for $IrC_{28}H_{30}$: 559.1977; found: 559.1980

$[Rh(COD)(C_{20}H_{18})]PF_6$ (119)

To a vial containing tetramethylfluoranthene (30 mg, 0.116 mmol) and $[Ir(COD)Cl]_2$ (38.9 mg, 0.058 mmol) in CH_2Cl_2 (1.2 ml) was added dropwise a solution of $AgPF_6$ (29.3 mg, 0.116 mmol) in CH_2Cl_2 (0.5 ml) and the mixture (orange) stirred in the dark for 30 min. The resulting suspension was filtered through a pad of cotton/celite to eliminate the AgCl and the filtrate evaporated until ca. 0.1 ml. Ether (1.2 ml) and pentane (1 ml) were carefully layered and put in a freezer at -20 °C overnight. The resulting orange precipitate was decanted and washed with ether (3 x 2 ml) and pentane (2 x 2 ml) and dried in vacuo, yielding 73.5 mg (90%) of the desired compound.

^{1}H NMR (500 MHz, $C_2D_2Cl_4$, 298 K) δ (ppm) = 8.00 (d, J = 8.5 Hz, 2H), 7.55 (d, J = 8.5 Hz, 2H), 6.38 (s, 2H), 3.80 (bs, 4H), 3.00 (s, 6H), 2.95 (s, 6H), 2,14-2.24 (m, 4H), 1.93-2.03 (m, 4H)

^{13}C NMR (125 MHz, $C_2D_2Cl_4$, 298 K) δ (ppm) = 136.2, 135.7, 133.2, 130.0, 127.8, 127.1, 118.8, 116.8, 102.6, 83.1 (d, J_{Rh-C}= 12.5 Hz), 31.2, 25.9, 23.3

MS-ESI: m/z 469.1 $[RhC_{28}H_{30}]^+$ in chloroform. HRMS-ESI: calcd for $RhC_{28}H_{30}$: 469.1403; found: 469.1404

3.3.3. Crystal data

Table 3.11 Crystallographic data for 105

Crystallised from	CH_2Cl_2 / Et_2O
Empirical formula	$C_{27}H_{18}F_6PRh$
Formula weight [g mol^{-1}]	590.31
Crystal colour, habit	yellow, tablet
Crystal dimensions [mm]	0.10 × 0.12 × 0.25
Temperature [K]	160(1)
Crystal system	monoclinic
Space group	$P2_1/c$ (#14)
Z	4
Reflections for cell determination	71878
2θ range for cell determination [°]	4−60
Unit cell parameters a [Å]	10.5749(1)
b [Å]	23.0723(3)
c [Å]	9.8553(1)
α [°]	90
β [°]	114.9137(6)
γ [°]	90
V [Å^3]	2180.81(4)
F(000)	1176
D_x [g cm^{-3}]	1.798
μ(Mo $K\alpha$) [mm^{-1}]	0.921
Scan type	ϕ and ω
$2\theta_{(max)}$ [°]	60
Transmission factors (min; max)	0.785; 0.914
Total reflections measured	60690
Symmetry independent reflections	6376
R_{int}	0.060
Reflections with $I > 2\sigma(I)$	5279
Reflections used in refinement	6373
Parameters refined	316
Final $R(F)$ [$I > 2\sigma(I)$ reflections]	0.0345
$wR(F^2)$ (all data)	0.0851
Weights:	$w = [\sigma^2(F_o^2) + (0.0372P)^2 + 2.1632P]^{-1}$ where $P = (F_o^2 + 2F_c^2)/3$
Goodness of fit	1.076

Final Δ_{max}/σ	0.001
$\Delta\rho$ (max; min) [e Å^{-3}]	1.27; -0.72
$\sigma(d_{(C-C)})$ [Å]	0.003 – 0.005

Table 3.12 Crystallographic Data for 120

Crystallised from	CH_2Cl_2 / Et_2O
Empirical formula	$C_{28}H_{22}F_6PRh$
Formula weight [g mol^{-1}]	606.35
Crystal colour, habit	yellow, prism
Crystal dimensions [mm]	0.15 × 0.25 × 0.25
Temperature [K]	160(1)
Crystal system	orthorhombic
Space group	*Pbcn* (#60)
Z	8
Reflections for cell determination	109283
2θ range for cell determination [°]	4 – 55
Unit cell parameters a [Å]	23.4870(4)
b [Å]	9.9870(2)
c [Å]	19.8289(4)
α [°]	90
β [°]	90
γ [°]	90
V [Å^3]	4651.2(2)
$F(000)$	2432
D_x [g cm^{-3}]	1.732
μ(Mo $K\alpha$) [mm^{-1}]	0.866
Scan type	ϕ and ω
$2\theta_{(max)}$ [°]	55
Transmission factors (min; max)	0.776; 0.883
Total reflections measured	66170
Symmetry independent reflections	5325
R_{int}	0.077
Reflections with $I > 2\sigma(I)$	3743
Reflections used in refinement	5322
Parameters refined; restraints	506; 1029

Final $R(F)$ [$I > 2\sigma(I)$ reflections]	0.0432
$wR(F^2)$ (all data)	0.1009
Weights:	$w = [\sigma^2(F_o^2) + (0.0321P)^2 + 10.7281P]^{-1}$ where $P = (F_o^2 + 2F_c^2)/3$
Goodness of fit	1.046
Final Δ_{max}/σ	0.002
$\Delta\rho$ (max; min) [e Å^{-3}]	1.00; -1.13
$\sigma(d_{(C-C)})$ [Å]	0.003 – 0.006

Table 3.13 Crystallographic Data for 109

Crystallised from		CH_2Cl_2 / Et_2O / pentane
Empirical formula		$C_{31}H_{32}F_6PRhCl_4$
Formula weight [g mol^{-1}]		794.28
Crystal colour, habit		orange, prism
Crystal dimensions [mm]		0.12 × 0.15 × 0.28
Temperature [K]		160(1)
Crystal system		monoclinic
Space group		$P2_1/n$ (#14)
Z		8
Reflections for cell determination		193605
2θ range for cell determination [°]		4 – 50
Unit cell parameters	a [Å]	29.2924(4)
	b [Å]	7.7235(1)
	c [Å]	30.8558(4)
	α [°]	90
	β [°]	112.1888(8)
	γ [°]	90
	V [Å^3]	6463.8(2)
$F(000)$		3200
D_x [g cm^{-3}]		1.632
μ(Mo $K\alpha$) [mm^{-1}]		0.962
Scan type		ϕ and ω
$2\theta_{(max)}$ [°]		50
Transmission factors (min; max)		0.717; 0.925
Total reflections measured		81288

Symmetry independent reflections	11376
R_{int}	0.096
Reflections with $I > 2\sigma(I)$	8369
Reflections used in refinement	11376
Parameters refined; restraints	849; 285
Final $R(F)$ [$I > 2\sigma(I)$ reflections]	0.0936
$wR(F^2)$ (all data)	0.2685
Weights:	$w = [\sigma^2(F_o^2) + (0.1461P)^2 + 69.3966P]^{-1}$ where $P = (F_o^2 + 2F_c^2)/3$
Goodness of fit	1.022
Final Δ_{max}/σ	0.001
$\Delta\rho$ (max; min) [e Å^{-3}]	7.25; -1.22
$\sigma(d_{(C-C)})$ [Å]	0.01 – 0.02

Table 3.14. **Crystallographic Data for 110**

Crystallised from	CH_2Cl_2 / pentane / Et_2O
Empirical formula	$C_{43}H_{52}Cl_4F_6PRh$
Formula weight [g mol^{-1}]	958.57
Crystal colour, habit	red, prism
Crystal dimensions [mm]	0.20 × 0.22 × 0.28
Temperature [K]	160(1)
Crystal system	triclinic
Space group	P^{-},1 (#2)
Z	2
Reflections for cell determination	92384
2θ range for cell determination [°]	4 – 60
Unit cell parameters a [Å]	9.9158(2)
b [Å]	13.7606(3)
c [Å]	17.6211(4)
α [°]	111.476(1)
β [°]	106.383(1)
γ [°]	92.896(2)
V [Å^3]	2114.49(8)
$F(000)$	984
D_x [g cm^{-3}]	1.505

μ(Mo $K\alpha$) [mm^{-1}]	0.750
Scan type	ϕ and ω
$2\theta_{(max)}$ [°]	60
Transmission factors (min; max)	0.769; 0.909
Total reflections measured	64302
Symmetry independent reflections	12177
R_{int}	0.077
Reflections with $I > 2\sigma(I)$	10289
Reflections used in refinement	12177
Parameters refined; restraints	584; 453
Final $R(F)$ [$I > 2\sigma(I)$ reflections]	0.0697
$wR(F^2)$ (all data)	0.1813
Weights:	$w = [\sigma^2(F_o^2) + (0.0843P)^2 + 10.7317P]^{-1}$ where $P = (F_o^2 + 2F_c^2)/3$
Goodness of fit	1.067
Final Δ_{max}/σ	0.001
$\Delta\rho$ (max; min) [e Å^{-3}]	1.64; -1.30
$\sigma(d_{(C-C)})$ [Å]	0.005 – 0.006

Table 3.15 . Crystallographic Data for 122

Crystallised from	CH_2Cl_2 / Et_2O / pentane
Empirical formula	$C_{60}H_{81}F_{12}O_{1.5}P_2Rh_2$
Formula weight [g mol^{-1}]	1322.04
Crystal colour, habit	colourless, prism
Crystal dimensions [mm]	0.30 × 0.40 × 0.45
Temperature [K]	160(1)
Crystal system	triclinic
Space group	$P\bar{}$,1 (#2)
Z	2
Reflections for cell determination	48841
2θ range for cell determination [°]	4 – 60
Unit cell parameters a [Å]	13.8491(2)
b [Å]	13.9159(3)
c [Å]	17.1299(3)
α [°]	103.385(1)

β [°]	107.818(1)
γ [°]	95.833(1)
V [Å^3]	3004.1(1)
F(000)	1362
D_x [g cm^{-3}]	1.461
μ(Mo $K\alpha$) [mm^{-1}]	0.678
Scan type	ω
$2\theta_{(max)}$ [°]	60
Transmission factors (min; max)	0.543; 0.914
Total reflections measured	82559
Symmetry independent reflections	17460
R_{int}	0.116
Reflections with $I > 2\sigma(I)$	12246
Reflections used in refinement	17460
Parameters refined; restraints	764; 574
Final $R(F)$ [$I > 2\sigma(I)$ reflections]	0.0891
$wR(F^2)$ (all data)	0.2639
Weights:	$w = [\sigma^2(F_o^2) + (0.1741P)^2 + 0.9193P]^{-1}$ where $P = (F_o^2 + 2F_c^2)/3$
Goodness of fit	1.086
Secondary extinction coefficient	0.010(1)
Final Δ_{max}/σ	0.001
$\Delta\rho$ (max; min) [e Å^{-3}]	2.92; -2.02
$\sigma(d_{(C-C)})$ [Å]	0.006 – 0.009

Table 3.16. Crystallographic Data for 118A

Crystallised from	CH_2Cl_2 / Et_2O / pentane
Empirical formula	$C_{28}H_{30}F_6IrP$
Formula weight [g mol^{-1}]	703.71
Crystal colour, habit	yellow, plate
Crystal dimensions [mm]	0.03 × 0.14 × 0.30
Temperature [K]	183(1)
Crystal system	monoclinic
Space group	$P2_1/c$ (#14)
Z	4

Reflections for cell determination	16784
2θ range for cell determination [°]	4.8 – 65.4
Unit cell parameters a [Å]	8.8792(1)
b [Å]	28.3455(3)
c [Å]	10.2934(2)
α [°]	90
β [°]	108.046(2)
γ [°]	90
V [Å^3]	2463.26(7)
$F(000)$	1376
D_x [g cm^{-3}]	1.897
μ(Mo $K\alpha$) [mm^{-1}]	5.562
Scan type	ω
$2\theta_{(max)}$ [°]	65.4
Total reflections measured	36419
Symmetry independent reflections	8392
R_{int}	0.035
Reflections with $I > 2\sigma(I)$	6312
Reflections used in refinement	8392
Parameters refined	329
Final $R(F)$ [$I > 2\sigma(I)$ reflections]	0.0254
$wR(F^2)$ (all data)	0.0543
Weights:	$w = [\sigma^2(F_o^2) + (0.0271P)^2]^{-1}$ where $P = (F_o^2 + 2F_c^2)/3$
Goodness of fit	0.967
Final Δ_{max}/σ	0.003
$\Delta\rho$ (max; min) [e Å^{-3}]	0.93; -0.84
$\sigma(d_{(C-C)})$ [Å]	0.003 – 0.005

Table 3.17 Crystallographic Data for 119

Crystallised from	CH_2Cl_2 / Et_2O / pentane
Empirical formula	$C_{28}H_{30}F_6PRh$
Formula weight [g mol^{-1}]	614.41
Crystal colour, habit	orange, prism
Crystal dimensions [mm]	0.12 × 0.17 × 0.20

Temperature [K]	160(1)
Crystal system	monoclinic
Space group	$P2_1/c$ (#14)
Z	4
Reflections for cell determination	57867
2θ range for cell determination [°]	4 – 60
Unit cell parameters a [Å]	8.8630(1)
b [Å]	28.3665(4)
c [Å]	10.2968(1)
α [°]	90
β [°]	108.3534(7)
γ [°]	90
V [Å^3]	2457.06(5)
$F(000)$	1248
D_x [g cm^{-3}]	1.661
μ(Mo $K\alpha$) [mm^{-1}]	0.821
Scan type	ϕ and ω
$2\theta_{(max)}$ [°]	60
Transmission factors (min; max)	0.813; 0.907
Total reflections measured	61933
Symmetry independent reflections	7176
R_{int}	0.071
Reflections with $I > 2\sigma(I)$	5562
Reflections used in refinement	7172
Parameters refined	346
Final $R(F)$ [$I > 2\sigma(I)$ reflections]	0.0355
$wR(F^2)$ (all data)	0.0878
Weights: $w = [\sigma^2(F_o^2) + (0.0430P)^2 + 0.2620P]^{-1}$ where $P = (F_o^2 + 2F_c^2)/3$	
Goodness of fit	1.038
Secondary extinction coefficient	0.0018(4)
Final Δ_{max}/σ	0.001
$\Delta\rho$ (max; min) [e Å^{-3}]	0.85; -1.11
$\sigma(d_{(C-C)})$ [Å]	0.003 – 0.004

3.3.4. Build-up curves

Compound 107 (277 K in CD_2Cl_2)

$\tau_m = 10^{-6}$ s, 0.02s. 0.08 s, 0.15 s, 0.3 s, 0.6 s, 1.0 s, 1.6 s, 2.2 s, 2.8 s.

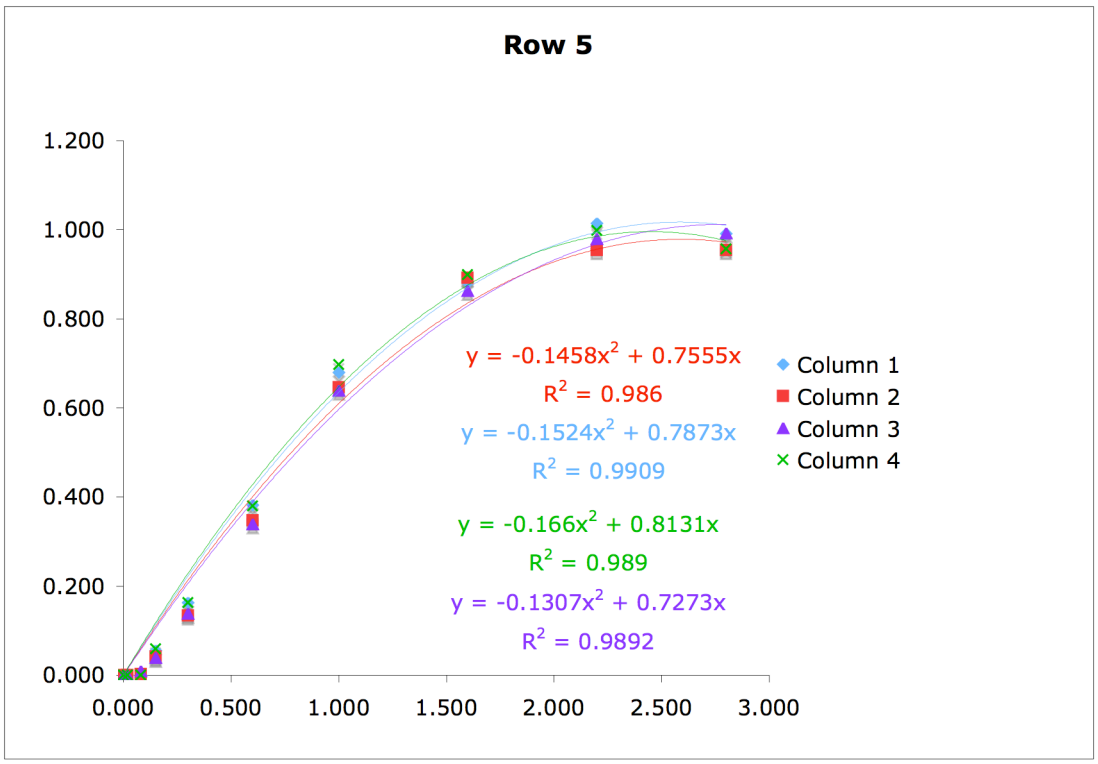

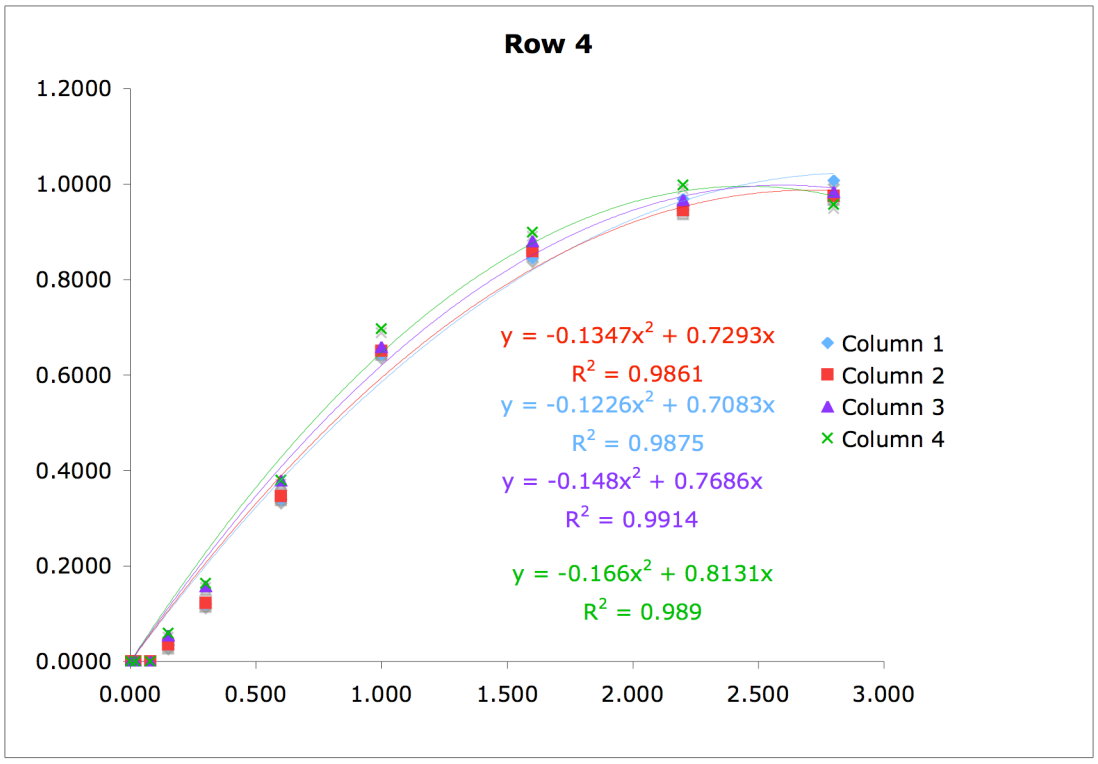

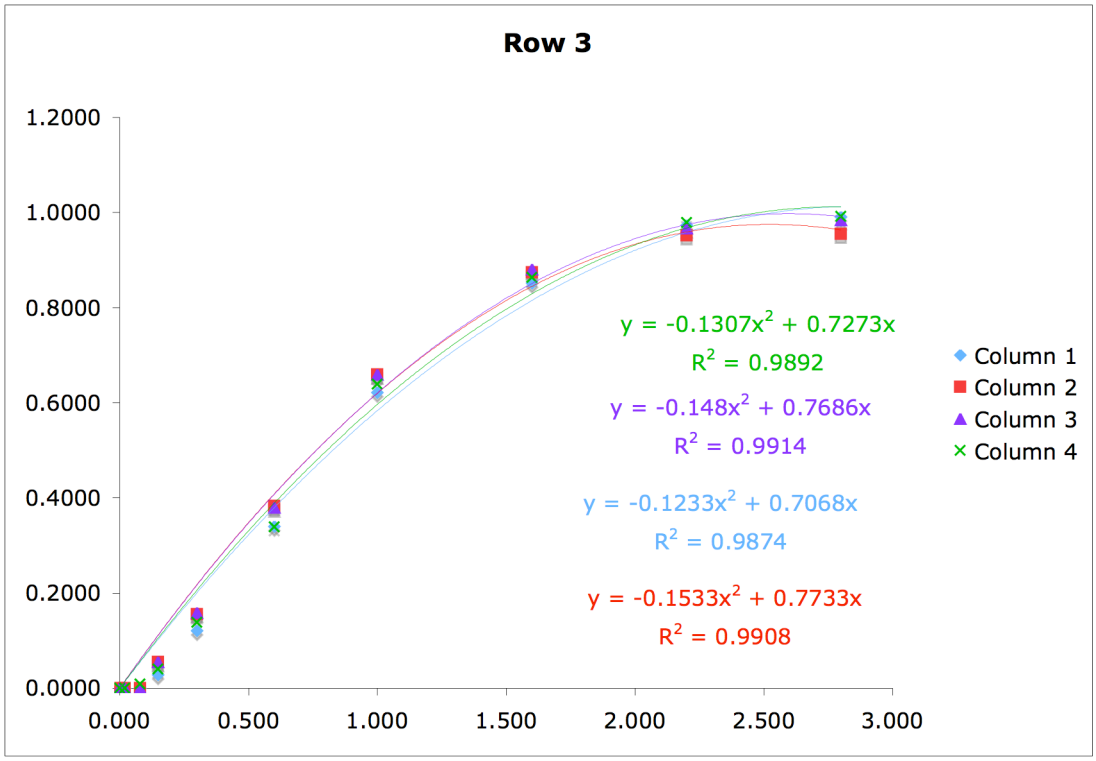
Row 3
1.2000
1.0000
0.8000
0.6000
0.4000
0.2000
0.0000
0.000
0.500
1.000
1.500
2.000
2.500
3.000
y = -0.1307x2 + 0.7273x
R2 = 0.9892
y = -0.148x2 + 0.7686x
R2 = 0.9914
y = -0.1233x2 + 0.7068x
R2 = 0.9874
y = -0.1533x2 + 0.7733x
R2 = 0.9908
Column 1
Column 2
Column 3
Column 4

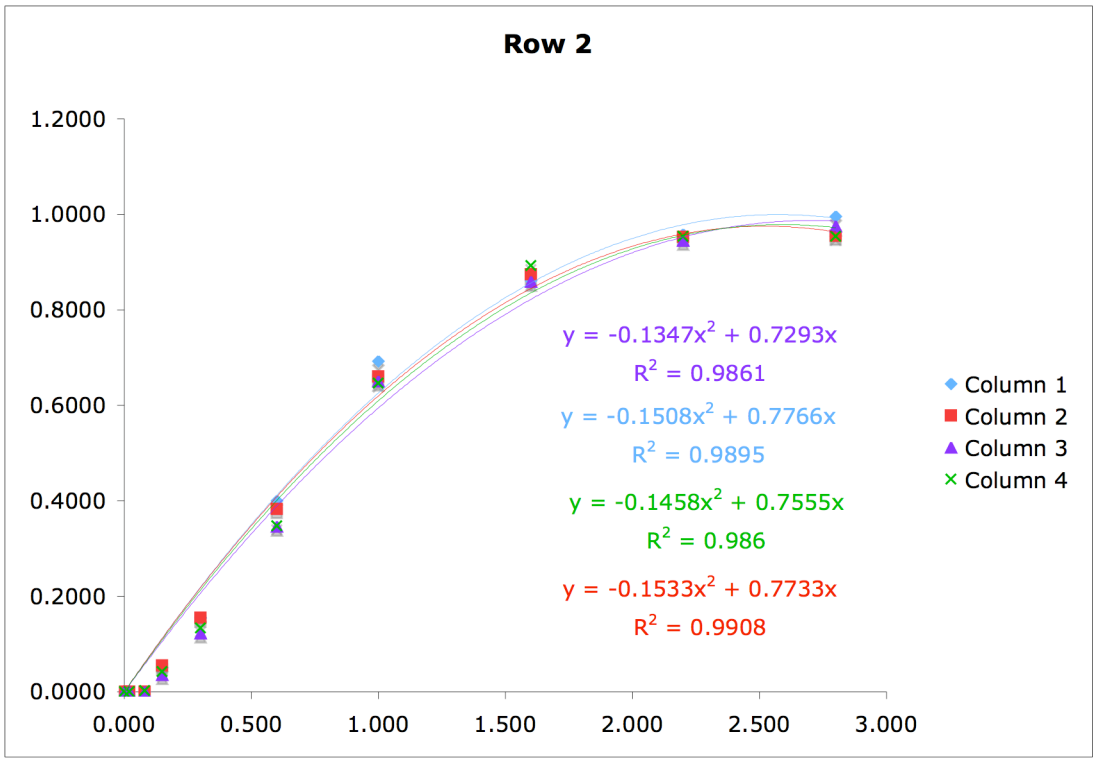
Row 2
1.2000
1.0000
0.8000
0.6000
0.4000
0.2000
0.0000
0.000
0.500
1.000
1.500
2.000
2.500
3.000
y = -0.1347x2 + 0.7293x
R2 = 0.9861
y = -0.1508x2 + 0.7766x
R2 = 0.9895
y = -0.1458x2 + 0.7555x
R2 = 0.986
y = -0.1533x2 + 0.7733x
R2 = 0.9908
Column 1
Column 2
Column 3
Column 4

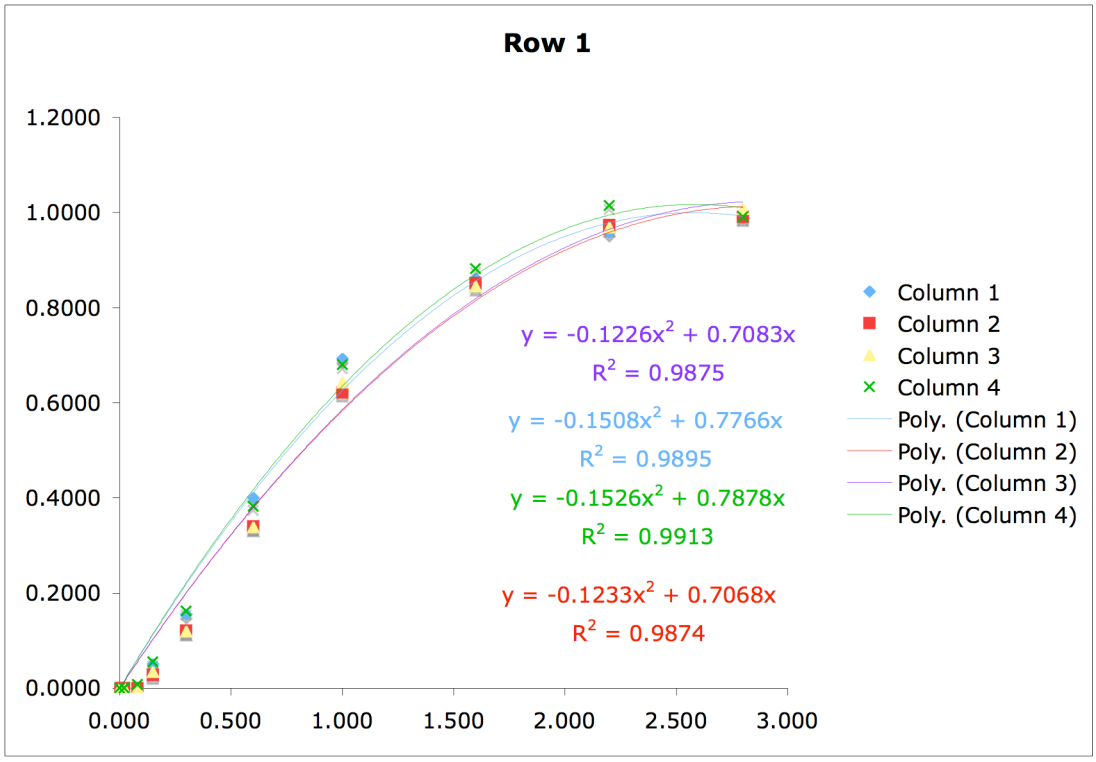

Compound 107 (282 K, CD_2Cl_2)

$\tau_m = 10^{-6}$ s, 0.02s. 0.08 s, 0.15 s, 0.3 s, 0.6 s, 1.0 s, 1.6 s, 2.2 s, 2.8 s.

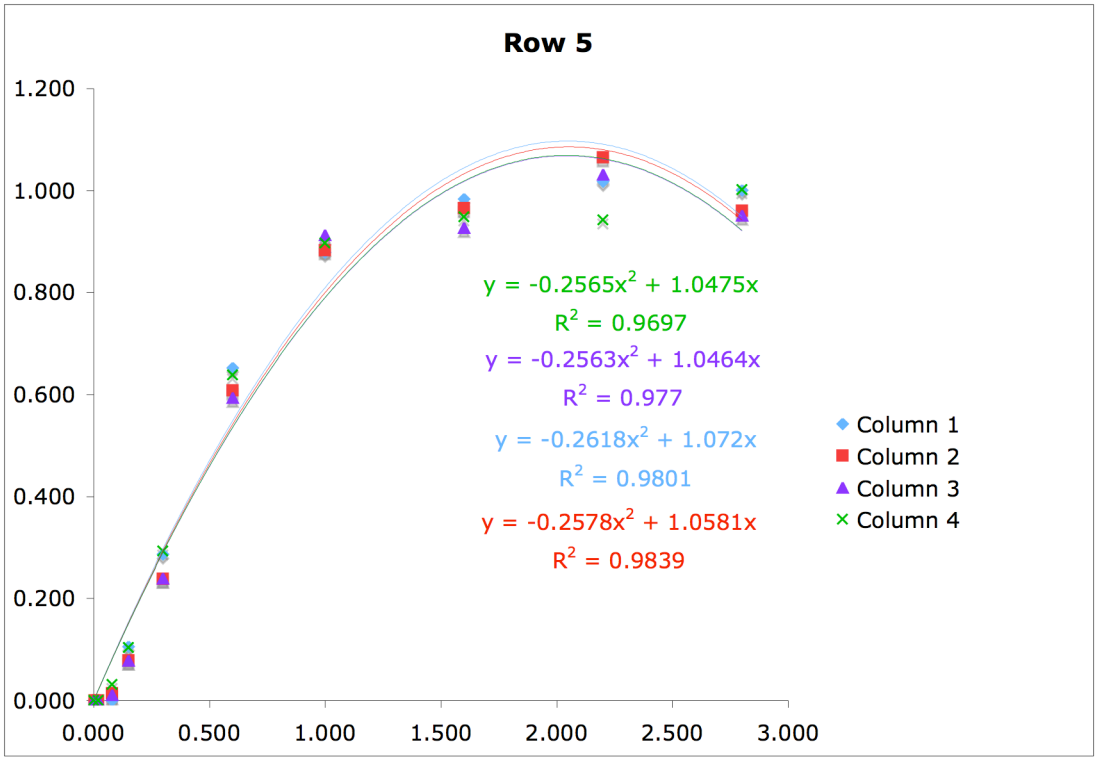

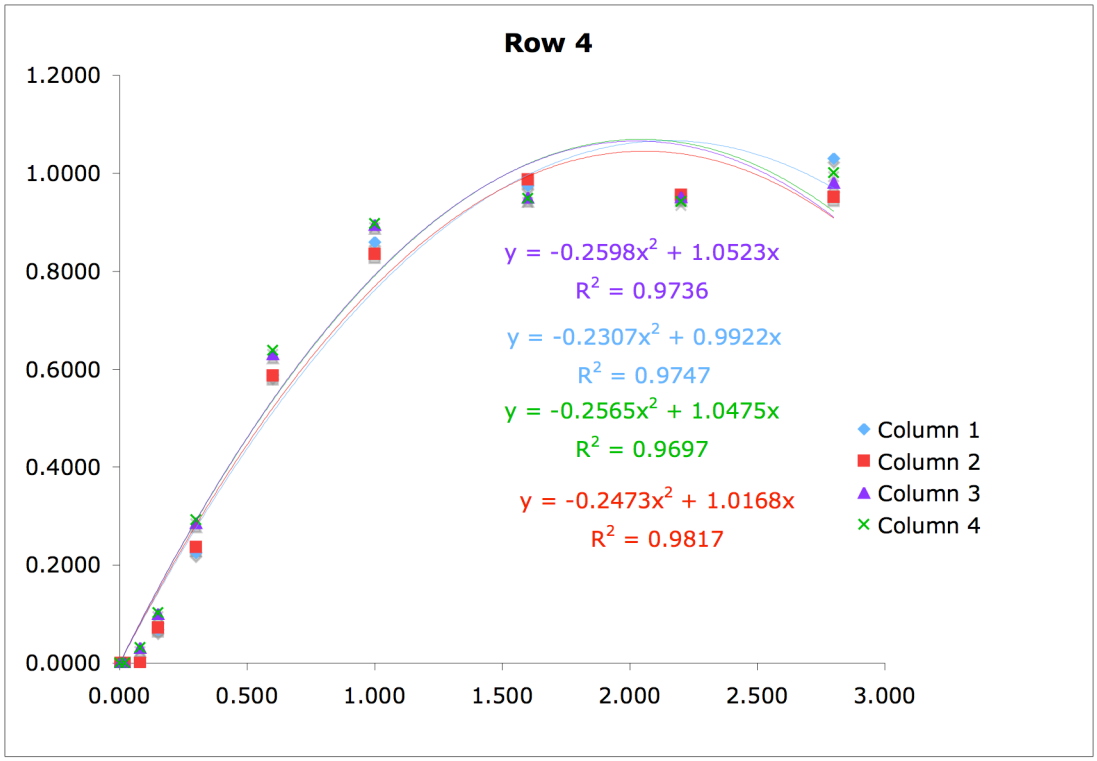
Row 4
1.2000
1.0000
0.8000
0.6000
0.4000
0.2000
0.0000
0.000
0.500
1.000
1.500
2.000
2.500
3.000
y = -0.2598x2 + 1.0523x
R2 = 0.9736
y = -0.2307x2 + 0.9922x
R2 = 0.9747
y = -0.2565x2 + 1.0475x
R2 = 0.9697
y = -0.2473x2 + 1.0168x
R2 = 0.9817
Column 1
Column 2
Column 3
Column 4

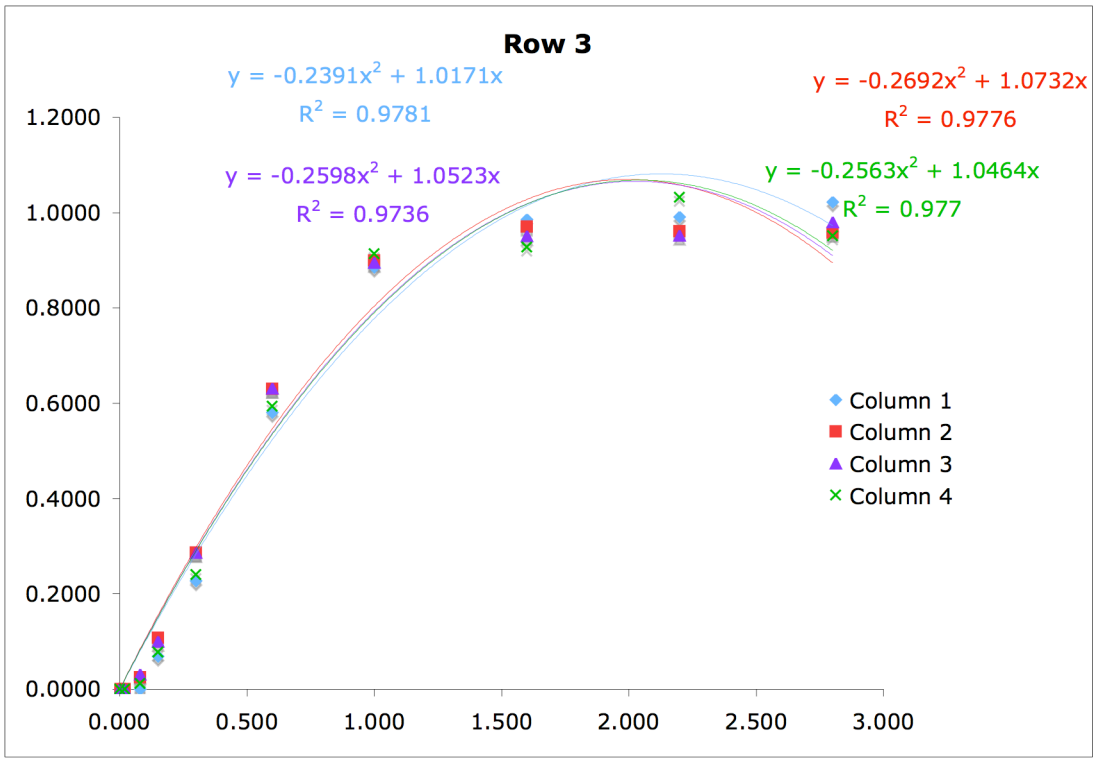
Row 3
y = -0.2391x2 + 1.0171x
R2 = 0.9781
y = -0.2692x2 + 1.0732x
R2 = 0.9776
y = -0.2598x2 + 1.0523x
R2 = 0.9736
y = -0.2563x2 + 1.0464x
R2 = 0.977
1.2000
1.0000
0.8000
0.6000
0.4000
0.2000
0.0000
0.000
0.500
1.000
1.500
2.000
2.500
3.000
Column 1
Column 2
Column 3
Column 4

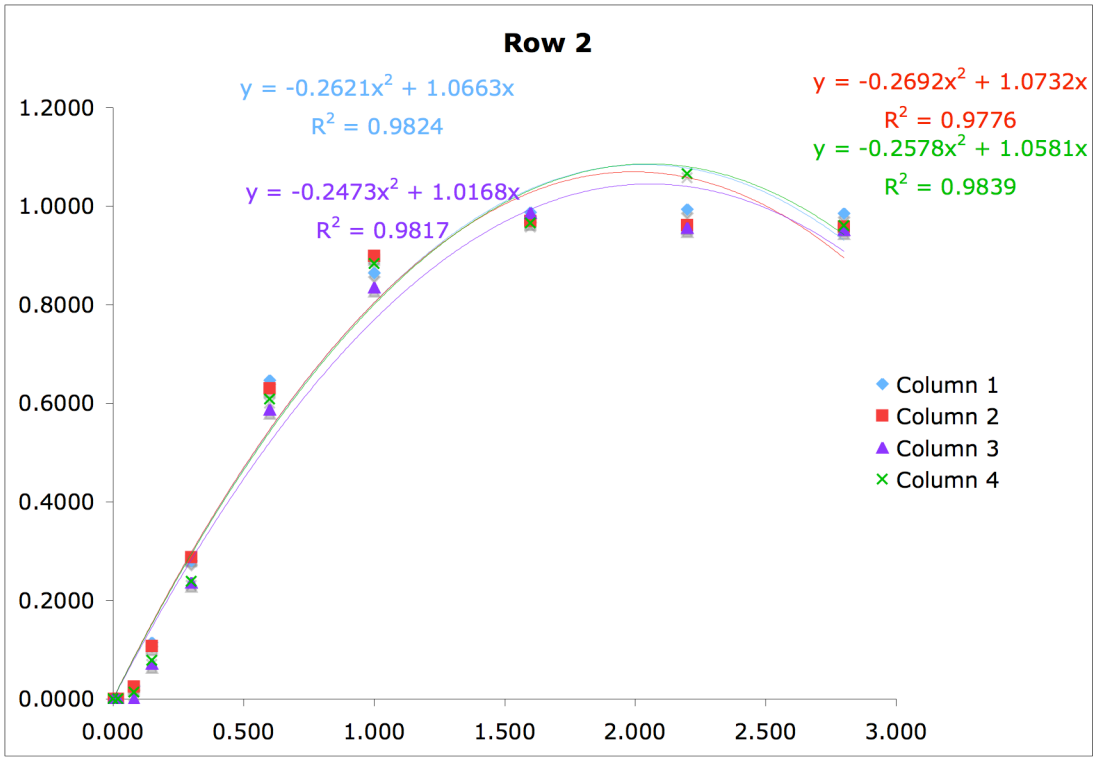
Row 2
y = -0.2621x2 + 1.0663x
R2 = 0.9824
y = -0.2692x2 + 1.0732x
R2 = 0.9776
y = -0.2578x2 + 1.0581x
R2 = 0.9839
y = -0.2473x2 + 1.0168x
R2 = 0.9817
1.2000
1.0000
0.8000
0.6000
0.4000
0.2000
0.0000
0.000
0.500
1.000
1.500
2.000
2.500
3.000
Column 1
Column 2
Column 3
Column 4

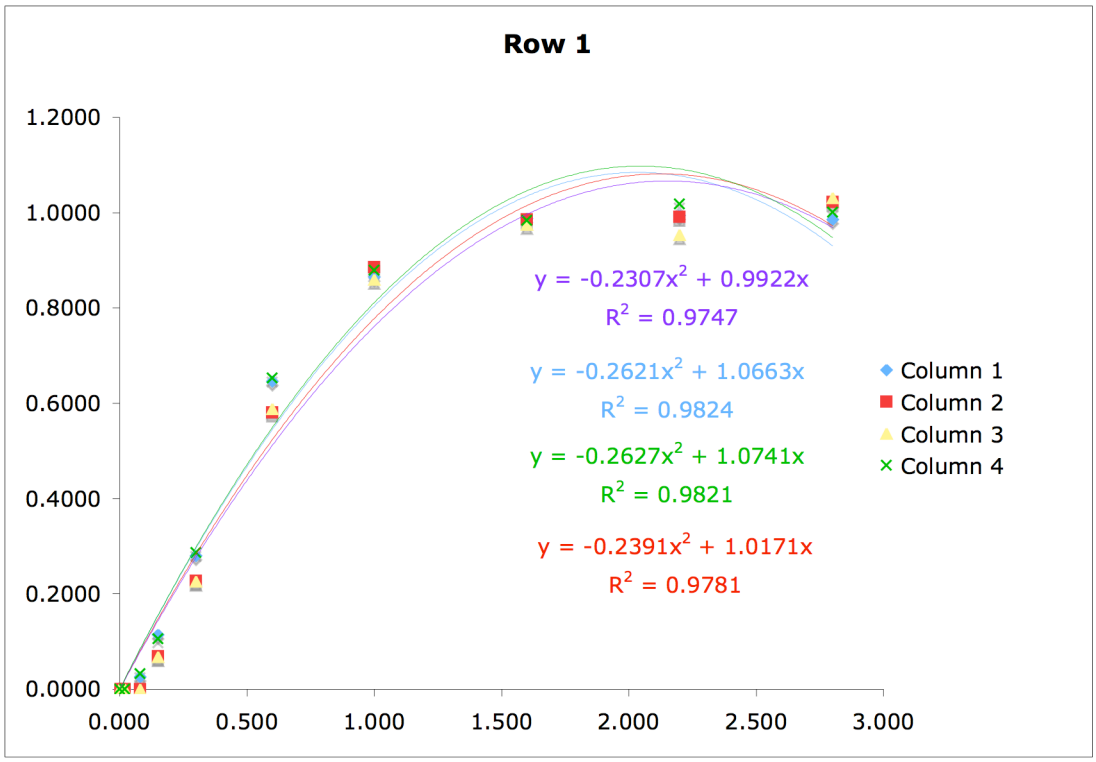
Row 1
y = -0.2307x2 + 0.9922x
R2 = 0.9747
y = -0.2621x2 + 1.0663x
R2 = 0.9824
y = -0.2627x2 + 1.0741x
R2 = 0.9821
y = -0.2391x2 + 1.0171x
R2 = 0.9781
1.2000
1.0000
0.8000
0.6000
0.4000
0.2000
0.0000
0.000
0.500
1.000
1.500
2.000
2.500
3.000
Column 1
Column 2
Column 3
Column 4

Compound 111 (314 K, in $CDCl_3$)

$\tau_m = 10^{-6}$ s, 0.02s. 0.08 s, 0.15 s, 0.3 s, 0.6 s, 1.0 s, 1.6 s, 2.2 s, 2.8 s.

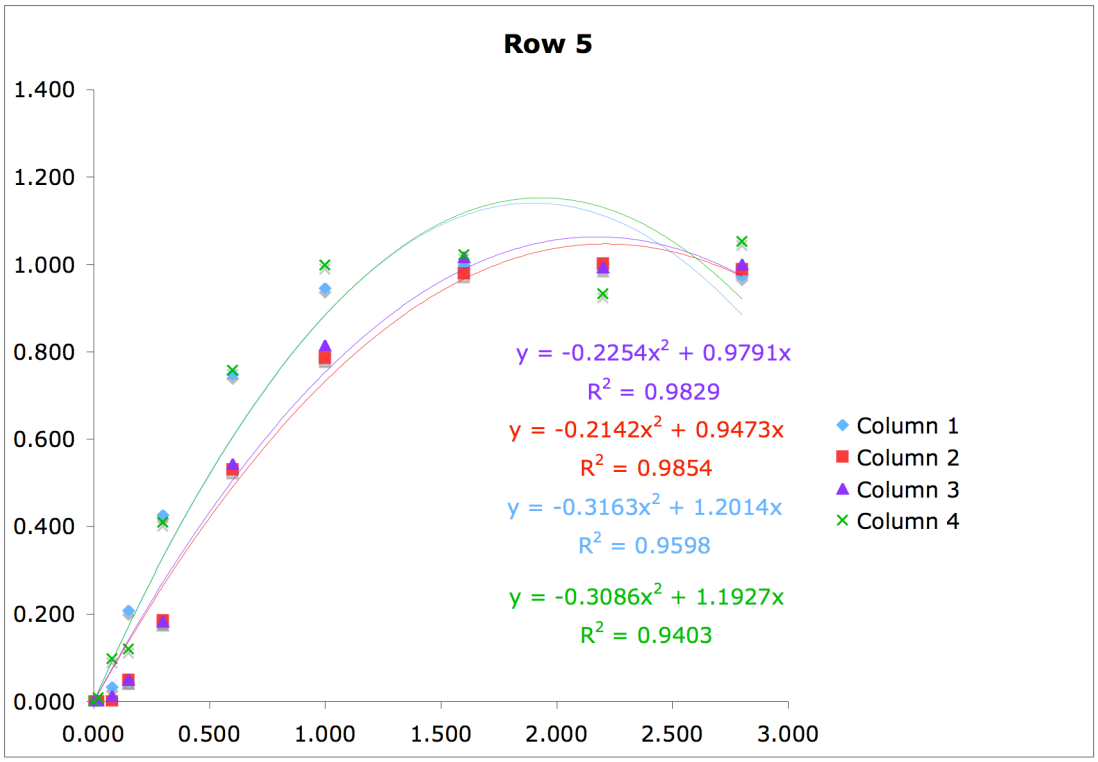

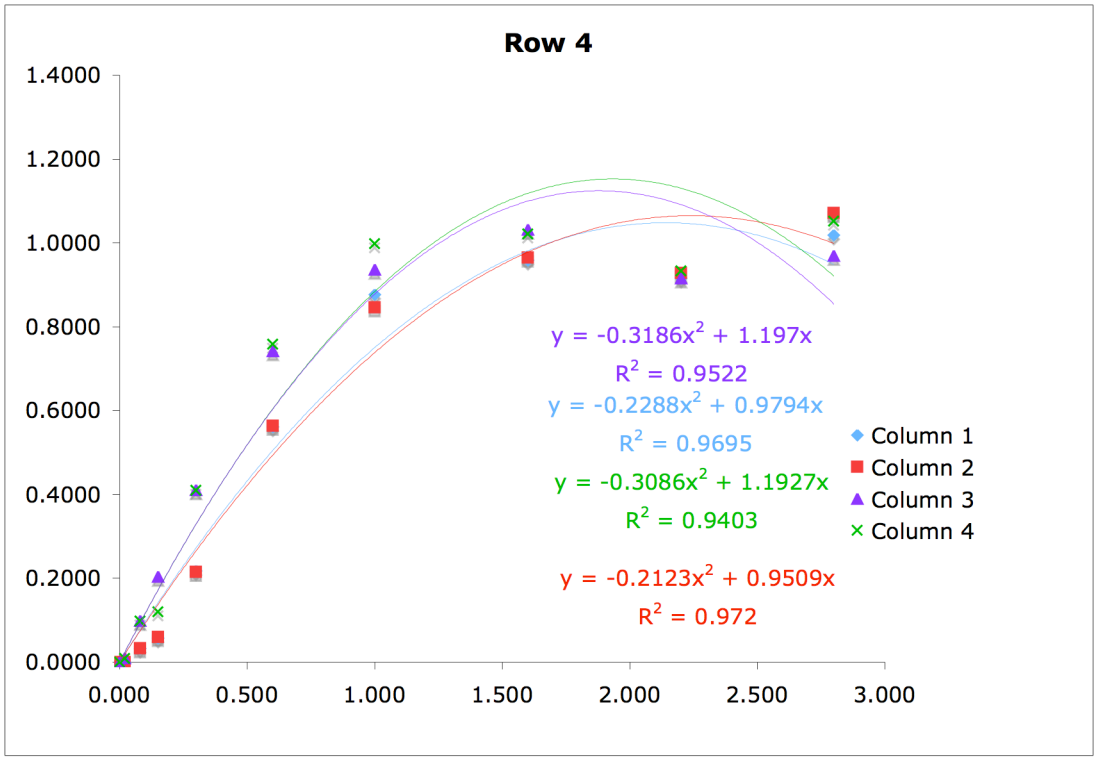

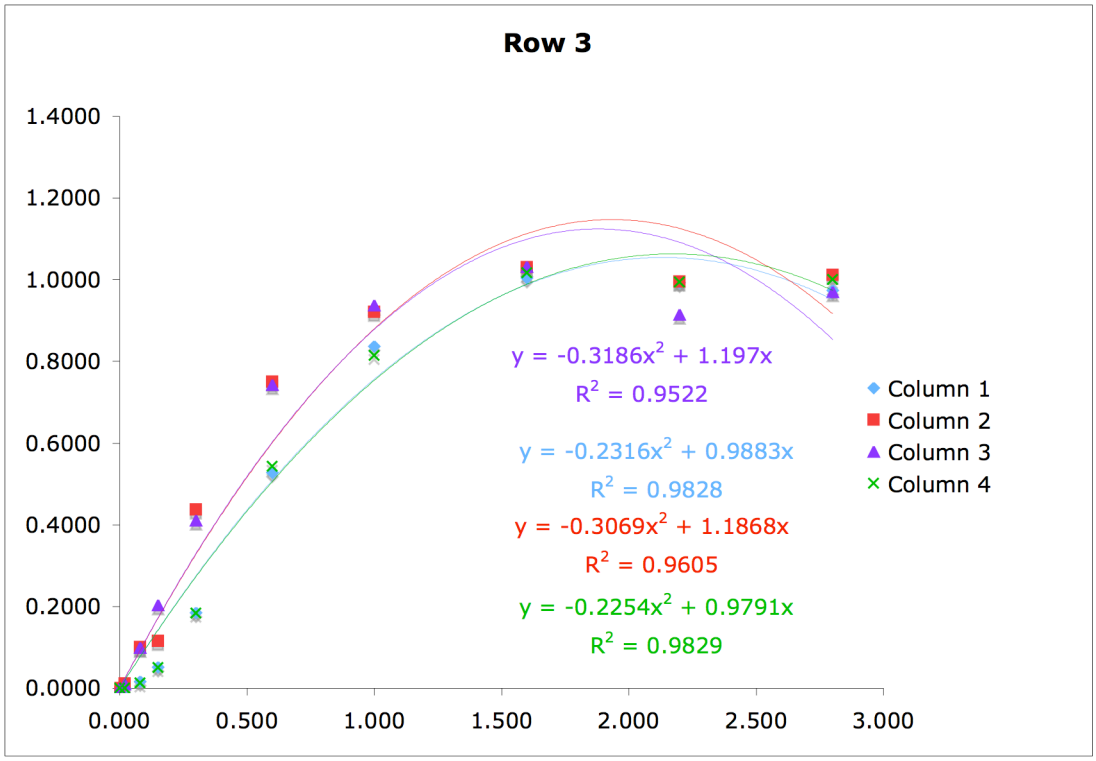
Row 3
1.4000
1.2000
1.0000
0.8000
0.6000
0.4000
0.2000
0.0000
0.000
0.500
1.000
1.500
2.000
2.500
3.000
y = -0.3186x2 + 1.197x
R2 = 0.9522
y = -0.2316x2 + 0.9883x
R2 = 0.9828
y = -0.3069x2 + 1.1868x
R2 = 0.9605
y = -0.2254x2 + 0.9791x
R2 = 0.9829
Column 1
Column 2
Column 3
Column 4

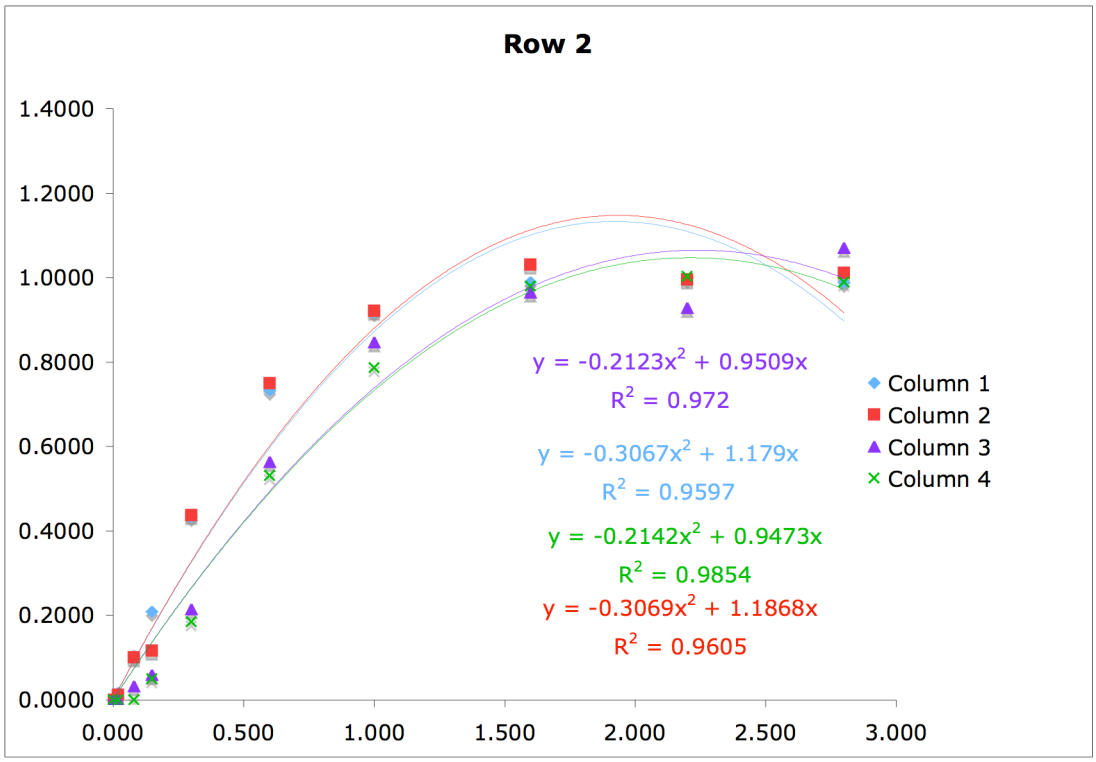
Row 2
1.4000
1.2000
1.0000
0.8000
0.6000
0.4000
0.2000
0.0000
0.000
0.500
1.000
1.500
2.000
2.500
3.000
y = -0.2123x2 + 0.9509x
R2 = 0.972
y = -0.3067x2 + 1.179x
R2 = 0.9597
y = -0.2142x2 + 0.9473x
R2 = 0.9854
y = -0.3069x2 + 1.1868x
R2 = 0.9605
Column 1
Column 2
Column 3
Column 4

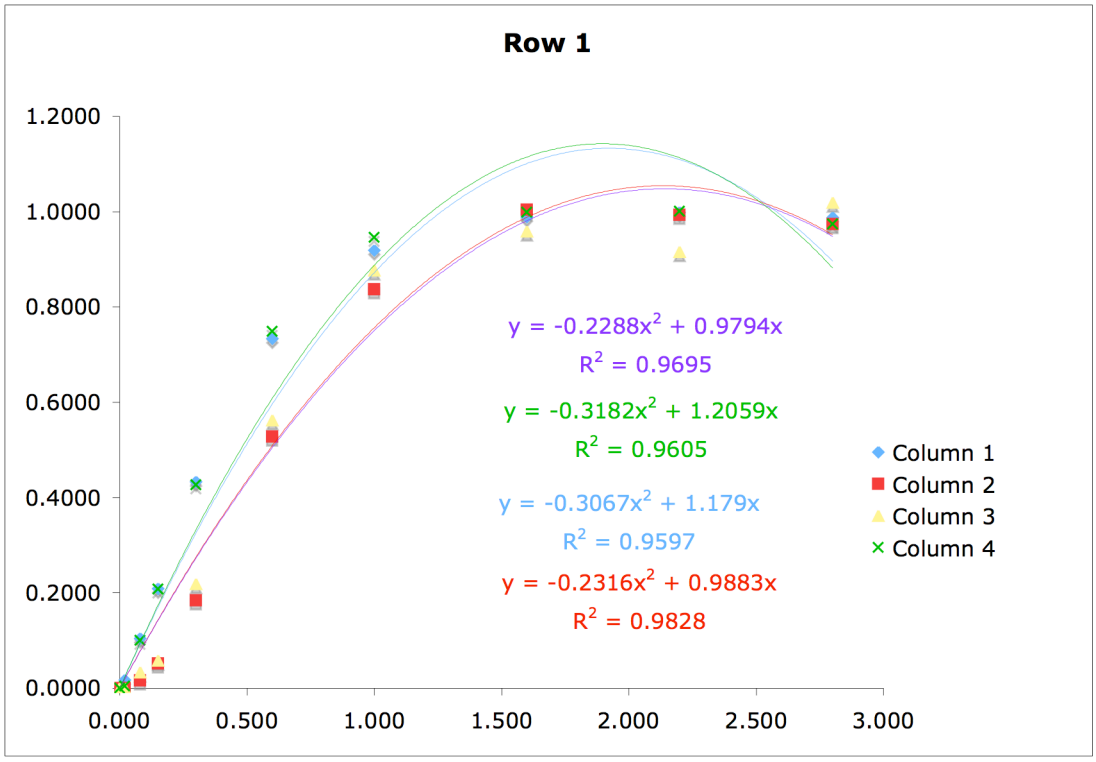

Compound 111 (309 K, in $CDCl_3$)

$\tau_m = 10^{-6}$ s, 0.02s. 0.08 s, 0.15 s, 0.3 s, 0.6 s, 1.0 s, 1.6 s, 2.2 s, 2.8 s.

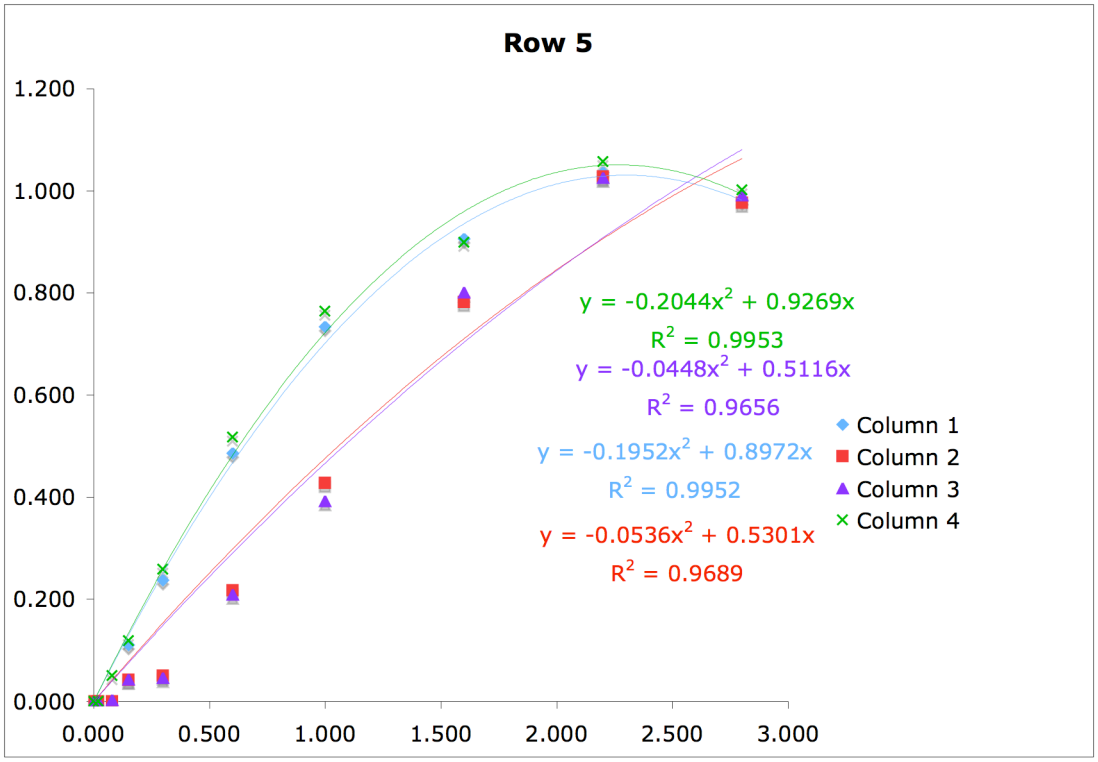

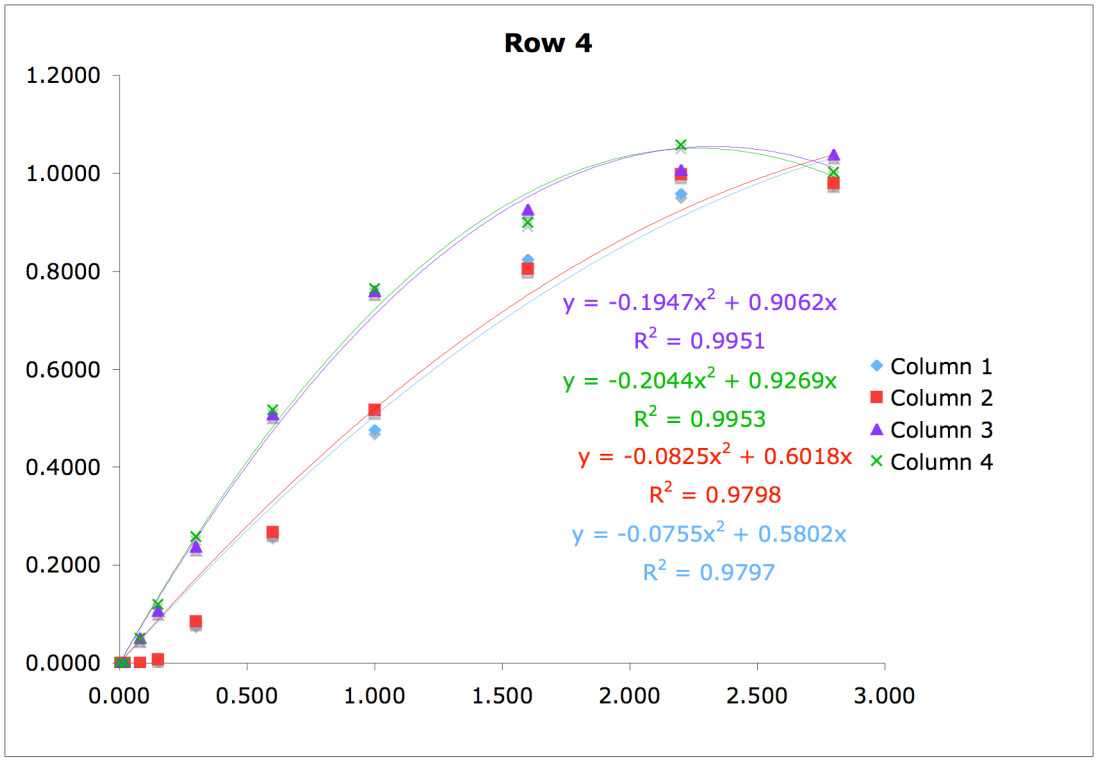
Row 4
1.2000
1.0000
0.8000
0.6000
0.4000
0.2000
0.0000
0.000
0.500
1.000
1.500
2.000
2.500
3.000
y = -0.1947x2 + 0.9062x
R2 = 0.9951
y = -0.2044x2 + 0.9269x
R2 = 0.9953
y = -0.0825x2 + 0.6018x
R2 = 0.9798
y = -0.0755x2 + 0.5802x
R2 = 0.9797
Column 1
Column 2
Column 3
Column 4

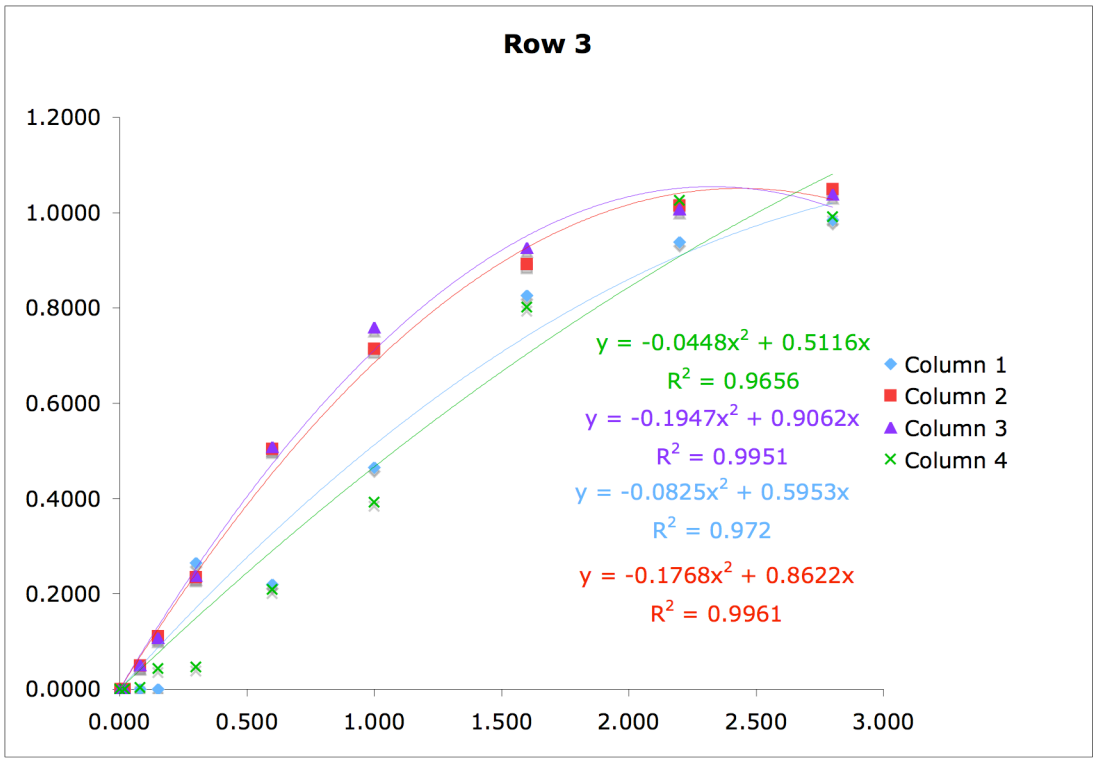
Row 3
1.2000
1.0000
0.8000
0.6000
0.4000
0.2000
0.0000
0.000
0.500
1.000
1.500
2.000
2.500
3.000
y = -0.0448x2 + 0.5116x
R2 = 0.9656
y = -0.1947x2 + 0.9062x
R2 = 0.9951
y = -0.0825x2 + 0.5953x
R2 = 0.972
y = -0.1768x2 + 0.8622x
R2 = 0.9961
Column 1
Column 2
Column 3
Column 4

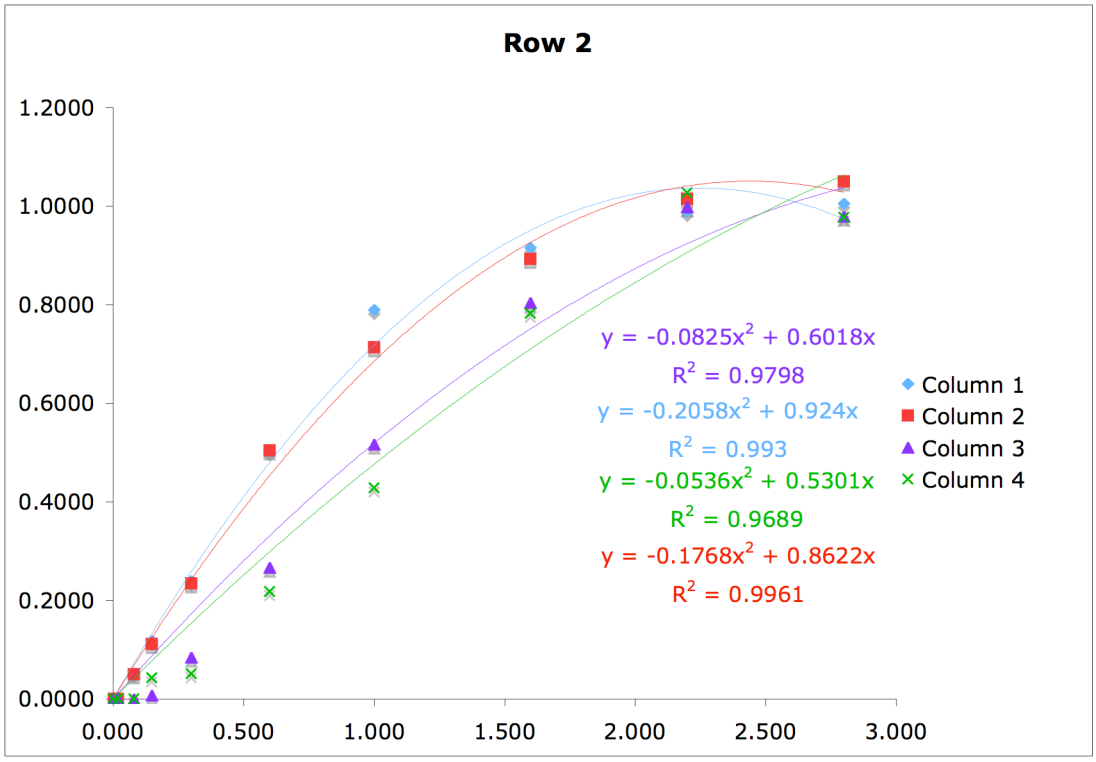
Row 2
1.2000
1.0000
0.8000
0.6000
0.4000
0.2000
0.0000
0.000
0.500
1.000
1.500
2.000
2.500
3.000
y = -0.0825x² + 0.6018x
R² = 0.9798
y = -0.2058x² + 0.924x
R² = 0.993
y = -0.0536x² + 0.5301x
R² = 0.9689
y = -0.1768x² + 0.8622x
R² = 0.9961
Column 1
Column 2
Column 3
Column 4

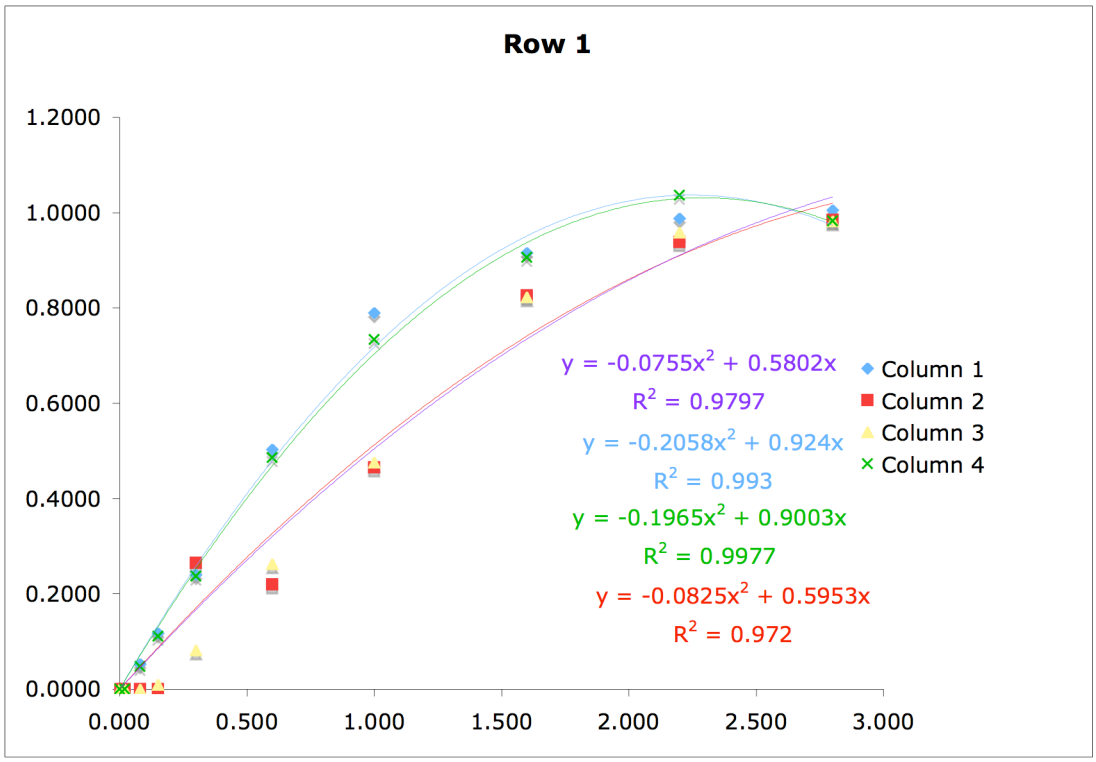
Row 1
1.2000
1.0000
0.8000
0.6000
0.4000
0.2000
0.0000
0.000
0.500
1.000
1.500
2.000
2.500
3.000
y = -0.0755x² + 0.5802x
R² = 0.9797
y = -0.2058x² + 0.924x
R² = 0.993
y = -0.1965x² + 0.9003x
R² = 0.9977
y = -0.0825x² + 0.5953x
R² = 0.972
Column 1
Column 2
Column 3
Column 4

Compound 113 olefin exchange (297 K in CD_2Cl_2)

$\tau_m = 10^{-6}$ s, 0.02s. 0.08 s, 0.15 s, 0.3 s, 0.5 s, 0.6 s, 1.0 s, 1.6 s.

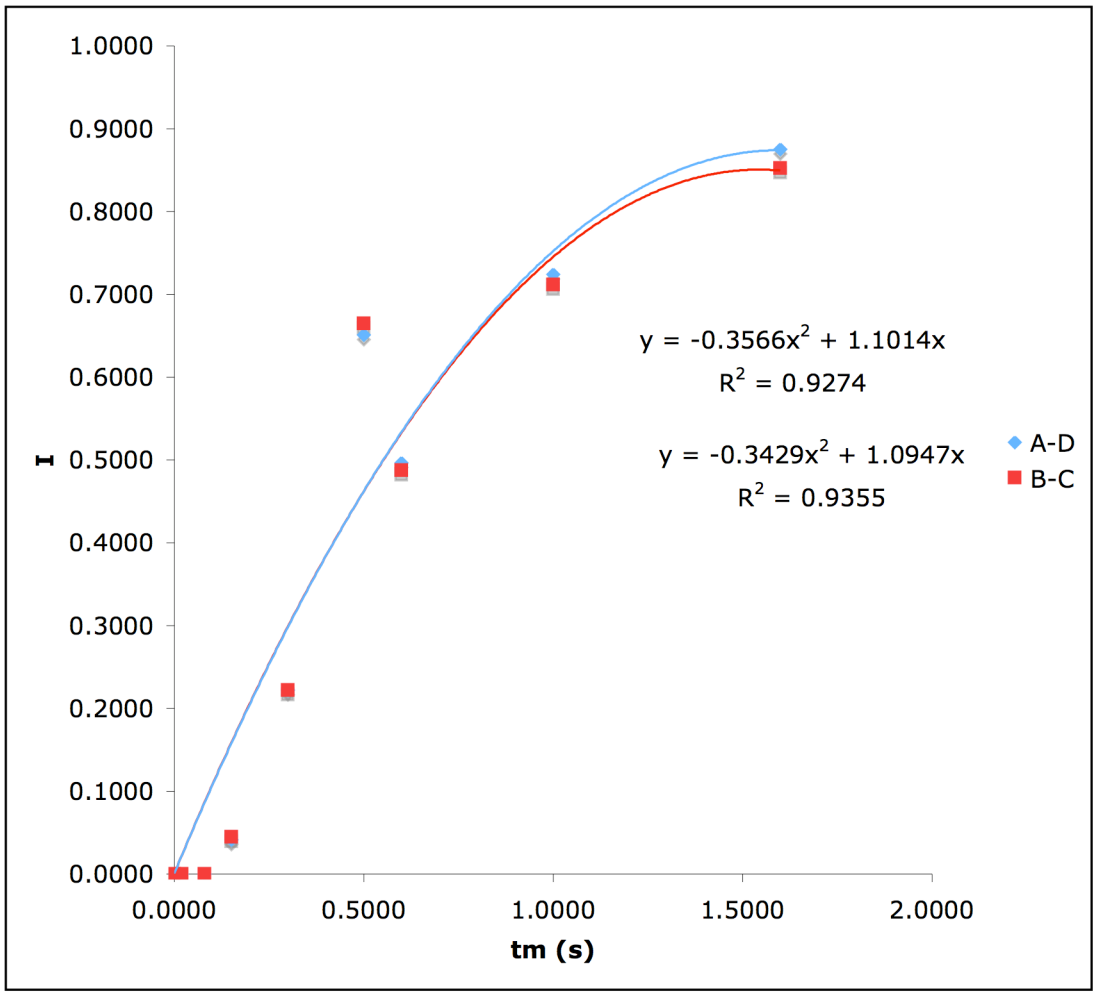

Compound 113 olefin exchange (302 K in CD_2Cl_2)

$\tau_m = 10^{-6}$ s, 0.02s. 0.08 s, 0.15 s, 0.3 s, 0.5 s, 0.6 s, 1.0 s, 1.6 s.

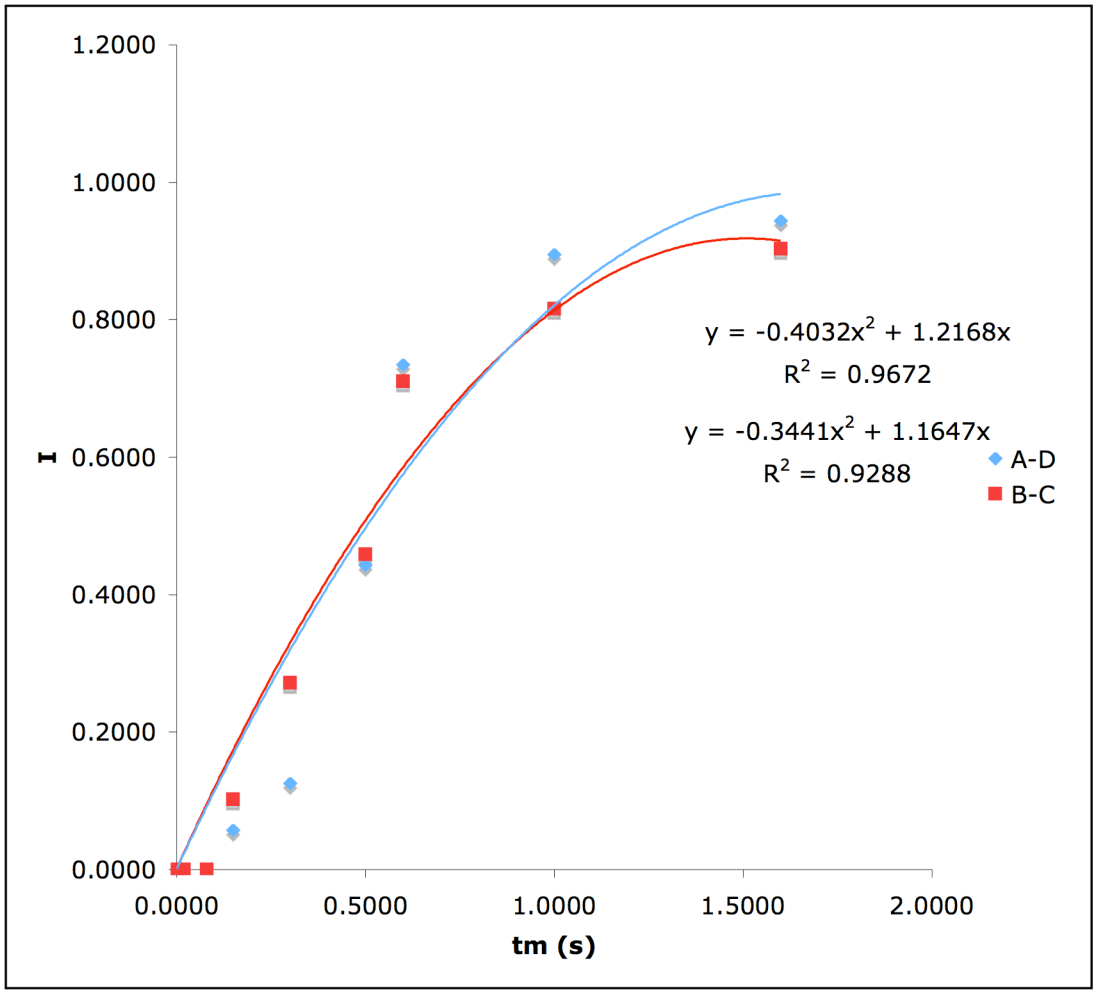

3.3.5. HOMO and LUMO for 1 and 54.

Table 3.18. HOMO and LUMO for $C_{20}H_{10}$ (1) and $C_{25}H_{20}$ (54)

Orbital	**1**	**54**
LUMO	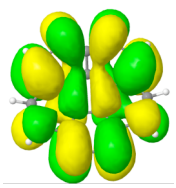	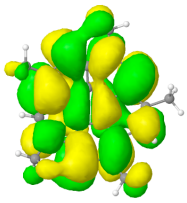
HOMO	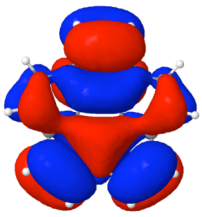	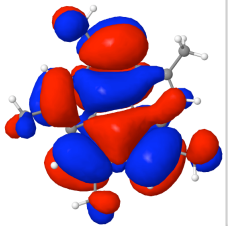
HOMO-2	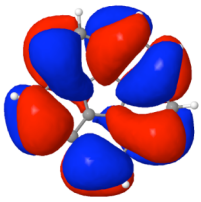	
HOMO-4	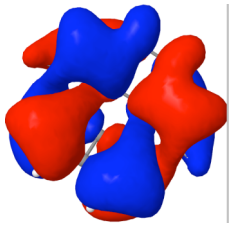	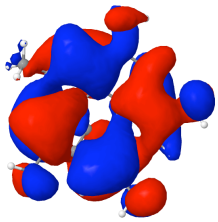
HOMO-6	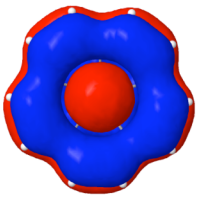	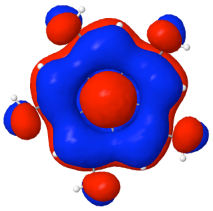
HOMO-7	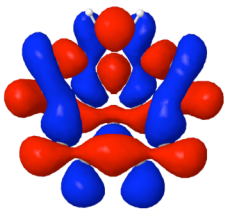	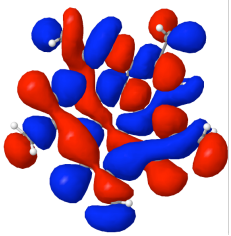

[a] side views for LUMO and from HOMO to HOMO-4, calculated at the level TZVP + LANL2TZ+f.

3.1 References

1 (a) Fagan, P. J.; Calabrese, J. C.; Malone, B. *Acc. Chem. Res.* **1992**, *25*, 134. (b) Balch, A.; Olmstead, M. M. *Chem. Rev.* **1998**, *98*, 2123. (c) Lee, K.; Song, H.; Park, J. T. *Acc. Chem. Res.* **2003**, *36*, 78.

2 (a) Rubin, Y. *Chem. Eur. J.* **1997**, *3*, 1009; (b) Rubin, Y. *Top. Curr. Chem.* **1999**, *199*, 67.

3 (a) Petrukhina, M. A. *Angew. Chem. Int. Ed.* **2008**, *47*, 2. (b) Petrukhina, M. A.; Scott, L. T. *J. Chem. Soc., Dalton Trans.* **2005**, 2969.

4 Ayers, T. M.; Westlake, B. C.; Preda, D. V.; Scott, L. T.; Duncan, M. A. *Organometallics* **2005**, *24*, 4573.

5 Stoddart, M. W.; Brownie, J. H.; Baird, M. C.; Scmider, H. L. *J. Organomet. Chem.* **2005**, *690*, 3440.

6 This complex was previously used for the preparation of metal complexes η^2 bound: Fagan, P. J.; Calabrese, J. C.; Malone, B. *Science* **1991**, *30*, 3980. For examples η^6 bound, see: (a) Chavez, I.; Cisternas, A.; Otero, M. Romàn, E. *Z. Naturforsch.* **1990**, 45*b*, 658. (b) Denbeck, A.A.; Fagan, P.J. *Organometallics* **1995**, *14*, 3741.

7 Seiders, T. J.; Baldridge, K. K.; O'Connor, J. M.; Siegel, J. S. *J. Am. Chem. Soc.* **1997**, *119*, 4781.

8 (a) Scott, L.T.; Hashemi, M. M.; Brachter, M. B. *J. Am. Chem. Soc.* **1992**, *114*, 1920. (b) Scott, L. T. *Pure & Appl. Chem.* **1996**, *68*, 291. (c) Seiders, T. J.; Baldridge, K. K., Siegel, J. S. **1996**, *118*, 2754.

9 Caraiman, D.; Koynagi, G. K.; Scott, L. T.; Preda, D. V.; Bohme, D. K. *J. Am. Chem. Soc.* **2001**, *123*, 8573.

10 Alvarez, C. M.; Angelici, R. J.; Sygula, A.; Sygula, R.; Rabideu, P. W. *Organometallics*, **2003**, *22*, 624.

11 White, J.; Thompson, S. J.; Maitlis, P. M. *J. Chem. Soc., Dalton trans.* **1977**, 1654.

12 Seiders, T. J.; Baldridge, K. K.; O'Connor, J. M. ; Siegel, J. S. *Chem. Comm.*. **2004**, 950.

13 (a) Seiders, T. J.; Elliot, E. L.; Grube, G. H.; Siegel, J. S. *J. Am. Chem. Soc.* **1999**, *121*, 7804. (b) Sygula, A.; Abdourazak, A.H.; Rabideau, P.W. *J. Am. Chem. Soc.* **1996**, *118*, 339.

14 (a) Haddon, R. C.; Scott, L. T. *Pure Appl. Chem.* **1986**, *58*, 137. (b) Haddon, R. C.

Acc. Chem. Res. **1988**, *21*, 243. (c) Haddon, R. C. *J. Am. Chem. Soc.* **1990**, *112*, 3385. (d) Haddon, R. C. *Science* **1993**, *261*, 1545.

[15] (a) Lee, K.; Song, H.; Park, J. T. *Acc. Chem. Res.* **2003**, *36*, 78. (b) Balch, A. L.; Olmstead, M. M. *Chem. Rev.* **1998**, *98*, 2123.

[16] Vecchi, P. A.; Alvazer, C. M.; Ellern, A.; Angelici, R. J.; Sygula A.; Sygula, R.; Rabideu, P. W. *Organometallics,* **2005**, *24*, 4543.

[17] Vecchi, P. A.; Alvrez, C. M.; Ellern, A.; Angelici, R. J.; Sygula, A.; Sygula, R.; Rabideu, P. W. *Angew. Chem. Int. Ed.* **2004**, *43*, 4497.

[18] (a) Hanson, J. C.; Nordman, C. E. *Acta. Crystallogr., Sect. B* **1976**, *B32*, 1147. (b) Sevryugina, Y.; Rogachev, A. Y.; Jackson, E. A.; Scott, L. T.; Petrukhina, M. A. *J. Org. Chem.* **2006**, *71*, 6615.

[19] Zhu, B.; Ellern, A.; Sygula, A.; Sygula, R.; Angelici, R. J. *Organometallics*, **2007**, *26*, 1721.

[20] (a) Lai, Y.-H.; Tam, W.; Vollhardt, K. P. C. *J. Organomet. Chem.* **1981**, *216*, 97. (b) Grundy, S. L.; Smith, A. J.; Adams, H.; Maitlis, P. M. *J. Chem. Soc., Dalton Trans.* **1984**, 1747. (c) Bennett, M. A.; Goh, L. Y.; Willis, A. C. *J. Am. Chem. Soc.* **1996**, *118*, 4984.

[21] Domaille, P.J.; Ittel, S. D.; Jesson, J. P.; Sweigart, D. A. *J.Organomet. Chem.* **1980**, *202*, 191.

[22] Siegel, J. S.; Baldridge, K. K.; Linden, A.; Dorta, R. *J. Am. Chem. Soc.* **2006**, *128*, 10644.

[23] (a) Windmüller, B.; Nürnberg, O.; Wolf, J.; Werner, H. *Eur. J. Inorg. Chem.*. **1999**, 613. (b) Dorta, R.; Rozenberg, H.; Shimon, L. J.; Milstein, D. *J. Am. Chem. Soc.* **2002**, *124*, 188.

[24] Schrock, R. R.; Osborn, J. A. *J. Am. Chem. Soc.* **1971**, *93*, 3089.

[25] Amaya, T.; Sakane, H.; Hirao, T. *Angew. Chem. Int. Ed.* **2007**, *46*, 8376.

[26] (a) Cotton, F. A.; Dikarev, E. V.; Petrukhina, M. A.; Stiriba, S.-E. *Polyhedron*, **2000**, *19*, 1829. (b) Cotton, F. A.; Dikarev, E. V.; Petrukhina, M. A. *J. Am. Chem. Soc.* **2001**, *123*, 11655.

[27] Petrukhina, M. A.; Andreini, K. W.; Mack, J.; Scott, L. T. *Angew. Chem. Int. Ed.* **2003**, *42*, 3375.

[28] Petrukhina, M. A.; andreine, K. W.; Peng, L.; Scott, L. T. *Angew. Chem. Int. Ed.* **2004**, *43*, 5477.

[29] Petrukhina, M. A.; Sevryugina, Y., Rogachev, A. Y.; Jaackson, E. A.; Scott, L. T.; *Angew. Chem. Int. Ed.* **2006**, *45*, 7208.

[30] Petrukhina, M. A.; Sevryugina, Y.; Rogachev, A. Y.; Jackson, E. A.; Scott, L. T. *Organometallics*, **2006**, *25*, 5492.

[31] Elliott, E. L.; Hernandez, G. A.; Linden, A.; Siegel, J. S. *Org. Biomol. Chem.* **2005**, *3*, 407.

[32] (a) Kakkar, A, K.; Taylor, N. J.; Calabrese, J. C.; Negent,W. R.; Roe, D. C.; Connaway, E. A.; Marder, T. B. *J. Chem. Soc., Chem. Comm.* **1989**, 990. (b) Mlekuz, M.; Bougeard, P.; Sayer, B. G.; McGlinchey, M. J.; Rodger, C. A.; Churchill, M. R.; Ziller, J. W.; Kang, S.-K.; Albright, T. A. *Organometallics* **1986**, *5*, 1656.

[33] Albright, T.A.; Burdett, J. K.; Whangbo, M. H. *Orbital Interactions in Chemistry*; Wiley-Intersceinece: NY, 1985

[34] (a) Dewar, M. J. S. *Bull. Soc. Chim. Fr.* **1951**, *18*, C79. (b) Chatt, J.; Duncanson, L. A. *J. Chem. Soc.* **1953**, 2939. (c) Dewar, M. J. S.; Ford, G. P. *J. Chem. Soc.* **1979**, *101*, 783.

[35] Zeise, W. C. *Ann. Phys. und Chem.* **1831**, *97*, 497.

[36] (a) Muetterties, E. L.; Bleeke, J. R.; Wucherer, E. J.; Albright, T. A. *Chem. Rev.* **1982**, *82*, 499. (b) Hrovat, D. A.; Borden, W. T. *J. Am. Chem. Soc.* **1988**, *110*, 4710. (c) Smith, J. M.; Hrovat, D. A.; Borden, W. T.; Annan, M.; Asmis, K. r.; Buillard, C.; Haselbach, E.; Meier, U. C. *J. Am. Chem. Soc.* **1993**, *115*, 3816. (d) Rondan, N. G.; Paddon-Row, M. N.; Caramella, P.; Houk, K. N. *J. Am. Chem. Soc.* **1981**, *103*, 2436. (e) Mastryukov, V. S.; Chen, K.-H.; Allinger, N. L. *J. Phsy. Chem. A* **2001**, *105*, 8562. For conformation of cyclones see: (f) Favini, G.; Rubino, C.; Todeschini, R. *J. Mol. Str.* **1977**, *41*, 305. (g) Pauncz, R.; Ginsburg, D. *Tetrahedron*, **1960**, *9*, 40.

[37] Sievert, A. C.; Muetterties, E. L. *Inorg. Chem.* **1981**, *20*, 489

[38] Sevryugina, Y.; Rogachev, A. Y.; Jackson, E. A.; Scott, L. T.; Petrukhin, M. A. *J. Org. Chem.* **2006**, *71*, 6615.

[39] Acton, N.; Roth, R. J.; Katz, T. J.; Frank, J.; Maier, C. A.; Paul, I. C. *J. Am. Chme. Soc.* **1972**, *94*, 5446.).

[40] (a) Perrin, C. L.; Dwyer, T. J. *Chem. Rev.* **1990**, *90*, 935. (b) Jeener, J.; Meier, B. H.; Bachmann, P.; Ernst, R. R. *J. Chem. Phys.* **1979**, *71*, 4546. (c) Kumar, A.; Wagner, G.; Ernst, R. R.; Wütrich, K. *J. Am. Chem. Soc.* **1981**, *103*, 3654.

[41] Cramer, R. *J. Am. Chem. Soc.* **1964**, *86*, 3089.

[42] Szajek, L. P.; Lawson, R. J.; Shapley, J. R. *Organometallics* **1991**, *10*, 357.

[43] (a) Adams, H.; Bailey, N. A.; Mann, B. E.; Taylor, B. F.; White, C.; Yavari, P. *J. Chem. Soc., Dalton Trans.* **1987**, 1947. (b) Nambu, M.; Mohler, D. L.; Hardcastle, K.; Baldridge, K.K.; Siegel, J. S. *J. Am. Chem. Soc.* **1983**, *115*, 6138. (c) Kilway, K. V.; Siegel, J. S. *J. Am. Chem. Soc.* **1991**, *113*, 2332.

[44] $\Delta G^{\neq} = 19.1 \cdot 10^{-3} T_c \cdot \left(9.97 + \log T_c - \log\left|\upsilon_A - \upsilon_B\right|\right)$ (a) Sandstrom, J. *Dynamic NMR Spctroscopy*; Academic press: NY, **1982**; p97. (b) Gutowski, H. S.; Holm, C. H. *J. Chem. Phys.* **1956**, *25*, 1228..

[45] (a) Ustynyuk, N. A.; Lokshi, B. V.; Orpunenko, Y. F.; Roznyatovsky, V. A.; Luzikov, Y. N.; Ustynyuk, Y. A. *J. Organomet. Chem.* **1980**, *202*, 279. (b) Rogers, R. D.; Atwood, J. L.; Albright, T.A.; Lee, W. A.; Rausch, M. D. *Organometallics*, **1984**, *3*, 263. (c) Brydges, S.; Reginato, N.; Cuffe, L. P.; Seward, C. M.; McGlinchey, M. J. *C. R. Chemie* **2005**, *8*, 1497. (d) Rigby, S. S.; Decken, A.; Bain, A. D.; Mcglinchey, M. J. *J. Organomet. Chem.* **2001**, 372. (e) Dötz, K. H.; Jahr, Holger, C.; *Chem. Rec.* **2004**, *4*, 61. (f) Dötz, K. H.; Stendel, J. Jr.; Müller, S.; Nieger, M.; Ketrat, S.; Dolg, M.; *Organometallics*, **2005**, *24*, 3219.

[46] (a) Heise, J. D.; Raftery, D.; Breedlove, B. K.; Washington, J.; Kubiak, C. P. *Organometallics*, **1998**, *17*, 4461. (b) Abel, E. W.; Coston, T. J.; Orrell, K. G.; Sik, V.; Stephenson, D. *J. Magn. Res.* **1986**, *70*, 34. (c) Dimitrov, V. S.; Vassilev, N. *Magn. Res. Chem.* **1995**, *33*, 739.

[47] (a) Macura, S. *J. Magn. Res. A.* **1995**, *112*, 152. (b) Zolnai, Z.; Juranic, N.; Vikic-Topic, D.; Macura, S. *J. Chem. Inf. Compt. Sci.* **2000**, *40*, 611.

[48] The growth of the cross peaks is almost the same and almost linear, thus the exchange matrix has all the elements equal. The diagonal peaks have also the same intensities and this means the process is only one.

[49] (a) Willem, R. *Prog. Nucl. Magn. Res. Spectrosc.* **1987**, *20*, 1. (b) Ramachandran, R.; Knight, C. T. G.; Kirkpatrick, R. J.; Oldfield, E. *J. Mag. Res.* **1985**, *65*, 136. (c) Willem, R.; Biesemans, M.; Hallenga, K. Lipens, F.; Mailasse-Lagae, F. Mailasse, W. J. *J. Biol. Chem.* **1992**, *267*, 210.

[50] Jimenéz-Halla, J. O. C.; Robles, J.; Solà, M. *J Phys. Chem. A.*, **2008**, *112*, 1202.

[51] $\Delta G^{\neq} = RT \cdot \left[\ln\left(\frac{k_B}{h}\right) - \ln\left(\frac{k}{T}\right) \right]$ in which k_B = 1.381 10^{-23} J K^{-1}, h = 6.626 10^{-34} J s, R = 8.314 J K^{-1} mol^{-1}.

[52] Jones, C. S.; Elliott, E.; Siegel, J. S. *Synlett*. **2004**, 187.

[53] Seiders, T. J.; Elliot, E. L.; Grube, G. H.; Siegel, J. S. *J. Am. Chem. Soc*. **1999**, *121*, 7804.

[54] Sevryugina, Y.; Rogachev, A. Y.; Jackson, E. A.; Scott, L. T.; Petrukhin, M. A. *J. Org. Chem*. **2006**, *71*, 6615.

[55] (a) Abel, E. W.; Bennett, M. A.; Wilkinson, G. *J. Chem. Soc*. **1959**, 3158. (b) Herde, J. L.; Lambert, J. C., Senoff, C. V.; Cushing, M. A. *Inorganic Syntheses*, **1974**, *15*, 18-20. (c) Girdano, G.; Crabtree R. H.; Heintz, R. M.; Forster, D.; Morris, D. E. *Inorganic Syntheses*, **1990**, *28*, 88. (d) Giordano, G.; Crabtree, R. H.; Heintz, R. M.; Forster, D.; Morris, D. E. *Inorganic Syntheses*, **1990**, *28*, 91. (e) Komiya, S. *Synthesis of Organometallic Compounds*, Wiley & Sons, Chichester, UK, 1997, p237.

Chapter 4.

Synthesis and Properties of Rh(I) Complexes of $C_{20}H_{10}$, $C_{25}H_{20}$ and $C_{40}H_{50}$ with a Metal Fragment Bearing an Enantiomerically Pure Ligand.

4.1. Introduction

The discovery of fullerenes, the first molecular allotropes of carbon in 1985[1] and their synthesis in macroscopic amount by arc vaporization of graphite in 1990[2] have profoundly influenced several aspects of contemporary chemistry. Some of the higher order fullerenes are chiral[3] and the isolation of the enantiomerically pure bucky-balls, as well as the study of their properties, has lead to the development of a new field of stereochemistry. The functionalization and metallation of the carbon spheres has resulted in variety of unprecedented new molecular structures and shapes that have been investigated for their reactivity, physical properties and applications in advanced materials.

The fragments of fullerenes, the so called bucky-bowls, can also be chiral. Some examples are: monosubstituted corannulene derivatives,[4] hemibuckminsterfullerene,[5] benzo[*a*]acecorannulene,[6] substituted indenocorannulenes,[7] *sym*-pentaaryl-[8] and *sym*-penta(arylethynyl)-corannulene derivatives.[9] These chiral bucky-bowls are, however, prepared as racemic mixtures. Recently, a stereoselective synthesis of trimethylsumanene[10] and the first chiral complex of sumanene[11] were reported.

In the previous chapter, we have addressed the issues of the synthesis and dynamics of some Ir(I) and Rh(I) metal complexes of alkylsubstituted corannulene derivatives but still some questions remain. In fact, data suggest that the metal migration on the corannulene nucleus occurs *via* the *hub* ring and most likely, in a intramolecular fashion. However, a strong evidence for this mode of migration is still missing. Furthermore, it is uknown whether chiral racemic, corannulene derivatives having C_5 symmetry (Figure 4.1) like 1,3,5,7,9-pentamethylcorannulene (**54**) and 1,3,5,7,9-pentakis(*t*-butyl)corannulene (**104**) can react with an enantiomerically pure metal fragment, to give diastereoisomerically enriched compounds.

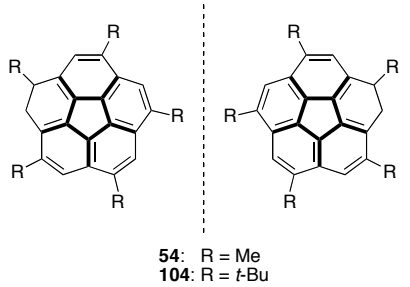

54: R = Me
104: R = *t*-Bu

Figure 4.1. Corannulene derivatives having C_5 symmetry.

4.1.1 Inherently chiral fullerenes

In 1993, the first chiral fullerene C_{76} was isolated,[12] opening a new chapter of stereochemistry in which new structural motifs and nomenclature had to be developed. C_{76} (Table 4.1, **124**) has a D_2 symmetric structure and was first predicted by Manolopoulus[13] as the only possible isomer. After its discovery,[12] the structure was confirmed by ^{13}C NMR, which gave a spectrum consisting of nineteen, equally intense lines. Achiba, by an ^{13}C INADEQUATE experiment observed that the chemical shifts correlate with the curvature of the spheroids: the more strongly pyramidalized carbon center, being shifted to lower magnetic field.[14]

Table 4.1. Structure and symmetry of some higher fullerenes.

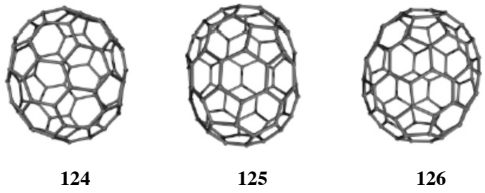

124 **125** **126**

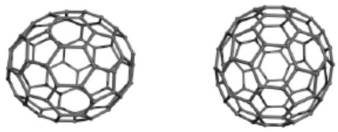

127 **128**

Compound	C_n	Point Group
124	C_{76}	D_2
125	C_{78}	D_3
126	C_{80}	D_2
127	C_{82}	C_2
128	C_{84}	D_2

Among the five possible isomers of C_{78}, only one is chiral and has D_3 symmetry. It was first isolated as minor component next to C_{78}-C_{2v}, by HPLC purification of the higher fullerene fraction of soot extract. (Table 4.1, **125**).[15,16]

Due to its very low abundance in fullerene soot, it took several years to isolate the next higher fullerene C_{80}.[17] Its ^{13}C NMR spectrum showed twenty groups of four symmetry-equivalent carbon atoms and, in combination with calculations,[18] a D_2 symmetric structure was proposed (Table 4.1, **126**).

A chiral isomer of C_2 symmetry (41 ^{13}C NMR peaks) has been shown to be the major component of the C_{82} fraction of fullerene soot.[14] Due to the fact that three structures with this symmetry are possible, an assignment seemed difficult at first. Calculation of the ^{13}C NMR spectrum, in conjunction with stability considerations, have identified the $C_{82}(3)$-C_2 symmetric fullerene as **127** (Table 4.1).[19]

Due to its relatively large abundance in fullerene soot, as well as its structural (isomeric) diversity, C_{84} is one of the most interesting higher order fullerenes. Early ^{13}C NMR studies revealed the presence of two major isomers of D_2 and D_{2d} symmetry in a 2:1 ratio.[20] Theoretical calculations,[21] X-ray analyses of an Ir derivative,[22] together with 2D ^{13}C NMR spectroscopy,[14] allowed the assignment of the $C_{84}(22)$-D_2 symmetric structure (Table 4.1, **128**). Enriched samples of fullerene with more than 84 C-atoms, have been obtained and their symmetric structure assigned, in particular C_{86}, C_{88}, C_{90}, C_{92}, C_{94}.[23]

Within this section on inherently chiral carbon allotropes, it should be mentioned that most carbon nanotubes, which can be considered as extremely large and oblong fullerenes in their idealized single–walled form, are chiral (Figure 4.2, **129**). In fact, the central part represents a graphite lattice that is rolled up into a cylinder. This roll up "process" does not necessarily occur parallel or perpendicular to opposite edges of the constituting hexagons. Any intermediate orientation leads to an arrangement in which the tube walls can be considered as interlocking helical strands of edge-sharing hexagons winding around the axis of the tube. Helical carbon nanotubes where discovered by Iijima[24] and later confirmed by STM (scanning tunnel microscopy) images of single nanotube surfaces resolved at the atomic level.[25]

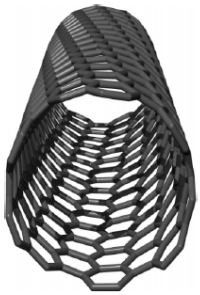

129

Figure 4.2. Chiral (9, 6)-SWNT.

Chiral fullerenes like C_{76}-D_2 and $C_{84}(22)$-D_2 have been resolved. In particular, Hawkins and Meyer performed a kinetic resolution of C_{76}-D_2 by asymmetric Sharpless osmylation of the racemic fullerene, using OsO_4 complexes with an enantiomerically pure ligand derived from a cinchona alkaloid (Scheme 4.1).[26]

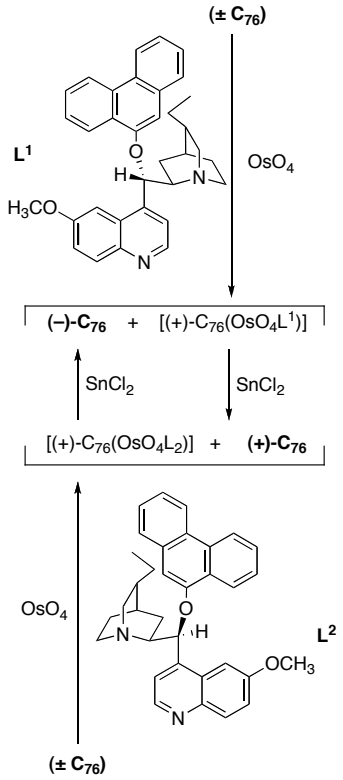

Scheme 4.1. Kinetic resolution of (±)-C_{76}-D_2.

Incomplete osmylation of (±)C_{76} afforded enantiomerically enriched unreacted [76]fullerene and a diastereoisomerically enriched osmate complex. Removal of the addend from the latter with $SnCl_2$ yielded C_{76} enriched in the other enantiomer. When a pseudoenantiomeric ligand was used in the reaction, the enantiomers of the carbon cage were enriched in the starting material and in the product.[26] The first CD spectra were also recorded. Following this first report, the same procedure was used for the resolution of C_{78}-D_3 and $C_{84}(22)$-D_2.[27] The first reported CD data from different group had some discrepancies.[27,28] Thus, the chiroptical properties were reinvestigated. In particular, a new procedure was used for the separation of the enantiomers of C_{76}. The resolution was performed by a Bingel/retro Bingel approach.[29] This separation consistsed of three steps, starting with the cyclopropanation of a fullerene mixture with 2-halomalonates (Bingel reaction).[30] The fullerene-derived esters are easier to separate and, thereafter, the Bingel addends are removed by exhaustive constant

potential electrolysis,[31] regenerating the clean fullerene. In summary, the method involves a reversible functionalization of fullerene including a facilitated separation of the covalent derivatives (see ref.1 for CD spectra and structures of the Bingel addends). The Bingel cyclopropanation was also applied to the separation of $C_{84}(22)$-D_2 and the CD spectra were recorded (See Ref. 1 for CD spectra).[32]

Direct chromatographic resolution of a chiral fullerene was achieved for the first time by Okamoto for C_{76} through recycling HPLC on amylose tris[(3,5-dimethylphenyl)carbamate] with hexane/$CHCl_3$ 80:20 as eluent.[33] Several other derivatives of C_{60} and C_{70} bearing chiral moieties have been prepared and characterized, as reviewed by Thilgen and Diederich.[3]

4.1.2 Some examples of chiral organometallic complexes and derivatives of fullerene

The aim of this section is to show some examples of chiral organometallic complexes and derivatives of C_{60} (**2**) and C_{70} (**129**). Treatment of C_{60} with organocopper reagents[34] leads to addition of five organic groups in high yield to the far ends of the 6–6 bonds radiating from a pentagon, turning the latter into a cyclopentadienyl anion, which, upon protic workup, affords pentakis-adducts **130**.[35]

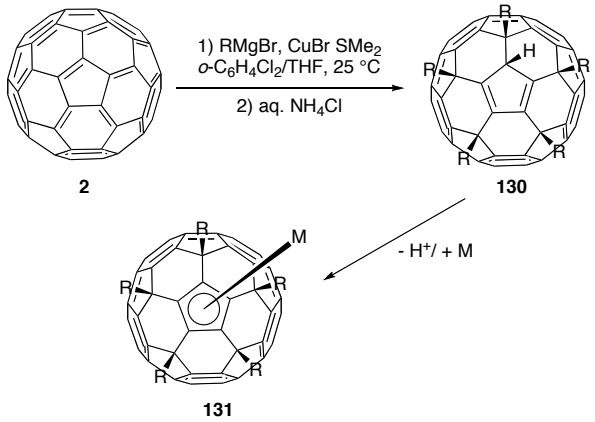

Scheme 4.2. Adddition of organocopper reagents to C_{60}.

The anionic cyclopentadienides, in addition to forming small bilayer vesicles in water,[36] can be used as η^5-ligands in a variety of metal complexes.[35] If the added residues in such complexes (**131**) are aryl groups, they adopt a chiral, propeller-

shaped, C_5-symmetric arrangement,[35c] whereas they can freely rotate in the protonated species (**131**) unless the R groups are fluorenyl residues (Scheme 4.2).[37]

When a Grignard reagent is added to a 1,4-bisadduct of C_{60}, the reaction stops at the stage of tris-adduct formation (Scheme 4.3, **132** and **133**).[38] In this case, the anionic fragment (**134**) corresponds to a indenyl anion[39] and the protonation of the corresponding pentagon takes place in an unsymmetric way, leading to an inherently chiral pattern.

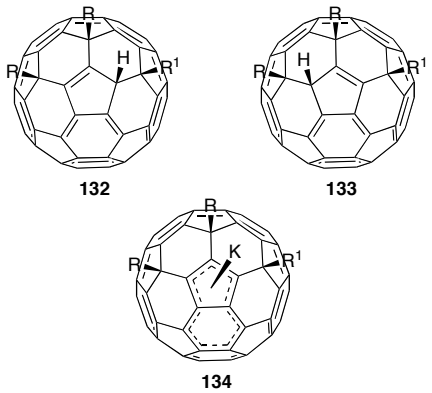

Figure 4.3. Tris-Adducts of C_{60}.

By twofold application of the "cyclopentadiene addition mode" to C_{60}, Nakamura was able to access an interesting class of compounds in which opposite corannulene caps are functionalized and the fullerene chromophore is reduced to a [10]cyclophenacene belt with 40 π-electrons, which represents the shortest version of a (5,5) armchair, chiral, carbon nanotube (See Ref. 1, Scheme 37).[40]

Nakamura and co-workers have also reported the use of a ligand possessing a concave cavity in "remote chirality transfer".[41] This idea emerged from the observation that, for istance, the reaction of $[Ru(\eta^5\text{-Cp})Cl(PPh_3)_2]$, with a chiral diphosphine ligand of modest steric demand, (*R*)-1,2-bis(diphenylphoshpino)propane (*R*-prophos), gives an essentially 1:1 mixture of two diastereoisomers (Scheme 4.3).[42] The diastereoselectivity could be improved by the use of sterically more demanding pentamethylcyclopentadienide ligand.[43]

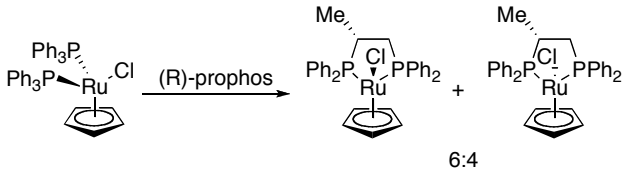

Scheme 4.3. Reaction of [Ru(η^5-Cp)Cl(PPh_3)$_2$] with (*R*)-prophos.

Nakamura considered that the installation of a ligand with a concave structural motif on the metal center would limit the conformational mobility of the other ligands and would enhance the steric effect of one ligand to the other. Nakamura's ligands of choice were a new class of cyclopentadienide (Cp) moieties in which the Cp belongs to the concave cavity built on the skeleton of a fullerene.[41]

According to the procedure shown in Scheme 4.2, several pentaorgano fullerene metal complexes can be prepared. The protruding R groups provide a new type of environment for the metal which protects, in the case that the R groups are big enough, the metal center itself. The modulation of the hight of the protecting "wall", might control the coordination chemistry of the metal atom by limiting the mobility of the ligands.

Reaction of **135** with (*R*)-prophos at 150 °C, gives compound **136** (Scheme 4.4) as a single diastereoisomer as determined by NMR and HPLC analyses.[41] X-ray analyses allowed the determination of the configuration at the Ru stereogenic center as S_{Ru}. The methyl substituent points away from the chlorine atom on the Ru. The excellent diastereoselectivity induced Nakamura to examine the formation of the corresponding cationic complex **137** by treatment of **136** with $AgSbF_6$. In particular, this reaction was performed in the presence of a nucleophile **L** to see whether the reaction proceeded with a degree of diastereoselectivity to give **138**. Distereoselectivities ranging from 84 to100% were found.

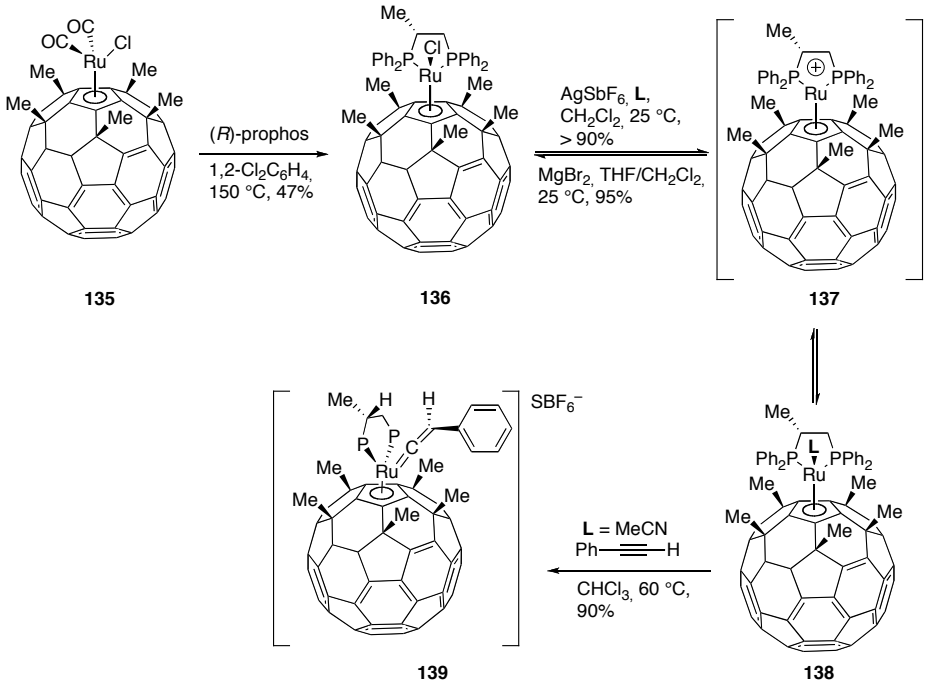

Scheme 4.4. Nakamura's example of "remote chirality transfer".

Furthermore, reaction of **138** (with **L** = MeCN) with phenylacetylene gave **139** as a sigle diastereoisomer. The basic system shown here opens new opportunities in asymmetric synthesis of organic and inorganic compounds.

C_{60} and C_{70}, can complex chiral enantiomerically pure metal fragments. For example, Sokolov and co-workers submitted the above mentioned fullerene to a reaction with $Pd_2(dba)_3$ in the presence of a chiral, enantiomerically pure ligand **140** ((-)TertraMe-BITIOP),[44] and obtain the complexes **141** and **142** (Scheme 4.5). Circular dichroism spectra were recorded and exhibited ill-resolved Cotton effects shifted to longer wavelength with respect to the ligand **140** that probably comes about by an electron transfer from the ligand to the fullerene as has already been observed.[45] Other complexes of C_{60} with chiral metal fragments have been reported,[46] for example, the complexes of W and Mo in the presence of (+) or (-) DIOP.[47]

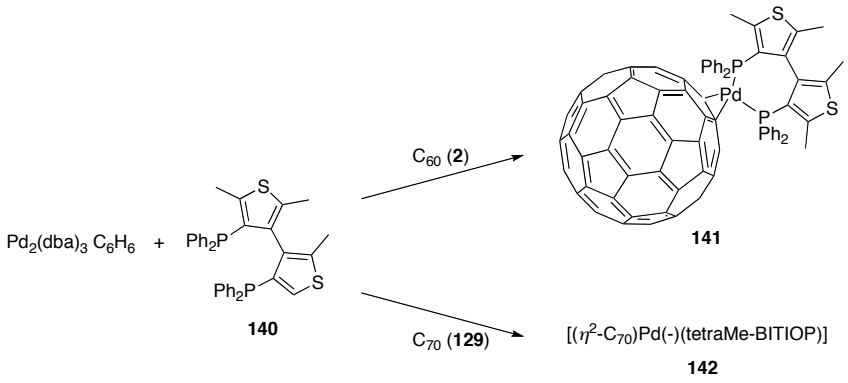

Scheme 4.5. Reaction of C_{60} and C_{70} with a chiral metal fragment.

4.1.3. Interaction of corannulene with surfaces.

Ernst and co-workers have investigated the interaction of the C_{5v}, corannulene, with the C_{2v} surface of copper[110].[48] The twofold symmetry of this surface provides the right degree of mobility for small aromatic molecules to establish long-range order at and below room temperature. Long-range STM topographies reveal the formation of ordered lattice structures. Two mirror domains of a quasi hexagonal superlattice were observed together with a tilting of the corannulene with respect to the surface (Figure 4.4).

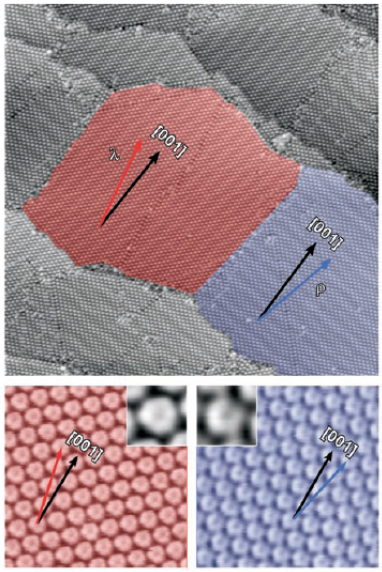

Figure 4.4. STM images of corannulenene and the enantiomorphous domains, red and blue.

The same group was also involved in the study of substituted, chiral, C_5 symmetric racemic derivatives of corannulene on different metal surfaces to elucidate their assembly.[49] In particular, it was found that substituted derivatives such as in *sym-*

pentachloro- and *sym*-pentamethyl-corannulene (on Au (12 12 12) and Cu(111) respectively) do not allow for a tilting of the corannulene core, due to steric bulk leading to hexagonal lattices with dislocations or azimuthal disorder at a local length.[49]

4.1.4. Chiral fragment of C_{60}: trimethylsumanene

Sakurai and co-workers have recently reported the first asymmetric synthesis of a chiral buckybowls: trimethylsumanene having C_3 symmetry.[10] The synthetic patway starts with enantiomerically pure (1*S*,4*S*)**147**, that is converted with high diastereoselectivity to *anti*-**146** by a cyclotrimerization reaction. The carbonyl groups on **146** were treated with MeMgI to obtain the benzonorbornene derivative **145**. Treatment of **145** first with the Grubbs first generation catalyst, followed by the Grubbs second generation catalyst, afforded by ring opening/ring closing reactions, the desired compound **144**. The latter was converted to the final product (*C*-**143**) by treatment with DDQ with and overall yield of 4.8% (Scheme 4.6).

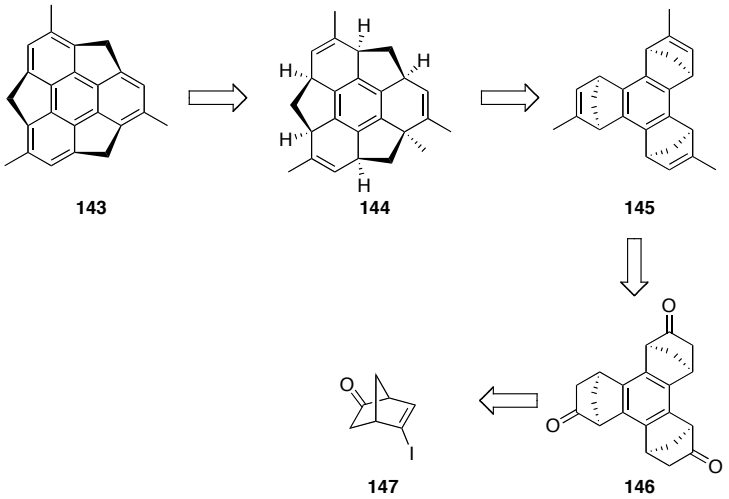

Scheme 4.6. Synthesis of Trimethylsumanene.

A CD spectra was recorded at -40°C and the intensity scarcely changed. Measurement at 10°C showed gradual decrease of the Cotton effect due to bowl-to-bowl inversion. The barrier of inversion was determined by the decay of the CD spectra and estimated to be 21.6 kcal mol^{-1}. The enatiomeric excess of **143**, was determined on the derivative bearing (*S*)-Ph(CF_3)(OMe)CCO (**148**) groups on the sp^3

C-atoms of trimethylsumanene. ^{1}H NMR analysis showed an enantiomeric excess for **143** of 90% based on the distereoisomeric ratio of **148** (Figure 4.5).

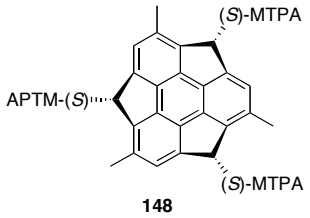

148

Figure 4.5. Derivative 148 (MTPA = (*S*)-Ph(CF$_3$)(OMe)CCO).

4.1.5. Chiral complex of sumanene.

Sumanene was found to form ferrocene-like complexes in which the is metal was bound on the *endo* face.[50] In a recent study, it was found that substitution of the Cp ligand in such a complex with Me-Cp showed a partially restricted rotation, observed by VT-NMR experiments, in the temperature range -60– +45 °C. The reaction of the enantiomerically pure *sec*-butyl-substituted ferrocene complex, with sumanene in the presence of Al powder and $AlCl_3$ afforded compound **149**, which is the first chiral complex of a bucky-bowl (Scheme 4.7). The ^{1}H NMR spectrum of **149** showed four different signals for the Cp ring and a splitting of the *endo*-benzylic proton and the proton on the coordinated benzene. CD spectra displayed Cotton effects at 272, 303, and 517 nm.

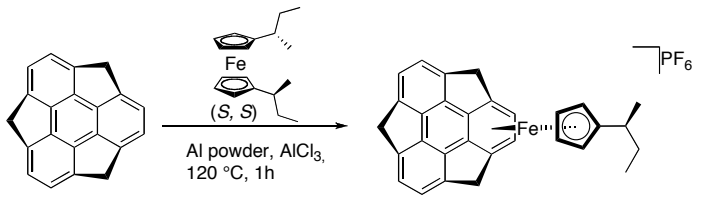

80 **149**

Scheme 4.7. Preparation of the chiral complex 149.

4.2 Present work

In this section, the synthesis and properties of Rh(I) complexes in cases in which a chiral ligand is used for the preparation of the metal fragment will be shown. Particular emphasis will be given to the stereochemical outcome of such reactions and to the properties of the recently synthesized compounds.

4.2.1. The hypothesis

The main idea of this project is to determine which stereoselectivity is afforded by the reaction of an enantiomerically pure metal fragment with a chiral, C_5, racemic corannulene derivative. When an enantiomerically pure metal fragment is used for the complexation of corannulene (**1**), 1,3,5,7,9-pentamethylcorannulene (**54**) and 1,3,5,7,9-penta(*t*-butyl)corannulene (**104**), the growing steric bulkiness of the substituents on the corannulene core drives the stereochemical outcome of the reaction towards diastereoisomerically enriched products, due to repulsive interactions with the ligands L (Figure 4.6).

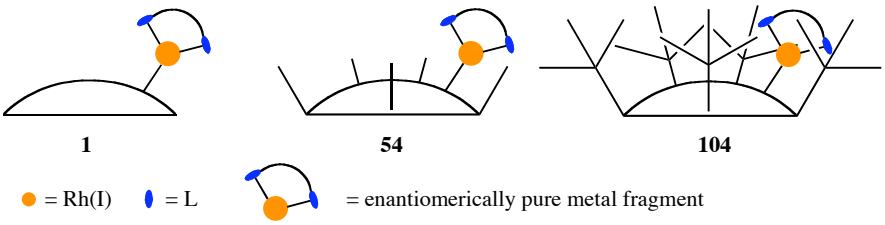

Figure 4.6. The concept at the base of the project.

In particular, based on the structural information obtained from the crystallographic analysis of the complex $\{[Rh(NBD)]_2(C_{40}H_{50})\}(PF_6)_2$ (**122**) and the NMR studies on the conformation of Rh(I) complexes shown in Chapter 3, the chiral (*R*,*R*)-2,5-dimethyl-bicyclo[2.2.1]hepta-2,5-diene was selected to as the ligand for this study. The favored or unfavored steric interactions between the methyl groups on the olefinic ligand and the alkyl groups on the corannulene core will result in a preference of the chiral metal fragment towards the *M* or *P* enantiomers of the corannulene (Figure 4.7). Furthermore, the pentasubstituted corannulene derivatives, possessing C_5 symmetry, are chiral but the low inversion barrier[8] leads to racemization of the enantiomers. This means that not only a diastereoselective complexation, but also a dynamic kinetic resolution of the two enantiomers is possible.[51]

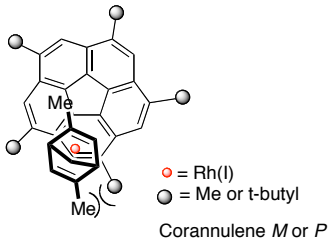

Figure 4.7. Steric interaction of the chiral diene with C_5 corannulene derivatives.

4.2.2. Synthesis of the ligand.

The use of chiral olefins as ligands for Rh(I) and Ir(I) in asymmetric catalysis has grown in the recent years.[52] Such ligands have been applied in diastereoselective and enantioselective reactions with good results.[53] For this type of ligand, the mode of space differentiation is different compared to conventional ligands such as BINAP. In biphosphanes, the stereochemical outcome of reactions is controlled by face/edge orientations of the aryl substituents on the phosphorus atoms, while, in dienes, it is controlled by the size of the substituents attached to the double bonds.[52b]

In 2006[54] new C_2-symmetric chiral diene ligands derived from bicyclo[2.2.1]hepta-2,5-diene bearing methyl and phenyl substituents at the 2 and 5 positions were introduced. In this report the isolation of the dienes was achieved by formation of the corresponding $[RhCl(diene)]_2$ complexes. The synthesis of these ligands starts from enantiomerically pure (1*R*,4*R*)-bicylco[2.2.1]hepta-2,5-dione **152** that is first converted to the ditriflate **151** and finally to the corresponding disubstituted dienes **150** (Scheme 4.8).

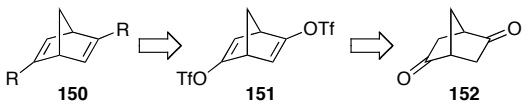

Scheme 4.8. Retrosynthetic scheme for the preparation of 150.

The preparation of the Rh(I) complex containing the ligand of choice **155** (Scheme 4.9), starts from **153** by means of double enantioselective hydrosilylation using (*R*)-MeO-MOP[55] in the presence of $[PdCl(C_3H_5)]_2$, followed by oxidation, giving diol **154**.[56] This diol is then oxidized, by Swern conditions to yield **152**.[56] Compound **152** is converted to the ditriflate **151** by treatment with KHMDS in the presence of the mild triflating agent 2-$PyNTf_2$.[57] Complex **155** is then prepared by the reaction of **151** with MeMgBr in the presence of $Fe(acac)_3$ to give the intermediate (*R*,*R*)-2,5-dimethyl-bicyclo[2.2.1]hepta-2,5-diene, which is then treated with $[Rh(C_2H_4)Cl]_2$ to give the desired compound **155**.[54]

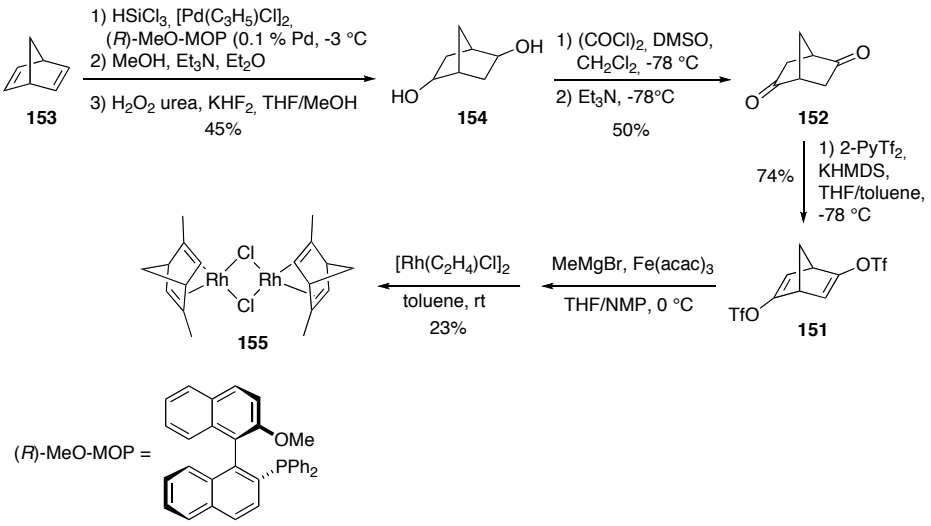

Scheme 4.9. Synthesis of the complex 155.

4.2.3. Synthesis of the new complexes bearing a chiral, enantiomerically pure metal fragment

The syntheses of these complexes has been achieved *in situ* by the procedure discussed in Chapter 3.[58] The reaction of corannulene and its racemic C_5 derivatives with the chiral complex {Rh[(*R*,*R*)-2,5-dimethyl-bicyclo[2.2.1]hepta-2,5-diene]Cl}$_2$ in the presence of $AgPF_6$ gave the desired products in good yields (Scheme 4.10).

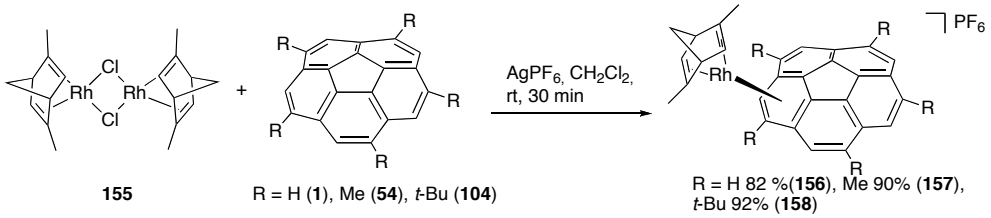

Scheme 4.10. Synthesis of complex bearing a chiral metal fragment.

It is important to analyze the possible stereochemical outcomes of these reactions. In particular, only one product is possible for **156**. In the case of compounds **157** and **158**, two diastereoisomers are possible due to the C_5 symmetry of the corannulene derivatives, (Figure 4.8).

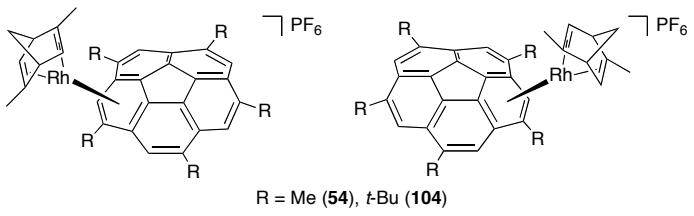

Figure 4.8. Possible diatereoisomers in 157 and 158.

The chiral metal fragment contains a diene having C_2 symmetry: [(*R*,*R*)-2,5-dimethyl-bicyclo[2.2.1]hepta-2,5-diene. Such a diene will drive the stereochemical outcome of these reactions towards one diatereoisomer or to diastereoisomerically enriched products. This selectivity is related to the possible preferential interactions with the *M* or *P* enantiomers of the C_5 symmetric corannulene derivatives **54** and **104**.

4.2.4. Stereochemical analysis of the chiral complexes 156-158.

The ^{1}H NMR spectra of complexes **156**-**158** provides fundamental insights regarding the stereochemical outcome of the reactions described in Scheme 4.10. In particular, the reaction between {Rh[(*R*,*R*)-2,5-dimethyl-bicyclo[2.2.1]hepta-2,5-diene]Cl}$_2$ and **1** yields one product (**156**), which is the only possible. The ^{1}H NMR spectrum displays a set of non-resolved proton signals at 300 K in the aromatic region. This is commonly observed for complexes in which the metal fragment migrates (see Chapter 3). Upon cooling, the signals undergo de-coalescence to a set of ten proton signals, which is typical for an η^6 bound metal, due to a slowed migration process (Figure 4.9). When the same complex is warmed, the aromatic region signals coalesce to one broad peak at 338 K without decomposition and, upon cooling no changes are observed in the low temperature ^{1}H NMR spectra.

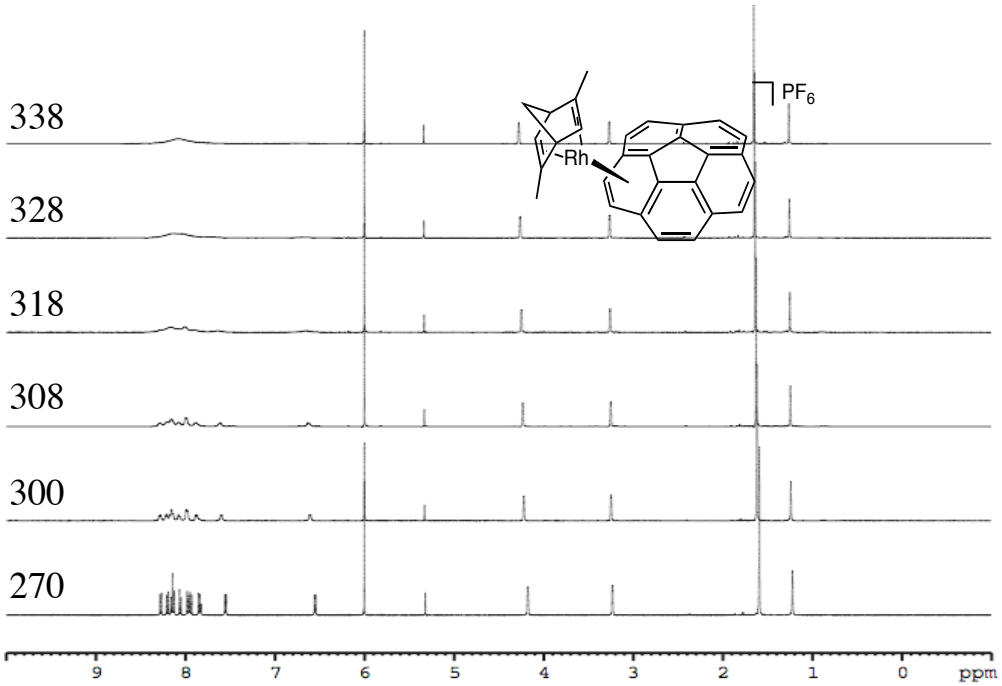

Figure 4.9. Variable temperature ^{1}H NMR spectra for 156 in $C_2D_2Cl_4$.

The reaction between {Rh[(*R*,*R*)-2,5-dimethyl-bicyclo[2.2.1]hepta-2,5-diene]Cl}$_2$ and the C_5 derivatives are more interesting. In fact, diastereoselectivity was observed in these two examples.

Compound **157**, having 1,3,5,7,9-pentamethylcorannulene as one of the ligands, shows, by analysis of the ^{1}H NMR spectrum (Figure 4.11, bottom), a mixture of two compounds. The aromatic region displays two sets of five signals supporting the presence of two diatereoisomers in a 1.8:1 ratio. Sets of two split signals are also observed for the protons (Figure 4.10) of the diene ligands belonging to the two different diastereoisomers. These observations are in agreement with the initial hypothesis for which a complementary steric interaction (Figure 4.7) between the C_2, chiral norbornadiene ligand and the enantiomers of the C_5 corannuelene derivative could lead to diastereoisomerically enriched products.

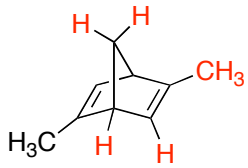

Figure 4.10. ^{1}H NMR signals in the C_2 ligand.

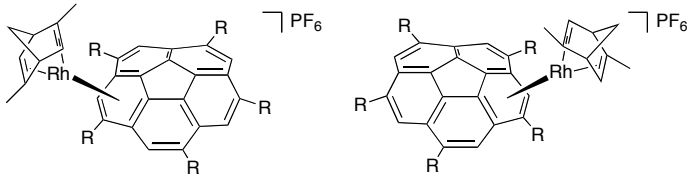

R = Me (**54**), *t*-Bu (**104**)

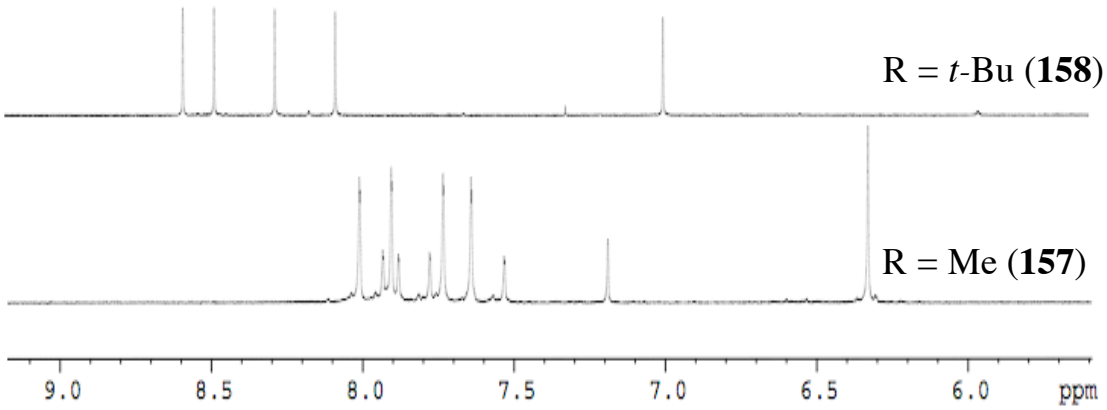

Figure 4.11. ^{1}H NMR spectra for 158 (top) and 157 (bottom).

Compound **158** having 1,3,5,7,9-penta(*t*-butyl)corannulene as one of the ligands, shows, by analysis of the ^{1}H NMR spectrum, only one set of signals in the aromatic region (Figure 4.11, top) and for the diene ligand. These observations suggest that, in this case, the steric interactions occurring between the diene ligand and the *t*-butyl substituents on the corannuele core are much more effective compared to the one observed in **157** and lead to the formation of a highly diastereoisomerically enriched product **158**.

The results presented above not only show the possibility of preparing chiral complexes of corannulene derivatives, but also show that, during these reactions, a dynamic kinetic resolution (DKR) process takes place.[51] DKR involves a one-pot procedure in which racemization is coupled to an irreversible enantiomer-differentiating reaction. The aim of this process is the quantitative conversion of a racemate to a single stereoisomer of a new compound and neither of the enantiomers is recovered because enantioconversion is combined with an asymmetric reaction that consumes the starting material. Dynamic resolution obeys the Curtin-Hammet principle,[59] as the ratio of the products formed by the enantiomer-differentiating step is determined by the difference in the free activation energies (Figure 4.12).

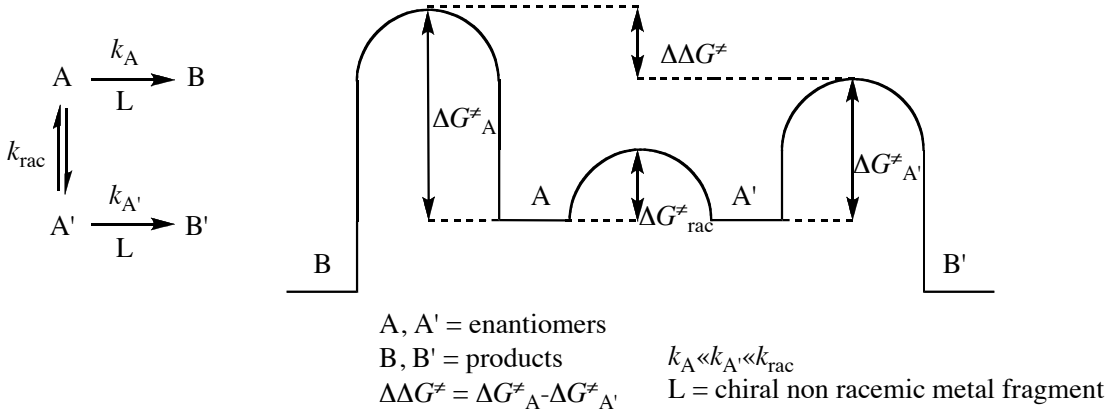

Figure 4.12. Illustration of dynamic kinetic resolution.

In addition, the rate costant for racemization k_{rac}, should be higher than the rate costant for the faster of the two conversions, $k_{A'}$, or at least several times higher than k_A in the case of very high selectivity. In figure 4.11, L and A' constitute a matched pair, whereas A gives a mismatched pair. In our examples, A and A' are the rapidly

interconverting[4] (by bowl inversion) *M* and *P* enantiomers of the C_5-symmetric corannulene derivatives. L is the enantiomerically pure metal fragment, B and B' are the two products.

The outcome of the reaction leading to **157** suggests that $k_{A'}$ is three time larger than k_A and, in fact, a 2.5:1 ratio in the product was observed. In the case of **158** the $k_{A'}$ is much bigger than k_A and only one diastereoisomer is displayed in the ^{1}H NMR spectrum. This phenomenon is also bound to the so-called Pfeiffer effect in which a racemic mixture is desymmetrized by complexation and optical activity is observed.[60]

The reaction of a chiral, enantiomerically pure metal fragment with C_5-symmetric corannulene derivatives thus unveils the possibility of selective complexation of the *M* or *P* intercorverting enantiomers, under dynamic kinetic resolution conditions but does not provide any insights into the nature of the formed diastereoisomers. Due to the impossibility of analyzing the metal complexes by chiral HPLC or ^{1}H NMR in the presence of chiral shift agents and in the absence of a X-ray crystal structure, quantum chemical calculations offer some help.

Theoretical calculations on the difference in energy between the *M*-C_5 1,3,5,7,9-pentamethylcorannulene (**54**) and 1,3,5,7,9-penta(*t*-butyl)corannulene (**104**) with the (*R*,*R*) and (*S*,*S*) enantiomers of the diene ligand provide information about the stereochemical nature of the products. Figure 4.13 shows that the repulsive interaction occurring between the *t*-butyl groups on the corannulene core and the methyl groups on the diene (in green) are indeed responsible for the diastereoselectivity observed in the formation of **158**. It also serves as a picture for explaining the facial enantioselectivity observed during the reaction.

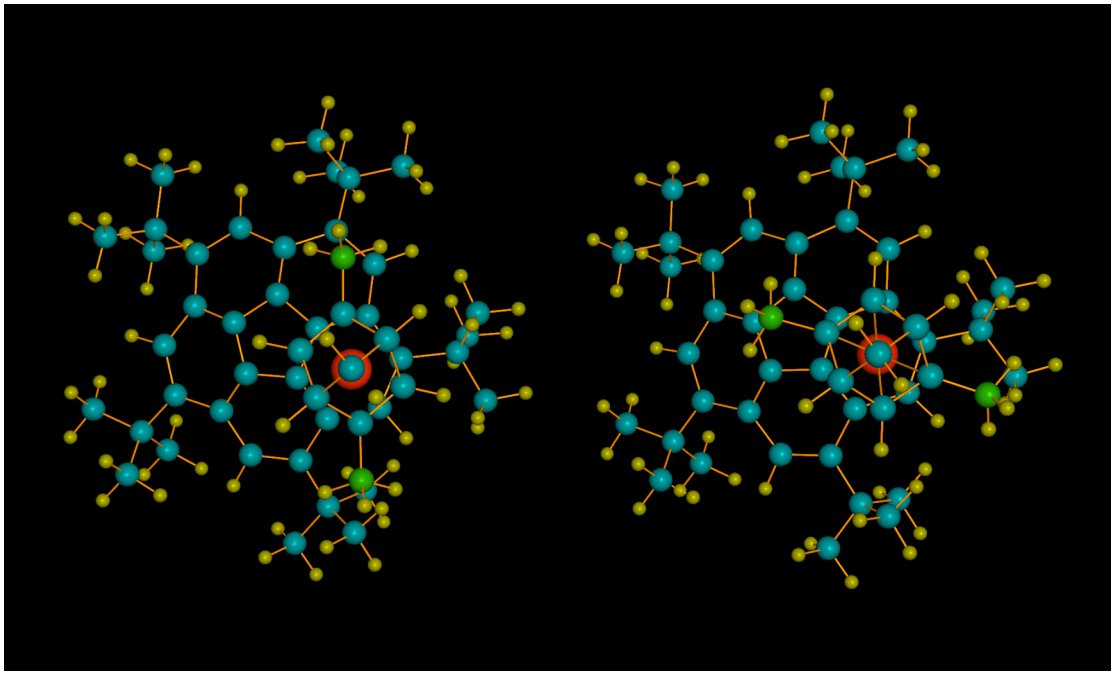

Figure 4.13. Ball and stick calculated structure for *M-RR* (right) and *M-SS* (left).

The calculated energy difference for **157** is 1.5 kcal mol^{-1} and this low value is reflected in the experimental observation for which two products are observed in a 1.8:1 ratio. In the case of **158** a difference in energy is 3.2 kcal mol^{-1} which accounts for the high selectivity that leads to one product. Calculations also predict that the *M*-(*S,S*) product is the favored (Figure 4.14), which means that, in the experiment, the *P*-(*R, R*) isomer is favored by symmetric analogy (calculations with M06/SDD method). An experimental observation for the chiral nature of the compounds is the appearance of a Cotton effect in the circular dichroism (CD) spectra.[61] CD spectra were recorded in CH_2Cl_2 solutions (Figure 4.15).[62] The chiral diene ligand displays a negative Cotton effect with a minimum at 255 nm and only the last part of the curve is measurable, as supported by optical rotatory dispersion curves of non-conjugated norbornadienes as discussed by Mislow.[63]

Compound **156** displays Cotton effect with a maximum at 355 nm, whereas **158** shows a maximum at 347 nm. The shifted Cotton effects to longer wavelengths for **156** and **158** compared to the diene ligand probably points to electron density transfer from the ligand to the corannulenes.

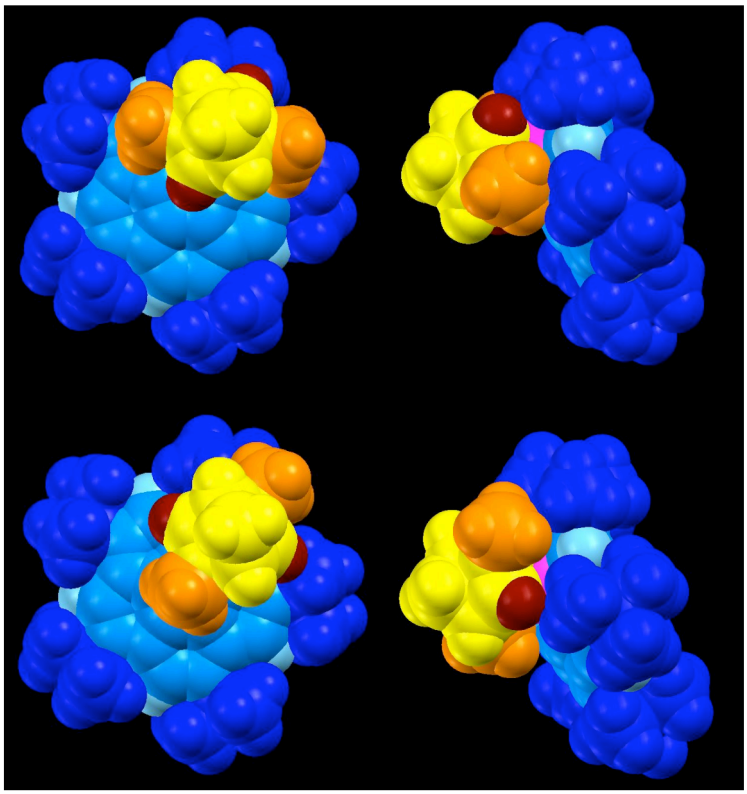

Figure 4.14. Calculated space fill model for *M-RR* (top) and *M-SS* (bottom), methyl groups on the diene in orange.

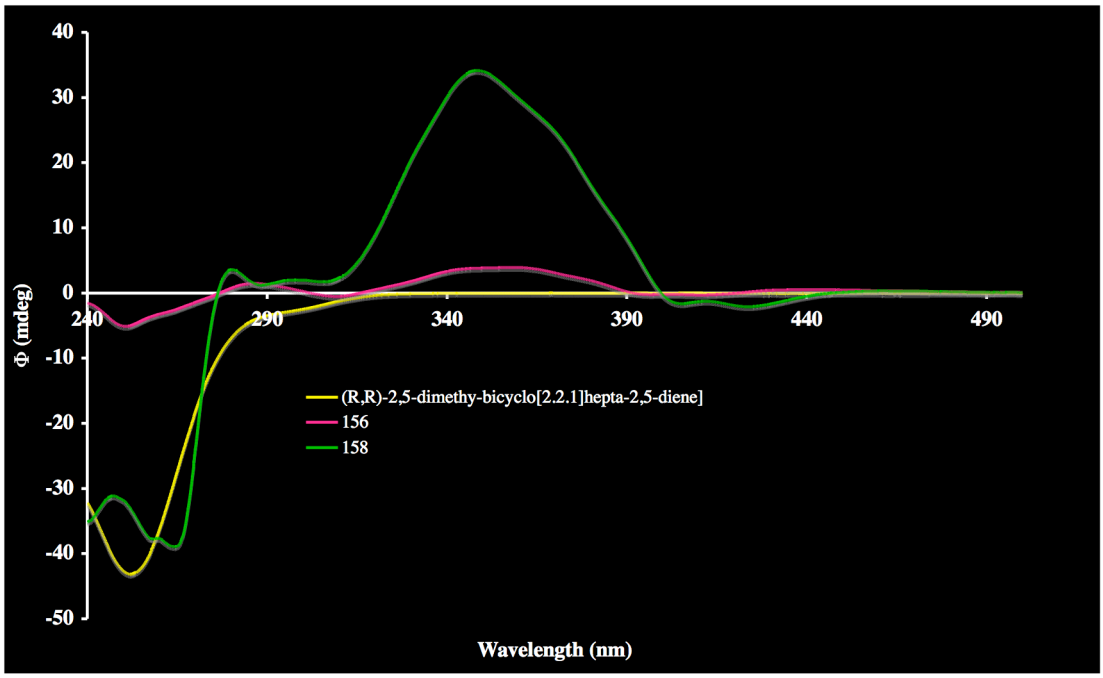

Figure 4.15. CD spectra for the chiral diene ligand (yellow), 156 and 158.

4.2.5. Proof of the intramolecular nature of the migration of metal fragment on corannulene

In chapter 3, it was demonstrated that metal migration on corannulenes occurs via a *hub* migration path. The observation of split ^{1}H NMR signals for the diene ligands also upon heating, when the migration is fast, and only one signal is observed for the aromatic region suggest that the migration process is likely intramolecular but does not prove it.

An experiment was designed to solidly prove the intramolecular nature of the migration process. Specifically, if the phenomenon is intramolecular, then in the case of the complex **156**, two sets of five exchanging proton signals should be observed in a 2D ^{1}H EXSY spectrum, due to stereochemical arguments (Figure 4.16).

Such a spectrum was recorded at 273 K in CH_2Cl_2 with increasing mixing times (τ_m) and the rapid growth of the cross peaks suggest that the migration process is occurring. For τ_m = 1.2 s, the optimal mixing is reached and, as hypothesized, two sets of five exchanging protons are observed, proving the intramolecular nature of haptotropic migration in corannulene derivatives (Figure 4.17).

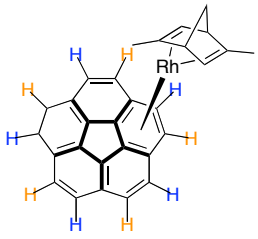

156

Figure 4.16. Possible sets of observable exchanging protons in 2D ^{1}H EXSY experiment of 156.

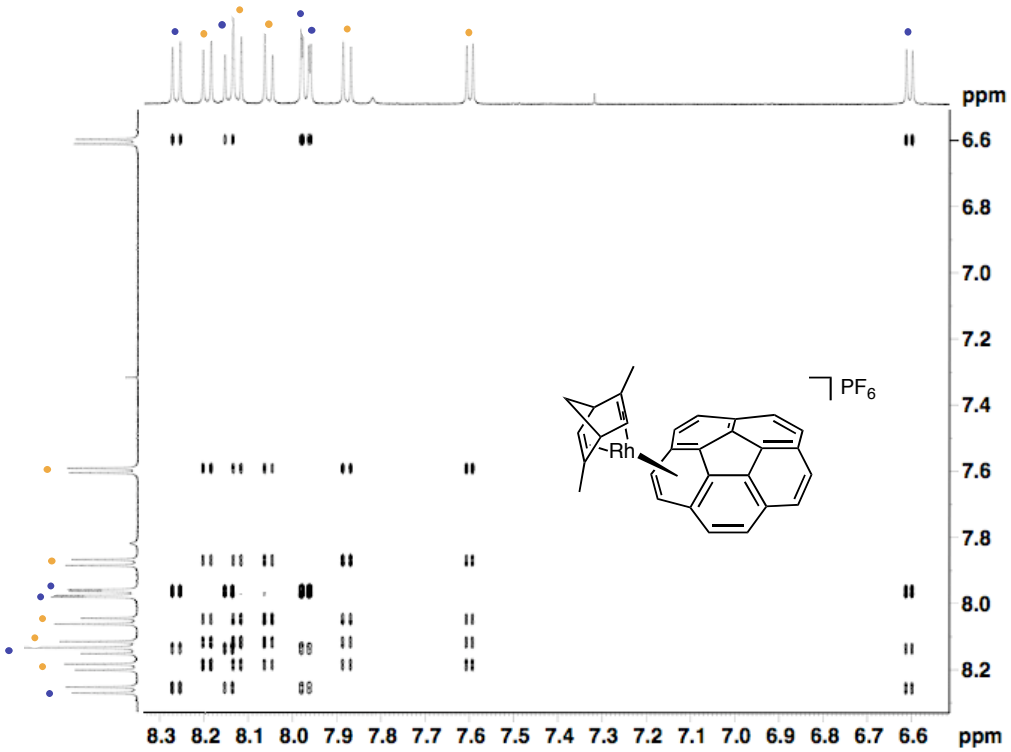

Figure 4.17. 2D ^{1}H NMR EXSY spectrum for 156 (two sets of five exchanging protons in blue and orange).

4.2.6. Conclusion and outlook

In this chapter, we have answered two fundamental questions. First, the selective complexation of a C_5 racemic corannulene derivative by use of a chiral dienic metal fragment is possible. Furthermore, this process involves a dynamic kinetic resolution, which, the first time, has been applied to a buckybowl. Second, the intramolecular migration of a metal fragment on corannuelene was proved by a 2D EXSY experiment in which the migrating fragment is chiral, showing the power of stereochemical arguments in the elucidation of complex phenomena.

4.3. Experimental section

4.3.1. Materials and method

General: ^{1}H and ^{13}C NMR were recorded using Bruker AV2-400 (400 and 101 MHz) or AV2-500. 2D EXSY spectra were recorded on Bruker AV2-500 equipped with BBI probe. – ESI-MS: Bruker EsquireLC MS. – Chromatography: Merck silica gel 60 (230–400 mesh) or Fluka neutral alumina (Brockmann I, Activity II). – Fluka acid washed celite was use for the organometallic complxes. – All experiments were carried out under nitrogen in anhydrous solvents (by passage through alumina colums in a MC Brown solvent system and degassed with N_2 for organometallic complexes) unless otherwise noted. – Solvent for NMR spectroscopy were degassed with nitrogen and dried over molecular sieves. – Solvents for chromatography were technical grade and freshly distilled before use – Corannulene,[64] *sym*-pentachlororcorannulene,[8c] *sym*-pentamethylcorannulene,[8c] 1,3,5,7,9-penta(*t*-Butyl)corannuelene,[65] tetramethylfluoranthene,[64] $[Rh(C_2H_4)_2(\mu^2\text{-}Cl)]_2$,[66] **155** (following Scheme 4.9),[54,55b,56] (*R*)-MeO-MOP,[55] 2-PyNTf$_2$[57] were prepared according to the literature procedures and the spectral data in agreement with them. – The synthesis of the organometallics complexes **156**-**158** were performed in a MCBrown glove box with a nitrogen atmoshphere. – Reaction involving the use of silver salts were carried out in the dark. – CD spectra: Jasco J-815 spectropolarimeter. – UV-vis: Prekin-Elmer Labda 19.

4.3.2. Synthetic procedures

{Rh[(*R*,*R*)-2,5-dimethyl[2.2.1]bicyclohepta-2,5-diene](η^6-corannulene}PF$_6$ (156)

To a vial containing corannulene (10 mg, 0.04 mmol) and {Rh[(*R*,*R*)-2,5-dimethyl-bicyclo[2.2.1]hepta-2,5-diene]Cl}$_2$ (10 mg, 0.02 mmol) in CH_2Cl_2 (0.3 ml) was added dropwise a solution of $AgPF_6$ (10.1 mg, 0.04 mml) in CH_2Cl_2 (0.2 ml) and the mixture (yellow) stirred in the dark for 30 min. The resulting suspension was filtered through a pad of cotton/celite to eliminate the AgCl and the filtrate evaporated until ca. 0.1 ml. Ether (1 ml) and pentane (1 ml) were carefully layered and put in a freezer at -20 °C overnight. The resulting yellow precipitate was decanted and washed with ether (2 x 1 ml) and pentane (2 x 1 ml) and dried in vacuo, yielding 20.3 mg (82%) of the desired compound.

^{1}H NMR (500 MHz, CD_2Cl_2, 270 K) δ (ppm) = 8.26 (d, *J* = 8.5 Hz, 1H), 8.19 (d, *J* = 9.0 Hz, 1H), 8.14 (d, *J* = 9.0 Hz, 1H), 8.13 (d, *J* = 9.5 Hz, 1H), 8.05 (d, *J* = 8.5 Hz,

1H) 7.98 (d, *J* = 8.5 Hz, 1H), 7.97 (d, *J* = 9.0 Hz, 1H), 7.88 (d, *J* = 9.0 Hz, 1H), 7.60 (d, *J* = 6.7 Hz, 1H), 6.60 (d, *J* = 6.7 Hz, 1H), 4.20-4.24 (m, 2H), 3.21-3.24 (m, 2H), 1.60 (s, 6H), 1.21 (dd, *J* = 1.5, 1.5 Hz, 2H).

^{13}C NMR (125 MHz, CD_2Cl_2, 270K) δ (ppm) = 140.1, 137.0, 136.4, 134.5, 134.0, 133.6, 133.3, 130.6, 130.4, 129.2, 128.9, 123.4, 123.3, 120.8, 119.1, 112.9, 107.0, 98.4 (d, J_{Rh-C} = 3.75 Hz), 94.0 (d, J_{Rh-C} = 3.75 Hz), 77.3 (d, J_{Rh-C} = 8.75 Hz,), 59.3 (d, J_{Rh-C} = 8.75 Hz), 54.3 (d, J_{Rh-C} = 2.5 Hz), 48.7 (d, J_{Rh-C} = 10 Hz), 21.3.

MS-ESI: m/z 473.1 $[RhC_{29}H_{22}]^+$ in chloroform. HRMS-ESI: calcd for $RhC_{29}H_2$: 473.0776; found: 473.0777.

{Rh[(*R*,*R*)-2,5-dimethyl[2.2.1]bicyclohepta-2,5-diene](η^6-1,3,5,7,9-pentamethylcorannulene}PF_6 (157)

To a vial containing 1,3,5,7,9-pentamethylcorannuelene (16 mg, 0.05 mmol) and {Rh[(*R*,*R*)-2,5-dimethyl-bicyclo[2.2.1]hepta-2,5-diene]Cl}$_2$ (12.7 mg, 0.025 mmol) in CH_2Cl_2 (0.5 ml) was added dropwise a solution of $AgPF_6$ (12.6 mg, 0.05 mmol) in CH_2Cl_2 (0.2 ml) and the mixture (yellow) stirred in the dark for 30 min. The resulting suspension was filtered through a pad of cotton/celite to eliminate the AgCl and the filtrate evaporated until ca. 0.1 ml. Ether (1 ml) and pentane (1 ml) were carefully layered and put in a freezer at -20 °C overnight. The resulting yellow precipitate was decanted and washed with ether (2 x 1 ml) and pentane (2 x 1 ml) and dried in vacuo, yielding 31 mg (90%) of the desired compound.

^{1}H NMR (400 MHz, CD_2Cl_2, 300 K) δ (ppm) = 8.02 (d, *J* = 1.2 Hz, 1H), 7.94 (d, *J* = 1.2 Hz, 1H'), 7.92 (d, *J* = 1.2 Hz, 1H), 7.89 (d, *J* = 1.2 Hz, 1H'), 7.79 (d, *J* = 1.2 Hz, 1H'), 7.75 (d, *J* = 1.2 Hz, 1H), 7.65 (d, *J* = 1.2 Hz, 1H), 7.54 (d, *J* = 1.2 Hz, 1H'), 7.18 (s, 1H'), 6.33 (s, 1H), 4.01-4.05 (m, 2H') 3.87-3.9 (m, 2H), 3.22-3.25 (m, 2H), 3.18-3.21 (m, 2H'), 2.98 (s, 3H), 2.93 (d, *J* = 0.8 Hz, 3H'), 2.90-2.92 (m, 9H), 2.86 (d, *J* = 0.8 Hz, 3H'), 2.84 (d, *J* = 0.8 Hz, 3H), 2.79 (d, *J* = 0.8 Hz, 3H), 1.62 (s, 3H), 1.51 (s, 1H'), 1.23 (t, *J* = 1.6 Hz, 3H), 1.15 (dd, *J* = 1.6 Hz, 3H').

^{13}C NMR (125 MHz, CD_2Cl_2, 270K) δ (ppm) = 145.5, 144.8, 141.2, 141.0, 139.2, 139.1, 138.6, 135.6, 135.5, 135.3, 135.1, 134.5, 134.1, 134.0, 133.9, 133.7, 133.4, 133.19, 133.3, 129.6, 129.1, 126.87, 126.5, 125.2, 125.0, 122.0, 120.7, 119.9, 119.2, 119.0, 118.6, 113.1 (d, J_{Rh-C} = 3.75 Hz), 111.6, 11.1, 109.8, 106.1, 96.0, 91.7 (d, J_{Rh-C} = 3.75 Hz), 76.1 (d, J_{Rh-C} = 8.75 Hz), 72.7 (d, J_{Rh-C} = 8.75 Hz), 49.5 (d, J_{Rh-C} = 10 Hz),

49.3 (d, J_{Rh-C} = 10 Hz), 21.5, 20.3, 20.01, 19.97, 19.6, 19.5, 19.30, 19.28, 19.24, 19.21, 19.19, 18.2

MS-ESI: m/z 543.2 $[RhC_{34}H_{32}]^+$ in chloroform. HRMS-ESI: calcd for $RhC_{34}H_{32}$: 543.1559; found: 543.1563.

{Rh[(*R*,*R*)-2,5-dimethyl[2.2.1]bicyclohepta-2,5-diene](η^6-1,3,5,7,9-penta(*t*-butyl)corannulene}PF_6 (158)

To a vial containing ,3,5,7,9-penta(*t*-Butyl)corannuelene (21.2 mg, 0.04 mmol) and {Rh[(*R*,*R*)-2,5-dimethyl-bicyclo[2.2.1]hepta-2,5-diene]Cl}$_2$ (10.0 mg, 0.02 mmol) in CH_2Cl_2 (0.4 ml) was added dropwise a solution of $AgPF_6$ (10.1 mg, 0.04 mmol) in CH_2Cl_2 (0.2 ml) and the mixture (yellow) stirred in the dark for 30 min. The resulting suspension was filtered through a pad of cotton/celite to eliminate the AgCl and the filtrate evaporated to dryness. The resulting yellow solid was washed with pentane (3 x 2 ml) and dried in vacuo, yielding 33.6 mg (92%) of the desired compound.

^{1}H NMR (500 MHz, CD_2Cl_2, 300 K) δ (ppm) = 8.58 (s, 1H), 8.48 (s, 1H), 8.28 (s, 1H), 8.17 (s, 1H), 8.08 (s, 1H), 7.00 (s, 1H), 3.80-3.85 (br s, 2H), 3.14-3.18 (m, 2H), 1.92 (s, 9H), 1.77 (s, 9H), 1.73 (s, 9H), 1.63 (s, 9H), 1.47-1.51 (br s, 6H), 1.22-1.24 (m, 2H)

^{13}C NMR (125 MHz, CD_2Cl_2, 215K) δ (ppm) = 157.2, 151.8, 150.0, 144.8, 136.9, 135.3, 134.4, 130.4, 129.9, 129.2, 128.7, 128.5, 124.7, 124.0, 121.7, 116.8, 116.1, 112.5, 101.1, 88.7, 78.6, 74.3, 59.6, 48.9, 46.3, 37.9, 37.3, 37.2, 37.19, 37.16, 36.9, 32.0, 31.9. 31.6 (2C), 31.5, 23.1, 18.1

MS-ESI: m/z 753.6 $[RhC_{49}H_{62}]^+$ in chloroform. HRMS-ESI: calcd for $RhC_{49}H_6$: 753.3907; found: 743.3902.

4.3.3. Computational part

Computation were performed with the method M06/SDD at the level TZVP+LANL2TZ+f.

4.4. References

[1] Kroto, H. W.; Heath, J. R.; O'Brein, S. C.; Curl, R. F.; Smalley, R. E. *Nature* **1985**, *318*, 162.

[2] Krätschmer, W.; Lamb, L. D.; Fostiropoulos, K.; Huffman, D. R. *Nature* **1990**, *347*, 354.

[3] Thilgen, C.; Diederich, F. *Chem. Rev.* **2006**, *106*, 5049.

[4] Scott, L. T.; Hashemi, M. M.; Bratcher, M. S. *J. Am. Chem. Soc.* **1992**, *114*, 1920.

[5] Abdourazak, A. H.; Marcinow, Z.; Sygula, A.; Sygula, R.; Rabideau, P. W. *J. Am. Chem. Soc.* **1995**, *117*, 6410

[6] Tsefrikas, V. M.; Arns, S.; Merner, P. M.; Warford, C. C.; Merner, B. L.; Scott, L. T.; Bodwell, G. *J. Org. Lett.* **2006**, *8*, 5195.

[7] Wu, Y. T.; Hayama, T.; Baldridge, K. K.; Linden, A.; Siegel, J. S. *J. Am. Chem. Soc.* **2006**, *128*, 6870.

[8] (a) Hayama, T; Baldridge, K. K.; Wu, Y.-T.; Linden, A.; Siegel, J. S. *J. Am. Chem. Soc.* **2008**, *130*, 1583. (b) Grube, G. H.; Elliott, E. L.; Steffens, R. J.; Jones, C. S.; Baldridge, K. K.; Siegel, J. S. **2003**, *5*, 713. (c) Seiders, T. J.; Elliot, E. L.; Grube, G. H.; Siegel, J. S. *J. Am. Chem. Soc.* **1999**, *121*, 7804.

[9] Wu, Y.-T.; Bandera, D.; Maag, R. ; Linden, A.; Baldridge, K.K.; Siegel, J. S. *J. am. Chem. Soc.* **2008**, *130*, 10729.

[10] Higashibayashi, S., Sakurai, H. *J. Am. Chem. Soc.* **2008**, *130*, 8592.

[11] Sakane, H.; Amaya, T.; Moriuchi, T.; Hirao, T. *Angew. Chem. Int. Ed.* **2009**, *48*, 1640.

[12] Ettl, R.; Chao, I.; Diederich, F., Whetten, R. L. *Nature* **1991**, *353*, 149.

[13] Manolopoulos, D. E. *J. Chem. Soc., Faraday Trans.* **1991**, *87*, 2861.

[14] Achiba, Y.; Kikuchi, K.; Aihara, Y.; Wakabayashi, Y.; Miyake, Y.; Kinoso, M. On *Higher Fullerenes: Structure and Properties*; Bernier, P; Bethune, D. S.; Chiang, L. Y.; Ebbesen. T. W.; Metzeger, R. M.; Mintmire, J. W. Eds. Material Society Symposium Proocedings, Vol. 359; Material Research Society: Pittsburgh, PA, 1995; P3.

[15] Diederich, F.; Whetten, R. L.; thilegen, C.; Ettl, R.; Chao, I.; Alvarez, M.M. *Science*, **1991**, *254*, 1768.

[16] Kikuchi, K.; Nakahara, N.; Wakabayashi, T.; Suzuki, S.; Shiromaru, H.; Miyake,

Y.; Saito, K.; Ikemoto, I.; Kainosho, M.; Achiba, Y.
Nature (London) **1992**, *357*, 142.

[17] Henrich, F. H.; Michel, R. H.; fischer, A.; Richard Schneider, S.; Gilb, S.; Kappes, M.M.; Fuchs, D.; Bürk, M.; Kobayashi, K. Nagase, S. *Angew. Chem. Int. Ed.* **1996**, *35*, 1732.

[18] Kobayashi, K.; Nagase, S.; Akasaka, T. *Chem. Phys. Lett.* **1995**, *245*, 230.

[19] Sun, G. Y.; Kertesz, M. *J. Phys. Chem. A* **2001**, *105*, 5468

[20] (a) Diederich, F.; Whetten, R. L. *Acc. Chem. Res.* **1992**, *25*, 119. (b) Taylor, R.; Langley, G. J.; Avent, A. G.; Dennis, T. J. S.; Kroto, H.W.; Walton, D. R. M. *J. Chem. Soc., Perkin Trans. 2* **1993**, 1029.

[21] Fowler, P. W.; Manolopoulos, D. E. *An Atlas of Fullerenes*; Clarendon Press: Oxford, U.K., 1995.

[22] Balch, A. L.; Ginwalla, A. S.; Lee, J. W.; Noll, B. C.; Olmstead, M. M. *J. Am. Chem. Soc.* **1994**, *116*, 2227.

[23] (a) Kimura, T.; Sugai, T.; Shinohara, H.; Goto, T.; Tohji, K.; Matsuoka, I. *Chem. Phys. Lett.* **1995**, *246*, 571. (b) Miyake, Y.; Minami, T.; Kikuchi, K.; Kainosho, M.; Achiba, Y. *Mol. Cryst. Liq. Cryst.* **2000**, *340*, 553. (c) Sun, G. Y.; Kertesz, M. *Chem. Phys.* **2002**, *276*, 107. (d) Sun, G. Y. *Chem. Phys. Lett.* **2003**, *367*, 26. (e) Tagmatarchis, N.; Arcon, D.; Prato, M.; Shinohara, H. *Chem. Commun.* **2002**, 2992.

[24] (a) Iijima, S. *Nature (London)* **1991**, *354*, 56. (b) Iijima, S.; Ichihashi, T. *Nature (London)* **1993**, *363*, 603.

[25] (a) Ge, M.; Sattler, K. *Science* **1993**, *260*, 515. (b) Wildoer, J. W. G.; Venema, L. C.; Rinzler, A. G.; Smalley, R. E.; Dekker, C. *Nature (London)* **1998**, *391*, 59. (c) Odom, T. W.; Huang, J. L.; Kim, P.; Lieber, C. M. *Nature (London)* **1998**, *391*, 62.

[26] Hawkins, J. M.; Meyer, A. *Science* **1993**, *260*, 1918.

[27] Hawkins, J. M.; Nambu, M.; Meyer, A. *J. Am. Chem. Soc.* **1994**,*116*, 7642.

[28] Herrmann, A.; Diederich, F. *Helv. Chim. Acta* **1996**, *79*, 1741.

[29] Kessinger, R.; Crassous, J.; Herrmann, A.; Ruttimann, M.; Echegoyen, L.; Diederich, F. *Angew. Chem., Int. Ed.* **1998**, *37*, 1919.

[30] Bingel, C. *Chem. Ber.* **1993**, *126*, 1957.

[31] Herranz, M. A.; Diederich, F.; Echegoyen, L. *Eur. J. Org. Chem.* **2004**, 2299.

[32] Crassous, J.; Rivera, J.; Fender, N. S.; Shu, L.; Echegoyen, L.; Thilgen, C.;

Herrmann, A.; Diederich, F. *Angew. Chem., Int. Ed.* **1999**, *38*, 1613.

[33] Yamamoto, C.; Hayashi, T.; Okamoto, Y.; Ohkubo, S.; Kato, T. *Chem. Commun.* **2001**, 925.

[34] Matsuo, Y.; Nakamura, E. *Chem. Rev.* **2008**, *108*, 3016.

[35] (a) Nakamura, E.; Sawamura, M. *Pure Appl. Chem.* **2001**, *73*, 355. (b) Nakamura, E.; Isobe, H. *Acc. Chem. Res.* **2003**, *36*, 807. (c) Sawamura, M.; Iikura, H.; Nakamura, E. *J. Am. Chem. Soc.* **1996**, *118*, 12850. (d) Sawamura, M.; Iikura, H.; Ohama, T.; Hackler, U. E.; Nakamura, E. *J. Organomet. Chem.* **2000**, *599*, 32. (e) Sawamura, M.; Nagahama, N.; Toganoh, M.; Hackler, U. E.; Isobe, H.; Nakamura, E.; Zhou, S. Q.; Chu, B. *Chem. Lett.* **2000**, 1098. (f) Sawamura, M.; Kuninobu, Y.; Nakamura, E. *J. Am. Chem. Soc.* **2000**, *122*, 12407.

[36] Zhou, S. Q.; Burger, C.; Chu, B.; Sawamura, M.; Nagahama, N.; Toganoh, M.; Hackler, U. E.; Isobe, H.; Nakamura, E. *Science* **2001**, *291*, 1944.

[37] Murata, Y.; Shiro, M.; Komatsu, K. *J. Am. Chem. Soc.* **1997**, *119*, 8117.

[38] (a) Toganoh, M.; Suzuki, K.; Udagawa, R.; Hirai, A.; Sawamura, M.; Nakamura, E. *Org. Biomol. Chem.* **2003**, *1*, 2604. (b) Toganoh, M.; Matsuo, Y.; Nakamura, E. *J. Organomet. Chem.* **2003**, *683*, 295. (c) Sawamura, M.; Toganoh, M.; Suzuki, K.; Hirai, A.; Iikura, H.; Nakamura, E. *Org. Lett.* **2000**, *2*, 1919.

[39] Iikura, H.; Mori, S.; Sawamura, M.; Nakamura, E. *J. Org. Chem.* **1997**, *62*, 7912.

[40] (a) Nakamura, E.; Tahara, K.; Matsuo, Y.; Sawamura, M. *J. Am. Chem.Soc.* **2003**, *125*, 2834. (b) Matsuo, Y.; Tahara, K.; Sawamura, M.; Nakamura, E. *J. Am. Chem. Soc.* **2004**, *126*, 8725.

[41] Matsuo, Y.; Mitani, Y.; Zhong, Y.-W.; Nakamura, E. *Organometallics* **2006**, *25*, 2826.

[42] Morandini, F.; Consiglio, G.; Straub, B.; Ciani, G.; Sironi, A. *J. Chem. Soc., Dalton Trans.* **1983**, 2293.

[43] Morandini, F.; Dondana, A.; Munari, I.; Pilloni, G.; Consiglio, G.; Sironi, A.; Moret, M. *Inorg. Chim. Acta* **1998**, *282*, 163.

[44] Bashilov, V. V.; Dolgushin, F. M.; Petrovskii, P.V.; Sokolov, V.; I.; Sada, M.; Benicori, T.; Zotti, G. *J. Organomet. Chem.* **2005**, *690*, 4330

[45] Sokolov, V. I. *Russ. J. Org. Chem.* **1999**, *35*, 1257.

[46] Sokolov, V. I. *Pure & Appl. Chem.* **1998**, *70*, 789.

[47] Song, L.-C.; Liu, P.-C.; Liu, J.-T.; Su, F-H.; Wang, G.-F.; Hu, Q.-M.; Zanello, P.; Laschi, F.; Fontani, M. *Eur. J. Inorg. Chem.* **2003**, 3201**.**

[48] Parschau, M.; Fasel, R.; Ernst, K.-H.; Gröning, O.; Brandenberger, L.; Schillinger, R.; Greber, T., Seitsonen, A. P.; Wu, Y.-T.; Siegel, J. S. *Angew. Chem. Int. ed.* **2007**, *46*, 1.

[49] Parschau, M.; Merz, L.; Bandera, D.; Ernst, K.-H.; Siegel, J. S. *J. Am. Chem. Soc.* **2009**, *131*, 3460.

[50] Amaya, T.; Sakane, H.; Hirao, T. *Angew. Chem. Int. Ed.* **2007**, *46*, 8376.

[51] Wolf, C. *Dynamic Stereochemistry of Chiral Compounds Principles and Applications*, RCS publishing, Cambridge, UK, 2008, P 331.

[52] (a) Glorius, F. *Angew. Chem. Int. Ed.* **2004**, *43*, 3364. (b) Defieber, C.; Grützmache, H.; Carreira, E. M. *Angew. Chem. Int. Ed.* **2008**, *47*, 4482.

[53] (a) C. Fischer, C. Defieber, T. Suzuki, E. M. Carreira, *J. Am. Chem.Soc.* **2004**, *126*, 1628. (b) T. Hayashi, K. Ueyama, N. Tokunaga, K. Yoshida, *J. Am. Chem. Soc.* **2003**, *125*, 11508. (c) C. Defieber, J.-F. Paquin, S. Serna, E. M. Carreira, *Org. Lett.* **2004**, *6*, 3873. (d) Y. Otomaru, K. Okamoto, R. Shintani, T. Hayashi, *J. Org. Chem.* **2005**, *70*, 2503. (e) Y. Otomaru, N. Tokunaga, R. Shintani, T. Hayashi, *Org. Lett.* **2005**, *7*, 307. (f) Y. Otomaru, A. Kina, R. Shintani, T. Hayashi, *Tetrahedron: Asymmetry* **2005**, *16*, 1673.

[54] Berthon-Gelloz, G.; Hayashi, T. *J. Org. Chem.* **2006**, *71*, 8957

[55] (a) Uozomi, Y.; Lee, S.-Y.; Hayashi, T. *Tetrahedron Lett.* **1992**, *33*, 7185. (b) Uozumi, Y.; Tanahashi, A.; Lee, S.-Y.; Hayashi, T. *J.Org. Chem.* **1993**, *58*, 1945. (c) Uozumi, Y.; Kawatsura, M.; Hayashi, T. *Organic Syntheses*, vol 78, Rausch, W. R. Ed.

[56] Noël, T.; Vandyck, K.; Van der Eycken, J. *Tetrahedron* **2007**, *63*, 12961.

[57] Comins, D. L.; Dehghani, A. *Tetrahedron Lett.* **1992**, *33*, 6299.

[58] (a) Schrock, R. R.; Osborn, J. A. *J. Am. Chem. Soc.* **1971**, *93*, 3089. (b) Siegel, J. S.; Baldridge, K. K.; Linden, A.; Dorta, R. *J. Am. Chm. Soc.* **2006**, *128*, 10644.

[59] Carey, F. A.; Sundberg, R. J. *Advanced Organic Chemistry*, 5th Ed., Spring Science, New York, USA, 2007, p296.

[60] Pfeiffer, P.; Quehl, K. *Ber. Deutsch. Chem. Ges.* **1931**, *64*, 2667.

[61] Observation of optical activity support the chiral nature of compounds but in some cases even though the compound is chiral, optical activity is not measurable as observed in: K. Mislow, Bickart, P. *Isr. J. Chem.* **1977**, *15*, 1.

[62] For **156** and **158** an accurate concentration was not measured. For [(*R*,*R*)-2,5-dimethyl-bicyclo[2.2.1]hepta-2,5-diene the concentration was 5.4 10^{-4} M.

[63] Mislow, K. *Annals of the New York Academy of Science*, **1962**, *93*, 459 and references cited therein.

[64] Jones, C. S.; Elliott, E.; Siegel, J. S. *Synlett*. **2004**, 187.

[65] Sevryugina, Y.; Rogachev, A. Y.; Jackson, E. A.; Scott, L. T.; Petrukhin, M. A. *J. Org. Chem.* **2006**, *71*, 6615.

[66] S. Komiya, *Synthesis of Organometallics Compounds*, Wiley & Sons, Chichester, UK, 1997. p237.